

STUDIES OF THE COALESCENCE OF DISPERSIONS  
IN PARTICULATE PACKINGS

by

David Wilkinson

A thesis submitted to the University  
of Aston in Birmingham for the  
degree of Doctor of Philosophy

THESIS  
660-22  
WIL  
181682 E-6 FEB 1975

Department of Chemical Engineering  
The University of Aston in  
Birmingham

November, 1974.

## SUMMARY

Droplet hydrodynamics and coalescence mechanisms in a packed bed have been studied using a mono-sized primary inlet dispersion with a packing of equal sized glass spheres. Four systems were studied and a correlation was developed using a dimensional analysis to evaluate the parameters affecting the exit drop size of a packed bed. A technique was developed to evaluate the mean exit drop size by producing a Shadowgraph capable of automatic analysis on an Image Analysing Computer.

Two distinct processes of droplet behaviour were identified within a packed bed. In the first, droplets entered and passed through the packing until they met a restriction, at which droplet retention and subsequent coalescence occurred. The second process was drop formation at the exit of the packing, which was related to the release mechanisms which occurred after the retained droplets had grown by coalescence.

A mathematical model was developed to relate the buoyancy and surface forces in terms of the drop size and shape in the aperture of a packing element. The model can be used to predict the range of drop diameters that will not pass through a packing restriction. The lower and upper limits refer to the initial point of drop retention and the eventual point of drop release, and this has been related to the geometry of the packing within the bulk of the bed and in the exit layer respectively. Good agreement was found between predicted and experimental values for both simulated single packing restrictions and packed beds.



SUMMARY (continued)

A definition of a packing efficiency has been proposed by equating the experimental mean exit drop size with the theory of droplet release and the probability of droplet retention. This has enabled a quantitative comparison to be made of the theoretical and experimental limitations of a packed bed as a coalescing aid.

## ACKNOWLEDGEMENTS

The author is deeply indebted and wishes to record his sincere thanks to all the members of staff and the postgraduates of the Department of Chemical Engineering, particularly :-

Professor G. V. Jeffreys

for providing the facilities for this research and for his helpful guidance and personal interest in the supervision of this project.

Dr. C. J. Mumford

for his constant advice and encouragement.

D. W. Moore

for his stimulating comments, suggestions and interest shown.

The author also wishes to express his sincere gratitude to:-

Mrs. A. Mellings of the Photographic Section of the Department of Chemical Engineering .

The Science Research Council, without whose assistance this research would not have been possible .

Professor S. J. Hartland, of Eidgenossische Technische Hochschule Zurich, who provided facilities for part of this study .

Finally, I acknowledge my great debt to Miss A. Wootton for her kind help in typing numerous pages to finalize this thesis .



## LIST OF CONTENTS

	<u>Page</u>
INTRODUCTION	
<u>CHAPTER 1.</u>	
1) Single Droplet Coalescence	1
1.1) Drop Interface Coalescence	2
1.1.1) Coalescence Times	3
1.1.2) Factors affecting Coalescence	4
1.1.3) Theoretical Models	8
1.2) Drop-Drop Coalescence	11
 <u>CHAPTER 2.</u>	
2) Coalescence of Dispersions in Packed Beds	14
2.1) Primary Dispersions	
2.1.1) Conventional Packings - Raschig Rings and Berl Saddles	16
2.1.2) Volumetric Throughputs	21
2.2) Primary Dispersions-Knitted Mesh Packings	23
2.2.1) Wetted Packings	24
2.2.2) Composite Packings	26
2.2.3) Non-Wetted Packings	28
2.3) Secondary Dispersions	30
2.3.1) Flow Through Porous Media	32
2.3.2) Coalescence in Fibrous Beds	32
2.3.3) Flow through Particulate Beds	36
 <u>CHAPTER 3.</u>	
3) Drop Formation	
3.1) Drop Formation at Low Velocity	38
3.2) Drop Formation below jetting	38

LIST OF CONTENTS (contd)

3.3)	Predicting jetting velocities	42
3.4)	Drop Formation from Jets	43

CHAPTER 4.

4)	Surface Energy Considerations	45
4.1)	Theoretical Considerations	46
4.2)	Factors affecting Contact Angle Values	47
4.2.1)	Surface Roughness	47
4.2.2)	Temperature	48
4.2.3)	Rate of Motion	48
4.2.4)	Hysterisis	49
4.2.5)	Experimental Procedures	50

CHAPTER 5.

5)	Experimental Investigation	53
5.1)	Design of Apparatus	53
5.1.1)	Packing Selection	53
5.1.2)	Materials of Construction	56
5.1.3)	Selection of Systems	57
5.1.4)	System Preparation	58
5.2)	Pilot Plant Equipment	60
5.2.1)	6" Diameter Column	60
5.2.2)	9" Diameter Column	61
5.3)	Laboratory Apparatus - Single Drop Studies	62
5.3.1)	Inlet Drop Studies	62
5.3.2)	Exit Drop Studies	63
5.3.3)	Surface Energy Studies	64



## LIST OF CONTENTS (contd.)

	<u>Page</u>
<u>CHAPTER 6.</u>	
6) Data Acquisition and Treatment ; Drop Size Analysis	67
6.1) Direct Measurement	67
6.2) Automatic Measurement	70
6.2.1) Image Analysing Computers (I.A.C)	70
6.2.2) Schlieren Photography	70
6.2.3) Light -Emitting Compounds	73
6.3) Drop Size Analysis on the I.A.C.	
<u>CHAPTER 7.</u>	
7) Theoretical Considerations for Mathematical Model	77
7.1) Single Drop Studies	77
7.1.1) Film Drainage Models	78
7.2) Idealized Drop at a Plane Orifice	82
7.3) Model for a Drop Residing in a Ballotini Packing Restriction	85
<u>CHAPTER 8.</u>	
8) Discussion of Results	89
8.1) Inlet Model	89
8.2) Lower Limit	91
8.3) Upper Limit	92
8.4) Experimental Errors	93
8.5) Application of the Inlet Model to Packed Bed Behaviour	94
8.6) Previously Reported Packed Bed Phenomena	96
<u>CHAPTER 9.</u>	
9) Discussion of Results Exit Drop Mechanisms	99

## LIST OF CONTENTS (contd)

9.1)	Packed Bed Results	100
9.1.1)	Effect of Ballotini Diameter	100
9.1.2)	Effect of Flow Rate	101
9.2)	Determination of Exit Packing Geometry	106
9.2.1)	Drop Void Number	106
9.3)	Single Nozzles	110
9.4)	Drop Formation Mechanism on "release"	114
9.5)	Design Considerations	116

### CHAPTER 10.

10)	Discussion of Results Application of Inlet Model to a definition of Packing efficiency	119
10.1)	Packed Bed Considerations	119
10.2)	Discussion of Results	122
10.3)	Packing Efficiency Considerations	124

### CHAPTER 11.

11)	Discussion of Results	129
11.1)	Dimensional Analysis	129
11.2)	Results and Correlations	133
11.3)	Relationship of individual parameters to exit drop size	134
11.4)	Accuracy of General Correlation	137

Conclusions	139
-------------	-----

Recommendations for Further Work	141
----------------------------------	-----



## LIST OF CONTENTS (contd)

### Appendices

Surface Energetics	A.1
Physical Properties of Liquid Systems	A.2
Computer Programmes	A.3
Experimental Data	A.4
Correlations of Meister and Scheele	A.5

### Nomenclature

### References

## INTRODUCTION

Droplet dispersions occur in many fields of chemical engineering, especially in the manufacture of chemicals where liquid extraction forms part of the process. In liquid-liquid extraction, two liquid streams are contacted to facilitate transfer of solute from one phase to the other and, to accelerate the process, a high interfacial area is needed. This is obtained by forming a droplet dispersion of one phase in the other. Formation of dispersions may be achieved by means of nozzles, as in spray columns, or by mechanical agitation, as in mixing vessels, and in rotary agitated or pulsed columns. Internal baffles or packings may be used to aid dispersion and to reduce the extent of back mixing. Other cases where one liquid may be contaminated by another to produce a droplet dispersion include aviation fuel, which may be contaminated by water droplets, or effluent streams, which may be contaminated by an oil phase.

In all cases, the ultimate separation of the two liquid phases is an important operation. Many methods of separating droplet dispersions are available, but this study is concerned with the use of simple packed beds as an aid to droplet coalescence and subsequent phase separation.

The phenomena associated with the coalescence and separation of droplet dispersions in packings is dependent upon the nature and the droplet size range of the dispersion, the properties of the packing and the operating conditions. The hydrodynamics of flow through packed beds and the mechanisms of droplet coalescence are in fact little understood, and design is often by trial and error.



Therefore, in this study, the behaviour of primary dispersions (droplet diameters  $> 100 \mu\text{m}$ ) has been investigated in packings of equal sized glass spheres. Though of no commercial significance, this packing enabled a quantitative analysis to be made of the effect of packing geometry on droplet coalescence mechanisms.

CHAPTER 1.

SINGLE DROPLET COALESCENCE



1) Single Droplet Coalescence

Coalescence is a general term describing the fusion of two or more macroscopic quantities of the same material. This review will be restricted to the particular cases of:

- (a) a single drop coalescing with its parent liquid at an interface;
- (b) a single drop coalescing with a second drop.

These two processes are generally termed drop-interface and drop-drop coalescence respectively. In liquid-liquid systems, both forms of coalescence take place in a continuum of a second immiscible liquid.

Many studies have been made into the mechanisms of drop-interface and drop-drop coalescence. Different physical situations of droplet coalescence have been investigated and these include studies of single drop coalescence and large populations of drops in the presence, or absence, of mass transfer. Initially, work was generally concentrated on the study of drop-interface coalescence in the absence of mass transfer, since this is the most convenient experimentally and therefore enables a close inspection of the physical processes involved.

Essentially the same physical processes take place in all modes of droplet coalescence, but the situation is often complicated by the prevailing environment and its interaction upon the coalescence process. As a first step towards defining coalescence mechanisms within packed beds



the extensive literature available on single drop studies has been reviewed.

### 1.1) Drop-Interface Coalescence

Drop-interface coalescence involves the approach of a single drop to the parent interface, and the subsequent formation of a film of continuous phase between the drop and the interface. The film is forced out by the buoyancy forces between the dispersed phase and the continuous phase. The film drains until a critical thickness is reached when rupture takes place, allowing the contents of the droplet to be deposited into the bulk interface. Under some conditions, secondary droplets are formed during the initial coalescence process.<sup>(17)</sup> These drops must undergo a similar coalescence process and, dependent on conditions, may in turn form further secondary drops. This particular phenomenon leads to problems in industrial phase separation processes, owing to the much reduced settling velocities and the increased coalescence times associated with small droplets.

Whilst extensive<sup>(4 - 6)</sup> reviews are available for the mechanism of drop-interface coalescence, much conflicting information exists as to the relationship between the time required for drop coalescence and the properties of the system. The complexity of any coalescence process is well illustrated by the following summary of the main conclusions of earlier workers.



### 1.1.1) Coalescence Times

The process of coalescence experienced by a single drop at a plane interface consists of five consecutive stages;<sup>(4)</sup> (12)

- viz
- (a) the arrival of the drop at the interface and the subsequent deformation of the drop and interface profiles;
  - (b) the damping of oscillations caused by the impact of the drop at the interface;
  - (c) the formation and drainage of a continuous film between the drop and its bulk interface;
  - (d) rupture of the continuous film and the expansion of the resultant hole until the remaining film has been removed;
  - (e) deposition of the drop contents into the interface.

The time required for deformation and damping out of the oscillation of the drop, stages (a) and (b), has been defined as the pre-drainage time, and occupies a relatively short period, viz 0.1 seconds. High speed cine-photography of stage (e) has shown that the deposition time is of the order of 0.05 seconds. However, coalescence times can be measured with a stop watch, as stages (c) and (d), named respectively the "drainage time" and the "film removal time", are of the order of several seconds (or more). Although the total time is such as to nullify the errors inherent in measurement by a stop watch, all authors found a wide variation in coalescence

times. The distribution of times has been found to be approximately Gaussian (for the same size drop of an identical L/L system). Some discussion has arisen as to the number of drops which should be studied to obtain a reproducible mean coalescence time. The numbers of drops have varied from 70 to 200 for pure systems<sup>(7) (8)</sup> and from 30 to 40 for systems stabilized<sup>(9)</sup> with the use of surfactants. The coalescence time has been expressed as a mean rest time " $t_m$ " and also in the form of half life rest times " $t_{\frac{1}{2}}$ ". Generally,  $t_{\frac{1}{2}}$  has been more reproducible than  $t_m$ , and the ratio of ( $t_m/t_{\frac{1}{2}}$ ) has fallen within the range 1.01 - 1.27.<sup>(2)</sup>

Correlations of coalescence times have been evaluated for pure systems<sup>(8)</sup> and also for systems including surfactants<sup>(9)</sup> or electrolytes.<sup>(10)</sup> It is important to note that surfactants are known to reduce the interfacial tension and interfacial compressibility and to increase the surface viscosity. Similarly, electrolytes may have an effect on the interfacial behaviour, thus the presence of another component would be expected, in some way, to affect the film drainage process. However, the physical situation is not yet fully understood, which may explain the difficulties experienced in equating different correlations of coalescence times.

#### 1.1.2) Factors affecting coalescence

The coalescence of a single drop at an interface is accomplished through drainage and rupture of the trapped film of the continuous phase. Therefore,



those parameters which most affect the drainage and rupture control the overall coalescence process.

Many authors (2)(12) have discussed factors which affect the rate of coalescence of drops. Their conclusions have been well documented, and are summarized in Table 1.1.2. The table demonstrates that for parameters Nos.(v - XI) there is some agreement on the physical process taking place, however, this is not the case for parameters Nos.( i - iv). It is interesting to note that agreement generally occurs where the parameter under investigation is externally induced viz temperature effects, vibration, surfactants, mass transfer and electrical effects. The disagreement recorded for parameters Nos.(i - iv) is noticeably related to the more fundamental properties of the system, e.g. density difference and interfacial tension, and as such are more difficult to isolate.

Table 1.1.2

<u>No.</u>	<u>Parameter (increasing)</u>	<u>Physical description of effect</u>	<u>Coalescence time</u>	<u>Refs.</u>
(i)	Interfacial tension	Little deformation of drop hence area for drainage smaller	Decreases	(36)
		Increases strength of film, resistance to rupture	Increases	(14)
(ii)	Density difference	Greater drop deformation hence area for drainage greater	Increases	(16,17)
		Greater hydrostatic forces act on drainage	Decreases	(6)
(iii)	Drop Size	Drainage area greater	Increases	(16,17)
		Small area/volume hence surfactant area smaller	Decreases	(18)
		Depends on system investigated	Variable	(14)
		All forces balance	No effect	(9)

Table 1.1.2 (contd)

<u>No.</u>	<u>Parameter</u> <u>(increasing)</u>	<u>Physical description</u> <u>of effect</u>	<u>Coalescence</u> <u>time</u>	<u>Refs.</u>
(iv)	Distance of drop fall to interface	Exposure time to surfactants increases	Increases	(17,19)
		Independent (effect of apparatus design)	No effect	(17)
		Depends upon thermal and vibrational disturbance imposed on drainage of film	Variable	(21)
(v)	Viscosity of continuous phase	Increases resistance to film drainage	Increases	(90)
(vi)	Temperature	Decreases all physical properties particularly viscosity	Decreases	(19)
(vii)	Temperature gradients	Increases instability of film hence promotes rupture	Decreases	(7)
(viii)	Vibrational	Renews continuous film	Increases	(7)
		Produces random variations	Variable	(21)
(ix)	Electrical	Effectively produces forces greater than gravity	Decreases	(22)
(x)	Surfactants	Grouping of surface active molecules creates one mobile and one immobile interface, drop sinks and drainage area greater, or	Increases	(23)
		Initial internal circulation causes surface pressure differences, reduction of momentum transfer and consequently retards film drainage		(24)
(xi)	Mass Transfer	Solute from drop	Decreases	(24,12)
		Solute into drop	Increases	(25)



Controversy has arisen over the reproducibility of experimental results. The reasons for this are in general:

- (a) the effect of a particular parameter is not constant for all immiscible liquid-liquid systems;
- (b) the different experimental techniques employed during investigation.

This can be illustrated by considering the relationship between coalescence times and drop size. No effect was recorded for drop sizes of between 0.2 and 0.9 cms when a stabilized system of benzene-water was used, whereas a pure binary system has a relationship of  $t \propto d^n$ . Although various workers<sup>(2)</sup> have reported values of  $n$  ranging from  $n = -1.28$  to  $n = 3.15$ , Lang explained this<sup>(14)</sup> by the fact that there was no consistent variation with drop size. Rather it varied from system to system. This was carried further by Hitit<sup>(2)</sup> who proposed that the presence of contamination would supercede the effect of drop size.

Because of the difficulties of monitoring and observing film drainage, many hypothetical descriptions have been proposed for the physical process occurring within the film. For example, the effect of the drop fall distance to the interface is illustrated in Table 1.1.2. Lang<sup>(14)</sup> suggested a dependence upon the thermal and mechanical disturbance superimposed on the film drainage process. However, Jeffreys and Lawson<sup>(25)</sup> considered that the dimensions of the apparatus accounted for the variation of coalescence times noted by previous workers, and this must certainly be a contributory factor.

The effects of various parameters have been explained by numerous phenomena. More popular are the ageing effects of the interface<sup>(26)</sup>, surfactant contamination<sup>(2)</sup>, induced vibrational effects<sup>(14)</sup> and the randomness of drop approach to the interface<sup>(8)</sup>. It is possible

that each may act either independently or in conjunction with other known, or unknown effects. Further work is required to observe the drainage of the entrapped film before any firm conclusion can be reached.

### 1.1.3) Theoretical Models

The shape of a drop at an interface and the film thickness are equally important factors affecting the coalescence process. Therefore they have been the subject of investigation. This work has assisted the understanding of film drainage and has been used in the development of mathematical models to predict the time for film drainage.

#### (a) Shape of drop and the film profile

The shape of a drop at a plane interface was first formulated by Bashforth & Adams<sup>(13)</sup> who presented their work in a series of tables covering a wide range of physical properties. Princen<sup>(15)</sup>, and later Hartland<sup>(27)</sup> used a force balance on the drop surface to predict drop dimensions. From Hartland's work it can be concluded that the film thickness varies although the overall shape of the film is spherical. To reaffirm this conclusion, Jeffreys and Hawksley<sup>(16)</sup> using high speed cine-photography, found that the film was thinnest at its periphery. This result was based on the measurement of the principal radii of drop curvature and from these values they predicted the pressure drop over the profile. Though the above references are by no means complete, they serve to illustrate the investigations carried out into film and drop profiles. A further aid to predicting coalescence times has been in the evaluation of film thickness at rupture. This has been used in conjunction with film profiles to verify mathematical models of drainage times.



### (b) Film Thickness Evaluations

Three main methods of film thickness measurement have been employed:

- (i) an interference method (28)
- (ii) photographic techniques (16) (29)
- (iii) capacitance methods (29)

Mason et al<sup>(35)</sup> used an interference technique and found that rupture occurred at 900 Å. Hartland<sup>(29)</sup>, who used photographic and capacitance methods, found that rupture occurred at  $10^{-3}$  cms. This value, although large, was determined using a very viscous system of glycerol and golden syrup.

Other workers have recorded different values under various experimental conditions. Brown and Hanson<sup>(22)</sup> recorded a value between  $10^{-4}$  and  $10^{-5}$  cms for film rupture in the presence of an electrical field, whereas Vander Temple<sup>(30)</sup> found rupture to occur at 100 Å. The most recent analysis of film thickness at rupture is that of Allak<sup>(36)</sup>, who used an absorption technique of UV light and predicted from extrapolation that rupture would occur at 2 microns. He inferred that this value was an approximation and only indicated the order of magnitude.

The values recorded for the critical film thickness at rupture cover a wide range and further illustrate the difference which exists between systems investigated and experimental techniques employed.

### (c) Film Drainage Models

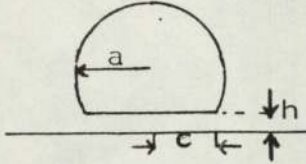
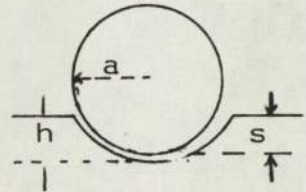
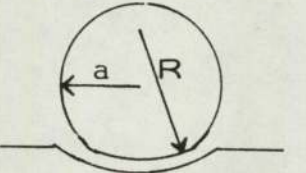
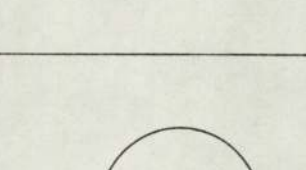
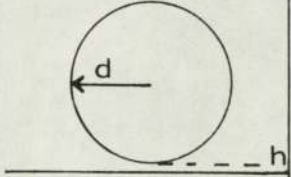
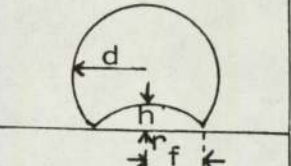
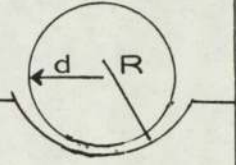
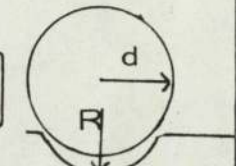
(7)(10)(15)(16)

Several mathematical models have been derived to explain the results obtained in determining coalescence times. The models derived to predict film drainage times are in two categories:



- (i) uniform film drainage models
- (ii) non-uniform film drainage models

These models have been described fully elsewhere<sup>(2)</sup> but are summarized in Table 1.1.3 for later reference.

Table 1.1.3 (a)	<u>UNIFORM FILM MODELS</u>	
(7) Deformable Drop Rigid Interface Uniform Film	$t = \frac{\mu_c \Delta \rho g d^5}{128 Y^2} \left( \frac{1}{h_2^2} - \frac{1}{h_1^2} \right)$	
(21) Rigid Drop Deformable Interface Uniform Film	$t = \left( \frac{9 \mu a^3 (a - s)^2}{(2a^3 - 3a^2 s - s^3) (\Delta \rho g)} \right) \frac{1}{h_2^2}$	
(15) Deformable Drop Deformable Interface Uniform Film	For small drops:- $t = \left( \frac{\mu_c \Delta \rho g d^5}{32 Y^2} \right) \frac{1}{h_2^2}$	
	where $R = 2d$ For large drops:- $t = \left( \frac{3 \mu_c d^3}{8 Y} \right) \frac{1}{h_2^2}$	
	a is the radius of the drop = $\frac{d}{2}$	
Table 1.1.3 (b)	<u>NON-UNIFORM FILM MODELS</u>	
(35) Rigid Drop Rigid Interface Non-Uniform Film	$t = \left( \frac{\mu_c}{2a \Delta \rho g} \right) \ln(h_1/h_2)$	
(3) Deformable Drop Deformable Interface Non-Uniform Film	$h = \left( \frac{0.0096 n^2 \mu_c r_f^6}{t a Y} \right)$ where n = number of surfaces that resist heat	
(1) Rigid Drop Deformable Interface Non-Uniform Film	(h' is the minimum film thickness at the periphery of the film)	
For $\lambda = R/d < 1$	$t = \frac{6 \pi \mu}{4 \phi^2 F L} \left[ \ln \left( \frac{h_2' - \theta}{h_1' - \theta} \right) + \ln \frac{h_1'}{h_2'} + \left( \frac{\theta}{h_2'} - \frac{\theta}{h_1'} \right) \right]$	
where	$\phi = \frac{1}{d} \left( 1 - \frac{1}{\lambda} \right); \theta = (\lambda - 1) \left( \frac{d}{2} - s \right)$	
For $\lambda = R/d > 1$	$t = \frac{6 \pi \mu}{4 \phi^2 F L} \left[ \ln \left( \frac{h_2}{h_1} \right) + \ln \frac{h_1 + \theta}{h_2 + \theta} + \left( \frac{\theta}{h_2 + \theta} - \frac{\theta}{h_1 + \theta} \right) \right]$	



## 1.2) Drop-Drop Coalescence

The "static" state of drop-interface coalescence has been favoured in most investigations as it is more convenient experimentally. The analysis of drop-drop coalescence, which represents a more dynamic situation, is difficult on two accounts. First, a controlled collision between two drops which have not been restrained in some way is extremely difficult to obtain. Secondly, the randomness with which the drops rebound or coalesce has made analysis very difficult.

Drop-drop studies necessitate consideration of both collision theory and the coalescence process. Hence the prediction of coalescence frequency requires knowledge of both collision frequency and coalescence probability.

Levich<sup>(31)</sup> has provided an excellent summary of collision frequency predictions for colloidal and aerosol systems for both laminar and turbulent flow. Although the analysis was valid only for particle diameters less than  $10^{-3}$  cms, Howarth<sup>(32)</sup> and Misek<sup>(11)</sup> have had limited success in extending the analysis to agitated systems containing larger drops in the range 0.01 to 0.2 cms.

Scheele and Lang<sup>(33)</sup> recently carried out an experimental study of the factors which promote coalescence although the simulated collision was similar to behaviour in a turbulent flow field. Using approach velocities of 1.9 to 11.2 cms/sec for 3.4 mm diameter drops, they concluded there was no obvious relationship between coalescence probability and impact velocity. Using high speed photography, they observed drop contact times of 0.01 - 0.07 seconds. If coalescence was to take place then, the film drainage time was of this order.

Scheele and Lang<sup>(33)</sup> applied the classical parallel disc rigid interface model<sup>(35)</sup> to describe the film thinning, and found that



this approach failed by several orders of magnitude to predict fast enough rates of film drainage to enable rupture. Experimentally, they observed more film thinning of the drops that did coalesce than in drops that rebounded. Although not proven experimentally, they suggested that coalescence was sensitive to the phase of oscillation at the point of drop-drop contact, and therefore the mobility of the interface would have to be included in the description of a film thinning model.

Work by Murdoch and Lang<sup>(34)</sup> attempted to relate a mathematical formulation of hydrodynamic film thinning to drop-drop coalescence. They equated the effects of interfacial mobility, rate of disc expansion, the force of impact, and both physical and interfacial property variables. Their analysis was based on transient solutions of the Navier Stokes flow equations with Newtonian liquids for film thinning between two drops during head-on collision. It was concluded that the film between two colliding drops thins most rapidly when there is an outward radial velocity inside the drop that sweeps out the liquid in the mobile continuous phase film. With decreasing radial velocity and decreasing interfacial mobility an increase of the film thinning time was predicted. However, no relationship was found between the approach velocity, internal circulation and the coalescence probability. This was verified by photographic analysis of the drops for possible internal circulation. Hence, it would appear that no internal circulation exists, and that coalescence is due to mobility of the interface alone. Random coalescence behaviour reported by Scheele and Lang<sup>(33)</sup> could be explained by the rate of disc expansion which is related to phase angle of drop oscillation at drop contact.

In conclusion, drop-drop coalescence occurs because either:



- (i) all colliding drops undergo very rapid film thinning, so that coalescence is associated with the statistical nature of rupture;
- (ii) or certain colliding drops undergo film thinning so that rupture can only occur in those cases.

The mechanisms of drop-drop coalescence are still not fully understood, and more experimental investigation is required before film drainage times can be predicted with any accuracy.

The information presented above indicates the difficulties inherent in the study of single droplet coalescence. Other equally important work on coalescence in a monolayer of drops at an interface and in dispersion bands within horizontal and vertical settlers has been reviewed elsewhere. However, these investigations are not of direct relevance to this study and therefore have not been considered.

CHAPTER 2.

COALESCENCE OF DISPERSIONS IN PACKED BEDS



## 2) COALESCENCE OF DISPERSIONS IN PACKED BEDS

The phase separation of immiscible liquids is a common chemical engineering problem. Examples occur in liquid-liquid extraction, direct contact heat transfer, de-salting and de-watering of crude oil, caustic washing of light distillates, the removal of water hazes from aviation fuels and the purification of effluent streams.

From some of the examples quoted, the need for separation is a by-product of increasing the efficiency of the overall industrial process. Frequently the phase separation operation is the rate-determining step, and thus is considerably studied. For instance, in liquid-liquid extraction, it is often desirable to generate a high interfacial area during contact of the phases to enhance mass transfer. This is achieved by dispersing one phase in the form of droplets. However, the resulting dispersion may be difficult to separate, and a problem of phase contamination exists.

Dispersions formed accidentally or by design consist of two types. The first is a primary dispersion or coarse emulsion and is characterized by droplets larger than  $100\mu\text{m}$  diameter. These drops will settle under the influence of gravitational forces to form a heterogeneous layer where eventually coalescence takes place. The other form of a dispersion is called a secondary or fine emulsion, and contains droplets less than  $100\mu\text{m}$  diameter. For small drops the gravitational forces are low, and settling rates of  $1\text{cm/day}$  are common. Similarly, the coalescence time associated with small drops is very high, and consequently the phase separation of a secondary dispersion may present a considerable problem.

Numerous mechanical and chemical methods<sup>(37)</sup> may be used to induce liquid dispersions to separate and coalesce. For



highly stable secondary emulsions, chemical techniques, such as the addition of electrolytes or de-emulsifying agents, are available to increase coalescence rates. The addition of finely divided solids or aeration techniques have been found to be successful in increasing settling rates. After enlargement of the dispersed phase droplets, recourse is made to mechanical techniques. The four main mechanical techniques are as follows:-

- (a) Induced coalescence on flow through packed beds;
- (b) Flow through selective membranes;
- (c) Simple gravity settlers;
- (d) Accelerated settling in centrifuges, hydrocyclones or electrical coalescers.

Although the criteria for selection is often governed by the throughput and economic specification, the design of mechanical coalescers is largely a matter of trial and error at the present time. This is particularly true of the packed bed coalescers considered in this research.

In packed beds, coalescence takes place within the packed section. The composition of the bed depends largely on the type of dispersion to be treated. Among the materials used are: fibrous beds consisting of cotton, glass-wool, metal and polymer strands; knitted mesh packings formed by interlocking loops of metals and polymeric material; particulate packings including ballotini beads, pebbles and gravel composites and the more conventional packings, such as ceramic Raschig Rings and Berl Saddles.

The literature on droplet behaviour and coalescence mechanisms within packed beds has been reviewed in order to assess the present knowledge of packing selection and design. The research



reported here is concerned with the fundamental analysis of droplet hydrodynamics of a primary dispersion within a bed of packed spheres. Thus, in the review, emphasis has been placed upon the more controlled investigations carried out under laboratory conditions.

## 2.1) Primary Dispersions

### 2.1.1) Conventional Packings - Raschig Rings and Berl Saddles

The most extensive study of droplet behaviour in packed columns is that of Pratt and others<sup>(38-43)</sup> who investigated coalescence within columns packed with Raschig Rings, in order to relate the droplet hydrodynamics to the interfacial area available for mass transfer. Consequently, their investigation was more concerned with defining the packing as a phase contacting-redispersing device for surface renewal of the dispersed phase. Nevertheless, the work was important in the analysis of droplet behaviour within a packing.

Pratt and Lewis<sup>(38)</sup> investigated droplet break-up and the coalescence of nine aqueous-organic systems in a 2" diameter column, packed with different sized Raschig Rings. For each liquid pair, it was found that there was a critical packing size, defined as :-

$$d_c = 2.42 \left( \frac{Y}{\Delta \rho g} \right)^{0.5} \quad (2.1)$$

The droplet behaviour within the packing depended upon whether the packing size was greater or smaller than the critical size,  $d_c$ . An analysis of photographed drops leaving the packing indicated that the exit drop diameter was independent of the inlet drop size, but dependent on the critical packing size. For packings larger than the critical packing size ( $d_c$ ) the exit drop was independent of the packing size and the flow rate until the onset of flooding. This was explained by the fact that the drop passed through the packing voids and broke down to an equilibrium size by impact with the packing element, whilst



small drops coalesced until the equilibrium size was attained. The exit drop diameter,  $d_{vs}$ , produced by passage of a range of aqueous-organic systems through six feet of packing with a diameter above the critical size, was correlated by :-

$$\left(\frac{\gamma \Delta \rho d_{vs}}{\mu_c}\right) = 1.62 \left(\frac{\Delta \rho \gamma^3}{\mu_{cg}}\right)^{0.475} \left(1 + 700 \left(\frac{u_c \mu_c}{\gamma}\right)\right) \quad (2.2)$$

In the case of packing smaller than  $d_c$  the entering drops were trapped in the interstices of the packing and coalescence occurred following impaction from behind by other drops. The mean exit diameter drop was found to be greater for packings  $< d_c$  than with packings  $> d_c$ , but no correlation was given. Such hydrodynamic behaviour was similar to that observed by Ballard and Piret<sup>(47)</sup>, but was contradictory to that reported by Morello and Beckmann<sup>(46)</sup>.

For packings equal to the critical size, the exit drop size was found to be strongly dependent upon flow rate. The overall process was similar to packings  $> d_c$  at low flow rates, but at high flow rates, a large outlet drop size was produced as in the manner for packings  $< d_c$ .

In a later investigation, Gayler and Pratt<sup>(39)</sup>, using the same equipment, attempted to relate more accurately the effects of phase flow rate and area for mass transfer upon the droplet size. From earlier work, they had derived a simplified dimensional analysis of the relationship between the physical properties and the equilibrium drop diameter, viz :-

$$\frac{d_{vs}^2 \Delta \rho g}{\gamma} = 1.25 \quad (2.3)$$

From consideration of this equation and collision theory, they concluded that the droplet diameter varied directly with the drop velocity relating to the packing, so that

$$d_{vs} = d_{vs}^o \left(\frac{\bar{V}_o}{\bar{V}}\right) \quad (2.4)$$



where  $\bar{V}$  is the mean velocity of the droplet in relationship to the stationary packing element and  $d_{VS}^0$  is the characteristic droplet diameter, i.e. the drop diameter at substantial zero flow rates. Since

$\bar{V} = V_d / \epsilon x$  then  $d_{VS}$  may be expressed as:-

$$d_{VS} = d_{VS}^0 \left( \frac{V_0 \epsilon x}{V_d} \right) \quad (2.5)$$

Hence, by expressing  $d_{VS}$  in terms of physical properties of the system, they found

$$d_{VS} = 0.92 \left( \frac{\gamma}{\Delta \rho g} \right)^{\frac{1}{2}} \left( \frac{V_0 \epsilon x}{V_d} \right) \quad (2.6)$$

The constant 0.92 was the best fit for their experimental data, and again the equation was applicable only for packing greater than the critical size  $d_c$ .

$V_0$  was defined as the droplet characteristic velocity, i.e. the mean velocity of the droplet in relation to the continuous phase at substantially zero rates. This was defined as

$$\frac{V_d}{x} + \frac{V_c}{1-x} = \epsilon V_0 (1-x) \quad (2.7)$$

$V_0$  could be found from experimental data by plotting  $V_d + \frac{xV_c}{1-x}$  against  $x(1-x)$  to give a straight line passing through the origin with a gradient of  $\epsilon V_0$ . These findings have been verified by Wicks<sup>(44)</sup>.

Thus, from a knowledge of  $V_0$ , the physical properties of the system, and the hydrodynamics, viz the hold-up and phase flow rates, the mean exit droplet diameter, could be predicted. Pratt<sup>(39)</sup> presented the prediction of  $V_0$  in the form of a graphical correlation, together with a monogram which relates  $V_0$  and the phase flow rates to the hold-up of the dispersed phase.

Further, from the relationship of the specific area for hold-up  $s = \left( \frac{6}{d_{VS}} \right)$  the superficial area was expressed as  $a = \left( \frac{6 \epsilon x}{d_p} \right)$ .

Thus, the interfacial area for mass transfer could be represented by :-

$$a = \left( \frac{6V_d}{0.92 (\gamma/\Delta\rho g)^{0.5} v_o} \right) \quad (2.8)$$

Hence, a rapid estimation of the interfacial area available for mass transfer could be made. No account was taken of the effect of mass transfer upon the interfacial area, shape, or behaviour of drops, but equation (2.8) was later verified experimentally by Paranik and Sharma<sup>(45)</sup>

Although Pratt et al correlated the equilibrium droplet size in terms of the properties of the extraction system, they did not report on the mechanism or rate of the break-down process. Ramshaw and Thornton<sup>(48)(49)</sup> considered this process first by studying the break-down of a single droplet on a baffle, and secondly by investigating the drop size distribution with respect to packing height. The break-down process was simulated in an impact cell in which single drops were allowed to collide with a laminar baffle. The subsequent break-down process was recorded by high speed cine photography.

From an energy balance, it was concluded that there was a critical drop size for any one system, below which droplets did not break-down on impact with the baffle. The critical drop size,  $d_{ec}$ , of a spherical drop, was represented by :-

$$1.79 (d_{ec} \Delta\rho g) + (d_{ec}^2 v_t^2 \rho_d) = 3.12 \gamma \quad (2.9)$$

and for the more representative case of a drop in the shape of an oblate spheroid,

$$\frac{\pi d_{ec} \gamma}{12} \left( d_{ec} \left( \frac{d_{ec} v_t^2 \rho_d}{\gamma} \right) + \left( \frac{d_{ec} \Delta\rho g}{\gamma} \right) \left( \frac{d_b + d_{ec}}{1.26} \right) - \frac{12}{\pi d_{ec}} \right) 1.26 d_{ec}^2 \left( \frac{\pi d_a^2 + d_b^2}{2} \frac{\ln \frac{1+e}{1-e}}{4e} \right) = 0$$

$$(2.10)$$



The equation was based on symmetrical collision producing two equal sized daughter droplets; however, asymmetrical collisions are equally probable, resulting in only a small portion of the original drop being sheared. This would produce a greater spread in the droplet size distribution.

Thornton observed that the experimental values of  $d_{ec}$  were generally higher than those predicted. This was attributed to the dissipation of energy in the form of frictional eddies within the droplet. However, further analysis was not presented, and Thornton concluded that a complex relationship existed between the observed  $d_{ec}$  and the baffle thickness. For this reason, it was difficult to predict break-down within a packed bed by the collision of a droplet with a packing element.

In the second part of their study, Thornton et al<sup>(49)</sup> examined the drop size distribution of a toluene water system in 18" packing sections of  $\frac{3}{4}$ " Raschig Rings in a column 6ft high and 3" diameter. The distribution became progressively skewed with the column height, and could be represented approximately by means of a log normal distribution function. A stable distribution was only reached after the droplets had passed through several feet of packing. Consequently, the Sauter mean diameter,  $d_{vs}$ , became progressively smaller with column height, and only approached equilibrium value towards the top of the packing. The change of  $d_{vs}$  with packing height could be represented by an exponential equation:

$$d_{vs} = d_{vs(eq.)} + 0.27 \exp(-0.0157 h) \quad (2.11)$$

To facilitate drop size analysis the packing was separated every 18" by a 4" observation cell. Thomas argued<sup>(50)</sup> subsequently that two 18" packed sections were not equivalent to

a continuous 36" section, since the droplets leaving each 18" section of packing were able to accelerate to a higher velocity than they could obtain in the voids of the packing. Consequently, break-down was greater, due to the higher impact velocity owing to acceleration between packing sections. Thornton also suggested that drops travelled at 80% of the terminal velocity within the packing. However, Thomas stated that calculation showed that 50% was a more realistic figure, although no data is available to substantiate this claim.

Thornton found that, for the range of system properties considered, there was a broad correlation between  $d_{VS}$  and  $d_{EC}$ . For the systems investigated, values of  $d_{VS}$  lay within 10% of the calculated values of  $d_{EC}$ , but Thornton stated that the exact form of the functional relationship required further study before  $d_{VS}$  could be predicted from first principles. The discrepancies between  $d_{VS}$  and  $d_{EC}$  were explained by the differences inherent in the break-down process of droplets with a laminar baffle and a packing element.

### 2.1.2) Volumetric Throughputs

Considerable work has been carried out concerning other important flow phenomena in packed extraction columns.

The most important of these has been the investigation into flooding, hold-up and pressure drop across packed beds. Gayler and Pratt<sup>(39)</sup> investigated the relationship between hold-up and the pressure drop,  $\Delta P$ , for counter current flow in columns packed with Raschig Rings. They obtained hold-up values by a displacement method where the flow was shut off with quick acting gate valves. Three distinct regions were identified. As flow rates were increased, the first region corresponded to a linear increase in hold-up. When the loading point was reached, an increased rate of hold-up occurred



and flooding was possible with systems of low density difference. However, for other systems, a third region was observed, where the hold-up remained constant for an increase in the dispersed phase velocity.

Flooding was defined as the limiting flow condition, and if this was exceeded, an accumulation of one phase took place. A knowledge of the limiting flow is essential for extraction column design, and numerous graphical correlations of flooding data have been published. The flooding condition was found to be a function of the particular liquid system and the packing under observation. Many investigations have been carried out, resulting in empirical and semi-empirical correlations of the data. Most of these correlations are presented in the form of graphs with coordinates of complex functions of liquid properties and phase flow rates ( $V_c$  and  $V_d$ ). A statistical study by Chin<sup>(51)</sup> compared all available data with several correlations, and led to the conclusion that the correlation of Crawford and Wilke<sup>(52)</sup> was the most suitable for use.

Crawford and Wilke presented their work in two parts, for:-

$$\left( \frac{V_{cf}^{\frac{1}{2}} + V_{df}^{\frac{1}{2}}}{a \mu_c} \right) \rho_c > 50 \quad (2.12)$$

Flooding occurred when: (2.13)

$$\left( V_{cf}^{\frac{1}{2}} + V_{df}^{\frac{1}{2}} \right)^2 = \left( \frac{694 \Delta \rho \epsilon^{1.5}}{\rho_c^{0.8} a^{0.5} \gamma^{0.2}} \right)$$

and for values of (2.12)  $< 50$ , flooding occurs when:

$$\left( V_{cf}^{\frac{1}{2}} + V_{df}^{\frac{1}{2}} \right)^2 = \left( \frac{79.7 \Delta \rho^{1.33} \epsilon^2}{\rho_c^{0.73} a \mu_c^{0.33} \gamma^{0.27}} \right) \quad (2.14)$$

The above correlations of Crawford and Wilke were found to be easier to use than the correlations of Hoffing and Lockhart<sup>(53)</sup> which Chin concluded were best compared to all available data.



## 2.2) Knitted Mesh Packings

The literature reviewed on packed columns has often been quoted out of context. The criteria of investigation was that of a breakdown-coalescence process to define the interfacial area for mass transfer. Consequently, the results of packed beds have been interpreted with the emphasis of a phase contacting device and not as a coalescing aid.

The current economic climate has now resulted in the single process of liquid-liquid extraction in packed towers being subdivided. In many cases, it is now thought more advisable to have a separate phase contacting device to enhance mass transfer which is then followed by phase separation with a coalescing aid. A typical example of this is a mixer settler device, such as the Scheibel column. Basically, a Scheibel column is a series of mixer settler units, in which the packed sections, under certain conditions, coalesce the dispersion formed by the turbines. Often knitted mesh packings are used not to coalesce the dispersion, but to isolate the mixing sections and prevent back-mixing within the column<sup>(61)</sup>. The hydrodynamic behaviour of droplets in knitted mesh sections in Scheibel columns has been studied by several workers<sup>(58-60)</sup>. The emphasis of the research has been placed more on the coalescence process, as this is the primary function of the packings.

Honeykamp and Burkart<sup>(58)</sup>, found that the mean exit drop size was dependent upon packing height, but independent of the inlet drop size and the dispersed or continuous phase flow rate. They also suggested that the droplet flow characteristics were similar to those in conventional packings greater than the critical size. Work by Piper<sup>(60)</sup> and, later, Slatter<sup>(59)</sup> found that the limiting flow was dependent on the inlet drop size. Both workers used knitted mesh



packings of known voidage in the range of 97.5 - 98.75%, and found that the limiting flow rate increased as the voidage increased.

One difficulty experienced by Piper was defining the onset of flooding - consequently his analysis of the factors affecting flooding were limited. Nevertheless, Thomas<sup>(50)</sup> suggested that Piper's results indicated that a general flooding correlation similar to that of Crawford and Wilke<sup>(52)</sup> was possible.

### 2. 2. 1.) Wetted Packings

The investigations so far reviewed were concerned with packings wet by the continuous phase. Some qualitative observations have been made regarding general flow phenomena in packed columns wet by the dispersed phase. However, the work by Jeffreys and Davies<sup>(62)</sup> was the first to analyze the importance of solid surface energy in relation to its effect on coalescence. The technique used in their work was to vary the concentration of Acetone in a Toluene-Acetone-Water system to produce a change in the interfacial tension values. Thus they illustrated the effect of disperse phase wetting and non-wetting conditions on the resulting drop diameter formed at an orifice. They stated that for primary dispersions, two basic mechanisms of coalescence took place within the packing. In the first case, drops formed a film on the packing and subsequent coalescence into this film took place by a drop-interface mechanism. The film eventually drained through the bed when the buoyancy forces were greater than the solid-liquid adhesion forces. The exit drops thus formed left by a drip point mechanism. The condition of a packing wet by the dispersed phase was characterized by a contact angle  $< 90^{\circ}$ .

Alternatively, the dispersed phase did not wet the packing and drop-drop coalescence occurred between moving drops and the



drops held up in the interstices of the packing. The non-wetting situation can be characterized by a contact angle  $>90^\circ$ . Thus they concluded that the surface properties of the solid in relation to the liquid-liquid system determined the mechanism of coalescence. This factor is of great importance in the selection of column packings if there is a composition change across the column. If the concentration effects ranged from non-wetting to wetting conditions, then careful design specification was required to achieve maximum efficiency.

To illustrate this fact, they investigated the size of drop leaving a perforated plate under various conditions. They found that for non-wetting conditions, if the ratio of nozzle to drop diameter  $d_n/d_{vs}$  was  $< 0.4$ , the drop did not pass through the perforation. However, if the ratio was  $0.4 < \frac{d_n}{d_{vs}} < 0.8$  the drops could deform and pass through the hole. From a force balance, they suggested the relationship:

$$V = \pi d_n \left( \frac{\gamma}{\Delta \rho g} \right) \quad (2.15)$$

However, if the plate was wet by the dispersed phase, a ten fold increase in exit drop diameter was observed. This fact could explain the many instances of phase reversal reported within packings wet by the dispersed phase.

Two important observations reported in their work were the importance of surface volume ratio for the non-wetted situation, and that no inter-droplet coalescence took place between two freely moving drops. Thus, for coalescence to take place, the drop must, in a non-wetted packing, be held up in the interstices against the hydrodynamic forces long enough for adjacent drops to collide and coalesce. This form of droplet behaviour has also been observed by Honeykamp and Burkart<sup>(58)</sup>.



The introduction of the interaction of the physical properties of the liquids with the solid surface energetics and the packing geometry with the subsequent droplet hydrodynamics, represented a considerable step forward in understanding the fundamental behaviour in a packed bed. It is now generally considered that a packing wet by the dispersed phase enhances coalescence. This is normally preferred, but the adhesion forces holding the dispersed phase to the packing can, in some cases, increase the hold-up and pressure drop. Consequently, the maximum throughput before flooding occurred could be lower for a wetted packing than for a non-wetted packing.

One particular problem at high hold-up values was that, above a certain fraction of dispersed phase volume, phase inversion was likely to occur, that is the continuous phase now became the dispersed phase. This has been reported, not only in packings, but in many phase contacting devices. This is particularly so in the Scheibel column<sup>(61)</sup>, and it has been suggested that the overall efficiency could be increased if the packing element were removed. For most systems, there is a range of phase ratios - the ambivalence range<sup>(63-65)</sup> where it is possible to disperse either phase. Thus the packing must be specified for the particular phase to be dispersed.

#### 2.2.2) Composite Packings

Work on dispersed phase bands in vertical settlers<sup>(66)</sup> led to an interesting observation regarding the coalescence effects at the boundary of a high and low energy surface. Ali,<sup>(66)</sup> using a 2" diameter column in which part of the surface had been treated with dichloro-dimethyl silane to render it hydrophobic, observed high rates of coalescence at the surface energy boundary. This observation led to the development of knitted mesh packings consisting of high and low energy filaments crimped together. Davies, Jeffreys

and Price-Bailey<sup>(72)</sup> found that a composite packing could separate both an oil in water and a water in oil dispersion. In this sense, the packing was universal<sup>(67,72)</sup> and was independent of the phase dispersed. In the table presented below, it is shown that, not only was the flooding rate much higher irrespective of which phase was dispersed, but the HETP (Height Equivalent of a Theoretical Plate) was 30% - 40% lower than with a single energy packing.

<u>PACKING</u>	<u>DISPERSED PHASE</u>	<u>FLOODING RATE</u> (ml/cm <sup>2</sup> sec)
Stainless Steel	Kerosene	0.069
	Water	0.993
Polypropylene	Kerosene	1.117
	Water	0.0475
Composite Packing Stainless Steel & Polypropylene	Kerosene	1.45
	Water	1.45

<u>PACKING</u>	<u>SYSTEM</u>	<u>H.E.T.P.</u>
Stainless Steel & Polypropylene	H <sub>2</sub> O - Ethanol	4 - 5 ins
Stainless Steel	H <sub>2</sub> O - Ethanol	9 - 15 ins

Further work<sup>(68)</sup> on the different ratios of high energy to low energy fibres showed that if the ratio exceeded 3.1 or 1.3, the efficiency of the process decreased for one of the phases dispersed.

Data on the flooding rate and the inherent pressure drop was presented which showed that the onset of flooding varied with packing height. It also indicated that the flooding velocity and the pressure drop was weakly dependent on the inlet drop. This effect was particularly pronounced at low bed heights.

The flooding velocity was also shown to be a function



of the phase viscosity ratio outside the limits 5:1 to 1:5. Using a 70% di-Butyl phthalate, 30% kerosene-water system, where the phase viscosity ratio was 10.75:1, the flooding velocity for the organic phase was  $15\text{m}^3/\text{m}^2\text{h}$ , and for the aqueous phase  $48\text{m}^3/\text{m}^2\text{h}$ .

No data was presented on exit drop size distributions and no analysis was carried out on the fundamental droplet hydrodynamics within composite packings. Thus, whilst the work presented was of considerable importance for industrial usage of a coalescing aid, it did little to aid the understanding of a general design equation.

### 2.2.3) Non-Wetted Packings

Considerable work into knitted mesh packing has been carried out to determine the mechanisms of coalescence taking place within the packing. The primary objective was to relate the exit drop size to the system hydrodynamics.

Thomas<sup>(50)</sup> investigated the change in mean drop size due to passage through a packed section of knitmesh. The investigation covered packings which were wet by either the dispersed phase or the continuous phase. For non-wetted packings with large inlet drops, behaviour was analogous to the break-down coalescence mode proposed by Thornton<sup>(48)</sup>. However, the equilibrium drop size was achieved much more rapidly for knitted mesh packings - 8" as opposed to - 6" for Raschig Rings.

Thomas investigated the breakdown process of drops on both wetted and non-wetted fibres. He found that for non-wetted fibres, the drops could be broken in two, whereas no breakdown was achieved with wetted fibres. Thus, Thomas concluded that drop-fibre collision in a high voidage, non-wetted, knitted mesh packing would closely resemble the ideal behaviour proposed by Thornton, whereas,



for wetted packings, coalescence predominates. The equilibrium drop size could be correlated by the following equation:-

$$\left( \frac{\Delta p d_{vs}^0 \gamma}{\mu_c^2} \right) = 2.44 \left( \frac{\Delta p \gamma^3}{\mu_c^4 g} \right)^{0.523} \quad (2.15)$$

This equation was similar to that proposed by Pratt<sup>(38)</sup> for Raschig Rings, and thus combining equation 2.15 with 2.6, the following relationship is found:-

$$\frac{d_{vs}^0 \text{ (knitmesh)}}{d_{vs}^0 \text{ (Raschig Rings)}} = 2.65 \quad (2.16)$$

In a similar investigation covering non-wetted packings<sup>(50)</sup> the following correlation was obtained:-

$$\left( \frac{d_{vs}^0 \Delta p \gamma}{\mu_c^2} \right) = 0.917 \left( \frac{\Delta p \gamma^3}{\mu_c^4 g} \right)^{0.503} \quad (2.17)$$

Thus, on simplification and comparison with equation(2.15), the following relationship is found:-

$$\frac{d_{vs}^0 \text{ (wetted knitmesh)}}{d_{vs}^0 \text{ (non-wetted knitmesh)}} = 2.65 \quad (2.18)$$

Equations 2.18 and 2.16 demonstrate the improved coalescence of knitted mesh packings wet by the dispersed phase, as opposed to non-wetted knitted mesh and Raschig Rings. From equations 2.16 and 2.18, it would appear that non-wetted knitted mesh packings and Raschig Rings can be described by similar equations. However, Thomas did not elaborate on this comparison.

Exit drop detachment has generally been observed to occur at some transition point between a drip point and jetting mechanism. Often, with very high void beds and high flow rates, jetting occurs and drop formation is due to interfacial instabilities imposed on the jet. This mode of drop formation may, however, lead to the formation of secondary drops. It has been suggested that exit drop formation is



dependent on a mean exit hydraulic radius,<sup>(50)</sup> but no quantitative analysis has been presented in the literature.

The fundamental analysis of coalescence in all packings has been hindered in that the packing geometry has been difficult to define. Voidage values and surface to volume ratios are often quoted but serve little purpose other than as a reference for the packing used. Inspection of these values in a real physical situation, especially in small diameter columns, illustrates how the wall effects can lead to large variations of local voidages. Thus it can be postulated that droplet hydrodynamics and coalescence near the periphery may be largely dependent on the high voidage values and also to some extent on the material of the column wall. Little attention has been paid to the low voidage beds with a packing less than the critical packing size. Thus the mechanism of drop-drop coalescence within the interstices has not been treated quantitatively. Likewise, the quantitative analysis of surface energetics has not been related to the system hydrodynamics except in the extremes of wetting and non-wetting conditions. Thus the design of a packed bed as a coalescing aid is still very much a matter of trial and error. However, the theory of coalescence of secondary dispersions has received considerably more attention. Consequently, a review is presented to illustrate the approach to the fundamental analysis and the different criteria for design of a coalescing aid.

### 2.3) SECONDARY DISPERSIONS

A secondary dispersion is often referred to as a "stable emulsion". This term loosely refers to the fact that if the dispersion were allowed to stand for an indefinite period of time, separation would not take place. However, this depends largely upon



the drop size and its density difference from the continuous phase. Whilst there is some disagreement as to the size range of secondary dispersions, this report refers to drop diameters in the range of 100 microns to the submicron level.

Secondary dispersions or emulsions have been described in various ways with respect to stability, drop size distribution, volume fraction of the dispersed phase and as to which phase is dispersed. Both oil in water and water in oil dispersions are common, and both present a considerable problem in separation. Separation of oil in water dispersions has, in the past, received scant attention, owing to the inherently low volume percentage of dispersed phase, and its economic insignificance. However, recent legislation on effluent stream discharge and increased knowledge of ecological damage attributable to pollution has led to an upsurge in industrial applications. On the other hand, water in oil dispersions have necessitated some industrial treatment because it was generally found that malfunction of the down-stream process would occur if separation were not carried out.

A variety of industrial processes may be used to separate secondary dispersions<sup>(37)(187)</sup>. These include alternating electric fields, magnetic fields, centrifugation, addition of chemical coagulants and flow through close packed beds. Some of these applications have had limited success, but often they are too specialized or too expensive when applied to general industrial use. Increased attention has been paid to the most simple form of coalescing aid - viz - flow through packed beds. This type of coalescer can be divided into three categories:-

- (a) Porous media (including porous rock, sponge etc);
- (b) Fibrous beds (including cotton, glass fibre, polymeric and metal threads;
- (c) Particulate packings (pebbles, gravel, polystyrene cubes etc.).



### 2.3.1) Flow through porous media

A wide range of natural and technological processes involve the capillary action associated with flow of immiscible liquids within the interstices of porous solids. The principles of capillary action are well documented<sup>(73,74)</sup> but their application to practical problems is often limited by the complicated geometry associated with porous solids. The difficulties are compounded when there is uncertainty as to the surface energetics or the wettability of the solid. However, the theory has received much attention<sup>(69)</sup> and is extensively applied in water filtration, soil science, and petroleum reservoir engineering. The theory is generally concerned with the displacement of one liquid by a second immiscible phase, both phases being in a continuous form. Nevertheless, this theory was used for the basis of a model to predict coalescence of a secondary dispersion in a fibrous bed.<sup>(79)</sup>

### 2.3.2) Coalescence in fibrous beds

Fibrous beds have been extensively used to coalesce secondary dispersions, and as such have been the subject of many studies.<sup>(70,81,82)</sup>

Several prerequisites have been proposed for successful operation. It is generally accepted that the bed should have a high voidage consistent with a close packing arrangement, combined with a high surface area to volume ratio. It has been found that coalescence increases with bed height, but an optimum exists between bed height and the pressure drop across the packing. To explain this, Sareen<sup>(71)</sup> et al reported that at high pressure drops, channels were formed within the bed which caused the coalesced drops to redisperse.

The effect of fibre wettability has been the subject of some controversy. Jeffreys and Davies<sup>(62)</sup> stated that successful



operation was independent of the wetting properties of the fibre. This was based on an equilibrium drop size as defined by Padday<sup>(76)</sup>, which was considerably larger than those found in secondary dispersions. Hazlett<sup>(77)</sup>, who agreed with the theoretical considerations of fibre wettability, proposed that wetting was important at the drop release point. Hazlett also suggested that the coalescence ratio should be different dependent upon which phase is dispersed.

Fibre roughness and fibre diameter are considered to be important factors affecting the coalescence efficiency.<sup>(70)</sup> Coalescence rates have been found to increase with decreasing fibre diameter, and increasing surface roughness. In this respect, cotton fibres have been very successful in coalescing secondary dispersions, but suffer from compression, and hence voidage reduction, at high flow rates. Composite beds of cotton and teflon fibres have been used to overcome this problem.<sup>(71)</sup>

For a given packing there is an optimum flow rate, above which the efficiency of separation decreases. This is due to the local shear forces within the bed being greater than the drop-fibre adhesion forces. However, the hypothesis is based upon the mechanism of drop attachment to the fibre, and to the subsequent drop collision and coalescence process.

Observation of the coalescence mechanisms within a fibrous bed is difficult, and consequently the process has not yet been clearly identified. Several coalescence mechanisms have been proposed and these are summarized below.

#### Pore Catchment or Direct Interception - Fig. 2.3.2. I

Drops larger than the pore diameter are held up and coalescence takes place by impaction of following drops. Hazlett<sup>(77)</sup>



Fig. 2.3.2

MECHANISMS OF COALESCENCE OF A SECONDARY DISPERSION

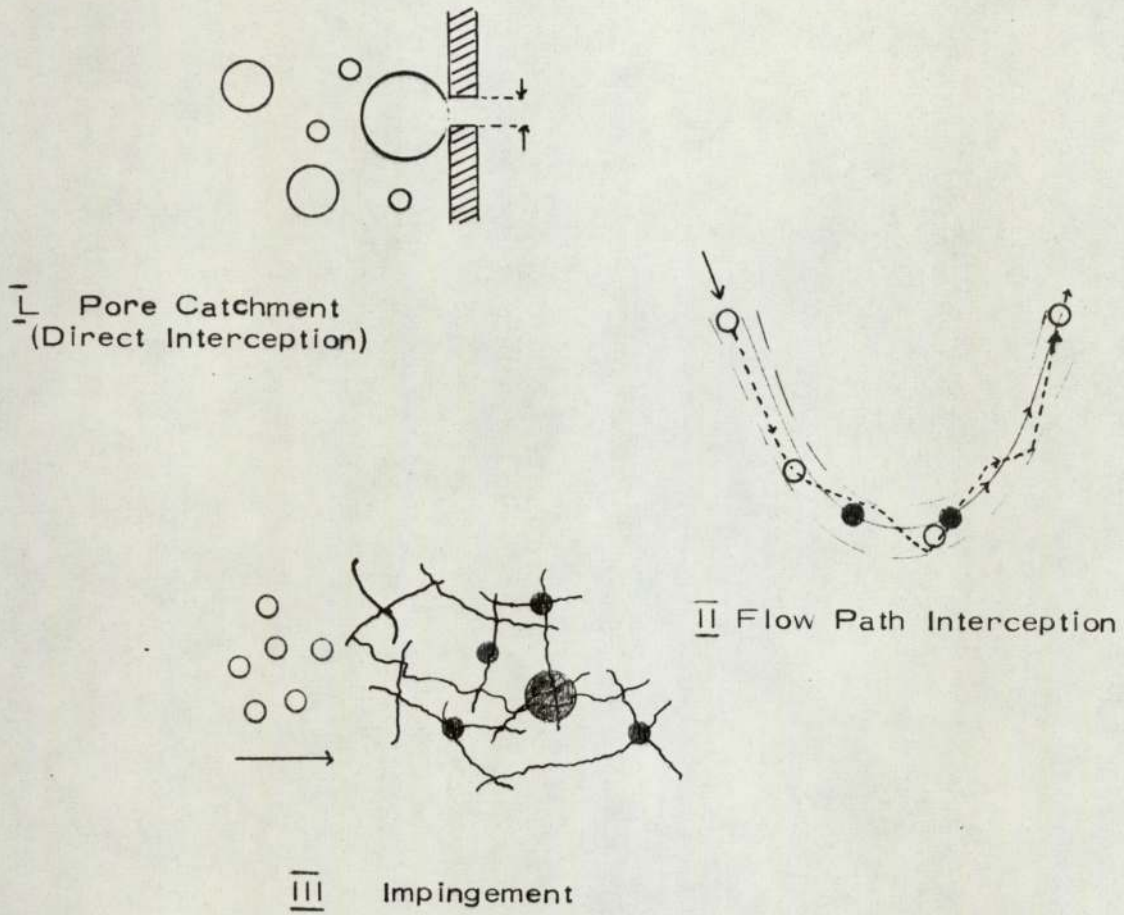
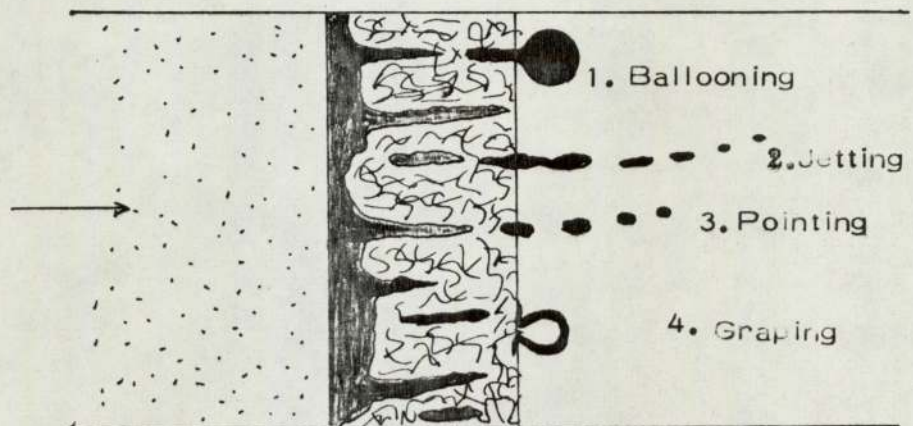


Fig. 2.3.3 Types of Droplet Release Mechanisms



suggested that this mechanism was similar to that in aerosol filtration but Sherony and Kintner<sup>(80)</sup> have argued that this is not applicable to fibrous beds, owing to the wide range of flow velocities.

Interdrop or Path Flow Interception - Fig 2.3.2 II

Bartle<sup>(83)</sup> suggested that repeated drop-fibre collision promoted coalescence of freely moving drops. However, on the basis of photomicrographic studies, Sareen<sup>(71)</sup> et al suggested that very little coalescence took place owing to this mechanism.

Impingement - Fig. 2.3.2 III

Droplets collide with the fibres and attach themselves to fibres irrespective of the surface energy of the fibre. These drops then move in the direction of the overall pressure gradient, to coalesce with other drops at fibre interstices.

Sareen<sup>(71)</sup> et al have proposed other coalescence mechanisms for droplets in the submicron range, which include the effect of Brownian motion and electrostatic effects.

Similarly, there are numerous descriptions of the mechanism of droplet release. Hazlett and Corhart<sup>(78)</sup>, who studied a water-oil system, suggested the modes of drop release shown in Fig. 2.3.3

- (1) Ballooning: the coalesced liquid drains through the bed and drop release is achieved when the buoyancy force and shear forces exceed the adhesion forces;
- (2) Jetting: rivulets flow through the bed, possibly via a high voidage channel, and leave the bed as a jet. Drops are then formed due to jet break-up by Rayleigh instabilities.
- (3) Pointing: fingers of coalesced liquid protrude from the packing and break into small drops, possibly due to local turbulence. This type of drop formation is believed to be a modification of jetting;



- (4) Grapping: the dispersed phase wets the area at a release site, causing the continuous phase flow to form a bubble. The bubble subsequently breaks away with the continuous phase entrapped in a film of dispersed phase.

The above mechanisms of drop release were observed for a water-oil system, but the same mechanisms are likely to occur for oil in water dispersions.

#### Theoretical Models for fibrous bed coalescers

Several theoretical models have been proposed to describe coalescence within a fibrous bed, but no generally accepted theory exists. Spielman and Goren<sup>(79)</sup> based their model upon globules held within the packing and drop capture by Van der Waals forces. Information from flow through porous media and assumptions based on experimental observations led to an empirical expression for the filter coefficient, (or deposition coefficient):

$$\lambda = (0.29 d_p^2 / d_f^3) (A d_f^2 / \rho_c U d_p^4)^{0.25} \quad (2.19)$$

They considered two phase flow through a porous media, and evaluated the permeability from consideration of the local geometric microstructure of a liquid-liquid configuration. However, no consideration was taken for the effect of the dispersed phase, which was assumed to exist as discrete spherical globules of uniform radius which in turn were related to the fibre diameter.

The second model developed by Sherony and Kintner<sup>(80)(81)</sup> was based upon the kinetic theory of gases, classical aerosol science and filtration theory. They assumed that the flow of the emulsion through the bed did not form a continuum. A method described by Hubburst and Katz<sup>(88)</sup> was used to solve the conservation of species



equation, leading to an expression for the filter coefficient:-

$$\lambda = 3S(1 - \epsilon)(1 + d_p/d_b) \mu_c/4 (1 - S) d_f \quad (2.20)$$

The most recent model is that of Rosenfeld and Wasan<sup>(82)</sup> who critically examined Spielman's and Sherony's model and discussed the shortcomings of several assumptions made by these workers. Rosenfeld and Wasan based their model on drops approaching the fibre by the mechanism of interception and being held until the drop produced by coalescence was sufficiently large to overcome the fibre attachment forces. The filter coefficient derived was as follows:-

$$\lambda = (8\beta(1 - \epsilon)d_p/\pi^2\epsilon(1 - S_m)d_f^2)(2d_{fe} + d_p)(d_{fe} + d_p) \quad (2.21)$$

where  $\beta$  was the fraction of collisions leading to coalescence and the average saturation was defined as :-

$$S = C(1 - \epsilon)V^{-n}/\epsilon \quad (2.22)$$

They also developed an empirical equation for the situation at high velocities, and found that both equations described the data of Spielman et al and Sherony et al.

### 2.3.3) Flow through particulate beds

Packed beds of pebbles, quartz, gravel and polymeric material such as polythene chips, have been used to coalesce secondary dispersions. In an initial investigation, Shackleton<sup>(84)</sup> et al found that the pumps used to feed the dispersed phase to the packed bed were of prime importance to the inlet size distribution. Douglas and Elliot<sup>(85)</sup> and later Farley and Valentine<sup>(86)</sup> both reported that particulate beds gave acceptably good performance as regards coalescing oil in water dispersions. However, the above investigations were mainly concerned with industrial usage and very little quantitative analysis was reported. Smith<sup>(87)</sup> recently has reviewed the work in this area, and the reader is referred to his work for further reference.



CHAPTER 3.

DROP FORMATION

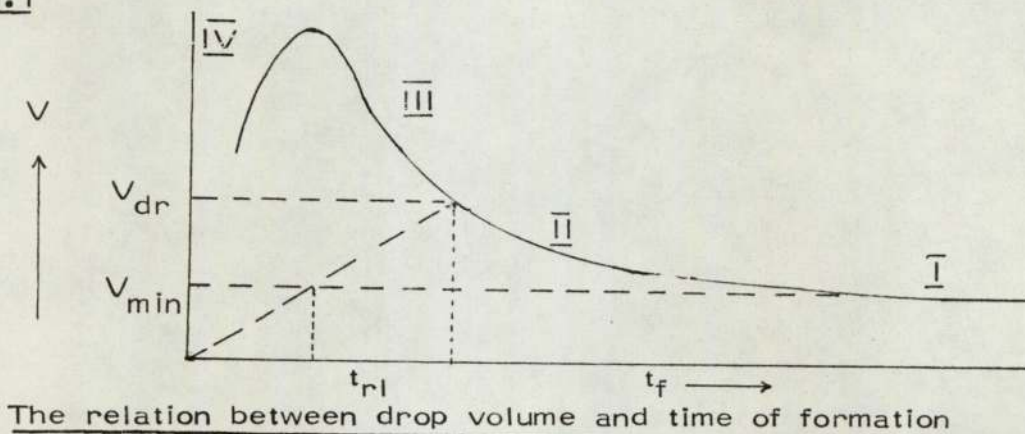
### 3) THE MECHANISMS & PREDICTION OF DROP FORMATION

In the review of secondary dispersions, it has been reported that Hazlett and Cohart<sup>(78)</sup> identified four different modes of droplet release from the bed. Similarly, for primary dispersions, Davies<sup>(67)</sup> and Thomas<sup>(50)</sup> both reported exit drop formation from jet break-up when operating knitted mesh packings at high dispersed phase flow rates. However, the mechanisms which control drop formation at the packing exit were not treated analytically. Thomas suggested that a definition of the mean exit hydraulic radius was necessary before further analysis could be undertaken. This presented a considerable difficulty as the packings used by previous workers were not amenable to geometric description. In this study, efforts have been made to evaluate the geometric properties of the packing, and to relate these properties to coalescence and exit drop mechanisms. Thus it was considered of particular importance to review the literature on the formation of drops at standardized nozzles.

The volume  $V$  of a drop released from a nozzle may be presented as a function of the time of formation  $t_f$ <sup>(93)</sup> in the form shown in Fig. 3.1.

In the Region  $\bar{I}$  the drop volume  $V$  is independent of the time of formation, and is often termed "static drop formation".

Fig. 3.1





Region  $\bar{\text{II}}$  has been the subject of extensive studies and many correlations have been proposed. Very little data has been presented for Region  $\bar{\text{III}}$ , which represents the transition from drop growth to jet break-up. In Region  $\bar{\text{IV}}$ , jetting is fully developed, and drop formation takes place by surface instabilities in the jet.

### 3.1) Region $\bar{\text{I}}$ : Drop Formation at Low Velocity

The first attempt to explain quantitatively the phenomena of "static" drop formation from circular nozzles was made by Tate<sup>(91)</sup>. This work was later expanded by Bashforth & Adams<sup>(13)</sup> in their evaluation of pendant drop profiles to predict surface tension values.

Harkins and Brown<sup>(94)</sup> derived an expression for calculating the drop volume at low injection velocities, by equating buoyancy and Interfacial forces. They introduced a correction factor 'F' to allow for the fraction of the pendant drop remaining at the nozzle when the drop detaches. This equation was as follows:

$$V_f = \left( \frac{\pi d_n Y}{\Delta \rho g} \right) F \quad (3.1)$$

where 'F' was a function of the ratio:

$$\phi / 2 (Y/\Delta \rho g)^{0.5} \quad (3.2)$$

### 3.2) Region $\bar{\text{II}}$ : Drop Formation below jetting

Treybal and Hayworth<sup>(95)</sup> were the first authors to give a theoretical prediction for drop volume in Region  $\bar{\text{II}}$ . They assumed that the buoyancy forces equalled the interfacial forces, and that the velocity within the drop was greater than that of the dispersed phase into the nozzle. They proposed the correlation:-

$$V_f + 4.11 \times 10^{-4} V_f \left( \frac{\rho_d U_n^2}{\Delta \rho} \right) = 21 \times 10^4 \left( \frac{Y_{d_n}}{\Delta \rho} \right) + 1.069 \times 10^{-2} \left( \frac{d_n^{0.767} U_n^{0.305} \mu_c^{0.185}}{\Delta \rho} \right)^{\frac{3}{2}} \quad (3.3)$$



This correlation was presented in a simplified form as a graphical solution from which it was possible to determine the drop diameter without resorting to the trial and error procedure. One major criticism of this work was the use of surfactants to evaluate the effects of surface tension, since Meister and Scheele<sup>(96)</sup> stated that for a given surfactant concentration the interfacial tension increases with increasing velocity through the nozzle as a result of the slow diffusion of surfactant to the interface. This caused a much greater increase in drop volume with increasing nozzle velocity than was observed with pure systems.

A different approach to describe drop formation was used by Null and Johnson<sup>(97)</sup>. From observations using a stroboscope, they presented their results in the form of a correlation which included Frode, Laplace and Weber numbers. They also concluded that there were two stages in the drop formation and their final graphical correlation was given in terms of two groups, viz

$$\left( \frac{d_n^2 \Delta \rho}{8\gamma} \right)^{0.5} \quad \text{and} \quad \left( \frac{8\mu_c \rho_d}{d_n g \Delta \rho} \right)^{0.5} \quad (3.4)$$

Roa et al<sup>(98)</sup> also based their correlation on a two stage process. In the first stage the drop is assumed to expand until the buoyancy forces balance the interfacial forces. The volume at this stage is given by: -

$$V_{sf} = \left( \frac{2 \pi d_n \gamma F(d_n / V_f^{1/3})}{(\rho_c - \rho_d)g} \right) \quad (3.5)$$

When the static stage is passed, the drop starts to ascend with a varying velocity, but still maintains its connection with the nozzle through a thread of liquid and continues to grow. Two models were proposed, the first was applicable to low viscosity liquids and the second to very viscous liquids. These were respectively: -

$$(a) \quad V_f = \frac{C}{A} + B \left( \frac{t}{A} - \frac{1}{A^2} \right) + \left( \frac{B}{A^2} - \frac{C}{A} \right) C \exp(-At) \quad (3.6)$$



$$\text{where } A = \frac{6\pi r\mu}{m} \quad B = \frac{Q(\rho_c - \rho_d)g}{m} \quad C = \frac{Q\mu_c \rho_d}{m}$$

$$(b) \quad A d_s = \frac{Bt^2}{2} \quad \text{where } t = \frac{2A d_s}{B} \quad (3.7)$$

The first model included a correction factor suggested by Davidson and Schuler<sup>(99)</sup> to account for the inertia of the continuous phase. They assumed the flow around the drop was irrotational and inseparable. The model of Roa<sup>(98)</sup> et al was modified by Kalyanasundaren<sup>(100)</sup> who included an extra resisting force, due to the tensile viscosity of the dispersed phase. This was particularly applicable when the influence of the dispersed phase viscosity was appreciable owing to high flow rate during drop formation. However, Roa used surfactants in his experimental work, and the comments of Meister and Scheele must be borne in mind when using this model.

At the present time, the most widely accepted correlation for predicting drop volumes at low flow rates is that of Meister and Scheele<sup>(96)</sup>. Their analysis is based on a two stage drop formation process, and it is claimed that drop volumes can be predicted with an error of the order of 11%. The model included four major forces acting on the drop during formation. The buoyancy forces and the kinetic forces associated with fluid flowing from the nozzle act to separate the droplet whilst interfacial forces at the nozzle tip and drag forces act to restrain the drop. Also included in their model was the analysis of additional flow into the drop during detachment. They also presented a plot of the Harkins Brown Factor  $|F|$  versus  $d_n \left(\frac{F}{V_d}\right)$  for use with their correlation:

$$V_f = F \left( \frac{\pi Y d_n}{g \Delta \rho} + 20 \frac{\mu_c Q d_n}{d_f g \Delta \rho} - \frac{4 \rho_d Q U_n}{3 g \Delta \rho} + 4.5 \left( \frac{Q^2 d_n^2 \rho_d Y}{(g \Delta \rho)^2} \right)^{\frac{1}{3}} \right) \quad (3.8)$$



Recently Heertjes de Nie and de Vries<sup>(101)</sup> developed a two stage drop formation model similar to that of Meister and Scheele. However, the second stage of drop release is dealt with much more vigorously. Models were developed for; forces acting on the drop; the way the dispersed phase enters the drop; the necking of the drop as a function of time; the velocity of the rise of the neck. An experimental relation was obtained for the leading edge velocity by analysis of high speed cine film. These workers also introduced an experimental correlation factor in order to fit the model to their data. Application of these models is difficult because of the changes in derived expressions with regard to different systems.

The preceding correlations are based to some extent on empiricisms and some recent authors feel that there is little justification for the complexity of models under these conditions.

de Chazel and Ryan<sup>(102)</sup> considered a simplified momentum balance combined with flow into the drop during necking, and presented the following equation:

$$V_f = \left( \frac{2\pi r_v \gamma}{g\Delta\rho} \right) F + 1.648 \left( \frac{g\Delta\rho r_v U V_d}{\gamma U t} \right) - 0.857 \left( \frac{\rho_d r_v U^2}{\gamma} \right) \quad (3.9)$$

Narayaman Baso and Roy<sup>(105)</sup> presented a complete empirical relationship based on the analysis of previous models. Using a dimensional analysis they obtained the following expression:-

$$\frac{d_d}{d_n} = a_1 \left( \frac{\Delta\rho}{\rho} \right)^{a_2} (Re)^{a_3} (We)^{a_4} (Fr)^{a_5} \quad (3.11)$$

where the constants were evaluated by fitting experimental data to the expression. Grignon<sup>(103)</sup> et al used a similar approach, and derived a correlation based on a polynomial of the Weber number.



In a recent paper, Izard<sup>(104)</sup> described a method based on the calculation of the shape of the drop formed at the nozzle tip by means of a pressure balance over the drop interface. The equation considered the vertical forces acting on the drop during formation at a horizontal section. A similar approach was used by Halligan and Buchard<sup>(106)</sup> to obtain the profile of a drop on an orifice plate. The latter, however, assumed that flow through the orifice into the drop impinged on the under side of the interface at the top of the drop surface before being deflected round the drop interface. Consequently, this model results in an abnormally high predicted pressure at the point of impingement when compared to the rest of the surface. Izard assumed that the entering dispersed phase circulates and therefore increases the outward pressure on the interface evenly throughout. The major drawback with the work of Izard is that a complicated reiteration procedure is required and that the drop profile needs to be known before calculation can commence.

Whereas considerable work has been carried out to predict the volume of a drop produced at low injection velocities from non-wetted nozzles, very little data has been presented for nozzles or orifices wet by the dispersed phase. Haynes<sup>(118)</sup> et al and later Jeffreys<sup>(62)</sup> et al both reported a tenfold increase in drop size using a wetted orifice plate, but no quantitative analysis was presented. Similarly, little information exists as to the effect of the geometry of the orifice on the drop formation mechanisms.

### 3.3) Predicting Jetting Velocities : $U_j$

Above certain dispersed phase velocities through the nozzle, the mechanism of drop formation changes. A jet of liquid is formed which breaks into drops by the amplification of disturbances which result from surface tension instabilities. The sizes of the drops



formed from the jet vary considerably from those of drops formed at subjetting velocities.

Several correlations can be found in the literature to evaluate the jetting velocity. Hayworth and Treybal<sup>(95)</sup> proposed a figure of 10cms/sec as an approximate guide, whereas Ryan<sup>(107)</sup> predicted the onset of jetting by the following correlation:

$$\left(\frac{\rho_d}{\Delta\rho}\right) \left(\frac{2U_j}{d_n g}\right)^{0.5} = 1.64 \left(\frac{\gamma}{\Delta\rho g d_n^2}\right)^{0.95} \quad (3.12)$$

Scheele<sup>(109)</sup> and Meister studied two kinds of jet formation theoretically, and presented the following correlation:

$$U_j = 2.0 \left[ \left(\frac{\gamma}{\rho_d d_n}\right) \left(1 - \frac{d_n}{d_f}\right) \right]^{\frac{1}{2}} \quad (3.13)$$

Heertjes de Née and de Vries<sup>(101)</sup> emphasised the difficulty in observing the transition stage between normal drop formation and jetting, and stated that jetting occurred when the necking of a drop begins before the preceding drop has been released.

### 3.4) Drop Formation From Jets Region III and IV

Tyler<sup>(113)</sup> first applied Rayleigh's<sup>(114)</sup> instability theory to the prediction of drop size, and suggested the following equation:

$$V_f = \frac{2 \pi a^3}{(Ka)_{\max}} \quad (3.14)$$

where  $(Ka)_{\max}$  is the dominant wave number predicted by the instability theory. Using inviscid liquid jets in air, Tyler found that the predicted volume agreed with the experimental data if a  $Ka$  value of 0.696 was used. Merrington and Richardson<sup>(181)</sup> who also used liquid jets in air, found that their results were in agreement with equation (3.14).

Perrut and Lowtay<sup>(108)</sup> using a photographic technique, proposed the following correlation to predict the drop size from jet break-up: -  $d_f/d_n = 2.07 (1 - 0.193 Eo)$  (3.15)



Where  $E_o = \text{Eotvos number} = \frac{g \Delta \rho d_n^2}{\gamma}$

Christiansen and Hixon<sup>(115)</sup> using a similar approach to that of Tyler, proposed a graphical correlation that can be expressed as:-

$$\frac{d_f}{d_n} = 2.07 / (0.485 E_o + 1) \quad \text{for } E_o < 0.615 \quad (3.16)$$

$$\frac{d_f}{d_n} = 2.07 / (1.15 E_o + 0.12) \quad \text{for } E_o > 0.615$$

Schiffler<sup>(112)</sup> in an experimental study of jets in liquid-liquid systems, found that drop sizes predicted by the above authors were generally low. He improved upon Christiansen and Hixon's equation by introducing a 'snap off' constant which decreased from a value of 6.0 for an interfacial tension value of 1.8 dynes/cms to 1.7 for an interfacial value of 40 dynes/cms.

None of the equations in the literature satisfactorily predicted the drop size over the entire range of properties studied in the present investigation. However, the predictions of Christiansen and Schiffler can be improved upon by using the correlation of Meister and Scheele<sup>(116, 117)</sup> viz:-

$$V_f = F \left[ \frac{2\pi\gamma_a}{g\Delta\rho} - \frac{4}{3} \frac{\rho_d Q U_n}{(a/a_n)^2 g\Delta\rho} + \frac{4Q\mu Q_a}{\Delta\rho d_f^2 g} + 7.15 \left( \frac{Q^2 a^2 \rho_d \gamma}{(g\Delta\rho)^2} \right)^{1/3} \right] \quad (3.17)$$

where 'a' is the jet radius on the end of the jet which can be predicted by the Schiffler Jet Construction<sup>(112)</sup>

$$\frac{1}{a^4} \left( g \Delta \rho d_n z + \rho_d U_n^2 + \frac{8\gamma}{d_n} \right) - \frac{3}{a} \left( \frac{8\gamma}{d_n} \right) = \rho_d U_n^2 \quad (3.18)$$

which also includes the prediction of the jet length 'L' in immiscible liquid systems.

$$L = \frac{1}{2a} \left( \left[ \frac{a^2 U \bar{I}}{a_n^2} \right]_{z=5} + \left[ \frac{a^2 U \bar{I}}{a_n^2} \right]_{z=L} \right) \ell_n \left( \frac{a_n}{\xi_0} \right) \quad (3.19)$$

CHAPTER 4.

SURFACE ENERGY CONSIDERATIONS



#### 4) SURFACE ENERGY CONSIDERATIONS

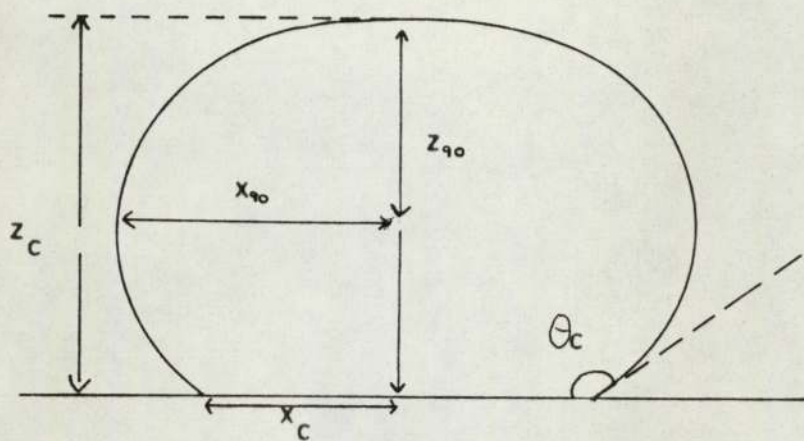
The importance of the solid surface properties on the coalescence mechanism taking place within a packed bed has been reviewed in Section (2.2.1). However, the relationship between coalescence mechanisms, droplet hydrodynamics and solid surface energies has not been treated quantitatively, and little data exists which could be conveniently applied to the design of packed bed coalescers. An index of the relationship between the solid surface energy and the overall coalescence mechanism is that of the contact angle of a sessile drop at the liquid-liquid-solid interface, (Fig. 4.1). If the angle is  $>90^{\circ}$ , the solid is referred to as a non-wetted surface, and vice-versa for angles  $<90^{\circ}$ . For coalescence of a primary dispersion in a wetted packing, the overall process is one of drop-interface coalescence between droplets and the film of dispersed phase which spreads on the packing surface. Conversely, for non-wetted packings, it is assumed that coalescence takes place by a drop-drop mechanism promoted by intimate contact of droplets passing through the packing.

The contact angle is a common and useful measure of the force balance between the cohesive force in the liquid and the adhesive forces between the solid surface and the liquid. It provides information about the solid surface energetics, surface roughness, and the surface heterogeneity. It is also a sensitive measure of surface contamination. The latter point is of particular importance if the contamination is soluted by either the dispersed phase or the continuous phase.

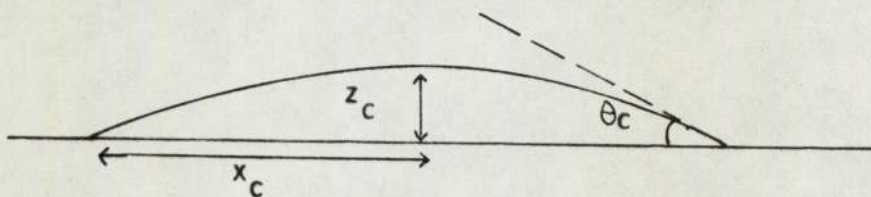
Schwartz<sup>(74)</sup> has reviewed the importance of solid surface energetics, particularly the contact angle in the macroscopic motion of liquids under the influence of their own surface and interfacial forces. It was suggested that when flow is extensive, as in wicking and blotting or in capillary imbibing systems, that consideration must be taken not only of the fluid dynamics, but also of the surface energetics. However, for the coalescence of dispersions, the detailed

Fig. 4.1

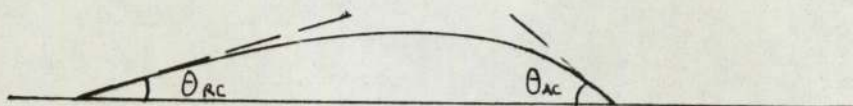
A SESSILE DROP ON A PLANE SURFACE



(1) CONTACT ANGLE  $> 90^\circ$



(2) CONTACT ANGLE  $< 90^\circ$



(3) SHOWING ADVANCING & RECEDING CONTACT ANGLE  
i.e. HYSTERESIS



dynamics of the process are of less practical interest than the statics of the initial and final states of the system. Thus, previous investigations into packed beds have been limited to observations of the inlet and outlet drop sizes.

Further work on the surface energetics and their relationship to flow in porous media has been presented by Morrow<sup>(70)</sup>. Morrow points out that much ambiguity exists in the terminology used in discussing surface energetics, and definitions are given for specific terms. Furthermore, it is of interest to note that, although contact angles were first related to surface energies in 1810 by Young<sup>(129)</sup>, much controversy still exists as to the validity of this fundamental equation.

#### 4.1) Theoretical Considerations

(129)

Young proposed the following equation for a sessile drop resting at equilibrium on a plane solid surface:

$$\sigma_{sv} - \sigma_{sl} = \sigma_{vl} \cos \theta_c \quad (4.1)$$

where s, v and l refer to solid, vapour and liquid respectively.

Various workers have commented upon the derivation, and assumptions inherent in Young's equation. Binkerman<sup>(140)</sup> suggests that Newton's 2nd Law of Mechanics was unaccounted for, whilst Zissman<sup>(139)</sup> argues that neither  $\sigma_{sv}$  nor  $\sigma_{sl}$  can be conveniently measured. Thus it was possible that any tensile stress existing in the solid would rarely be a system in equilibrium. Goodrich<sup>(138)</sup> pointed out Young's assumption that solid surfaces have surface tensions analogous to a liquid interface, and argues that the equation is only applicable when the drop produces a negligible strain energy in the solid.

However, Lester<sup>(137)</sup> with a sophisticated treatment of Young's equation, showed that equation 4.1 was valid, providing the surface was not "too deformable".



Pettica & Pettica<sup>(136)</sup> argued that if the drop were spherical, and not subjected to gravitational effects, the equation was valid. Johnson<sup>(130)</sup> suggested that gravitational and also adsorption effects have no bearing on the validity of the equation. According to Elliot and Riddiford<sup>(135)</sup> the equation must apply if the system is in equilibrium before and after drop deposition.

The basic thermodynamics of a surface were first published by Gibbs<sup>(134)</sup>. This work was used by Buff<sup>(132)</sup> and more recently by Johnson<sup>(130)</sup> to verify Young's equation. However, Rayleigh<sup>(133)</sup> first reported that a fundamental characteristic of wetting was the ability of a liquid drop to have many stable angles on a solid surface. This phenomena is now widely known as hysteresis, and is not a function of Gibbs' theory, which predicts that only one contact angle is possible for a given system.

Unfortunately, Young's equation has only been verified experimentally in a small number of cases, due to the difficulty in measuring the solid interfacial and surface tensions<sup>(131)</sup>. Even more disappointing is the controversy over experimental values of the contact angle of a sessile drop. In view of these discrepancies, the literature on the factors affecting contact angles has been reviewed.

#### 4.2) Factors affecting contact angle values

4.2.1) Surface Roughness: Much data exists for the effect of surface roughness on the contact angle. The effect of capillary grooves and the relationship between the angle and height of the asperity have been reported by Binkerman<sup>(144)</sup> and Bartell et al<sup>(149, 150)</sup> respectively. Wenzel<sup>(147)(148)</sup> who also investigated surface roughness, suggested a modified form of Young's equation, to equate the



surface roughness, viz

$$r^1 \cos \theta_c = \cos \theta_c^1$$

or

(4.2)

$$r^1 (\sigma_{sv} - \sigma_{sl}) = \sigma_{vl} \cos \theta_c^1$$

where  $r^1$  is the ratio of the actual surface area to the geometric surface area, and  $\theta_c^1$  is the angle of contact for the roughened surface. However, Bartell and Sheppard observed that their experimental results did not agree with Wenzel's equation.

The thermodynamic derivation of this equation was developed by Shuttleworth and Bailey<sup>(145)</sup>. The assumptions used by the latter workers were explicitly listed by Johnson and Dettre<sup>(146)</sup>, particularly the lack of consideration of the meta-stable states of the surface introduced by roughness.

4.2.2) Temperature: Investigations into the effect of temperature on the contact angle have shown that the coefficient  $\left(\frac{d\theta}{dt}\right)$  increased for polar liquids on low energy surfaces<sup>(162)</sup> and decreased for polar liquids on high energy surfaces<sup>(161)(167)</sup>. For organic-water systems, Adams and Elliot<sup>(163)</sup> found no detectable variation between 20° and 35°C. They suggested that an increase in temperature produced a decrease in its surface tension, and as such altered the work of cohesion but also that the adhesion to the solid was decreased to the same extent.

4.2.3) Rate of Motion: More important to this study is the effect of the rate of motion of a liquid-liquid interface across a solid surface. Elliot and Riddiford<sup>(160)</sup> observed that  $\theta_{ac}$  was independent of the interfacial velocity in the range 0 - 1 mm min<sup>-1</sup>, above which  $\theta_{ac}$  increased linearly up to a limiting value. Yarnold and Mason<sup>(159)</sup>, using a water-air system on paraffin wax, found little change in  $\theta_{ac}$  but the receding angle decreased with increased rate



of recession. Harkins<sup>(162)</sup> extended the equations of Dupre<sup>(184)</sup> to define the work of cohesion and adhesion, and from these equations derived an expression to define the spreading coefficient 'S':-

$$S = \gamma_a - (\gamma_b + \gamma_{ab}) \quad (4.3)$$

If  $(\gamma_b + \gamma_{ab})$  is less than  $\gamma_a$ , spreading will occur, but this equation is applicable only to the spreading of one liquid on a second liquid. However, the effect of interfacial velocity on the contact angle and its relationship to the hydrodynamics within a coalescing aid has received little attention.

4.2.4) Hysteresis: The concept of a dynamic contact angle can be described for an advancing or receding interface. The contact angle formed when the solid-liquid interface has moved into a previously 'dry' solid surface is the advancing angle  $\theta_{ac}$ . The angle formed after the solid-liquid interface has moved away from a previously wetted surface is the receding angle  $\theta_{rc}$ . Frequently, the two angles are different, and this is termed hysteresis - Fig. 4.1. Opinion is divided as to whether hysteresis can be avoided by careful experimental technique or whether it is a more fundamental phenomenon<sup>(142)(141)(152)(153)</sup>. Numerous theories have been proposed for explaining hysteresis. Several workers suggest that the adsorption at a solid-liquid-liquid interface is different for the advancing and receding angle<sup>(154)(155)</sup>. Other theories relate to change in orientation of polar groups<sup>(156)</sup> in the solid surface or the migration of polar groups of the impurities in the bulk of the solid to the surface<sup>(156)</sup>. It has also been suggested that surface heterogeneity<sup>(158)</sup> surface roughness<sup>(130)(152)</sup> and relaxation phenomena<sup>(157)</sup> have some effect. It is possible that



the above factors contribute either individually or collectively to hysteresis, however, further analysis is required before the phenomenon can be properly explained.

4.2.5) Experimental Procedures: The wide variation of results reported in the literature for the contact angle of a sessile drop for a given system is often attributed to hysteresis. A close inspection of the experimental techniques used to determine contact angle values leads to some interesting observations.

Many workers have quoted values on a glass surface, but often give no exact specification for the angle measured or the composition of the glass. The angle could be measured for the advancing interface or receding interface or a mean of the two.<sup>(177)</sup> Equally, the composition of the glass surface may have a pronounced effect. According to a review of the wettability of silica glasses<sup>(170)</sup> by water, values between  $0^{\circ}$  and  $40^{\circ}$  can be obtained, dependent on the composition of the glass.

Hair<sup>(171)</sup> has also suggested that for any given form of silica glass, the surface composition cannot be accurately described, owing to the evaporation of the more volatile compounds during the cooling process.

Perhaps more important is the consideration that the individual workers give to surface preparation. Microscopic evidence<sup>(169)</sup> has shown that grinding and polishing can produce changes in surface composition and surface heterogeneity. The heat generated and the shear process during grinding has been shown to produce the following effects:

- i) Surface bonding between the grinding compounds and the surface molecules
- ii) The "filling in" of cavities with the grinding compounds.



In some cases, conventional cleaning techniques may not totally eliminate these effects. Observations of the surface can be taken even further to the molecular level<sup>(161)</sup>. For instance, a glass surface can be shown to be molecularly rough owing to heat stress fissures, and consequent crystalline dislocations.

Equally important are the techniques used in cleaning solid surfaces. Typically, glass is cleaned with a range of compounds from acidified dichromate to alkaline detergent. Acid treatments are a surface renewal procedure<sup>(161)</sup>, leading to freshly exposed surface, not only of greater roughness, but also of different surface composition. Cleaning by surfactants presents the problem of ensuring complete removal of all surface active compounds

Similarly, care has to be taken during experimentation to minimize contamination of the liquids and adsorption on to the solid surfaces. The effect of adsorption on the surface of glass is shown in a remarkable way by silane compounds. A monolayer of dimethyl silane on a glass surface will render the glass completely lithophilic.

The contact angle is given the status of a thermodynamic property. As such, the contact angle of a liquid on a smooth rigid surface must be invariant at constant temperature and pressure. However, it is frequently observed that the advancing angle is different from the receding angle. Therefore, without further justification, the measured angle cannot be considered the equilibrium angle. Several problems stem from this conclusion. For example, it is questionable whether a relationship exists between the contact angle, the drop volume, and how the drop is positioned on a surface.



Experimental work was carried out to answer these fundamental questions and to evaluate how these relate to the dynamic situation within a packed bed. Comparisons were made between the contact angles measured directly from experiments and with those computed from the theory for the prediction of drop profiles. This has been discussed in detail in Appendix A.1

The literature presented in Chapters 1 - 4 has enabled a basic understanding of the problems inherent in the study of droplet hydrodynamics and coalescence mechanism within a packed bed coalescing aid. From the information presented an experimental programme was designed and this is described in more detail in Chapter 5.

CHAPTER 5.

EXPERIMENTAL INVESTIGATION



## 5) Introduction

In this study, the macroscopic effects of droplet hydrodynamics and coalescence rates were investigated using pilot plant equipment. More precise work on single droplet behaviour was carried out using laboratory apparatus.

A review of the literature on single drop coalescence mechanisms illustrates the difficulties arising in the analysis of experimental observations. Much disagreement exists in the interpretation of results and Hitit<sup>(2)</sup> concluded that it was often misleading to relate single drop behaviour to that in pilot plant equipment. Nevertheless, the extensive literature available was useful in evaluating the important criteria for the design of the experimental apparatus. The most important considerations are presented below, and illustrate the approach to the fundamental analysis of coalescence in packings.

### 5.1) DESIGN OF APPARATUS

#### 5.1.1) Packing Selection

The surface energy and the geometric properties of the packing have received scant attention in the literature. Similarly, observations of the droplet hydrodynamics within packed beds have been restricted to examination at the column wall. To obtain information in these areas, mono-sized glass ballotini<sup>\*</sup> were used to form a packed bed. The reasons for this choice of packing are presented below.

#### (a) Geometric Properties

In many unit operations, packings of various geometries have been related to that of a sphere by a shape factor, where a sphere has a shape factor equal to 1.0. In this respect, it is envisaged that the use of spheres as a packing may facilitate the use

\* derived from the Italian for spheres or balls



of a shape factor to equate the effect of surface area to volume ratios on the coalescence efficiency of different packings.

The theory and practice of packing arrangements of spheres has been widely reported in the literature<sup>(164-166)</sup>. Co-ordination numbers and voidage relationships have been evaluated for both regular and random packing of spheres. Pore sizes and channel diameter variations have been evaluated from a theoretical<sup>(164)</sup> and experimental<sup>(167)</sup> stand-point. Therefore, from these properties, it is possible to quantify the packing geometry and its effect on coalescence.<sup>(38)(50)(69)</sup> Previous workers have not included an analysis of packing geometry and have restricted the geometrical description to that of a voidage value. Whereas voidage values are important with respect to limiting flow conditions, they do not provide any information with regard to coalescence mechanisms within the bed. Sections(7 & 8) illustrate how droplet hydrodynamics are fundamentally related to a mean void diameter and independent of the voidage. Furthermore, examination of local voidage variations of either Raschig Rings or knitted mesh packing in small diameter columns shows that very large wall effects exist. This is also true for spheres and indicates the importance not only of packing selection, but also of using a column of adequate diameter. Ridgeway and Tarbuck<sup>(166)</sup> who investigated local voidage variations of spheres in cylindrical columns, concluded that the wall effects were virtually eliminated within two particle diameters from the wall.

Table 5.1 illustrates that, for small diameter columns, there are very large errors inherent in equating voidage values for different size packings.



Table 5.1.1

Diameter of sphere (cms)	Percent. cross sectional area with mean voidage for column diameter		
	3"	6"	9"
1.2	13.4	46.8	62.3
0.9	27.8	58.3	70.6
0.6	44.4	69.5	79.6
Volume/metre of column (litres)	18.6	74.4	167.4

Initially in this study, ballotini sizes of 1.2, 0.9 and 0.6 cms were used, with a column of 6" diameter. This provided a compromise between voidage effects and the total volume of continuous phase required. Later, however, to facilitate the counter current studies, a 9" diameter column was used.

A further advantage in the use of spheres was that it enabled incremental evaluation to be made of bed height and void diameter. This overcame the problems encountered in previous studies due to the inflexibility of packing sections.<sup>(50)(59)</sup>

#### (b) Surface Properties of Glass Ballotini

Coalescence mechanisms and droplet hydrodynamics within packed columns are, to a large extent, dependent on the surface energy of the packing. Considerable information is available on the surface properties of glass and its relationship to the contact angle, and wetting effects with many liquid-liquid systems. Therefore, the use of a glass packing made it possible to relate droplet behaviour within the bed to the system energetics.

In the main, this study was restricted to the coalescence process in a non-wetted packing. Glass, having a high surface energy value, was thus well suited when organic liquids were used as the dispersed phase.

Nevertheless, considerable expertise has been developed



for changing the surface energy of glass by preferential wetting and adsorption techniques, as described in Section 5.1.3(c). Thus, by pre-treatment of the ballotini surface, investigation into a wetted packing was possible without altering the packing geometry.

### (c) Optical Properties of glass ballotini

Glass ballotini are essentially transparent and observation within the packing was therefore possible with varying degrees of success using different techniques.

To observe the film drainage and drop shape in a close packed swarm of drops, Allak<sup>(36)</sup> matched the refractive index of the dispersed phase with that of the continuous phase. A similar technique was tried in this study by matching the refractive index of the glass to that of the continuous phase. Oil soluble dyes, fluorescent dyes or scintillating compounds were also used to permit observations within the packed bed.

### 5.1.2 Materials of Construction

Difficulties in reproducing results in coalescence studies have often been attributed to system contamination via the materials of construction. In this study, surface active contamination was minimized by using only glass, stainless steel and PTFE, with the exception of the brass distributor plates. The distributor plates, designed to specifications laid down by Treybal<sup>(185)</sup> were used to produce a primary dispersion with a narrow drop size distribution. Fabrication of a plate with the recommended sharp edged orifices was best carried out using a malleable material - viz brass. Distributor plates with 1.6, 1.2, 0.8 and 0.4 mm diameter orifices were used in this study to produce inlet drop size in the range 0.6 - 0.1cms. An orifice diameter of 0.4 mm was the smallest hole possible by conventional drilling techniques



and represented a serious limitation in analysis of the inlet drop size range.

The viton seals and glands within the centrifugal pumps, used to circulate the liquid phases, were found to be sources of contamination. This problem was overcome by replacing the standard seals and glands with stainless steel backing flanges and PTFE seals.

### 5.1.3) Selection of Organic-Aqueous Systems

Throughout this study, organic dispersions were investigated in a continuum of distilled water. Special attention was given to the distillation, storage and handling of all the liquid systems. Periodic checks of phase purity were carried out by using a Du Nouy Tensiometer to determine interfacial tension values. The fundamental process of film drainage and consequently coalescence times will not only differ with phase purity, but also from system to system. The adoption of systems used by recent workers made it possible to relate the present work to previous studies in different areas. Thus Lawson's<sup>(4)</sup> work on the coalescence of a single drop was used in the interpretation for the basis of a theoretical model for coalescence in a packing, as presented in Section(7.1). Similarly, comparisons were drawn with the work of Hitit<sup>(2)</sup> on vertical settlers, and Thomas,<sup>(50)</sup> who investigated droplet behaviour within knitted mesh packings.

The organic systems selected covered a range of interfacial tension values (9.8 - 51.5 dynes/cms) and a range of density difference values (0.025 - 0.306 g/cm<sup>3</sup>). Non viscous systems were selected to minimize the pressure drops associated with flow through packed beds. The organic liquids and their physical properties are listed in Appendix ( 2 ). A further advantage



of the systems used was that of general convenience. They were all relatively non toxic, non corrosive, readily available and economic to use in pilot plant studies.

#### 5.1.4) System Preparation (a) Liquid systems

Prior to use, the organic phase was distilled twice with a distillation cut of  $\pm 1^{\circ}\text{C}$  around its theoretical boiling point. The distilled organic was stored prior to use in cleaned containers in a darkened cupboard. This was to eliminate any polymerization due to sunlight, which Hitit<sup>(2)</sup> concluded was important to phase purity.

Tap water was continuously distilled in a standard Vigreux column, and the resulting distilled water was stored in 20 litre glass aspirators.

The physical properties of each system were determined prior to and during each set of experiments using conventional techniques<sup>(168)</sup>.

#### (b) Cleaning Techniques

The experimental apparatus in contact with the liquid phases was cleaned thoroughly before experimental investigations were started. A surface active cleaning solution, Decon 90, was found to be most suitable for cleaning pilot plant equipment. Before each series of experimental runs, the pilot plant apparatus was filled with a 2% solution of Decon 90 in distilled water. The apparatus was allowed to soak for 24 hours with periodic recirculation of the cleaning solution. After soaking, the whole apparatus was rinsed thoroughly with tap water until complete removal was achieved of all surface active compounds<sup>(2)</sup>. The apparatus was then rinsed with distilled water, before commencement of experimental investigation.







A monolayer of dimethyldichlorosilane has been reported molecularly to cover only 58% of the surface, but will render the glass to be completely wet by organics.<sup>(177)</sup> Similar effects from heavy metal soaps, long chain fatty acids and amines are caused, but the use of silane compounds was preferred, as these materials are bound so tightly they do not contaminate the surrounding liquids.

## 5.2) PILOT PLANT EQUIPMENT

### 5.2.1) 6" Diameter Column

The apparatus used to investigate coalescence within a packed bed is shown in Fig. 5.2.1. It was constructed entirely from standard Q.V.F. glassware with P.T.F.E. seals and valve seats, and the whole apparatus was enclosed in a thermostatically controlled cabinet (1). Temperature control was provided by a Fi-monitor Control Module connected to a 1 kw flameproof oil heater (2). The finned-tube heat exchanger was controlled by a simple capacitance device (3) in connection with the mercury thread of a low range thermometer (67°F - 75°F). This arrangement was found adequate in controlling the temperature to  $\pm 1^\circ\text{F}$ .

Before each series of experimental runs, the apparatus and packing was cleaned as described earlier (5.1.4). The central 6" column (4) was filled with distilled water and freshly distilled organic phase was admitted to the 9" reservoir (5). The flow diagram Fig. 5.2.2 indicates the method used for complete recirculation of the organic phase. A No. 10 Stuart Turner centrifugal pump (6) was used to pump the organic phase from the 9" reservoir (5) to the 6" column via the rotameters (7) and a sintered glass filter (8). The filter was used to trap any solid particles which could affect the coalescence process. Thermal and mass transfer gradients were eliminated by intermittent re-circulation over a period of 24 hours.



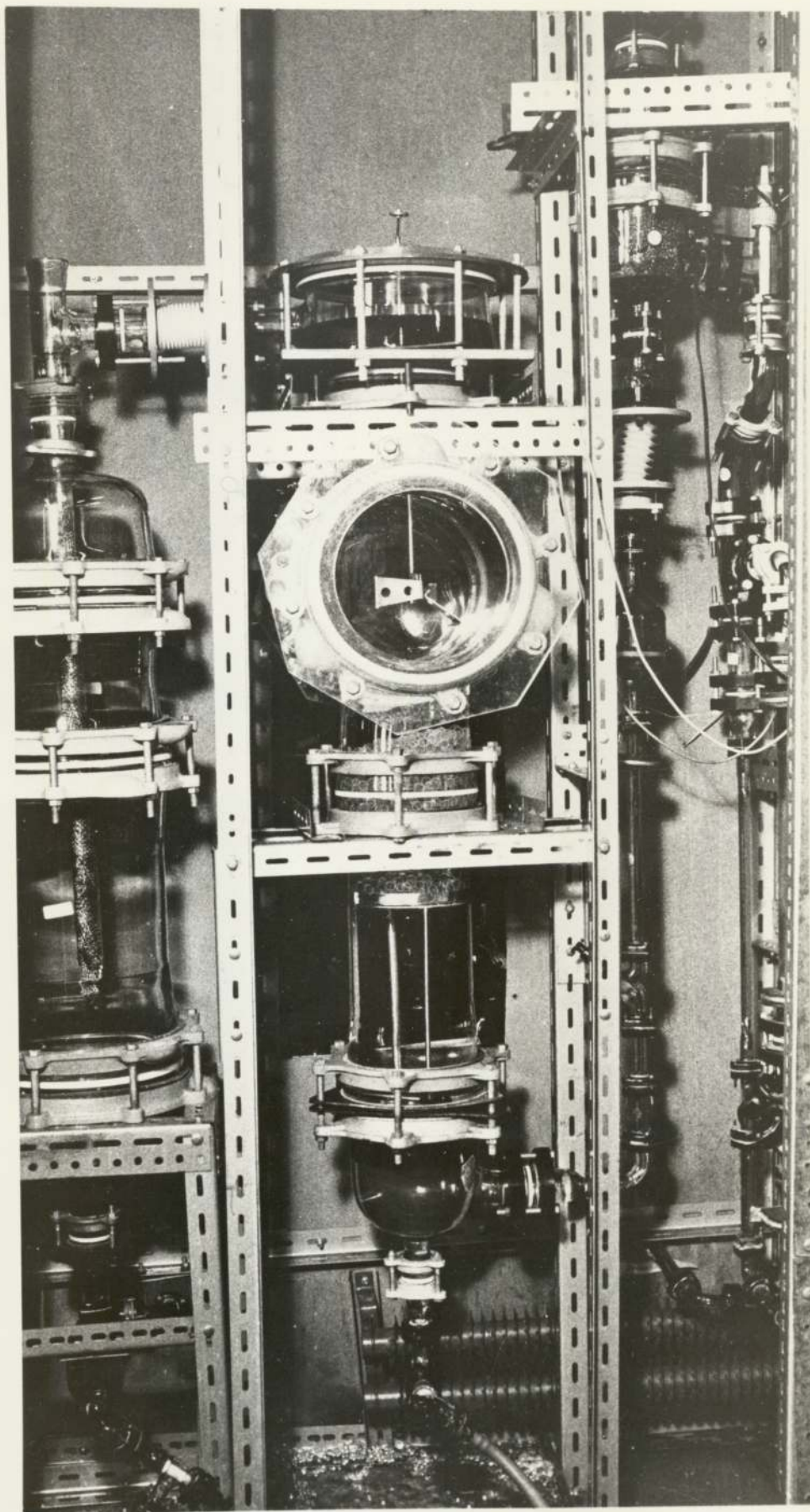
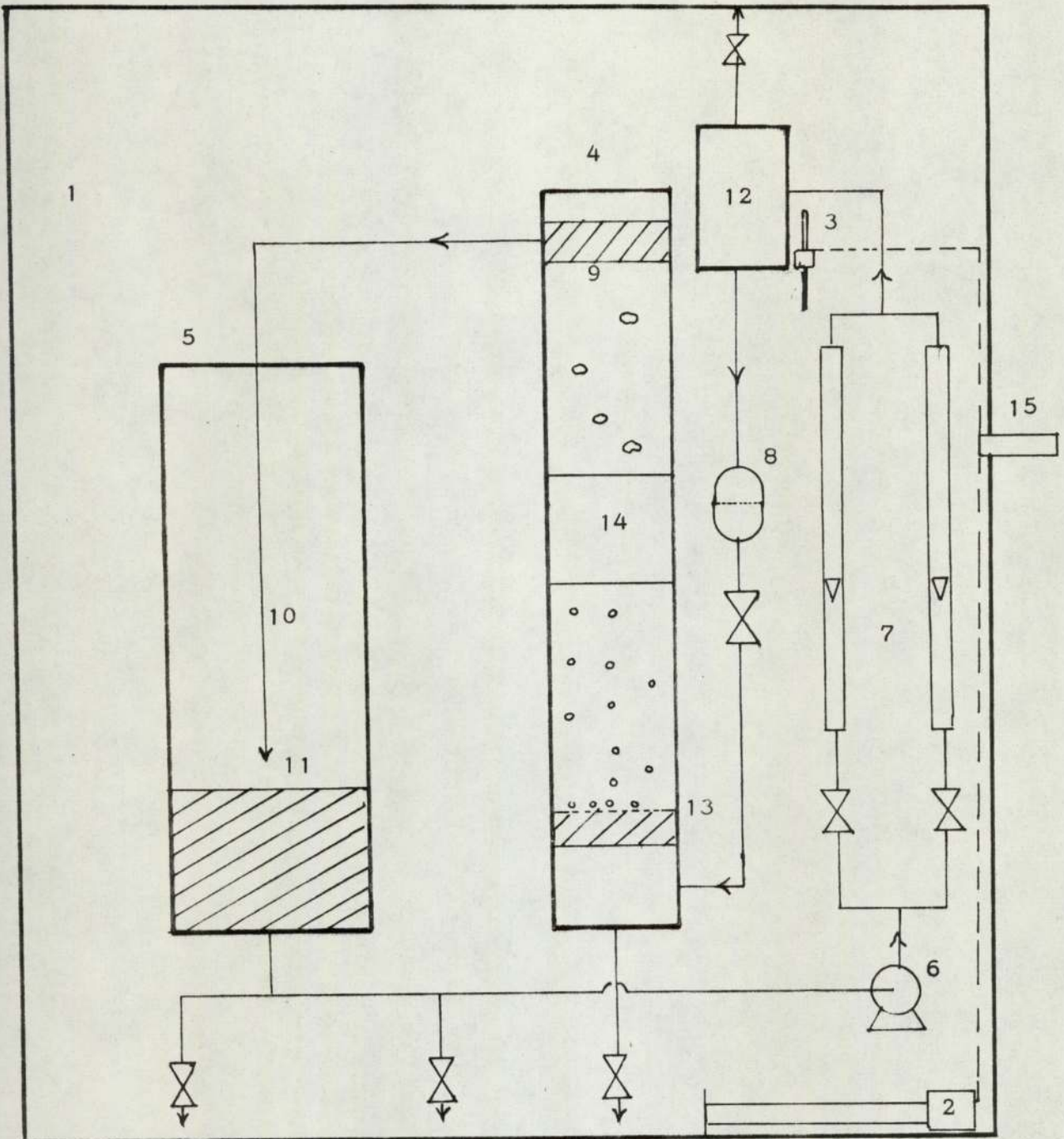


Fig. 5.2.1

6" DIAMETER COLUMN

Fig. 5.2.2

FLOW DIAGRAM FOR 6" DIAMETER COLUMN



1. Cabinet
2. Heat Exchanger
3. Capacitance Unit
4. 6" Column
5. Organic Reservoir
6. Centrifugal Pump
7. Rotameters
8. Filter
9. Organic Water Interface
10. Overflow Pipe
11. Organic Air Interface
12. Head Chamber
13. Brass Distributor Plate
14. Ballotini Packing
15. FI-Monitor Control Module



During experimental runs, the packing was added in the required amounts by means of a long stemmed glass funnel. This was used to minimize secondary droplet formation when the packing cascaded through the organic-water interface (9). The packing(14) was supported on a glass stand by a single layer of knitted mesh, crimped between two stainless steel bands. The supporting mesh was positioned 18" above the distribution plate (13) to allow the inlet drops to attain terminal velocity.

The overflow pipe (10) from the 6" column to the reservoir was filled with stainless steel knitmesh packing. This was used to reduce the impact velocity of the overflow, and consequently eliminated the problem of aeration at the organic-air interface (11) which occurred prior to the use of an overflow pipe.

During initial experimentation, the inlet and outlet drops were photographed for a range of disperse flow rates, bed heights, inlet drop sizes and packing diameters. Photographs were taken using a Pentax 35 mm camera with Kodak Plus X film. Illumination was provided by diffused rear lighting through a perspex window in the air bath cabinet. The mean drop size was evaluated by measuring the diameter of the drop from an enlarged photographic negative, c.f.(6.1). In later studies, a Schlieren technique was used to obtain a shadowgraph for automatic analysis on a Quantitative Television Microscope. The equipment and experimental apparatus for this technique have been fully discussed in Section (6.2).

#### 5.2.2) 9" Diameter Column

Work was carried out on a 9" diameter column to investigate the effect of counter-current flow on the rate of coalescence within a packing. This apparatus was originally constructed by Hitit<sup>(2)</sup> to study coalescence of the flocculation zones in a vertical



settler. The design and description of the 9" counter-current apparatus is given in detail elsewhere<sup>(2)</sup>. Essentially, it is similar to the 6" diameter co-current column, except for the provision to recirculate both phases either co-currently or counter-currently. Procedure for system preparation was identical to that described for the 6" column. Similarly, the data recorded during corresponding runs was comparable to that for co-current studies, but with the addition of the continuous phase flow rate values.

### 5.3) LABORATORY APPARATUS

#### Single Drop Studies

Pilot Plant investigations indicated that several areas of droplet behaviour required further analysis under more precise conditions. Small scale laboratory apparatus was therefore used to investigate:

- (I) Inlet drop mechanisms,
- (II) Exit drop mechanisms,
- (III) Surface energy effects.

#### 5.3.1) Inlet Drop Studies

The behaviour of a drop within a simulated packing geometry was investigated in order to understand the mechanism of coalescence within a non-wetted packing. The importance of whether a drop is held up in the packing interstices or passes through without retention is essential to understanding the overall mechanism of coalescence.

The apparatus shown in Fig. 5.3.1 was used to study inlet drop phenomena. The simulated packing geometries chosen were cubic and triangular packing arrangements shown in Fig.(5.3.2). This packing arrangement was considered most representative of the packed bed consistent with ease of construction, Table(10.1 ).



Fig. 5.3.1

APPARATUS USED FOR INLET & OUTLET DROP STUDIES  
INSERT - SHOWING ENLARGED TOP VIEW OF CUBIC  
BALLOTINI ORIFICE WITH AN EMERGING DROP AT THE  
CRITICAL POINT OF PASSAGE

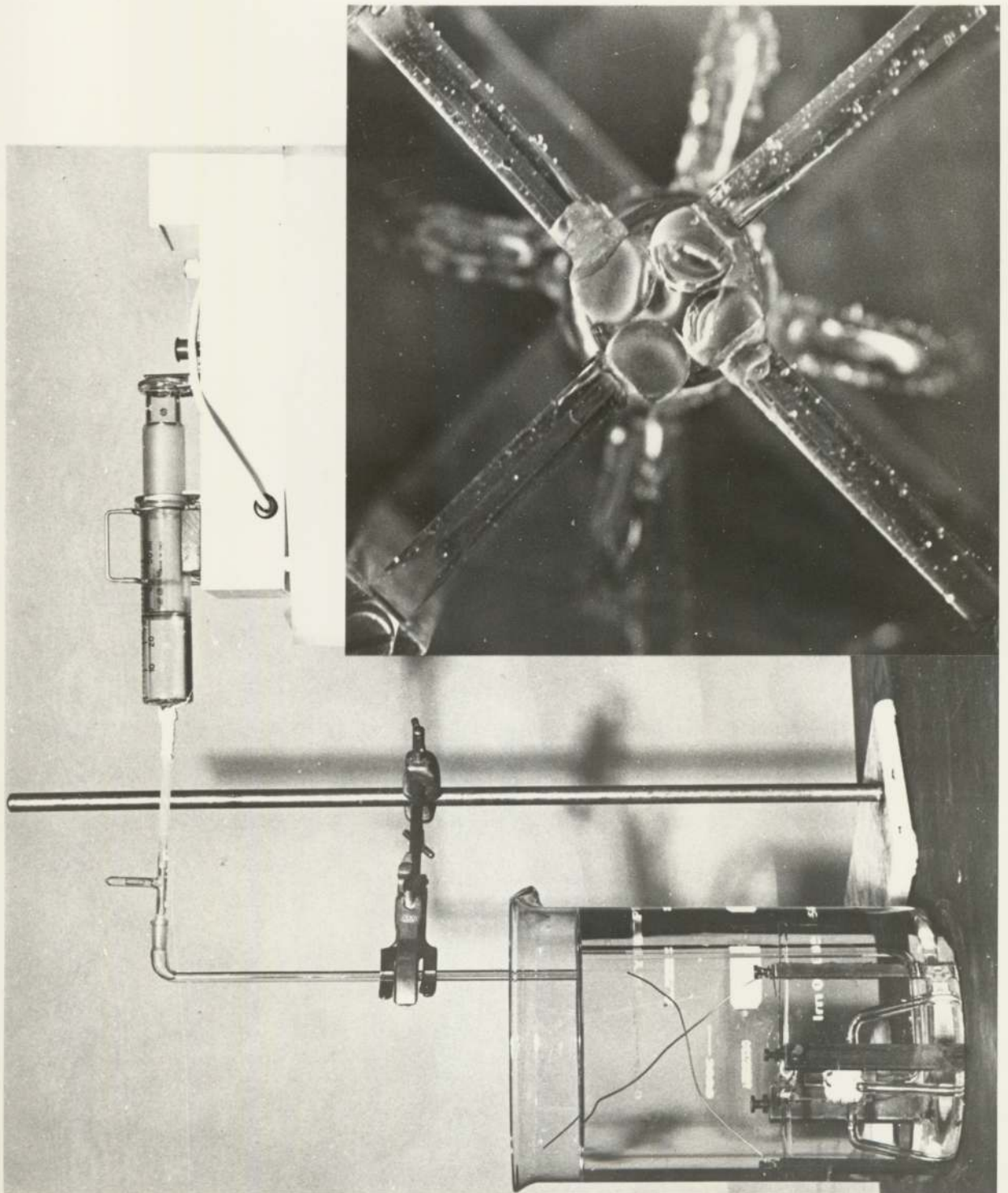
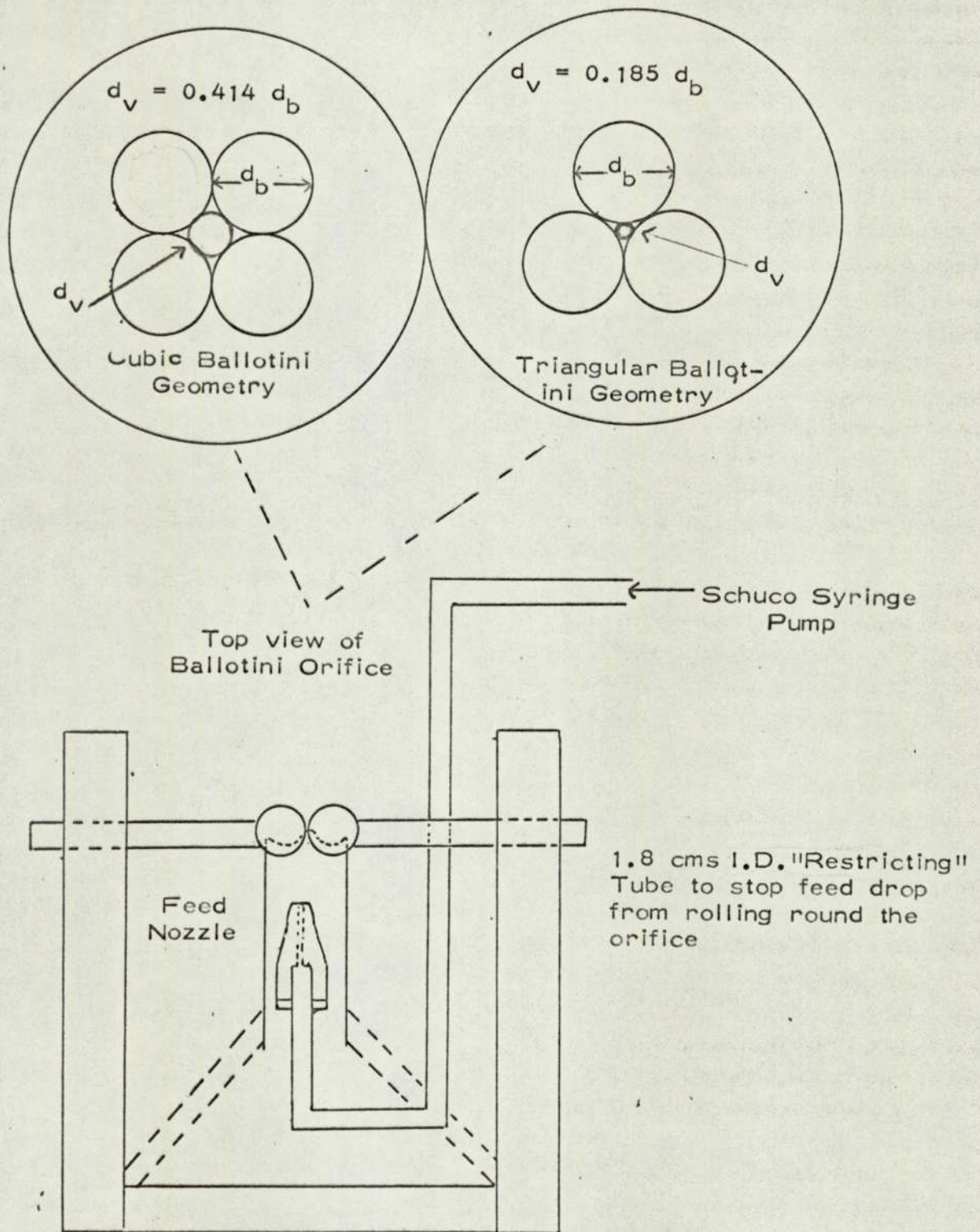


Fig. 5.3.2

SCHEMATIC DIAGRAM OF APPARATUS USED TO INVESTIGATE INLET & OUTLET DROP MECHANISMS



SUPPORT ARRANGEMENT FOR BALLOTINI ORIFICE



The simulated orifices were constructed by carefully fixing segmented ballotini on to glass rods with the use of epoxy resin adhesive. Care was taken to eliminate the presence of any resin on the surfaces in direct contact with the dispersed phase as this was found to change the wetting properties of the glass.

A Schuco model 'A' syringe pump was used to produce a constant flow rate into the feed nozzles. The flow rates could be altered by changing the syringe, thus facilitating investigation over a range of flow rates from 0.016 to 0.28 cc/s. Similarly, the diameter of the drop allowed to rise into the ballotini packing could be altered by inter changing the feed nozzles.

Drops formed at the standard glass feed nozzle were allowed to rise into the ballotini packing arrangement. If the drop was retained in the ballotini packing, the feed nozzle diameter was decreased until drop passage was achieved, and vice-versa if passage was initially obtained. The diameter of drop required for retention was evaluated from photographs and flow rate readings. This experimental procedure was repeated five times for a range of ballotini diameters and systems for both the cubic and triangular packing arrangements.

### 5.3.2) Exit Drop Studies

It was considered that the method by which the drop left the packing would determine the exit drop diameter. Once drop retention had taken place, further drops were allowed to rise into the packing arrangement until passage was achieved. The apparatus used to investigate exit drop behaviour was that described in the inlet drop studies, except a provision was made to stop the drop from rolling round the ballotini. This was achieved by supporting



the ballotini arrangement on a shaped piece of tubing as shown in Fig.(5.3.2).

The volume of drop required for passage was evaluated from photographs. Coalescence times within the void and passage of the dispersed phase through the interstices of the ballotini were recorded using high speed cine film. From these films the exit drop formation mechanism was studied with respect to the volume of drop required for passage, velocity of flow into the ballotini orifice during passage and the diameter of drop thus formed. The experimental procedure was repeated five times for each of the parameters investigated in the inlet drop studies.

### 5.3.3) Surface Energy Studies

The evaluation of any packing as a coalescing aid must take into account the relationship of surface energetics between the solid and the liquid systems. The most reported characteristic of surface energy is that of a contact angle. However, conflict exists in the literature as to the concept of a contact angle.

Hence, investigation was carried out into the following areas:

- a) Contact angle studies on solid surfaces for liquid-liquid systems and liquid-gas systems;
- b) the evaluation of drop profiles and the theoretical prediction of contact angle values from the dimensions of a sessile drop;

#### Contact Angle Studies

The apparatus used for the above investigations is shown in Fig.5.3.3(a) for a gas-liquid system and in Fig.5.3.3(b) for a liquid-liquid system.

Both mercury and water were used for the gas-liquid system, and mercury drops in water for the liquid-liquid system.



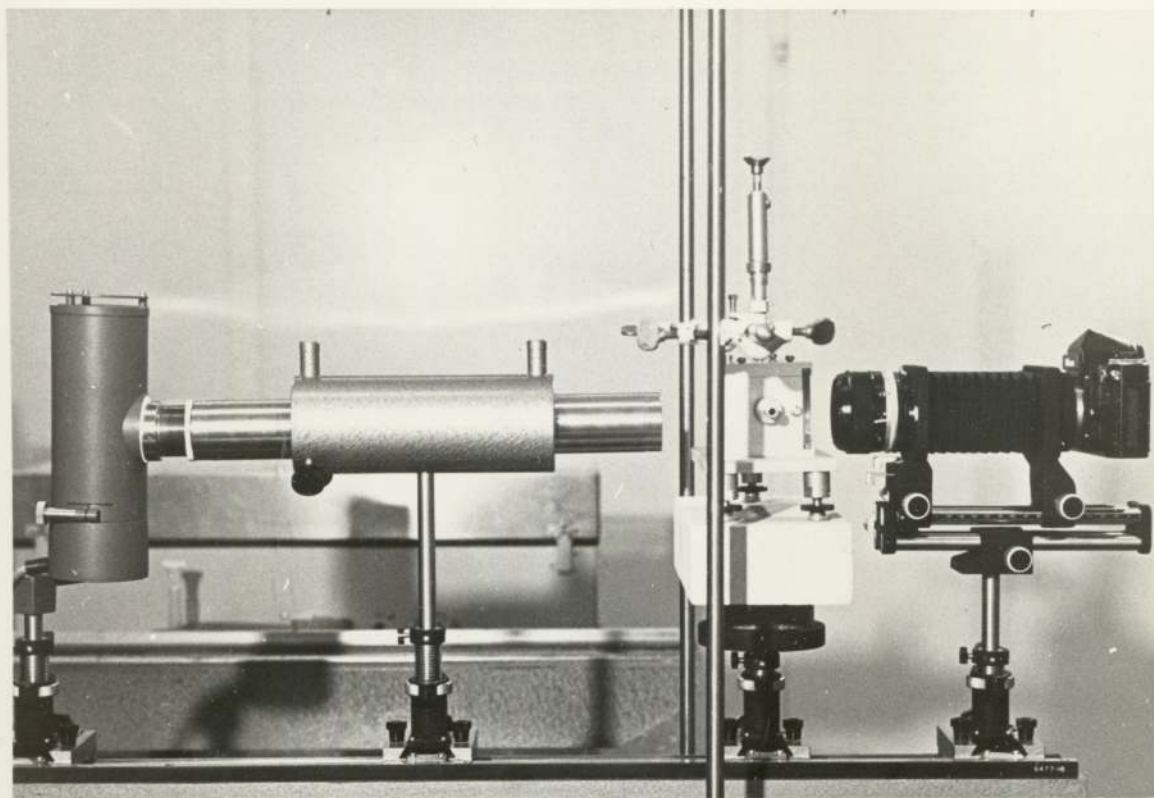


Fig. 5.3.3(a) APPARATUS USED FOR CONTACT ANGLE STUDIES (G/L) SIDE-VIEW. SHOWING USE OF REAR PARALLEL LIGHT SOURCE TO OBTAIN WELL DEFINED IMAGES

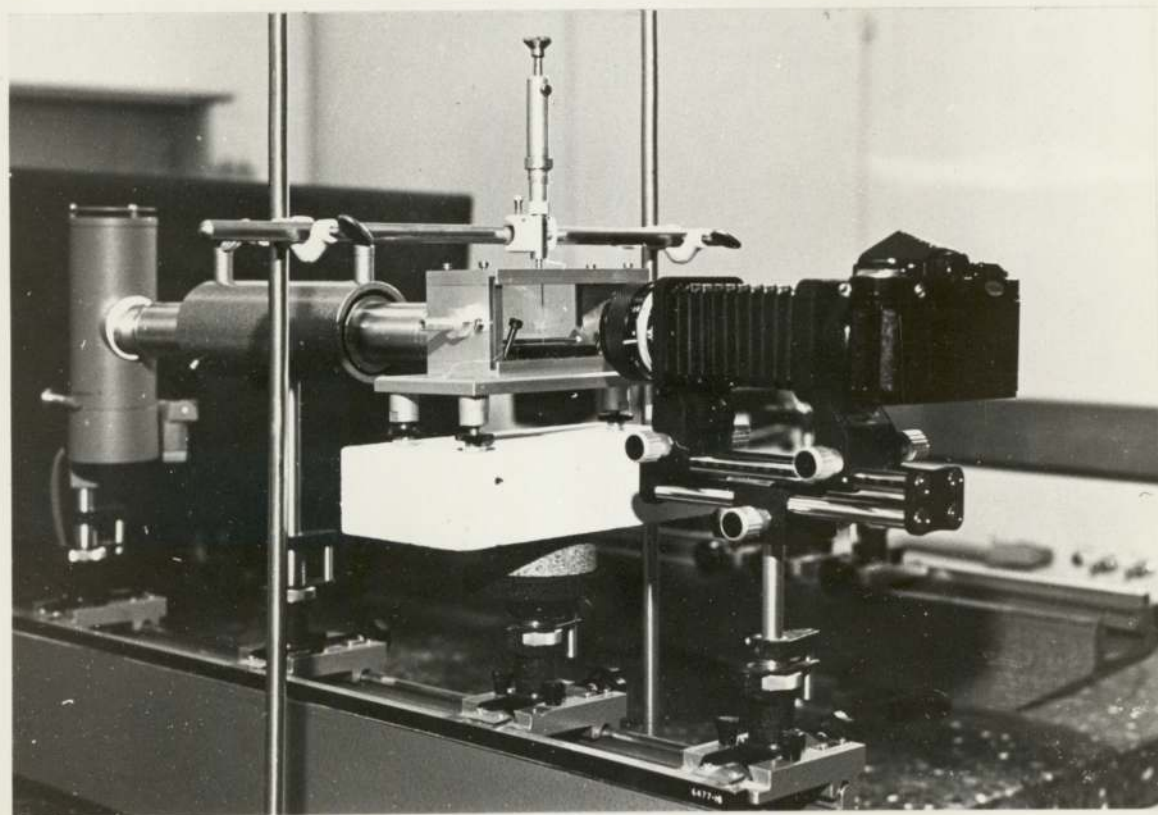


Fig. 5.3.3(a) APPARATUS USED FOR CONTACT ANGLE STUDIES (G/L) THREE QUARTERS VIEW. SHOWING OBSERVATION CELL.

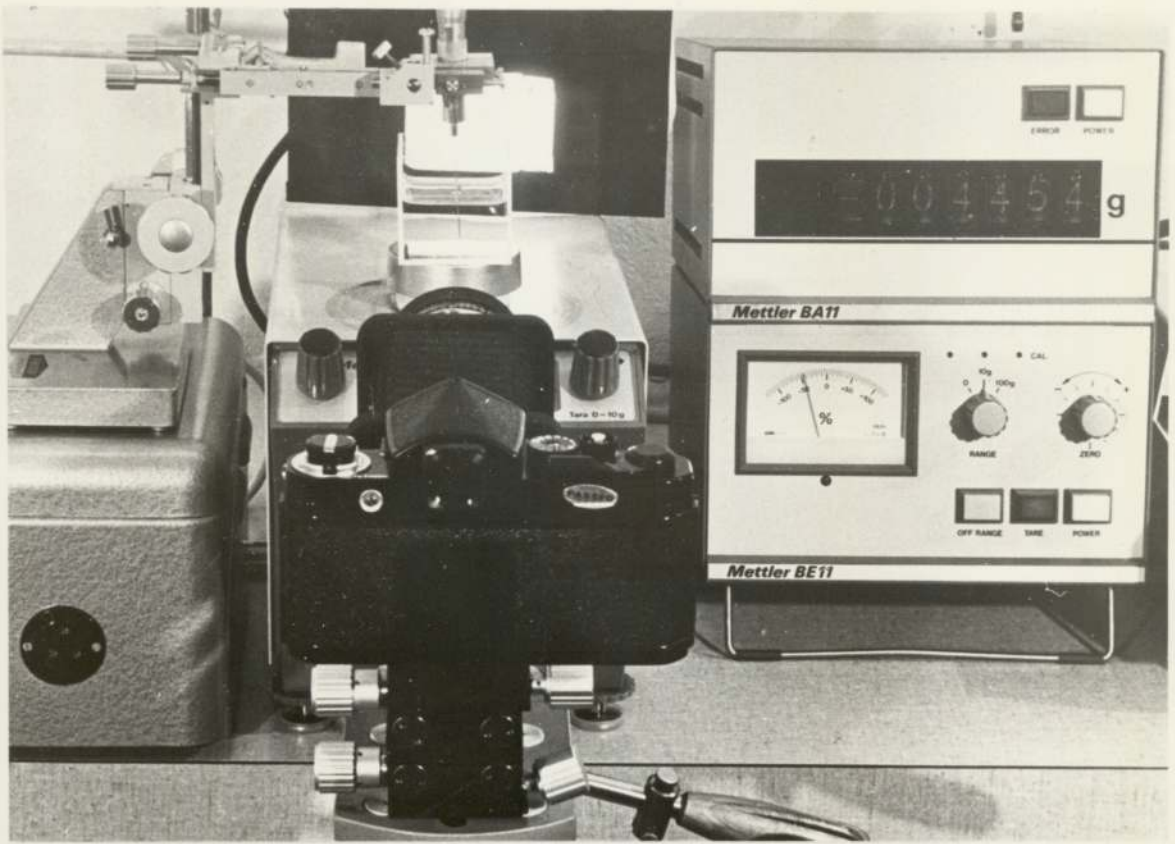


Fig. 5.3.3(b) APPARATUS USED FOR CONTACT ANGLE STUDIES (LIQUID-LIQUID)

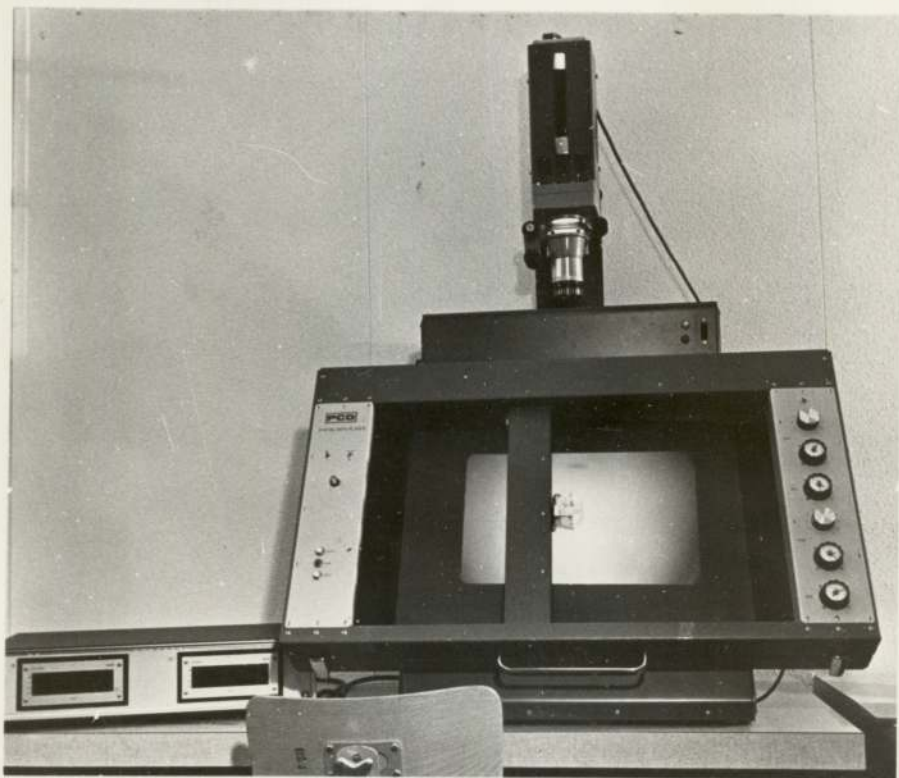


Fig. 5.3.3(c) P.C.D. DIGITAL DATA READER FOR MEASUREMENT OF DROP DIMENSIONS



Contact angles are sensitive to contamination, therefore great care was taken in system preparation. Ordinary tap water was first distilled, then re-distilled with a small quantity of potassium permanganate and finally distilled again. The potassium permanganate was to destroy any residual organics passed over during the initial distillation. Surface tension evaluations were carried out after each distillation stage. The mercury was purified by the following process: commercially available mercury was first washed in dilute nitric acid with the conventional bumping process, then passed through freshly prepared nitric acid from a jet column.<sup>(192)</sup> The mercury was then twice distilled under vacuum before being stored in a clean glass container inside a sealed dessicator.

A Hamilton CR 700 series syringe was used to form the drops and these were placed on cleaned microscope slides. Drop volumes were determined by direct syringe reading and also from weight measurements. In the liquid-gas system, weighing was carried out on a standard laboratory balance to 0.0001 g, whilst in the liquid-liquid system, a direct method was employed using a Mettler top pan balance with a digital display unit to 0.001 g. Contact angles were determined from photographs using a direct measurement technique. To enhance the definition of the drop profile, photography was carried out using a parallexed monochromatic light source as shown in Fig. 5.3.3. Investigations were carried out on the relationship of contact angle values with the following:

- (1) Surface cleaning and surface preparation.
- (2) Surface composition.
- (3) Surface roughness.
- (4) Drop volume and incremental values of drop volume.
- (5) Drop detachment mechanisms.

The investigations into (a) and (b) were carried out simultaneously by photographing the sessile drop on the solid surface. The following dimensions were recorded (Fig. 4.1):-

- I) Radius of drop contact with the solid;  $x_c$
- II) Maximum drop radius;  $x_{g0}$
- III) The maximum height of the drop;  $z_c$
- IV) The maximum height of the drop from the horizontal radius  $x_{g0}$  to the apex,  $z_{g0}$
- V) The contact angle  $\theta_c$

These dimensions were evaluated using a P.C.D. digital data reader screen and a capacitance device as shown in Fig. 5.3.3.(c)

The measurement by this method is reported to be accurate to 0.0001 cms.

The dimensions recorded above could be used in the theory of drop profiles to predict the contact angle or the surface tension value. Thus, the contact angle measured directly could be compared with a theoretically predicted value. By this analysis it was possible to test the theory of drop profile prediction and evaluate its applicability to the inlet model. The results, and limitations of the approach, are discussed in Appendix (A.1).



CHAPTER 6.

DATA ACQUISITION AND TREATMENT

## 6) DROP SIZE ANALYSIS

A measure of the coalescence efficiency of a packing is the ratio of the outlet to inlet mean drop diameter. Throughout this study the size distribution of droplets entering or leaving the packing was evaluated from photographic records. The inlet dispersions were produced from distribution plates with equal sized, sharp edged orifices and as such had a small distribution of sizes around the mean value. Consequently, analysis of the mean inlet drop diameter was carried out at selective intervals for each flow rate and liquid system. The drop size in the outlet dispersions, however, was dependent on local variation in geometry and also on the system hydrodynamics. This made the size distribution much wider, therefore a more detailed analysis was required.

### 6.1) Direct Measurement Technique

During each experiment, five minutes were allowed following any changes in the operating parameters for the system to reach hydrodynamic equilibrium before photography commenced. Analysis of the mean droplet diameter was made by directly measuring the drop dimensions with a graduated scale from an enlarged photographic negative. The number of drops present in any one negative is obviously a function of the flow rate. Therefore in the case of very low flow rates, several photographs were obtained at 15 second intervals so as to record sufficient drops for analysis.

Studies<sup>(38)(39)</sup> have been made to evaluate the definition of the mean diameter which best describes liquid-liquid dispersions. Generally the Sauter mean diameter, denoted as  $d_{32}$  has been favoured, owing to its relationship with the surface area available



for mass transfer. However, from a theoretical consideration of the coalescence mechanism within packed beds of ballotini, it would appear that a mean drop diameter based on the volume would be more applicable (7.3). In the results presented, the diameter was evaluated from both surface area and volumetric considerations.

It was found on analysis of the exit dispersion that the drops were irregular in shape. For purposes of analysis, a drop shape equivalent to that of an oblate spheroid was assumed. (38) Hence the individual drop diameters were determined by measuring the horizontal and vertical dimensions. Thus the diameter based on the surface area was evaluated from the following equation:

$$d_{xt}^s = \left( \frac{a^2}{2} + \frac{b^2}{4e} \ln \left( \frac{1+e}{1-e} \right) \right)^{0.5}$$

and the diameter based on the volume from:

$$d_{xt}^v = (a b^2)^{0.33}$$

where 'a' and 'b' are the major and minor axes of an oblate spheroid. The eccentricity 'e' which is always less than 1.0, is defined by:

$$e = \left( \frac{a^2 - b^2}{a^2} \right)^{0.5}$$

For any one set of experimental conditions, approximately 30 drops were measured, and the arithmetical mean was computed using Program 1 (Appendix 3.1). The number of drops required to be measured to produce a representative mean was evaluated using an experimental technique. Several tests were made on a large number of drops to evaluate the mean diameter. It was found



for all cases investigated, that a difference between the mean of a large sample and that for 30 drops was always less than 5%. The size distribution around the mean  $\bar{d}$  was calculated using a 95% Confidence Limit. This was obtained from the general equation of 0.95 probability that all the individual diameters lie within  $\bar{d} \pm 1.960/\sigma'\sqrt{N}$  of the mean drop diameter,  $\bar{d}$ , where  $N$  = number of drops measured, and  $\sigma'$  is the standard deviation defined as:

$$\sigma' = \sqrt{\frac{\sum_1^N (\bar{d} - d_i)^2}{N - 1}}$$

Hence the 95% Confidence Limit can be represented by the general equation:

$$C.L. = \bar{d} \pm 1.96 \sqrt{\frac{\sum_1^N (\bar{d} - d_i)^2}{N - 1}} / \sqrt{N}$$

In this way, the mean outlet drop size was analysed for changes in operating parameters, viz inlet drop size, bed height, flow rate, void and ball diameter and physical properties of the liquid systems. Initially, photography was carried out using 35mm Kodak Plus X Film with diffused rear lighting. Drop size analysis was carried out with individual measurement of the salient dimensions. In this way, some 50,000 measurements were taken. This represented a time consuming and demanding exercise. A review <sup>(127)(128)</sup> of the literature on automatic particle measurement indicated that no relevant information was available for the automatic analysis of translucent primary dispersions. Thus two methods for automatic drop size measurement were developed, and the experimental details are discussed below.



## 6.2) Automatic Measurement:

### 6.2.1) The use of image analysing computers such as the Quantitative television microscope to determine drop diameters of primary dispersions

Image analysing computers (I.A.C.) such as the Quantimet 720<sup>\*</sup> shown in Fig 6.2.1 are designed to make automatic analysis of selected features in photographs or in X Ray, electron and optical images. However, recognition of these features and subsequent counting is achieved by the critical property in boundary effects at a sharp contrast change.

Fig 6.2.2(B) shows a standard photograph of an exit dispersion using diffused rear lighting. This cannot be analysed on an I.A.C. owing to the lack of contrast throughout each drop. Similarly, the image on the screen in Fig. 6.2.1 is of a secondary dispersion and the same 'doughnut' effect is present. The use of dyes, the application of which is limited by their surfactant effect, and elaborate photographic development techniques failed to produce the required image contrast. To obtain high contrast images suitable for analysis on the Quantimet, the following two techniques were developed:

- (i) the use of parallel light to produce Schlieren effects
- (ii) the use of light emitting scintillating compounds

### 6.2.2) Schlieren Photography

The formation of Schlieren images depends essentially upon two superimposed optical systems<sup>(186)(187)</sup>. One produces general illumination and forms a silhouetted image of opaque objects. The other produces variations in light intensity within the subject area of transparent subjects dependent upon how the light is refracted within the Schlieren field. Shadow graphs, Interferometry and

\* For Quantimet 720 - read "Quantimet."



Fig. 6.2.1. QUANTIMET 720



Schlieren Photography all rely upon the deviation by the gradients of refractive index in the medium to produce images of different light intensity. These techniques are sufficiently sensitive to detect thermal and mass concentration gradients and as such are particularly useful in studying interfacial phenomena. Some of the more important applications in the study of interfacial phenomena associated with mass transfer have been presented by Sawistowski<sup>(20)</sup>. Generally, the optical arrangements are specifically designed for the particular needs of the experiment, but Lewis<sup>(57)</sup> and Liepman<sup>(75)</sup> have reviewed the more general scientific applications of Schlieren systems.

#### Experimental Arrangement for Schlieren Photography and Shadowgraph

A 250 watt mercury arc light with a variable iris diaphragm provided a source of light which was first condensed then passed through a pinhole onto the first parabolic mirror. The reflected beam of light was passed through the 6" diameter column onto a second parabolic mirror which in turn converged the light onto a photograph plate via a knife edge. The pinhole and knife edge were situated at the focal points of the respective mirrors, and accurate positioning was essential for high quality images - Fig. 6.2(a).

Initially, the 6" column was enclosed in a perspex box, and later in a glass box filled with the liquid which was used as the continuous phase within the column. Difficulties were encountered owing to the optical sensitivity of the column wall thickness with regard to the incident light path lengths. Similarly, the heat stress mark in the glass box and the extrusion lines in the perspex were found to be sources of distortion. These

Fig. 6.2.2

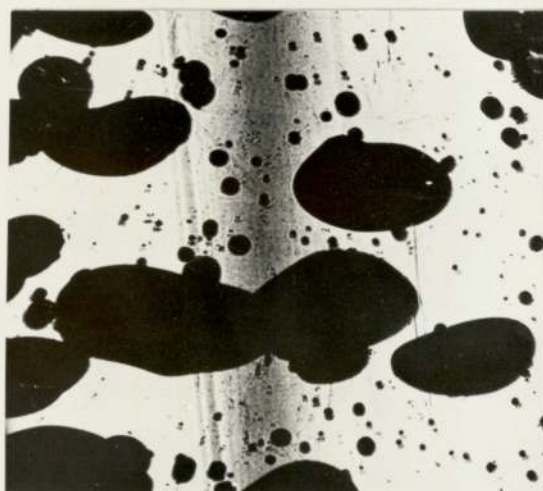
IMAGES OF DROPLETS AT THE EXIT OF THE BED



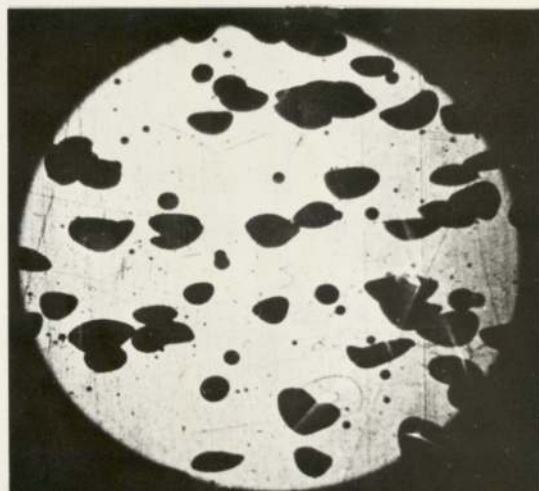
(A) Light emitting compounds with primary and secondary interference filters



(B) Normal - rear lighting



(C) Two mirror Schlieren



(D) Shadowgraph



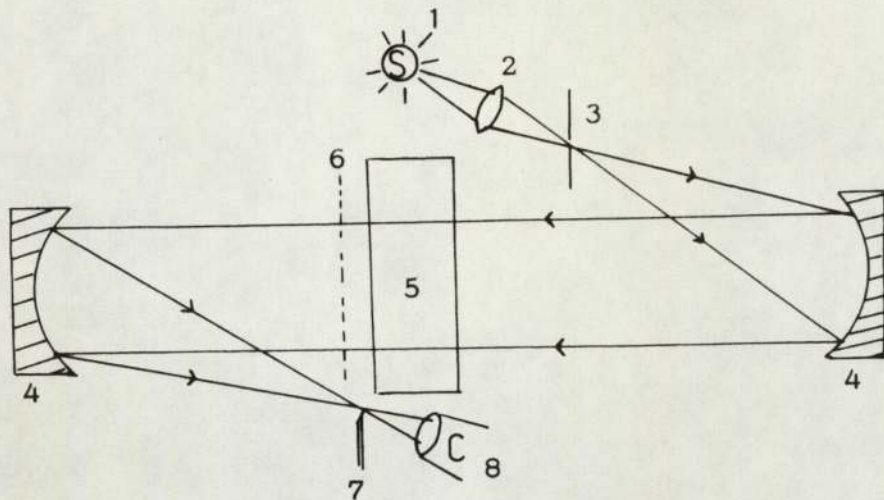


Fig. 6.2(a) Basic Arrangement - Two Mirror Schlieren with facility for Shadowgraph

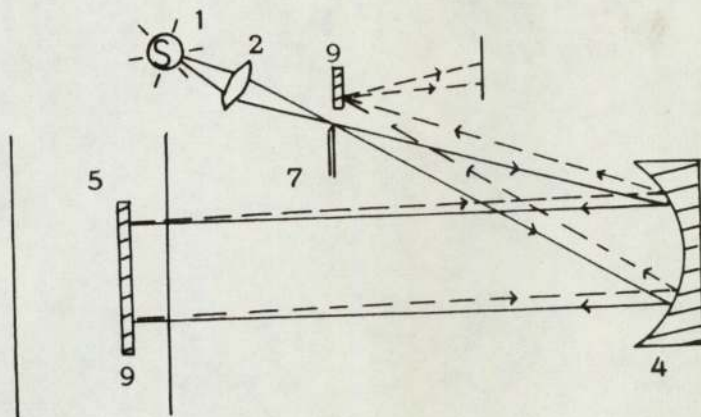


Fig. 6.2(b) One Mirror Schlieren - Including use of Plane Mirrors to minimize overlapping images

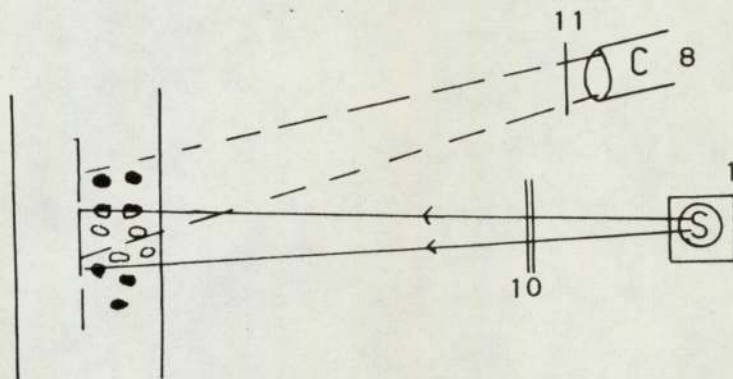


Fig. 6.2(c) Optical Arrangement for use with Light emitting compounds and interference filters

## NOMENCLATURE For Figs.(6.2.a-c)and(6.3.3)

### Fig.(6.2) - Optical Arrangements

1. Light source - Mercury Arc Lamp
2. Condenser
3. Pin-hole - (to obtain a "point" light source)
4. Parabolic mirrors with accurate focal point
5. Schlieren field, i.e. 6" diameter column
6. Transparent sheet for shadowgraph
7. Knife-edge - to separate images
8. 35 mm camera
9. Plane mirror
10. Filtraflex-R-UV Primary Interference Filter
11. 49 mm Skylight 1 A UV Camera Lens Filter - Secondary Filter

### Photographic Details

- a) Camera - Asahi Pentax Spotmatic 35 mm
- b) Film - 2485 Kodak high speed recording film 35 mm  
Estar - AH - base A.S.A. 1200 - 6000
- c) Developer - Kodak 857
- d) Scintillator dye Di-methyl Popop  $C_{26}H_{20}N_2O_2$   
1,4,-Di-(2-(4-methyl-phenyloxazolyl))-benzene  
Solubility in toluene = 3.9g/lit at 20° C  
Supplied by Koch Lite Laboratory Ltd.



problems were overcome by using a 6" diameter column with an 8" diameter crosspiece, as shown in Fig. 5.2.1. The ends of the crosspiece were sealed with high quality sheet glass using perspex flanges.

A Schlieren image using two mirrors is shown in Fig. 6.2.2 (C). The poor quality is attributable to the optical error inherent in the positioning of the two mirrors and also to the use of a non-finite light source. However, an image of sufficient contrast was obtained by inserting a semi-transparent material, such as ordinary tracing paper, at the rear of the column. The Shadowgraph thus produced was recorded using a high speed film (Fig. 6.2.2(D)). One disadvantage of the above methods was that the parallel beam of light had to travel the full diameter of the column. Consequently, at high flow rates, the drop number concentration was high and overlapping of recorded images led to problems in the classification by the Quantimet. Owing to the property of feature recognition by contrast changes at a boundary, the Quantimet cannot isolate overlapping images. To minimize overlapping, a plane silvered mirror was supported within the column above the packed section to reflect back the parallel beam of light. In this way, the light only travelled through a given fraction of the column diameter. The number of drops within the light path was less, thus proportionally reducing the probability of images overlapping (Fig. 6.2(b)).

Investigations were carried out into the effect of the 8" crosspiece and the plane mirror on the process of coalescence. No apparent differences were found in mean drop diameters, probably due to the fact that both are positioned above the packed section.



Schlieren techniques can be applied with equal success to organic - water and water-organic systems, also to systems where the density of the drop is greater than the continuous phase density. However, problems may arise with the positioning of the plane mirror below the packing, and with adhesion of drops to the mirror. These problems can be overcome by the design of a suitable mechanical device for supporting the mirror and by preferential surface treatment of the plane mirror to inhibit wetting effects.

### 6.2.3) The use of interference filters and light emitting compounds to produce high contrast images

It was considered that if compounds which emit light were photographed in the absence of external light sources, an image of high contrast would be obtained, suitable for analysis on the Quantimet.

An oil-soluble dye "Rubrene" was initially chosen, as the compound had the highest optical density in the emission spectra of the more common non-surfactant dyes. Unfortunately, several hours after the dye had been added to the organic phase, the light emitting properties deteriorated rapidly. The high cost and the exceptionally hazardous synthesis of this compound made its prolonged usage prohibitive. An intensive literature search led to the selection of a "scintillator" named dimethyl - popop.

The optical arrangement employed is shown in Fig.6.2(c). A standard mercury light, whose emission spectra coincided at certain wavelengths with the absorption spectra of the dye, was used as the light source. The light was first collimated, then passed through a Filtraflex R-UV Interference Filter, which had



transmittance peak at  $366 \text{ \AA}$ , (+ 1% tolerance). This was equivalent to the absorption peak of the dimethyl popop Fig.6.3.3. The resulting emission spectra of the activated dye was then photographed with the use of a camera lens UV filter, Fig.6.2.2(A).

One important criteria in the photography was that all external light sources had to be eliminated to reduce smearing effects which would reduce the contrast. Conversely, the photographic technique was complicated by the low levels of light intensity and because the drops were moving. To overcome this, a high speed recording film with an ASA rating 1500 - 6000 was used. The photographic details are given in Table(6.2). Inherent in the high ASA rating is the disadvantage of the loss of definition. However, this was not found to be significant with relatively large objects i.e. drops in primary dispersions. One advantage of this film is its sensitivity in the region corresponding to the emission spectra of dimethyl popop.

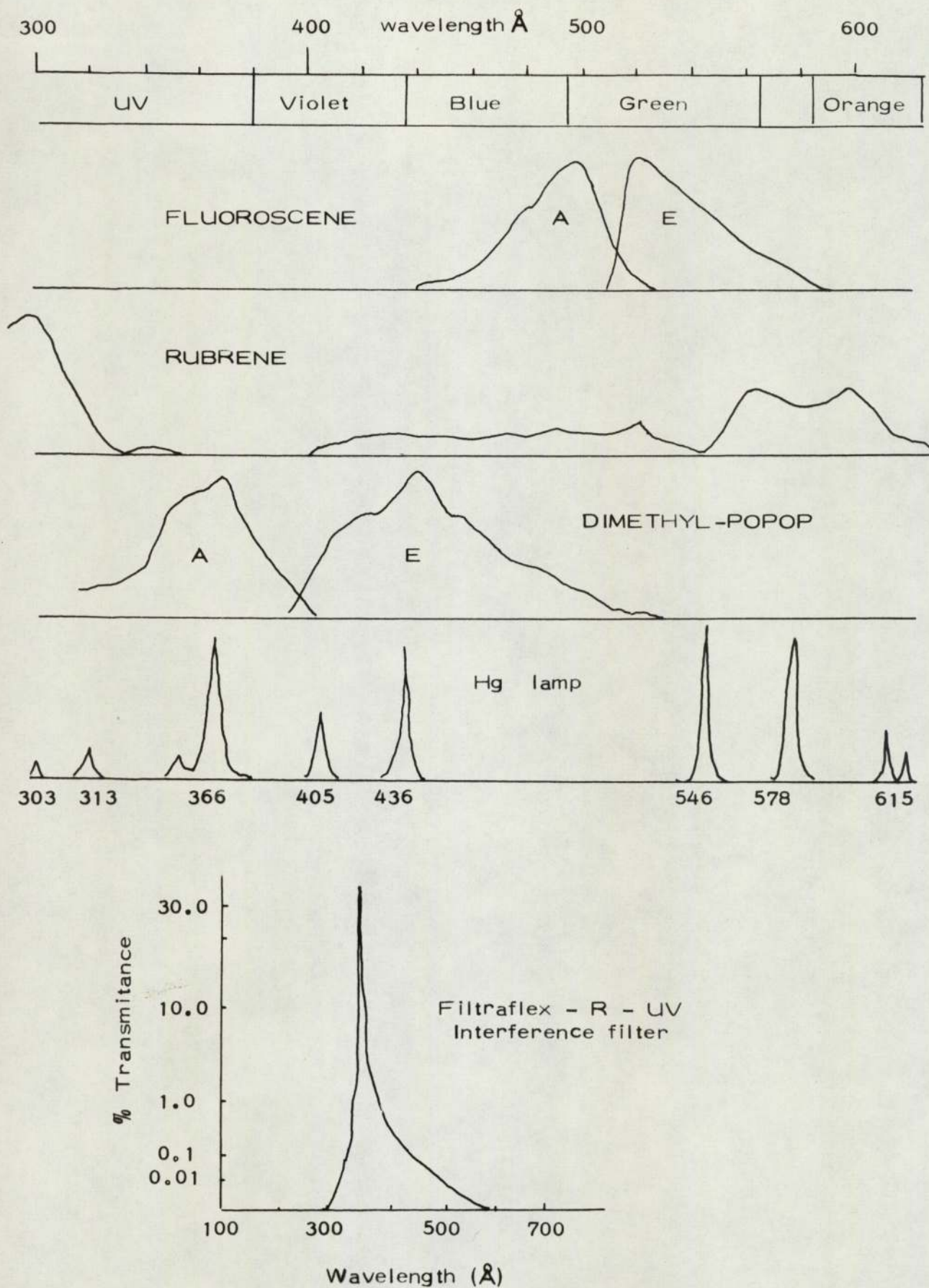
The use of primary and secondary interference filters and light emitting dyes can be applied to both organic-water and aqueous-organic systems. Particularly so in the latter case, as the most common water soluble dye is fluorescene. This compound has a very high value for the emitted light intensity and thus will produce excellent images. A further advantage of this optical technique is that observations could be made of the droplet behaviour within the packed section of the glass ballotini.

### 6.3) Evaluation of the mean drop size with the Image-Analysing Microscope

Fig.6.2.1 shows the Quantimet 720 used for analysis of the mean droplet diameter. During this study, the input of images from 35 mm negatives was achieved by replacing the microscope

Fig. 6.3.3

### ABSORPTION & EMISSION SPECTRA





attachment with that of an epidioscope. (The mode of operation<sup>(89)</sup> has been described fully elsewhere, and only the basic operational procedures are presented in this study). The chord length dial (A) is decreased from a maximum value until the largest particle is identified on the TV screen by a small dash. As the chord length value is decreased further, objects of decreasing size are identified. The numerical value of the objects identified is represented in a cumulative form on the number count meter (B). Thus for each negative, a series of dial readings is taken for the respective number count meter readings. To speed up data handling, the above values were punched directly on to paper tape for use with Program 2 on a Honeywell Computer ( Appendix 3.2.).

Initially, the instrument was calibrated by equating the chord length dial values to the diameter of a series of blackened circles. During analysis of the experimental data, certain factors have to be taken into consideration. The exit drops are usually in the form of oblate spheroids, hence both the major and the minor axes must be measured. However, the Quantimet can only evaluate dimensions in the horizontal direction<sup>(89)</sup>. To record both the major and minor axes the negative was first analysed in one direction, then the image was turned through  $90^{\circ}$  and the procedure repeated. A problem arose in matching the horizontal and vertical dimensions for each individual droplet. This was not possible directly, but a statistical approach was tried and found to be successful. A computer program was written to 'sort' the respective horizontal and vertical diameters in order of decreasing value. The largest diameter in the horizontal direction was paired with the largest in the vertical direction. This was repeated for the remaining values until one of the values was

exhausted. The paired values were used to calculate the Individual drop diameter and subsequently the mean drop diameter for each negative (Appendix A.3.3). These values were denoted as sorted means and analysis was carried out to evaluate the percentage error between the sort routine and direct measurement technique.

Data from Runs nos. 21 and 23 was evaluated for the mean error and mean percentage spread. This data represents 50 negatives each with a mean diameter evaluated from a distribution of drop sizes. The values quoted in Table 6.3 indicate the difference between sort and measured routines for all negatives in each run respectively. The significance of this approach is discussed fully in the evaluation of exit drop mechanisms (Section 9.2).

Table 6.3

Run	% Mean Error		% Standard Deviation		% Spread at 99.7% Confidence Limit	
	$d_{xt}^S$	$d_{xt}^V$	$d_{xt}^S$	$d_{xt}^V$	$d_{xt}^S$	$d_{xt}^V$
21	-1.7641	-2.8520	6.25	5.425	$\bar{+}$ 4.09	$\bar{+}$ 3.55
23	-0.3151	-1.8765	0.329	1.429	$\bar{+}$ 0.226	$\bar{+}$ 0.81

The mean percent error between the measured and sort is shown to be very low. However, the sort value appears to be slightly higher in all cases. The spread of the individual errors around the mean error is shown to be within 5% for a 99.7% Confidence Limit. Thus it was indicated that the spread and the mean error is within limits of reasonable acceptance.



CHAPTER 7.

MATHEMATICAL MODELS

## 7) Introduction

Generally the hydrodynamics within a packed bed have been classified with respect to the wetting properties of the dispersed phase and, to a lesser extent, the inlet drop size.

Many qualitative hypotheses have been suggested for the coalescence mechanisms inherent with the above dispersion characteristics, and these are the subject of much debate. In order to clearly define the coalescence mechanism within a packing, a systematic approach is presented, based on the following:

- (i) The application of film drainage models to the droplet hydrodynamics within a packing.
- (ii) An idealized model for drop behaviour at an orifice.
- (iii) A model for the hydrodynamic behaviour of droplets in a representative packing arrangement within a packed bed.

### 7.1) Single Drop Studies

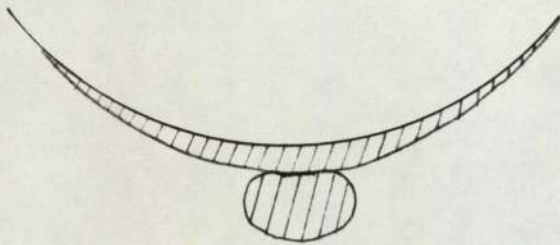
Fig. 7.1 shows the different forms of droplet behaviour that could possibly take place in a bed of uniform spheres.

Figs. 7.1.(A) and 7.1.(B) represent the case where the dispersed phase wets the packing, subsequently forming a film. In the first case (A) the drop coalesces with the film on the packing surface by drop-interface mechanism. Alternatively, the film formed, as in Fig.(B) will eventually drain through the bed until a restriction is reached. Dependent on the balance of the pressure gradient forces and wetting characteristics, the void may be filled with the dispersed phase, thus presenting

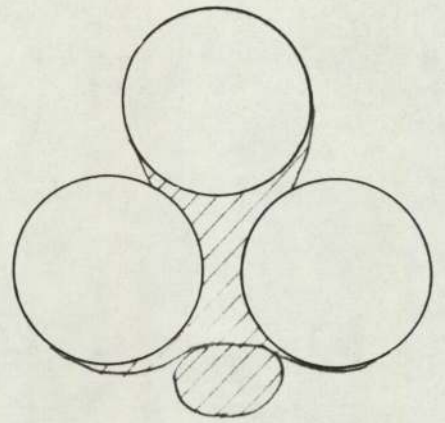


Fig. 7.1

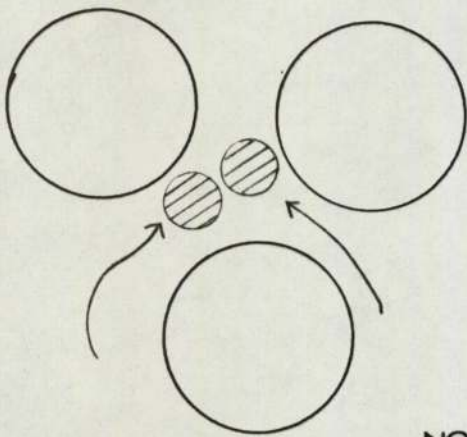
POSSIBLE COALESCENCE MECHANISMS IN A PACKED BED



(A) WETTED SURFACES

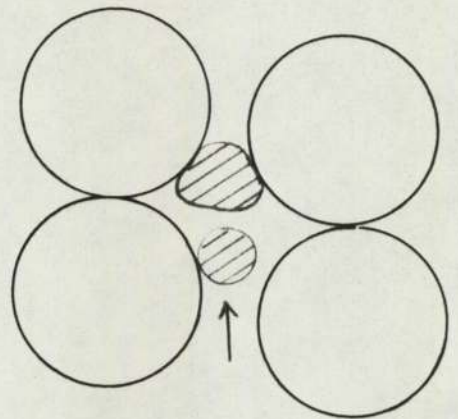


(B)

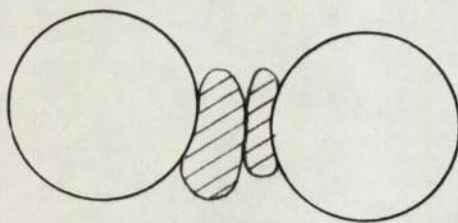


(C)

NON-WETTED SURFACES

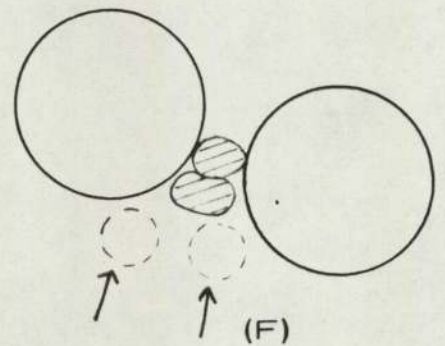


(D)



(E)

JOSTLING



(F)

an interface with which subsequent drops can coalesce.

In the non-wetted case, coalescence could occur by a drop-drop mechanism, either between two freely moving drops (Fig.7.1C) or between one moving drop and another held in a packing instercies (Fig.7.1D).

Alternatively, two drops enter the packing void simultaneously and squeeze through with an assumed rolling action, or the two drops jostle for priority in the void before passing through, as shown. The change in drop profile assists film drainage and coalescence takes place by some unknown mechanism.

#### 7.1.1) Film Drainage Models

The important criteria for all the above mechanisms of coalescence is whether the contact residence time between a 'free droplet' and the dispersed phase hold-up is sufficient for coalescence to take place. The theory of film drainage rates and coalescence times has been extensively reported in the literature. Investigation of drop-drop coalescence has shown that the drop contact time is very low  $\sim 0.05$  secs., and hence, for the non-wetted packings used in this study, this mechanism would seem most suitable. However, no work has been reported on the observation of drop-drop coalescence within packed beds. Moreover, the theoretical approach to predict film drainage rates has not been accurately defined. Scheele<sup>(33)</sup> et al reported that mathematical analysis failed by several orders of magnitude to predict the film thinning rates - hence they concluded that no satisfactory model exists to predict coalescence times for the dynamic situation of drop-drop coalescence.

However, most attention has been paid to the situation of coalescence of a single droplet at a plane interface. This work



has been reviewed earlier and several models were selected for analysis of the coalescence times, as shown in Table 7.1.1. The physical properties used in the evaluation of these models were taken for a toluene-water system (Appendix A.2).

Experiments using a toluene-water system showed that the mean coalescence time of 20 drops ( $\approx$  0.4 cms diameter) was 4.1 seconds. This compares favourably with that predicted by the eqn. of Jeffreys and Hawksley<sup>(16)</sup> who considered the factors affecting coalescence times and produced the following dimensional analysis: -

$$t_{\frac{1}{2}} = 4.5 \times 10^5 \left( \frac{\mu^{\frac{1}{2}} \Delta \rho^{1.2}}{\gamma^2} \right) \left( \frac{T}{25} \right)^{-0.7} \mu^{\frac{1}{2}} d^{0.02} \left( \frac{\gamma}{\mu} \right)^{0.001} \left( \frac{\gamma}{\mu^{\frac{1}{2}}} \right)^{0.91} \quad (7.1)$$

Later, Jeffreys and Lawson<sup>(25)</sup> modified this by stating that the temperature affected all physical properties and thus the following correlation was proposed:-

$$\frac{\gamma t}{\mu d} = 1.32 \times 10^5 \left( \frac{L}{d} \right)^{0.18} \left( \frac{d^2 \Delta \rho g}{\gamma} \right)^{0.32} \quad (7.2)$$

The correlation was found to fit their experimental results to  $\pm$  20%.

On substitution of the physical properties of toluene, and evaluating for effect of the length of fall 'L' and the drop size 'd', the following times 't' were obtained:

d = 0.2 cms	L = 1.0 cms	t = 3.1 secs
d = 0.2 cms	L = 10.0 cms	t = 5.2 secs
d = 0.4 cms	L = 1.0 cms	t = 3.7 secs
d = 0.4 cms	L = 10.0 cms	t = 5.6 secs

The above values would suggest that the order of magnitude is between 1 and 10 secs. However, from inspection of Table 7.1.1., the evaluated coalescence times appear to be greatly dependent on the values chosen for the film thickness at rupture.

Table 7.1.1

<u>Ref.</u>	<u>Model</u>	<u>Film Thickness at rupture</u> $h_2$ (cms)	<u>Approximate coalescence time</u> (secs)
(7)	Deformable Drop	$10^{-4}$	9.8
	Rigid Interface	$10^{-5}$	980
	Uniform Film	$10^{-6}$	98000
(35)	Rigid Drop	$10^{-4}$	$2.0 \times 10^{-3}$
	Rigid Interface	$10^{-5}$	
	Non-Uniform Film	$10^{-6}$	
(15)	Deformable Drop	$10^{-3}$	0.84
	Deformable Interface	$10^{-4}$	84
	Uniform Film	$10^{-5}$	8400
(1)	Rigid Drop		
	Deformable Interface		
	Non-Uniform Film		
	for $\lambda = R/d > 1$	$10^{-4}$	10
		$10^{-5}$	100
	for $\lambda = R/d < 1$	$10^{-4}$	1
	$10^{-5}$	10	

(See Table 1.1.3(A) for equations)

All the models used are based on an idealized drop or interface profile, but more important, as the evaluated coalescence times indicate, is the selection of  $h_2$ , the critical film thickness at rupture. Values of  $h_2$  have been reported in the range  $10^{-3} - 10^{-8}$  cms and, dependent on the choice of  $h_2$ , it is possible to obtain coalescence times differing by several orders of magnitude.



(16)(28)(29)

Several different techniques have been used to evaluate the film thickness at rupture, but no comment has been made on their accuracy. It was not within the scope of this study to investigate film thickness at rupture, but it can be assumed that a different phenomenological picture will exist for different systems. For example, some workers have used inhibitors<sup>(9)</sup> to slow down film drainage and facilitate experimental observation. The effect of inhibitors on the interfacial mobility is still the subject of much research, but no firm conclusions have been reached. Likewise, it could be postulated that the process of film drainage would be different between very viscous and non-viscous systems.

In a recent paper, Rushton and Davies<sup>(90)</sup> have shown the limitations of simplified models for film drainage rates. Often it was assumed that the radial velocity at the fluid-fluid interface was zero, ignoring the possibility of internal circulation within the drop. Moreover, it has been shown that internal circulation within the drop, set up as a consequence of interfacial shear forces, significantly influences the flow field, particularly in the entrapped film separating the drop from the bulk interface. This effect increases with the phase ratio of viscosity and becomes significant when the ratio is of the order of 10. In some cases, when the ratio is high the effect of viscosity on the internal circulation can lead to flow reversal and film renewal in the entrapped continuous phase.

In brief, the theoretical prediction of coalescence times is inconclusive, owing to the variation in film thickness ( $h_2$ ) at rupture for different systems; the inaccuracies of the models; and the uncertain range of physical properties for which each model is applicable. Moreover, the evaluation of  $h_2$  in a practical

situation within a packed bed presents considerable difficulties.

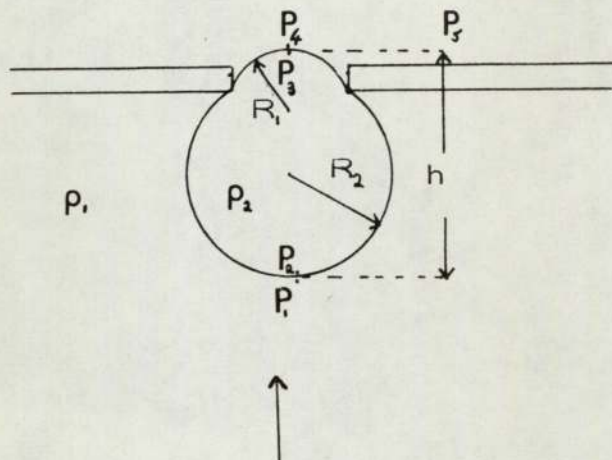
To overcome the difficulty in predicting coalescence times, an alternative approach was made, based on the hydrodynamic behaviour of a single droplet at a standard orifice.

### 7.2) Idealized drop at a plane orifice

For the hypothetical situation of a drop at an orifice (Fig. 7.2) it is possible to determine the relationship between the buoyancy and surface forces in terms of the drop dimensions with the following assumptions:

- (I) No viscous or drag forces act on the drop, i.e. it is purely a balance between buoyancy and interfacial forces;
- (II) The radius  $R_1$  is equivalent to the radius of the void;
- (III)  $R_1$  and  $R_2$  are the equivalent means of the respective segment radii, i.e. the segments are symmetrical about  $R_1$  and  $R_2$ ;
- (IV) The contact angle of the upper segment is equal to  $180^\circ$ , i.e. complete non-wetting is assumed.

Fig. 7.2







On substitution of the above values and solving the resulting quadratic, the following roots are found:

$$x = 1.94 \text{ or } 0.5 \text{ cms for a cubic void diameter} = 0.414 \text{ cms}$$

$$x = 5.27 \text{ or } 0.185 \text{ cms for a triangular void diameter} = 0.185 \text{ cms}$$

The roots of the quadratic equation represent the diameter of the drop when the buoyancy/surface forces just balance. On inspection it can be shown that retention occurs for drop diameters between the respective upper and lower limits. This fact is of great importance when applied to droplets within a packing. For an individual drop of a particular system, passage will take place if the drop diameter is less than the lower root value for that particular system. If the drop is above the lower root value, then retention occurs until subsequent drop coalescence forms a drop equal or greater than the upper root value. The buoyancy forces now exceed the surface forces and the coalesced mass breaks through the packing restriction.

Experiments were carried out using light emitting dyes and observations were made of droplet behaviour within a bed of ballotini. These observations confirmed that drops followed the above predicted behaviour. It was also observed in some cases that once break-through had been achieved, rivulets of dispersed phase passed through the remainder of the bed to the exit in a manner similar to that described by Hazlett<sup>(78)</sup> and Thomas<sup>(50)</sup>.

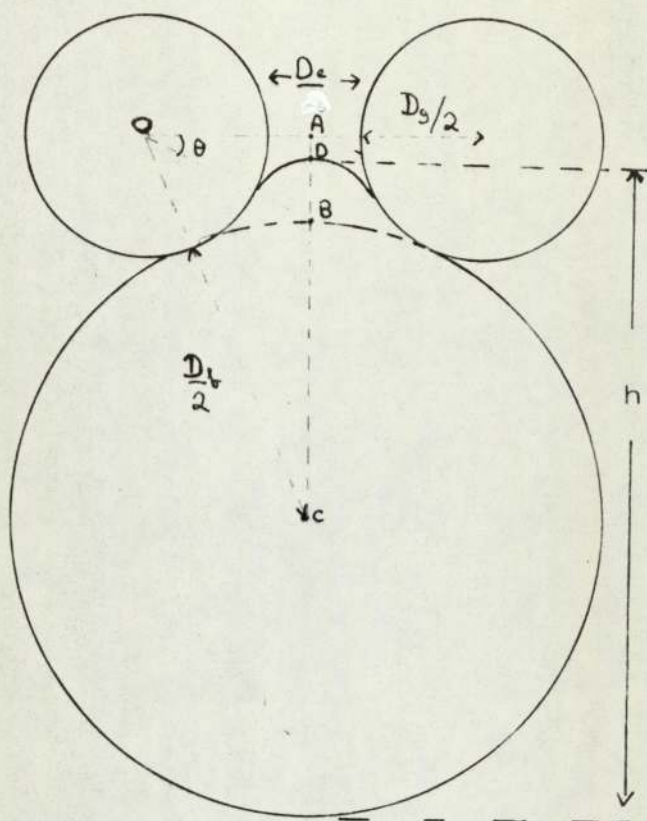
Therefore, if a mean void diameter can be determined for a particular packing and the inlet drop diameter and physical properties are known, then coalescence can be predicted by consideration of the previous theory.

In an attempt to refine the idealized approach, a more detailed consideration was carried out for the upper and lower limit of a drop at a representative packing arrangement of ballotini.

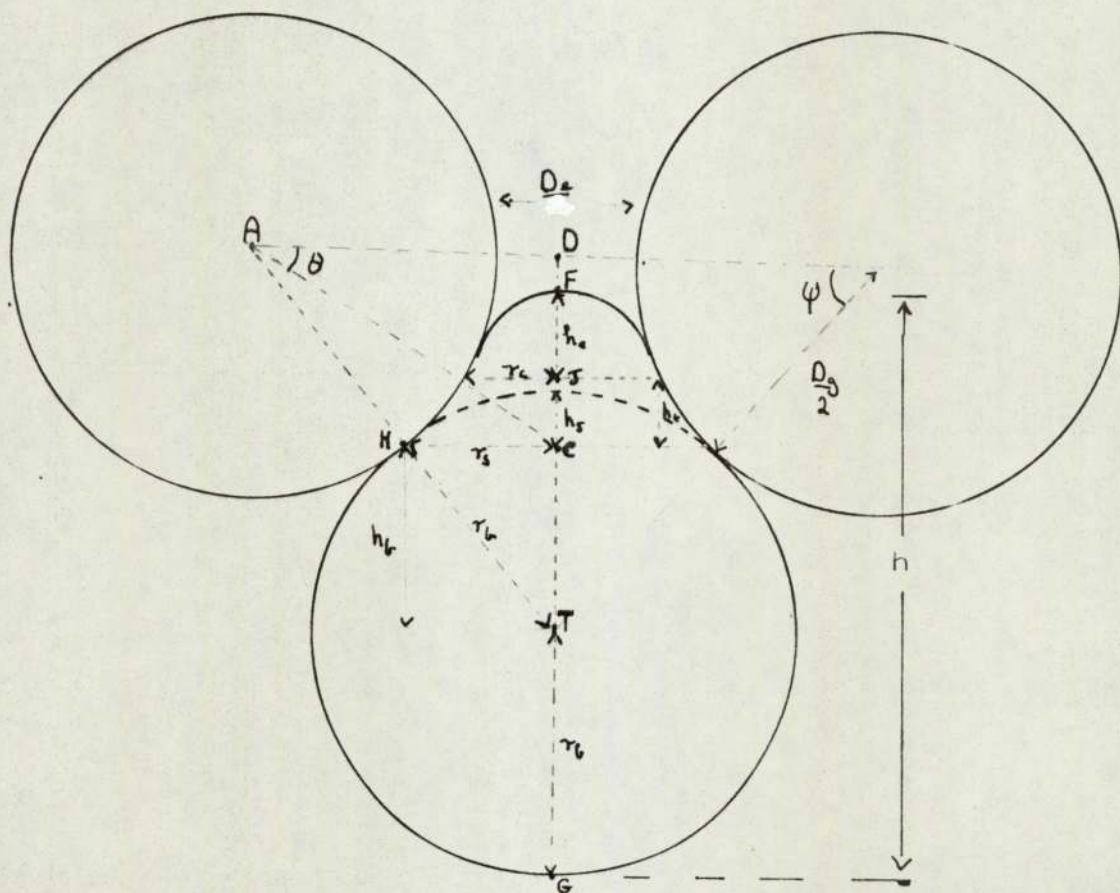


Fig. 7.3

IDEALIZED DROP RESIDING IN A BALLOTINI PACKING RESTRICTION



(B) LARGE DROP



(A) SMALL DROP

### 7.3) A model for a drop residing in a ballotini packing restriction

Figs.7.3(A) & 7.3(B) show schematically a small drop and a large drop residing at a ballotini restriction. In both cases,  $R_1$ ,  $R_2$  and  $h$  need to be solved with respect to the original drop diameter. However,  $R_1$ ,  $R_2$  and  $h$  are dependent on each other and have to be determined with respect to the diameters of the void, ballotini and inlet drop. The analysis of both the small and large drop can be carried out by considering Fig.7.3 A and using the assumption given in Section 7.2.

Radius of Upper Segment  $R_1$  (denoted in Fig. 7.3 as  $r_1$ )

$$AD = \frac{D_g + D_e}{2} \quad (7.10) \quad \text{where } D_g = \text{diameter of ballotini} \\ D_e = \text{diameter of void}$$

$$DC = \frac{D_g + D_e}{2} \tan \theta \quad (7.11) \quad \text{where } \theta = \text{the angle subtended} \\ \text{from the centre of packing} \\ \text{sphere (A) to the centre of the} \\ \text{leading interface (C)}$$

$$R_1 = r_1 = AC - \frac{D_g}{2} \quad (7.12) \quad \text{where } AC = \frac{D_g + D_e}{2 \cos \theta}$$

$$R_1 = r_1 = \frac{D_g(1 - \cos \theta) + D_e}{2 \cos \theta} \quad (7.13)$$

Radius of lower segment  $R_2$  (denoted in Fig.7.3 as  $r_b$ )

$$AT = \frac{(D_g + D_e)}{2 \cos \psi} \quad (7.14) \quad \text{where } \psi \text{ is the angle subtended} \\ \text{from (A) to the centre of the} \\ \text{lower segment (T)}$$

$$R_2 = r_b = AT - \frac{D_g}{2} = \frac{D_g(1 - \cos \psi) + D_e}{2 \cos \psi} \quad (7.15)$$

Height of the drop  $h$

$$h = r_b + DT - DF \quad (7.16)$$

$$DT = \frac{D_g + D_e}{2} \tan \psi \quad (7.17)$$

$$DF = DC - CF = \frac{D_g + D_e}{2} \tan \theta - \frac{D_g + D_e}{2 \cos \theta} - \frac{D_g}{2} \quad (7.18)$$



Substituting (7) (9) and (10) into (8)

$$h = r_b + \frac{D_g + D_e}{2} \tan \psi - \frac{1}{2} \left( D_g + D_e \left( \frac{\tan \theta - 1}{\cos \theta} \right) - D_g \right) \quad (7.19)$$

To evaluate equations (13) (15) (19) it is necessary to know the relationship of  $R_1$ ,  $R_2$  and  $h$  to the initial drop diameter  $D_{bo}$ .

This is found by equating the volume of the original drop to the following:

I Volume of upper segment

II Volume of truncated cone

III Volume of lower segment

Volume of upper segment of cone base  $V_I$

$$\text{General eqn.}^{(92)} \quad V_I = \frac{\pi h_t}{6} (3r_c^2 + h_t^2) \quad (7.20)$$

$$h_t = FJ = FC - JC = r_1 (1 - \sin \theta) \quad (7.21)$$

$$r_c = r_1 \cos \theta \quad (7.22)$$

Substituting (13) (14) into (12)

$$V_I = \frac{\pi r_1}{6} (1 - \sin \theta) (3r_1^2 \cos^2 \theta + r_1^2 (1 - \sin \theta)^2) \quad (7.23)$$

$$V_I = \frac{\pi}{6} r_1 (1 - \sin \theta) (3r_1^2 \cos^2 \theta + r_1^2 (1 - 2 \sin \theta + \sin^2 \theta)) \quad (7.24)$$

$$V_I = \frac{\pi r_1^3}{6} (1 - \sin \theta) (2 \cos^2 \theta + 2 - 2 \sin \theta) \quad (7.25)$$

Volume of truncated cone  $V_{II}$

$$\text{General eqn.}^{(92)} \quad V_{II} = \frac{\pi h_c}{3} (r_c^2 + r_c r_s + r_s^2) \quad (7.26)$$

$$GH = DC = \frac{D_g \sin \psi}{2} \quad \text{and} \quad RS = DJ = \frac{D_g \sin \theta}{2} \quad (7.27)$$

$$\text{and} \quad h_c = DC - DJ = \frac{D_g}{2} (\sin \psi - \sin \theta) \quad (7.28)$$

$$r_c = r_1 \cos \theta \quad (7.29)$$

on substitution of (7.28) and (7.29) into (7.26)

$$V_{II} = \frac{\pi}{6} D_g (\sin \psi - \sin \theta) (r_1^2 \cos^2 \theta + r_b r_1 \cos \psi \cos \theta + r_b^2 \cos^2 \psi) \quad (7.30)$$

Volume of lower segment

The volume of the lower segment can be calculated from the volume of sphere radius  $r_b$  less the volume of segment  $V_s$ , of height  $h_s$  and radius  $r_s$ .

$$\text{General equation } V_s = \frac{\pi}{6} h_s (3r_s^2 + h_s^2) \quad (7.31)$$

$$HP = h_b = r_b \sin \psi \quad (7.32)$$

$$h_s = r_b - h_b = r_b (1 - \sin \psi) \quad (7.33)$$

$$\text{and } r_s = r_b \cos \psi \quad (7.34)$$

Substituting (7.33) and (7.34) into (7.31)

$$V_s = \frac{\pi r_b}{6} (1 - \sin \psi) (3r_b^2 \cos^2 \psi + r_b^2 (1 - \sin \psi)^2) \quad (7.35)$$

$$V_s = \frac{\pi}{6} r_b^3 (1 - \sin \psi) (2 \cos^2 \psi + 2 - 2 \sin \psi) \quad (7.36)$$

$$V_s = \frac{\pi}{3} r_b^3 (2 - 2 \sin \psi + \sin \psi \cos^2 \psi) \quad (7.37)$$

$$V_{\text{III}} \text{ Volume of sphere } r_b: - V_s = \frac{\pi}{3} r_b^3 (2 + 2 \sin \psi - \sin \psi \cos^2 \psi) \quad (7.38)$$

$$\text{Total volume of deformed drop} = V_{\text{I}} + V_{\text{II}} + V_{\text{III}}$$

$$\text{Original drop volume } V_o = \frac{\pi D_{bo}^3}{6} = V_{\text{I}} + V_{\text{II}} + V_{\text{III}} \quad (7.39)$$

Therefore, on substitution of (7.25)(7.30) and (7.38) into (7.39) and simplifying

$$\begin{aligned} D_{bo}^3 = & r_b^3 (2 + 2 \sin \psi - \sin \psi \cos^2 \psi) \\ & + D_g (\sin \psi - \sin \theta) (r_1^2 \cos^2 \theta + r_b r_1 \cos \theta \cos \psi + r_b^2 \cos^2 \psi) \\ & + r_1^3 (1 - \sin \theta) (2 \cos^2 \theta + 2 - 2 \sin \theta) \end{aligned} \quad (7.40)$$

where  $r_1$  and  $r_b$  are given by equations (7.13) and (7.15)

The basic pressure balance equation (7.9) can only be solved when  $r_1, r_b$  and  $h$  are known; however, these terms are a function of  $\theta$  and  $\psi$  which in turn are related to  $D_{bo}, D_g$  and  $D_e$ . To enable analysis to be carried out, it was necessary to use the limiting condition at  $\theta = 0$ . This represents the critical point of



drop retention and drop passage. This can be explained by considering that at  $\theta = 0$ , the radius of the leading interface is equal to the minimum void radius, and consequently the surface forces acting on the drop are at a maximum. At this point, if the buoyancy and surface forces balance, then any further penetration of the leading interface will result in a decrease in the surface forces. Hence the drop will spontaneously eject itself by reason of the now dominant buoyancy forces.

Therefore, by use of the limiting condition  $\theta = 0$ , eqn(7.40) can be solved for  $\psi$  at given values of  $D_{b0}$ . This was carried out with a convergence procedure on  $\psi$  using a Honeywell 316 computer, as shown in Appendix (A.3.4).

Subsequently,  $r_1$ ,  $r_b$  and  $h$  can be evaluated for a given  $D_{b0}$ , and substituted into the basic pressure balance equation to evaluate whether the drop is in equilibrium at  $\theta = 0$ . The residual obtained on summation of eqn(7.9) is termed the E factor, and from inspection it can be seen that the following apply -

- when (a) E is + ve, drop passage will occur;
- (b) E is - ve, drop retention will occur;
- (c) E is 0, the drop is in equilibrium at the critical point of retention and passage.

CHAPTER 8.

DISCUSSION OF RESULTS

Inlet Model Studies using Single Nozzles



### 8.1) Inlet Model

A mathematical model has been presented to relate the buoyancy and surface forces in terms of drop size and shape in the aperture of a ballotini packing element. The quadratic equation describing the basic pressure balance over a drop at a packing restriction has been solved for the two roots. The lower root represents the point at which drop retention first occurs, and the upper root represents the point at which drop release takes place following retention.

Mathematically, the critical point of equilibrium between droplet retention and droplet passage is given for an E factor equal to zero when the drop dimensions are evaluated at  $\theta = 0$  (eqn. 7.9, 7.40). When the E factor is positive, the buoyancy forces are dominant and the drop will pass through the restriction. Conversely, for a negative E factor, the surface forces are dominant, and the drop is retained in the packing restriction.

Figs 8.1(A-D) illustrate the relationship between E and the variables of drop diameter, the physical property group and dimensions of the packing element. By holding two of the variables constant, the following are predicted:-

- (a) E values increase with increasing buoyancy values;
- (b) E values increase with increasing void diameters.

This is to be expected, but for increasing drop diameters, there exists a minimum in the E value. When the minimum is positive, Fig 8.1(A), then the drop will always pass through, irrespective of its size. If the minimum E value is negative, then in all cases, any increase or decrease in drop diameter will cause the E values to cross the axis, i.e.  $E = 0$ . The drop diameters at  $E = 0$  represent the two roots of eqn (7.9) at which the drop is in equilibrium at  $\theta = 0$ .

Fig. 8.1(A) VARIATION OF EQUILIBRIUM POINT  
WITH DROP DIMENSIONS AND SYSTEM PROPERTIES

Diameter of Sphere = 1.2 cms  
Diameter of Void = 0.497 cms

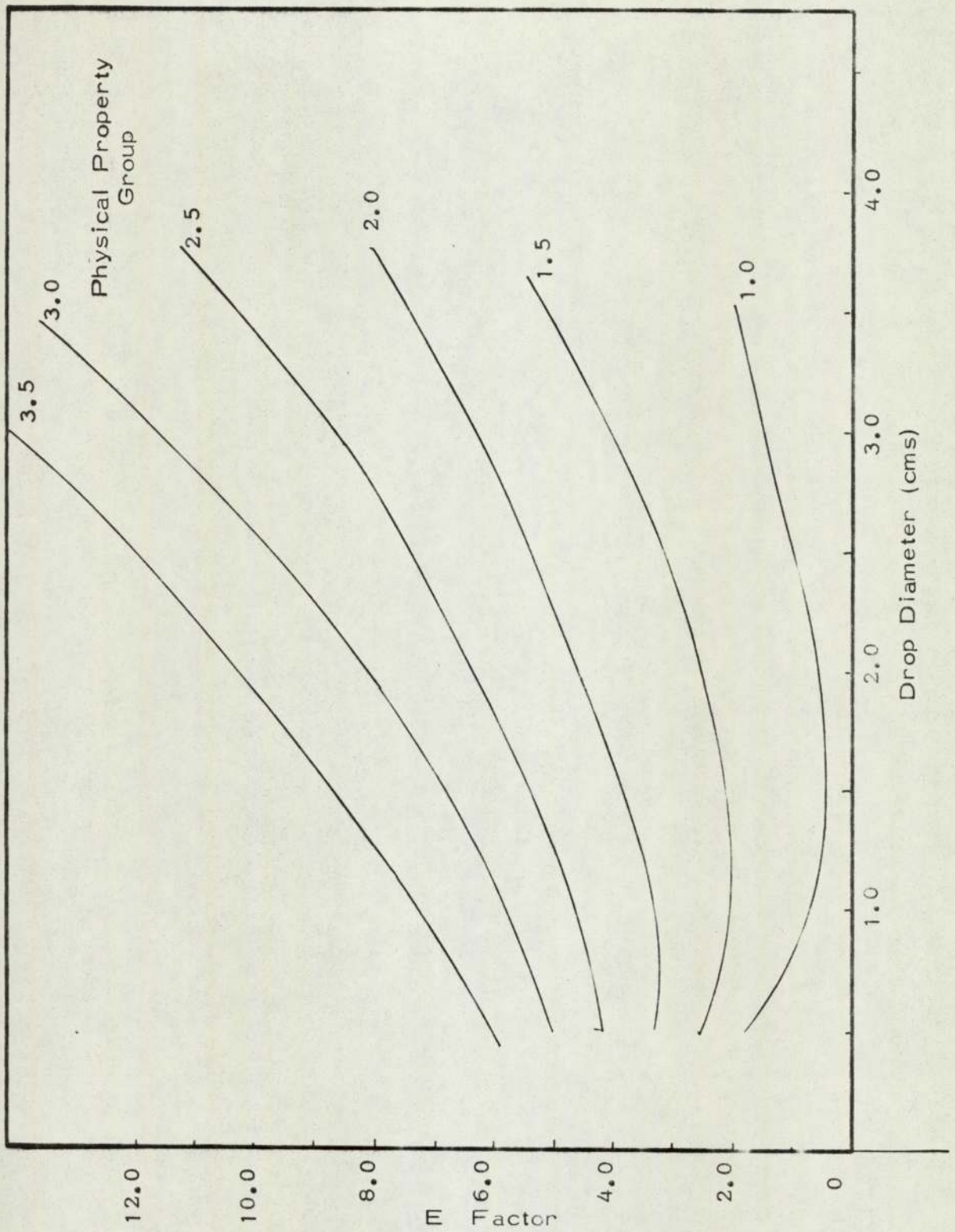




Fig. 8.1(B) VARIATION OF EQUILIBRIUM POINT  
WITH DROP DIMENSIONS AND SYSTEM PROPERTIES

Diameter of Sphere = 0.9 cms  
Diameter of Void = 0.375 cms

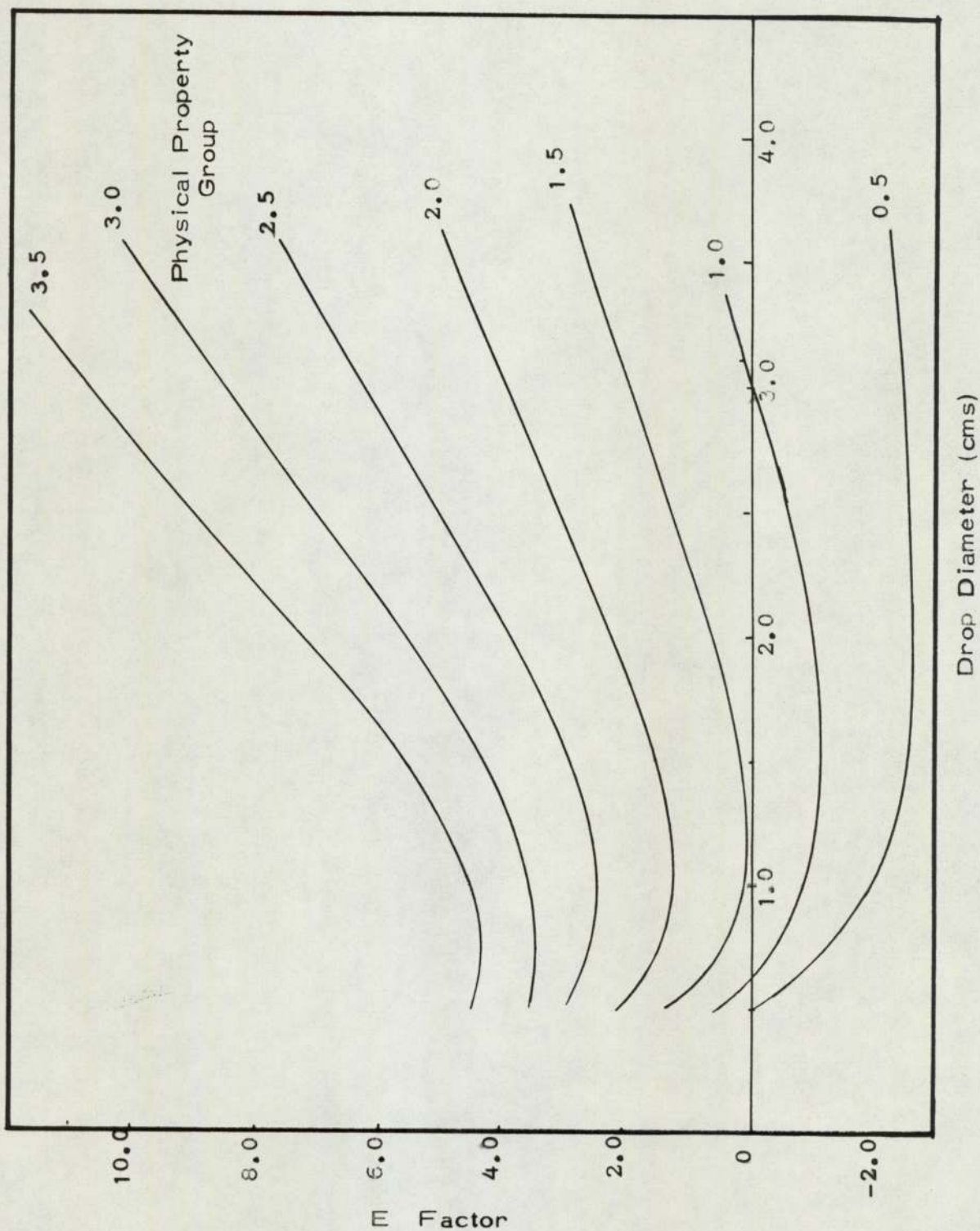


Fig. 8.1(C)

VARIATION OF EQUILIBRIUM POINT WITH  
DROP DIMENSIONS AND SYSTEM PROPERTIES

Diameter of Sphere = 0.6 cms  
Diameter of void = 0.248 cms

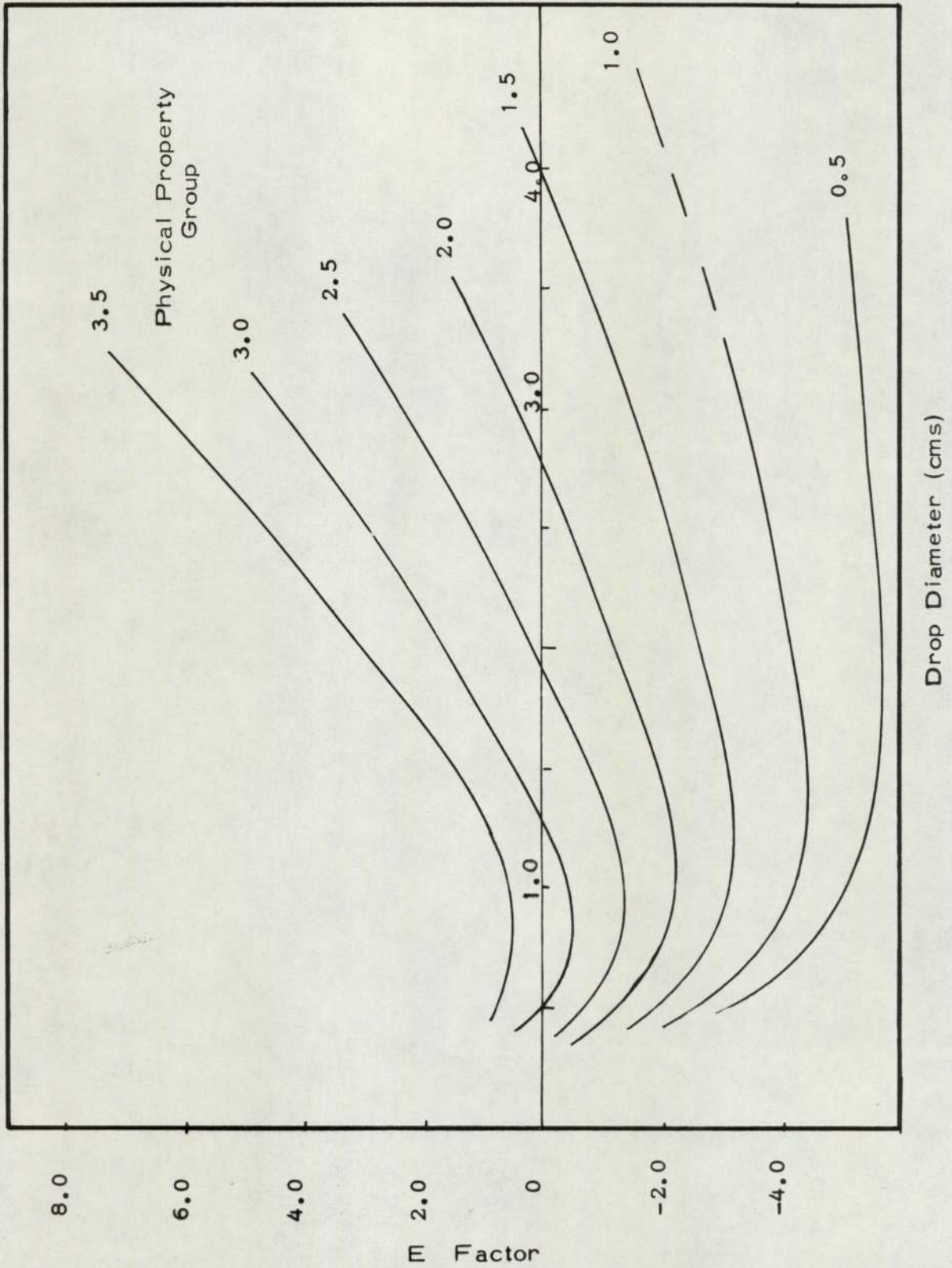
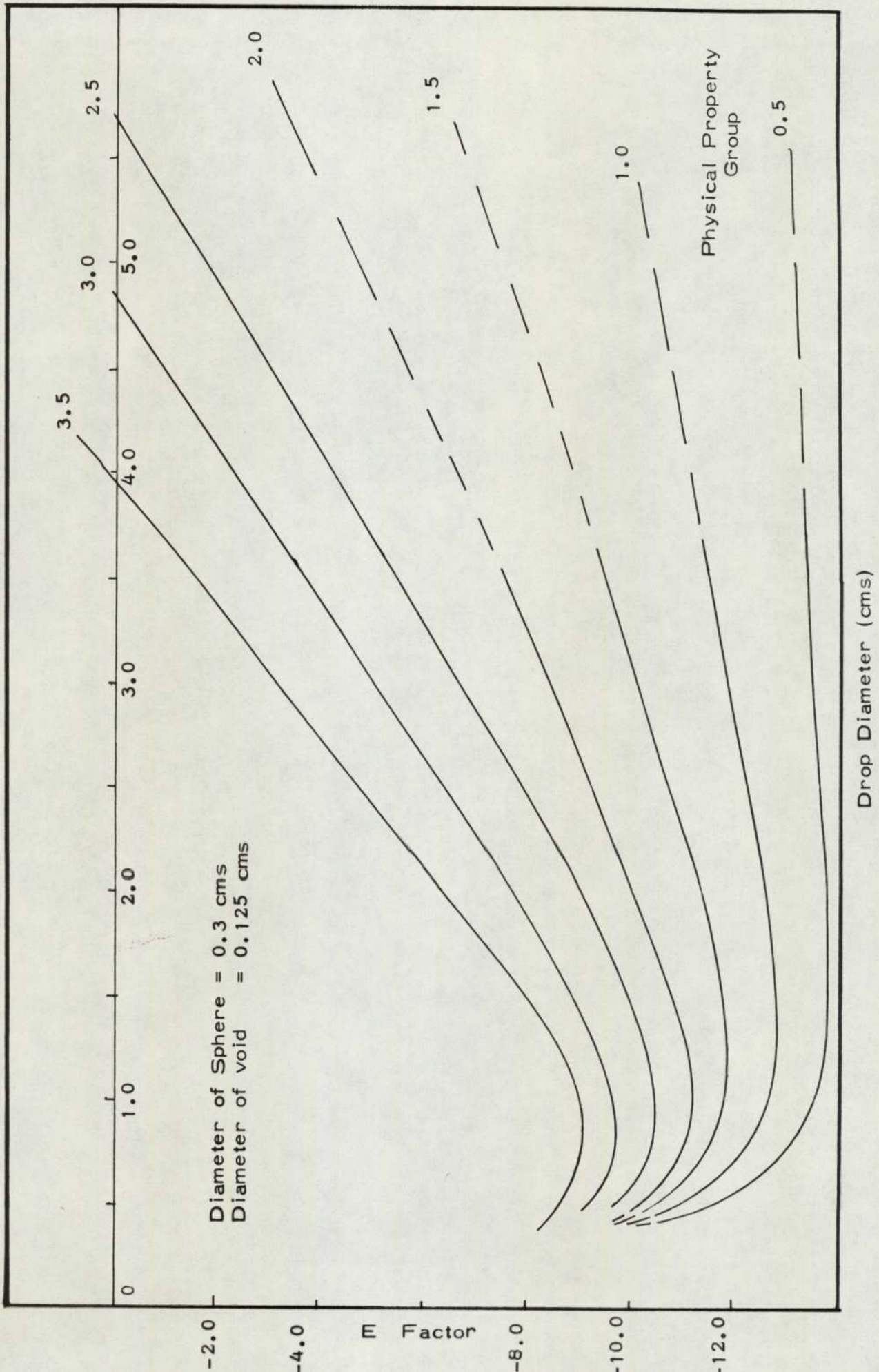




Fig. 8.1(D)

VARIATION OF EQUILIBRIUM POINT  
WITH DROP DIMENSIONS AND SYSTEM PROPERTIES



From inspection of Fig 8.1(B) it is seen that the lower roots represent the minimum drop diameter that will not pass through the restriction, and the upper root the maximum drop diameter that will be held in the restriction. As would be expected the range of drop diameters that will not pass through shows an increase for any decrease in the buoyancy force or void diameter.

To illustrate this more clearly, a second convergence procedure on the E values was carried out to determine the drop diameters which describe E values = 0 at  $\theta = 0$ . The results are shown in Fig 8.1.2, in which the drop diameters below the curves represent the retention of the drop for the respective physical properties of the system. Therefore, the range of drop diameters which will be held up can be predicted if the void aperture and physical properties are known.

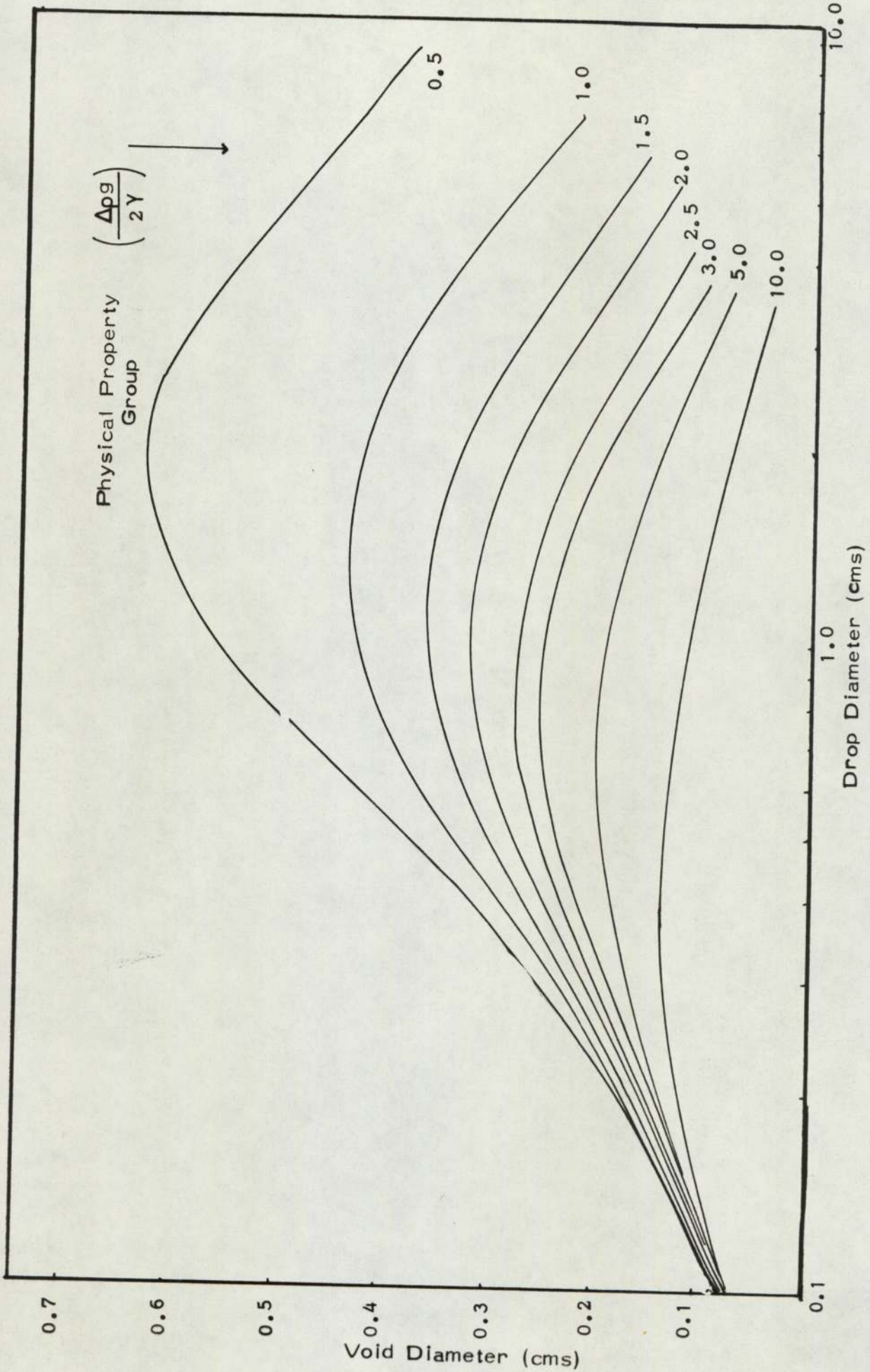
To test the applicability of the model, an experimental investigation was carried out using single nozzles. This covered both cubic and triangular ballotini geometries (Fig. 5.3.2). Drops formed at a sharp edged feed nozzle were allowed to rise into the restriction of a ballotini orifice. If retention was achieved, further drops were added until break through occurred. The apparatus and experimental technique is described more fully in Sections 5.3.1 & 5.3.2, and the results obtained are presented in Table 8.1.1.

To eliminate any kinetic energy which the drop may have obtained between release at the feed nozzle and entry into the packing restriction, the following technique was used. A specially shaped glass rod was inserted into the packing orifice to prevent passage. When the oscillation imposed by impact had been dampened, the rod was carefully removed, and drop behaviour was observed. To eliminate any wetting or adhesion effects, all glass surfaces were cleaned with acidified chromic acid, as described in Section 5.1.4(c).



Fig.8.1.2

RETENTION-RELEASE CURVES  
EVALUATED FROM FORCE-BALANCE CONSIDERATIONS  
Cubic Ballotini Geometry



System	Physical Property No. (cms) <sup>2</sup>	CUBIC			CUBIC			TRIANGULAR		
		d <sub>b</sub> (cms)	d <sub>vc</sub> (cms)	Lower limit Exp Theory (cms)	Upper limit Exp Theory (cms)	d <sub>vt</sub> (cms)	Lower limit Exp Theory (cms)	d <sub>vt</sub> (cms)	Lower limit Exp Theory (cms)	
Diethyl Carbonate - water	1.1	1.2	0.5	(0.72-NH)	NH	1.94	NH	0.22	0.3	0.25
		0.9	0.375	0.65	0.63	2.35	3.0	0.15	0.2	0.22
		0.6	0.26	0.40	0.32	4.1	6.5	0.12	0.2	0.15
Toluene - water	2.05	1.2	0.5	NH	NH	NH	NH	0.19	0.20	0.24
		0.9	0.375	(0.65-NH)	NH	1.9	NH	0.15	0.20	0.18
		0.6	0.25	(0.38-0.50)	0.45	2.5	2.6	0.11	0.20	0.14
Iso-Octane - water	2.9	1.2	0.5	NH	NH	NH	NH	0.20	0.34	0.28
		0.9	0.4	(0.8-NH)	NH	1.6	NH	0.14	0.25	0.17
		0.6	0.25	(0.45-0.55)	0.53	1.4	1.0	0.12	0.25	0.15
M I B K - water	11.1	1.2	0.5	NH	NH	NH	NH	0.19	NH	NH
		0.9	0.4	NH	NH	NH	NH	0.15	0.25	NH
		0.6	0.28	NH	NH	NH	NH	0.11	0.23	NH

(NH = No hold-up)

Table 8.1.1 DATA OBTAINED FOR SINGLE BALLOTINI NOZZLES AT LOWER AND UPPER LIMIT



The void diameters,  $d_v$ , were measured with a magnified graduated scale, owing to the difficulties in accurately positioning the ballotini in the cubic and triangular geometries. Each experiment was repeated 5 times and the results presented are an average value in all cases, except those in the brackets, which indicate special circumstances when the results were inconsistent.

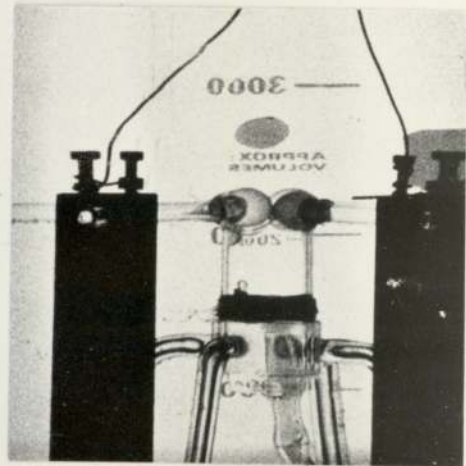
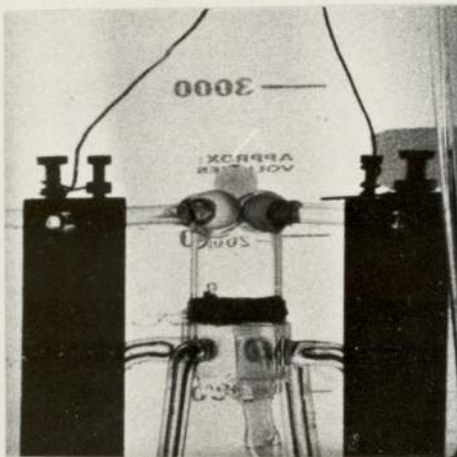
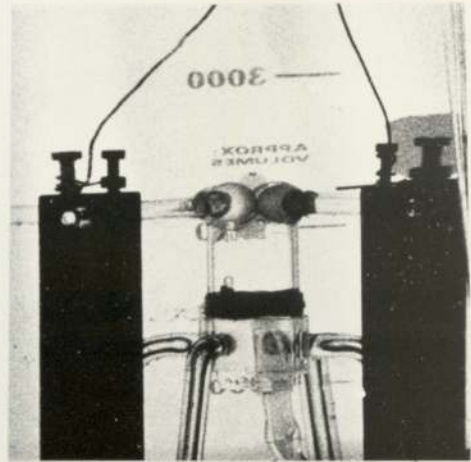
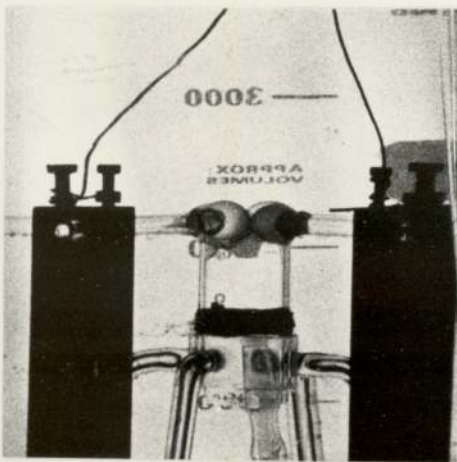
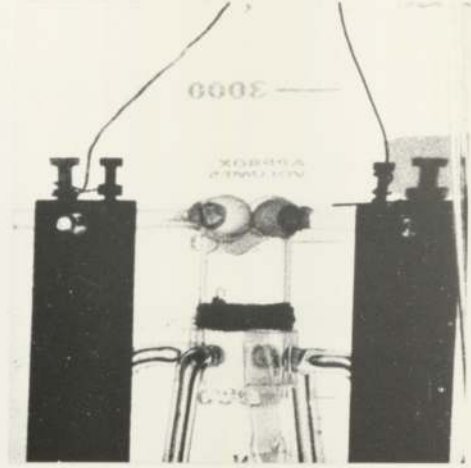
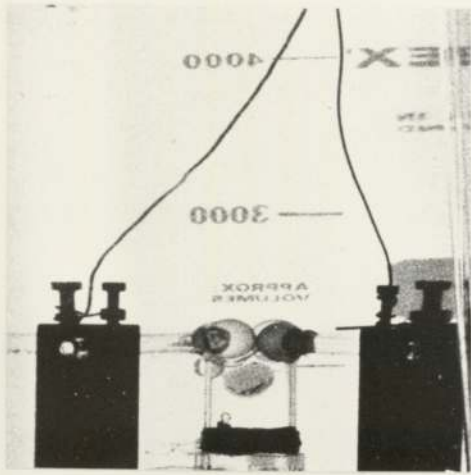
#### 8.2) Lower Limit

The experimental and predicted values for initial drop retention (i.e. - the lower limit) are in good agreement for the triangular geometry. However, for a cubic geometry, the agreement is less satisfactory. This was particularly evident at large drop sizes where 'no retention' was predicted but hold-up was obtained in practice. This may be because the model takes no account of drag forces acting on the drop, which would reduce the forces promoting passage. This effect is more evident with large drops because the effective surface forces are smaller and consequently, greater deformation is required during penetration and passage. A typical sequence of the drop deformation required for passage is shown in Fig. (8.2). However, for the results in brackets, the situation was difficult to reproduce experimentally and the range of behaviour is therefore quoted.

A severe limitation in the measurement of drop diameters which passed through or were retained was the inability of the feed nozzles to produce drop diameters which adequately covered the range required for experimentation. This was compensated for by promoting premature drop detachment by selective vibration of the feed line to the nozzle. (This was achieved by tapping the feed line with a glass rod - which, although

Fig. 8.2

DROPLET PASSAGE THROUGH CUBIC BALLOTINI ORIFICE





unsophisticated as a technique, proved successful in extending the range of diameters fed into the ballotini orifice).

### 8.3) Upper Limit

The upper limit values - i.e. the break-through point - indicate that in some cases, a large error exists between the experimental and predicted values. Surprisingly, in the majority of the upper limit results, the experimental values were lower than the predicted values. The reverse trend was expected from consideration of the drag forces. No conclusive evidence was found to explain this phenomena, but there are several possible sources of error.

During this study, a piece of 1.8 cms I.D. glass tubing was positioned below the ballotini orifice to prevent large drops rolling round the packing. The top of the glass tubing was shaped to fit the ballotini orifice to prevent unwanted penetration. However, whilst this technique was successful with the cubic orifices, fabrication problems precluded its use with triangular orifices. Therefore, no upper limit values were obtained for the triangular orifices. The effect of this tubing can be seen for large drops ( $\geq$  or  $>1.5$  cms) where distortion of the lower drop segment took place and, dependent on the size of the drop, the following effects are proposed:-

- (a) The surface area of the held-up drop is greater than that of an undistorted lower segment. Consequently, for the same volume extra buoyancy forces would be required to compensate this effect;
- (b) The hydrostatic forces are greater than those of an undistorted lower segment of the same volume. Hence break-through occurs at a smaller buoyancy force.

The model was derived for an ideal drop profile and no account was taken of distortion for the lower segment due to the gravitational forces of the drop. The above points require further investigation before any firm conclusion can be made as to which situation of drop deformation predominates.

#### 8.4) Experimental Errors

The controlling mechanism for coalescence in a packing is that of drop retention, which is described by the lower limit. The experimental results were in reasonable agreement with those predicted, where the accuracy increased as the void diameter decreased. The upper limit values represent the point of drop release after retention has occurred; although this has been related to the exit drop formation process, it is of less importance with regard to accurate prediction. This was justified in that the controlling parameters of drop formation on release were the void diameter and the physical properties and to a much lesser extent the velocity of flow into the orifice, as described in Section (9.3.1).

In the theoretical model, an ideal drop profile was used, and no account was taken of the drag forces or wetting effects. The latter were accounted for by assuming a contact angle for the advancing segment equal to  $180^{\circ}$ , i.e. complete non-wetting. This was difficult to confirm experimentally, since observation within the packing restriction was not possible. In practice, no liquid has a contact angle of  $180^{\circ}$ , but it is difficult to propose the exact relationship between contact angle values of a sessile drop on a flat surface to those of an advancing interface through a 'toroidal' ballotini aperture.

The experimental bias indicated by the upper limit values follows the same trend as the relationship of the break-through pressures



with contact angles as predicted by Mayer and Stowe<sup>(188)</sup>. That is to say, as the contact angle decreased from  $180^\circ$ , the pressure required for break-through also decreased. Whilst Mayer and Stowe studied the advancing interface of a continuous flow of mercury, a direct analogy may be possible. This hypothesis has been expanded in Appendix (A1) in an attempt to quantify the packing surface energetics with droplet hydrodynamics.

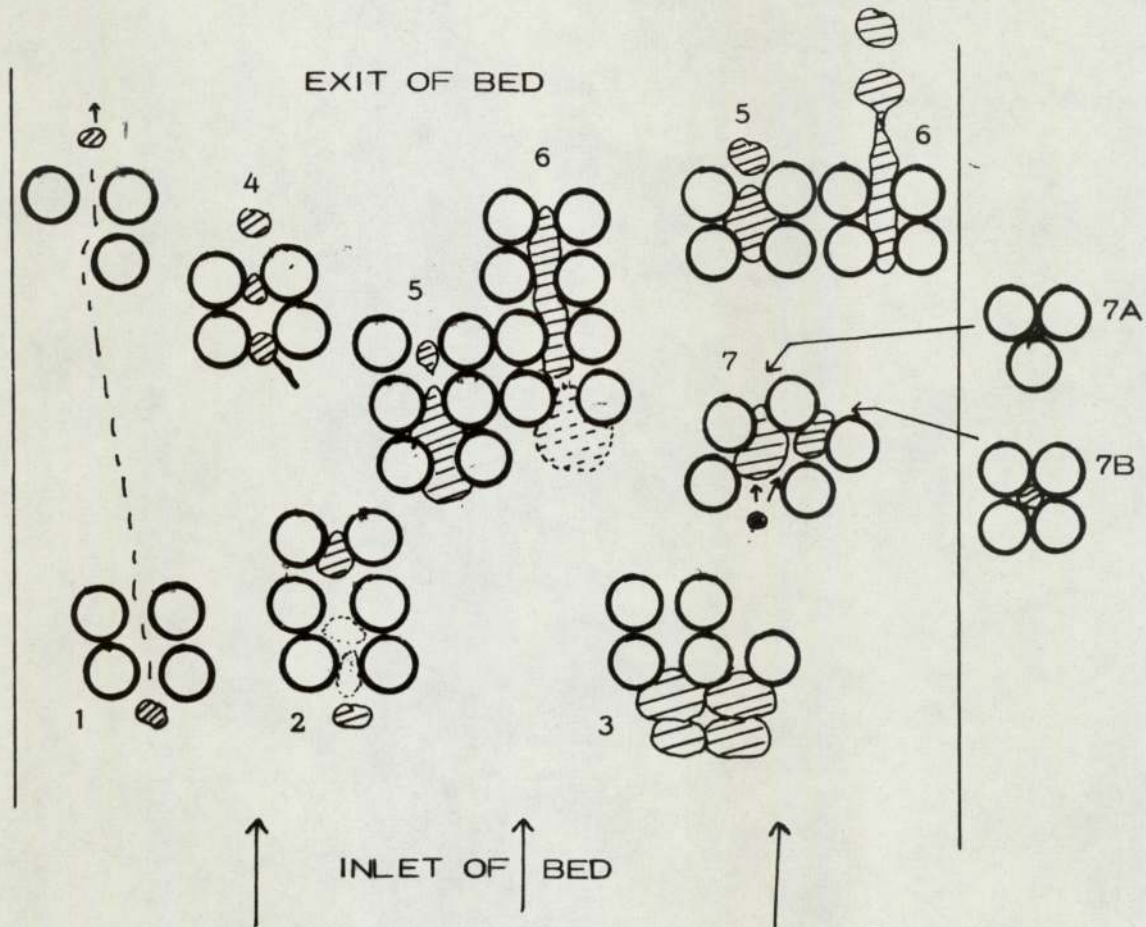
#### 8.5) Application of the inlet model to packed bed behaviour

Theoretical considerations and the experimental observation of the behaviour of droplets at single ballotini orifices have shown that the hydrodynamics can be characterized by a process of drop retention - coalescence - release. In principle, the above behaviour can be used to describe the more general conditions of dispersion within a packed bed coalescer. This is illustrated in Fig. (8.5) and discussed below:-

1. Unrestricted drop passage : The inlet drop is smaller than the packing apertures. Therefore the drop passes through the bed without retention or coalescence taking place.
2. Restricted drop passage : Drops enter the packing and may initially pass through the first few apertures which would normally promote retention, owing to the combined effect of kinetic and buoyancy forces. At each packing restriction, energy is lost on impact and deformation and also with oscillation about its equilibrium shape, after penetration has taken place. Likewise, energy is also dissipated on passage through the restriction by drag forces acting on the drop. The kinetic forces are consequently reduced and drop retention depends largely on a balance between buoyancy and surface forces.

Fig. 8.5

PROPOSED DROPLET HYDRODYNAMICS IN A NON-WETTED  
PACKING OF EQUAL SIZED SPHERES



- † Unrestricted drop passage
- 2 Restricted drop passage (penetration due to kinetic forces)
- 3 Inlet drop restriction
- 4 Retention-impact-release
- 5 Unrestricted drop release
- 6 Restricted drop release
- 7 Preferential flow-path



3. Inlet drop restriction: Penetration of the packing is by the same mode as in '12', but hold up occurs at the bed inlet because the buoyancy, and hence the kinetic forces, are low. Alternatively, a drop with a large diameter compared to that of the packing aperture, may also be retained at the inlet to the bed. Drops accumulate at the packing inlet and penetration occurs when the buoyancy forces overcome the surface forces. At this point, the bed will continue to operate without further increase in the layer of drops at the bed inlet.

Once the drop has been retained, however, its behaviour is dependent on the local geometric structure and the physical properties of the system.

4. Retention - Impact - Release : Fig. (4) shows an inlet drop which has been retained, but is near to the critical point of passage. Under these conditions, passage may be initiated by impact from a following drop. The initial drop is pushed through the restriction and its place is taken by the following drop. In this way, the drop may pass through the packing without coalescence taking place. This type of behaviour is particularly prominent at high values of  $\left(\frac{\Delta\rho g}{2\gamma}\right)$  i.e. where the buoyancy forces are much larger than the surface forces.

5. Unrestricted drop release : Droplet retention has occurred, and growth takes place by coalescence with following drops. On release, provided the penetrating meniscus is able to accelerate, drop formation will take place as shown in '15'. This behaviour is analogous to drop formation from a standard nozzle or orifice. Acceleration of the extruded interface may occur within the bulk of the packing at local packing dislocation as well as at the exit of the packed bed.

6. Restricted drop release : The advancing interface of a drop held in the bulk of the packing will probably be restricted by the packing above the orifice. Therefore, acceleration and drop formation is not possible and a rivulet of dispersed phase is formed which "snakes" through the bed. The rivulet may pass through to the packing exit where break up occurs, by acceleration of the penetrating interface into an unrestricted medium. Passage or retention of the rivulet is again subject to packing geometries and the physical properties of the system.
7. Preferential flow paths : The path chosen by the droplet is always dependent to some extent on the packing configuration and '7' illustrates a special example of this. Drop retention occurs at a restriction, and coalescence and subsequent drop growth occurs. If the volume of retained mass is sufficient to extend to a second, larger opening, then subsequent drops, before coalescing, may seek this preferential route. This is shown by '7A' and '7B' where A is the smaller original restriction.

The above descriptions, whilst founded on theoretical and experimental observations of drops at single balloting orifices, represent an idealized situation. Nevertheless, certain points illustrate that care is required in the interpretation of published data.

#### 8.6) Previously reported packed bed phenomena

Coalescence data for packed beds has often been related to phase velocities, voidage values and hold up measurements. However, voidage, whilst describing the amount of free space within the bed, gives no indication of the void size distribution or of the degree of interconnection between adjacent restrictions. Therefore, packings with the same voidage could have completely different



characteristics of coalescence. For example, with beds of monosized spheres, the bulk voidage value is approximately constant, but the aperture or void diameters depend on the size of the spheres. Similarly, total hold-up values comprise three possible types, each of which may have a different effect upon droplet hydrodynamics within the bed - viz :

<u>Type</u>	<u>Example</u>
Static hold-up	That which occurs in a restriction which does not release the retained mass - i.e. of the type shown in '7A'
Dynamic hold-up	Drops which are moving through the bed as either uncoalesced or coalesced drops, i.e. '11' '14' '15'.
Transient hold-up	Drops which are stationery at a packing restriction, but are active under the retention-coalescence release mechanism, i.e. '12' '13' '15'.

Many studies have been made of the important flow phenomena in packed beds. Correlations have been obtained for the prediction of flooding under the conditions described in '11'. These correlations<sup>(54)(47)(55)</sup> were found to be unsatisfactory when the packing size was decreased. These conditions effectively represent '12' and '14' and premature flooding was reported with systems of low density difference and high interfacial tension. This is to be expected by considering the relationship of  $\left(\frac{\Delta p g}{2 \gamma}\right)$  with drop retention. The degree of hold up, coalescence and "interface surging" was found to differ from system to system.<sup>(42)</sup> For the systems studied by previous workers, the trend was found to decrease with increasing values of  $\left(\frac{\Delta p g}{2 \gamma}\right)$ , which agrees with the predictions of this model.



The conditions describing the onset of flooding have been the subject of some debate. Recent workers<sup>(67)(172)</sup> have shown that high voidage packings can operate quite successfully with a layer of dispersed phase at the inlet, without further accumulation taking place. However, under conditions of flooding reported by early workers<sup>(57)(43)</sup>, and by recent workers<sup>(50)(60)</sup>, a different hydrodynamic behaviour obviously exists for the conditions described by '11' and '13' respectively. Other important flow conditions have been observed, for instance "snaking" has been reported for both primary<sup>(50)</sup> and secondary<sup>(78)</sup> dispersions, although the latter work was strongly criticized by later workers<sup>(79)</sup>.

Other authors<sup>(38)(39)</sup> have suggested that for coalescence, a relationship exists between inlet drop diameter and the void diameter, but they were unable to present any quantitative solution. Likewise, the exit drop diameter was thought to be related to a hydraulic mean diameter<sup>(50)</sup> described by the packing, but, as in the previous case, the packing was not amenable to description, and no quantitative work has been reported.

In this study, equal sized spheres were used. However, as the beds were randomly packed, there exists a distribution of void diameters. Therefore, work was carried out to investigate the process of drop release at the packing exit and the coalescence mechanism within the bulk of the packing. This has been described in more detail in Sections 9 and 10.



CHAPTER 9.

DISCUSSION OF RESULTS

Packed bed and Single Nozzle Exit Drop Formation Mechanisms

## 9) EXIT DROP MECHANISMS

Prior to this work, the mechanism of drop formation at the exit of the packing had received very little attention. Similarly, the effect of packing geometry on the drop release process had not been investigated. Thomas<sup>(50)</sup> suggested that exit drop size may be a function of a mean hydraulic diameter of the packing, but presented no supporting experimental or analytical work. Previous authors have been unable to separate and identify the effect of coalescence mechanisms within the bulk of the packing on the actual drop formation process at the packing exit. Accordingly, their results have been presented as a function of the overall process of coalescence and exit drop formation. The present study has identified two distinct processes, i.e., drop retention and drop release and each must be considered separately.

### Total Coalescence

The hydrodynamic behaviour of droplet coalescence within a packing can be predicted using the inlet theory of drop retention. Thus, under certain conditions, it is possible to isolate the effect of packing geometry on the exit drop mechanism. These conditions will be referred to as column operation under "total coalescence".

"Total coalescence" is characterized by all the inlet dispersion being coalesced within the bulk of the packing. This occurs by a process of drop retention and flow to the exit; a more detailed description has been given in Section 8.5.(6). Consequently, the exit drop size produced on release from the packing is only a function of the exit layer geometry and the physical properties of the system. Under the operating condition



of "total coalescence" the packed bed is analogous to a series of nozzles or orifices, supplied by a continuum of the phase which is normally dispersed. Experimentally, assuming a monodispersion, this condition can be achieved by selection of an inlet drop size which will be retained, and consequently coalesced, on passage through the bed. From the inlet drop theory of retention, a toluene-water system was selected with a mean inlet drop  $\approx 0.33$  cms. Toluene and water has often been referred to as an "easy system"<sup>(56)</sup> in that coalescence is readily promoted, and as such is well suited for the present investigation. A measure of the reliability of achieving "total coalescence" is shown by those results of the mean exit drop diameters which have been denoted at zero flow rates (Fig. 9.2.1-8) and Appendix (A.4). These results were obtained by operating the column first at very high dispersed phase flow rates at which there was a build up of droplets at the inlet to the bed. The flow was then quickly shut off, and the flocculation band at the bed inlet was observed to coalesce (Fig. 9.1) before passing through the bed to the exit. The exit drop diameters for this condition fall within the region of other results obtained at different flow rates for that particular packing.

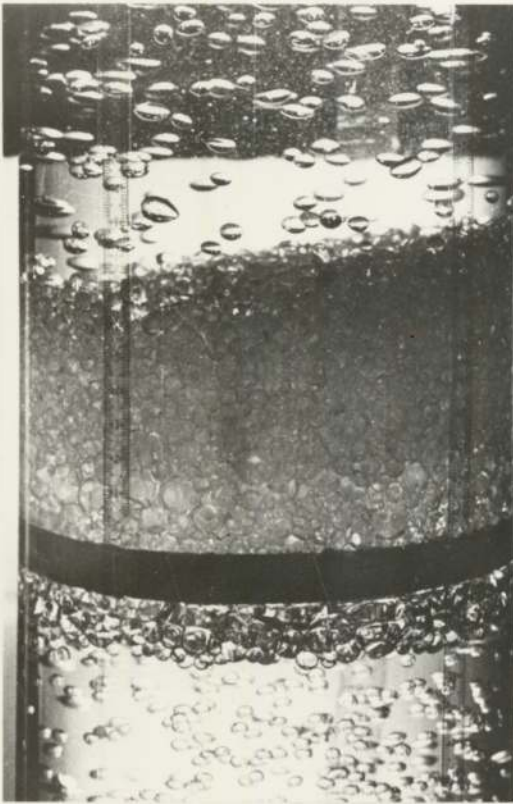
## 9.1) EXPERIMENTAL STUDY OF EXIT DROPS FROM A PACKED BED

### 9.1.1) Ball diameter

The 6" diameter column was operated as described in Section (5.1). The effect of flowrate, bed height, inlet drop and ballotini diameter on the exit drop size was investigated using the procedure detailed in (5.2.1). A representative set of results is shown in Fig.(9.1.1), from which it is clear that the ball diameter has a significant effect upon the exit drop size. This is to be

Fig. 9.1

PACKED BED OF 0.6 cms BALLOTINI OPERATING  
UNDER TOTAL COALESCENCE



(A)

Floculation band building-up  
beneath packing .



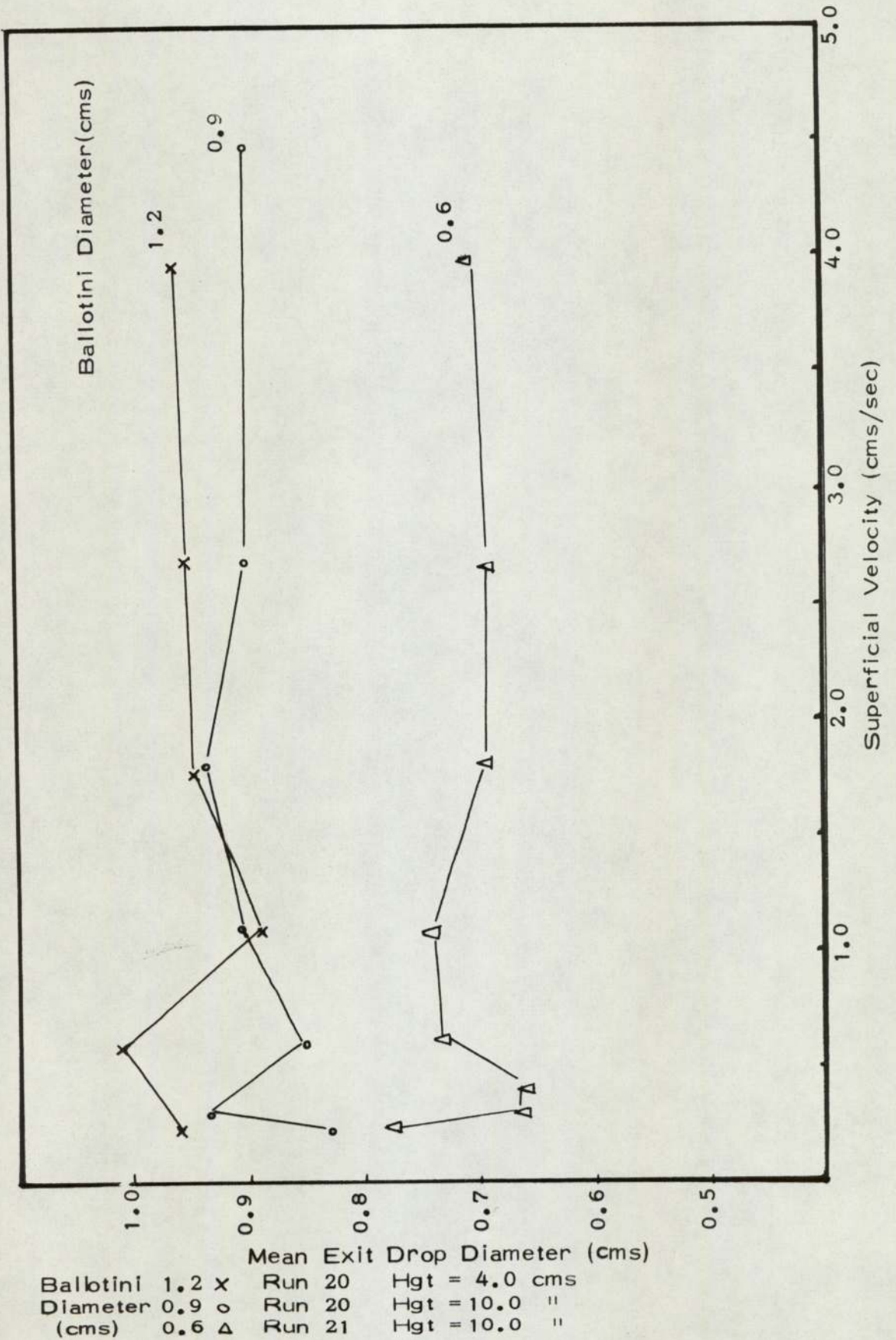
(B)

Flow rate shut-off.  
Floculation band coalesces and  
drains through the bed to exit.



Fig. 9.1.1

VARIATION OF EXIT DROP DIAMETER WITH SUPERFICIAL VELOCITY



expected if the exit drops are formed at a series of nozzles or orifices in the exit layer of the packing. The increase in the exit drop size with ballotini diameter arises since, for any random packing of spheres, the mean void diameter must increase as the particle size is increased.

To investigate the effect of packing size in the exit layer, incremental deposits of 1.2, 0.9, 0.6, 0.9 and 1.2 cms ballotini were added respectively to the existing bed, and the mean exit drop size was evaluated after each addition. The results presented in Fig.(9.1.2) show that a relationship does exist between packing size and exit drop size, and that the latter can be altered by simply altering the exit layer of packing. This is of importance in the design of a coalescing aid since, assuming that coalescence takes place within the packing, an increase in exit packing size will result in an increase in separation efficiency. It is of interest to note that previous workers have related the exit drop diameter to the amount of coalescence taking place within the bed, but the above results show that, in the case of the induced situation of "total coalescence", this approach is invalid.

#### 9.1.2) Flow rate

Fig.(9.1.1) indicates that the mean exit drop diameter is also very sensitive to flow rate. To explain this, it is necessary to consider the overall behaviour of a packed bed which is dependent upon:-

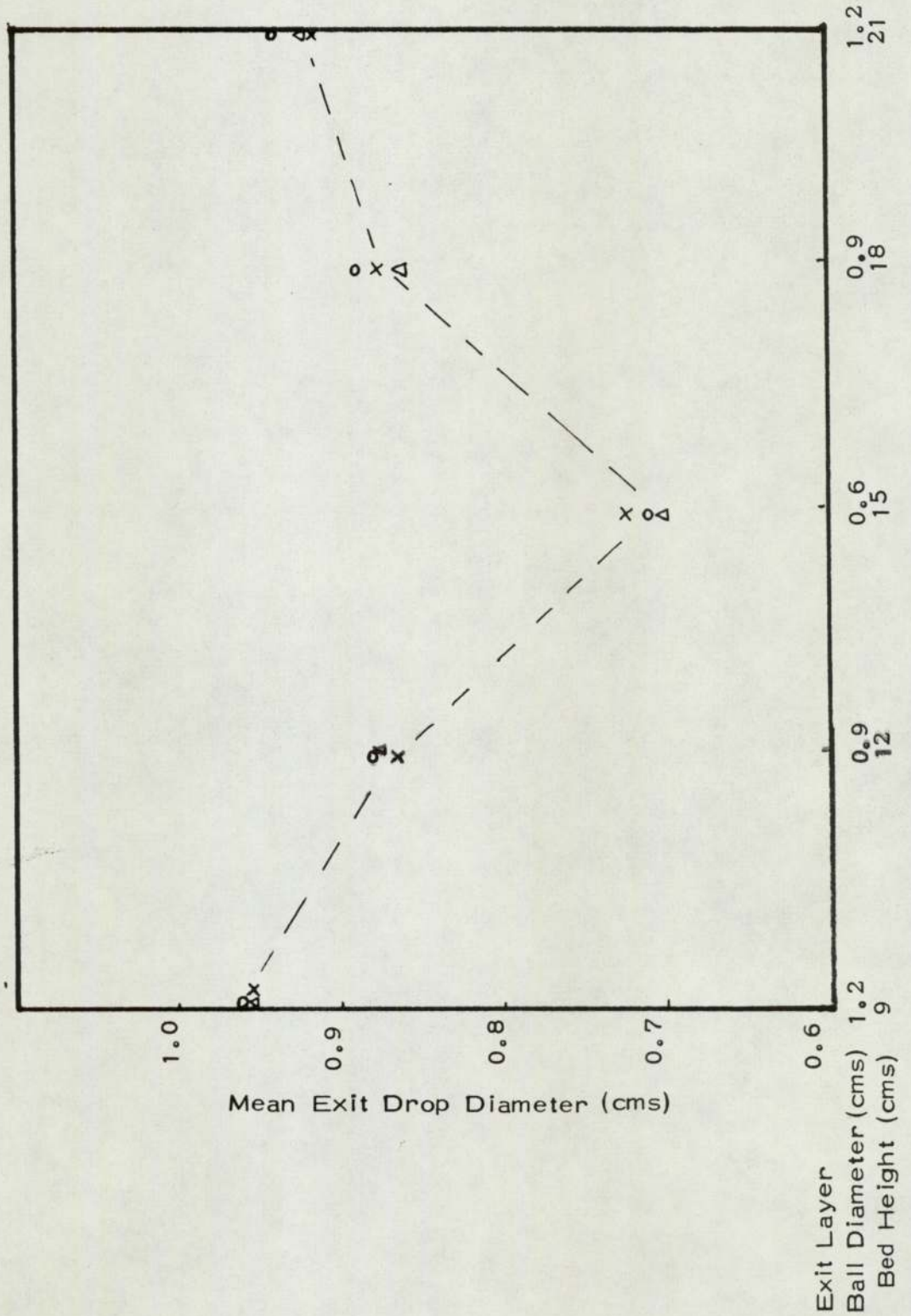
- (I) The geometry of a random packing of spheres;
- (II) Drop retention and drop release with respect to (I);
- (III) The effect of flow rate on the behaviour predicted by (II).



Fig. 9.1.2

VARIATION OF EXIT DROP DIAMETER WITH EXIT BALL DIAMETER

(For Toluene - Water System)



## I Packing Geometry

During the experimental study, it was observed that, at low flow rates, drops were released from only a certain number of the exit voids. Thomas<sup>(50)</sup> referred to this phenomenon as channelling, and its existence was assumed to be related to wetting effects of the dispersed phase on the solid surface. To evaluate this effect, experiments were carried out using non-wetted ballotini and ballotini packings which had been subjected to preferential wetting treatment before being placed in the column. Since no significant difference was detected for the mean exit drop size and its standard deviation, it was concluded that the exit release points were not a function of preferentially wetted channels - Table (9.2). This does not mean, however, that the exit drop is independent of the surface energy of the packing, but merely that the surface energy of glass ballotini was resistant to change by the preferential wetting technique described in paragraph (5.1.4.c). Initially, the "active exit release sites" were thought to be related to the local floculations in voidage, particularly at the column wall. For example, Ridgeway and Tarbuck<sup>(166)</sup> have predicted high voidage values for the region within two particle diameters of the wall. In the event, during this study the observed active release sites were randomly distributed over the total cross sectional area of the packing exit.

For any random packing arrangement of spheres, a distribution of channel diameters will exist throughout the bulk of the packing. Since the exit layer effectively constitutes a discontinuity of geometry, the mean void diameter in the exit layer will probably be greater than that in the bulk packing.



However, to explain the fluctuation of the exit drop size with flow rate, it is necessary to relate the existence of distribution of void sizes to the theory of drop retention and drop release.

## II Drop Retention & Release

It has been shown from theoretical considerations and experimental observation that droplets enter the bed and pass through until a restriction is reached where the surface forces required for retention are greater than the buoyancy forces for passage (7.3). Once the drop has been held up, passage will only occur when the buoyancy forces exceed the surface forces. The necessary increase in buoyancy forces is achieved by impact and coalescence of subsequent drops with the initial drop. It follows that, as the size of the restriction is increased, the buoyancy forces required for passage decrease. Thus, the effect of an exit void which is larger than its neighbours is two-fold:-

- (1) Assuming that the flow rate into each void is equal, release of the held up mass occurs more frequently.
- (2) If the drop size - void diameter relationship holds true, the drops formed at the large exit voids (at which release occurs more frequently) will be larger in diameter.

If "active sites" arise because of their size relative to other voids within the exit layer, it can be assumed that the cross-sectional area of the active sites operational at any one mass flow rate is constant, irrespective of the diameter of a mono-sized packing. From these assumptions, the data presented in Fig(9.1.1) was treated with respect to the flow rate through the "active sites" to give a more representative description of



the behaviour of the packing.

### III Flow Rate Consideration

The data presented in Fig.(9.1.1) has been characterized by superficial velocity,  $u_d$ , defined by the ratio of the volumetric throughput to the cross-sectional area of the column. However, the superficial velocity gives no indication of the droplet velocity or flow characteristics within the packed bed. Attempts were made to evaluate the drop velocity within the bed by injecting coloured drops into the inlet stream and measuring their residence times in the packing. The results proved inconclusive owing to a large scatter. This may be explained by considering the hydrodynamics of droplets at local variations in packing geometry and the theory of drop retention and release.

Based on the evidence given in the sections on packing geometry and droplet hydrodynamics, the flow rate was expressed as:

$$\text{Orifice Velocity No.} = U_o = \left( \frac{\text{Volumetric throughput}}{\text{CSA of one void}} \right) \times K$$

where K is a function of the fraction of active sites to non-active sites. The numerical value of the orifice velocity is unknown owing to the experimental difficulties in monitoring the number of active sites. Similarly, the exact geometric arrangement of the exit layer is unknown. However, the mean void diameter can be assumed to be related to the ballotini diameter by  $d_v = k d_b$  where k is a constant defining the packing geometry. The use of an orifice velocity number to illustrate the characteristics of a packed bed is valid, if the following assumptions are correct:-

- (1) The mean void size and packing geometry can be related

by the equation  $d_v = k d_b$



- (2) The parameters which control the existence of release sites are a function of the properties of one exit void relative to another, and this property is a constant function of the void size distribution of mono-sized packings.

The data from Fig.(9.1.1) is re-plotted with respect to the orifice velocity number, as shown in Fig.(9.1.3). Three distinct regions have been identified and these can be explained with the aid of qualitative observations made during the experimental study.

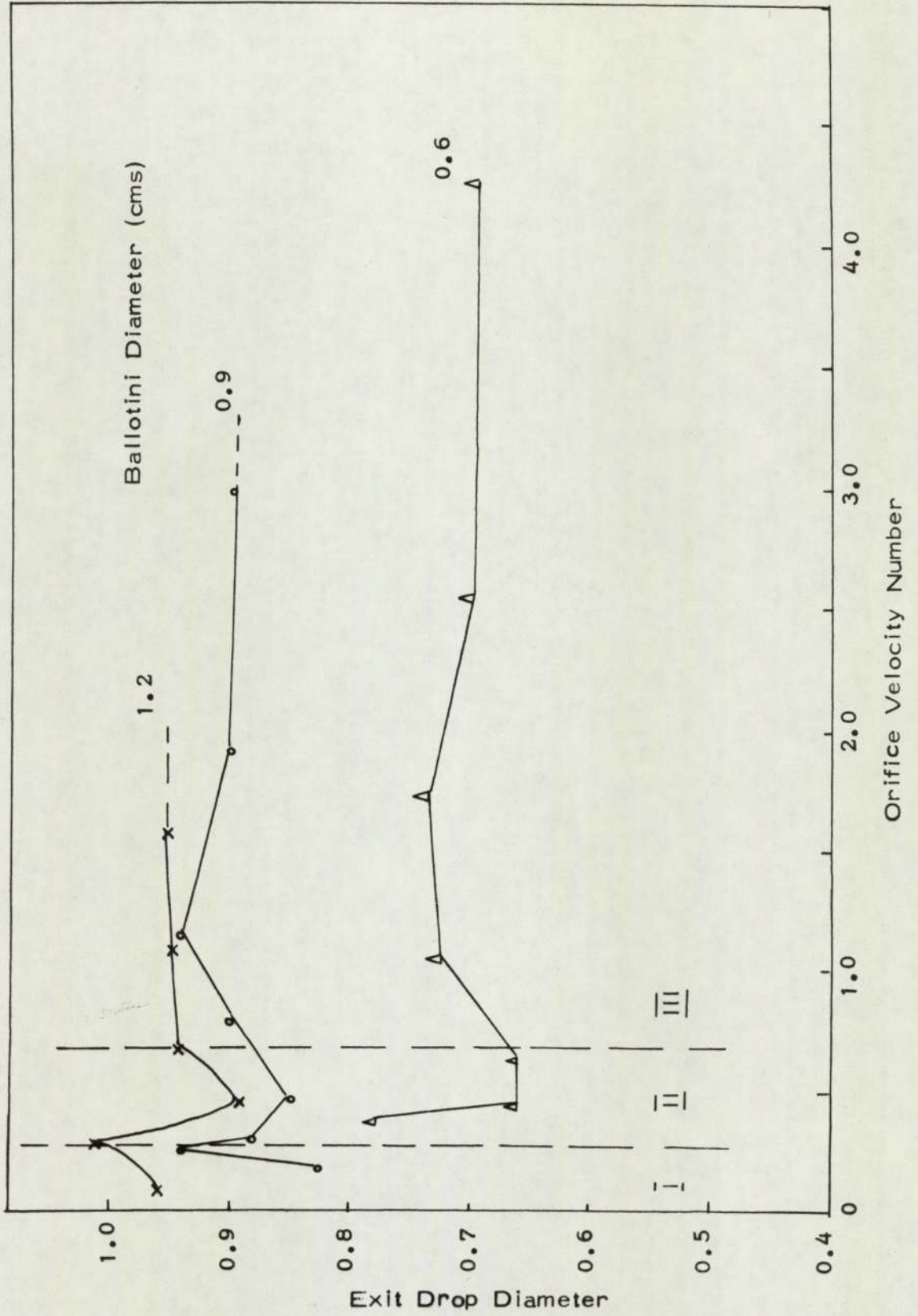
Region I : At low volumetric throughput only the largest exit voids are active, thus the exit drop size will be at its maximum if the relationship of drop size with void size holds true. The initial increase in drop size with flow rate can possibly be explained by considering the hydrodynamic behaviour at the largest exit voids where the packing geometry was ill-defined and the situation more closely resembled that of a "hole" at a packing dislocation. Where retention and release were generally observed at the exit voids, the "holes" were characterized by the absence of retention for the dispersed flow from within the bulk of the packing. Consequently, the mechanism of drop formation is difficult to define, but it was generally observed that the size of drop formed at these holes was smaller than that formed at other well-defined exit packing apertures.

Region II : As the volumetric flow increases, more exit voids of decreasing diameter become active. The average exit drop diameter therefore falls to a minimum corresponding to the maximum number of active voids.

Region III : At higher flow rates, a band of the inlet dispersion formed at the bed inlet, but the packing continued to operate without flooding occurring. The packing is now analogous to a series of nozzles, and the exit drop diameter increases in a manner similar to that of drop formation at single nozzles as shown by the Meister & Scheele<sup>(96)</sup> correlations - Figs (A.5.1-3).

Fig. 9.1.3

THEORETICAL RELATIONSHIP BETWEEN ORIFICE VELOCITY NUMBER AND BALL DIAMETER





## 9.2) Determination of the exit packing geometry

The above evidence suggests that the maximum exit drop size can be predicted if the mean exit void size and the drop release mechanisms are known. To investigate this a statistical approach was used to compare the mean drop diameter with the mean void diameter both of which are functions of their respective size distribution.

The void diameter is not only a function of the ball size but also of "k" which describes the geometric arrangement of the packing. Many packing arrangements associated with spheres have been reported, and it is recognized that a random packing of spheres will be a combination of many different geometries. Moreover, the exit packing layer, which controls the exit drop size distribution, will be more difficult to define.

As an initial estimate, the cubic and triangular packing arrangements were selected because most of the fundamental packing units consist of these two geometries - Fig.(10.1). For a cubic and triangular packing geometry the theoretical voidage is equal to 0.46 and 0.39 respectively. This value compares favourably with that experimentally determined for the random packed beds of ballotini used in this study - (that is  $\epsilon = 0.40 - 0.42$ ). This choice was also consistent with ease of fabrication of single ballotini nozzles used to investigate both the inlet and exit drop mechanisms (Table 10.1).

### 9.2.1) Drop Void Number

The experimental work was carried out as detailed in (5.2.1) and the results are presented in Fig(9.2.1-8) and Appendix (A4). To determine the geometry in the exit layer of the packing, the exit drop size was related to the void diameter by means of a

dimensionless Drop Void Number where :-

$$DV = \left( \frac{\text{Mean exit drop diameter}}{\text{theoretical void diameter}} \right) \quad (9.2)$$

For the cubic and triangular geometries, the Drop Void Nos., DVC and DVT were evaluated by using the respective void diameter relationships, that is  $d_{vc} = 0.414 d_b$  ;  $d_{vt} = 0.1545 d_b$  . Similarly, by the same method, a theoretical Drop Void Number can be obtained by using the theory of drop formation at standard nozzles and orifices. Thus, by comparing experimental and theoretical values for both a cubic and triangular geometry, it was possible to obtain an initial estimate of the mean exit packing geometry.

On inspection of Fig(9.2.1.-8) it can be observed that the bed height, superficial velocity, preferential surface treatment and Inlet drop diameter have little effect upon the Drop Void No. However, the Drop Void No. is strongly dependent on the ball diameter and similar discreet bands exist for each ball diameter. This was confirmed with a multiple regression analysis using a ICL 1905E Statistical Package on the experimental data, Appx.(A.3.5). Whilst a poor overall correlation was obtained, the results show that the exit drop diameter was virtually independent of all parameters except that of the ball diameter. On this basis, the Drop Void Nos. were averaged for each experimental run. The procedure for taking an average of each run was considered justified in that whilst bed heights and flow rates caused local fluctuation in the exit drop size, the regression analysis had shown that they had little effect. Further justification is that the effects of flow rate shown by the orifice velocity studies (9.1.2), follow similar trends for different packing diameters.



Fig. 9.2.1

RELATIONSHIP OF BED HEIGHT, SUPERFICIAL VELOCITY & BALL DIAMETER WITH DROP-VOID NUMBER (CUBIC)

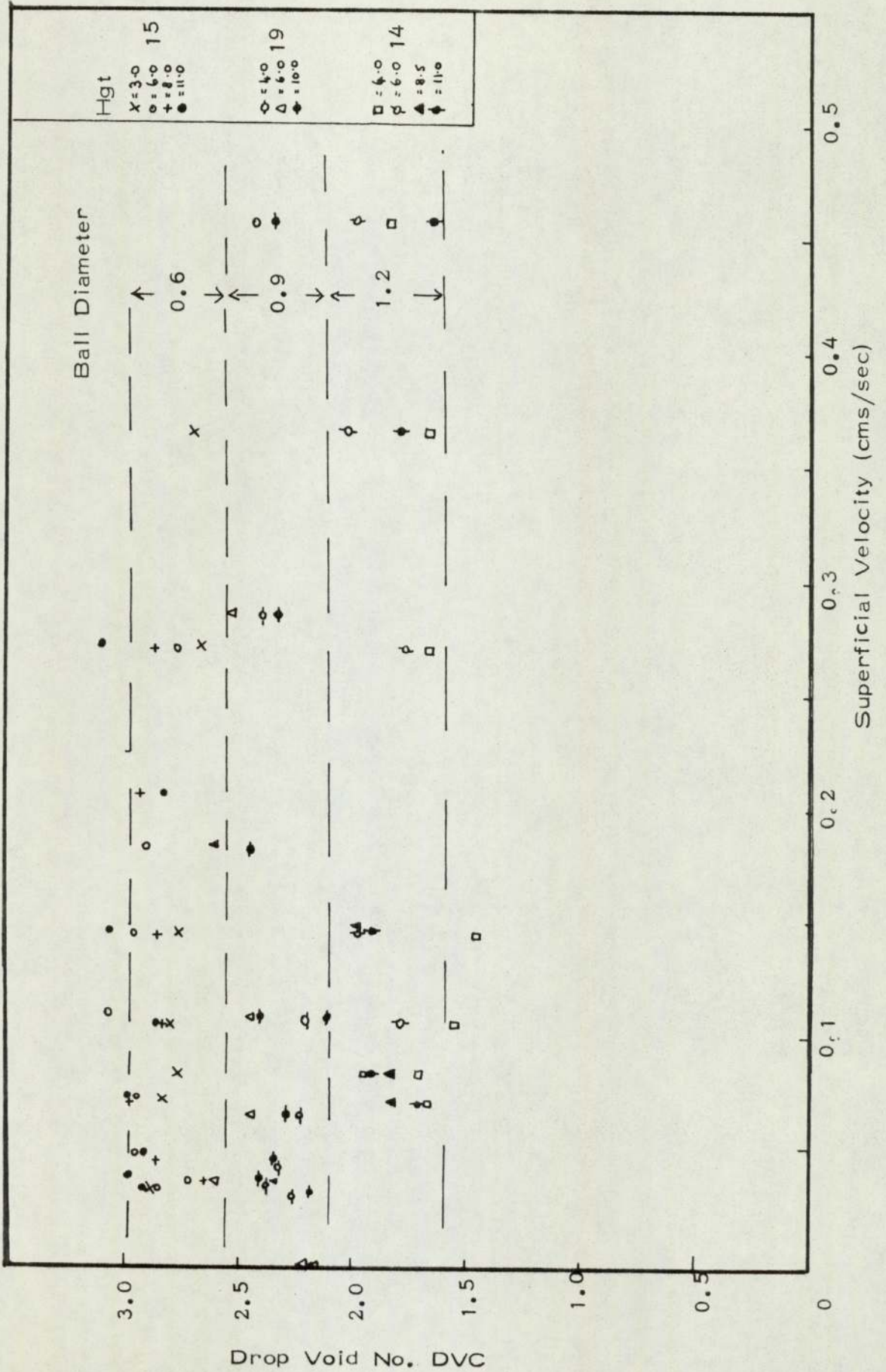


Fig. 9.2.2

RELATIONSHIP OF BED HEIGHT, SUPERFICIAL VELOCITY & BALL DIAMETER WITH DROP-VOID NUMBER (TRIANGULAR)

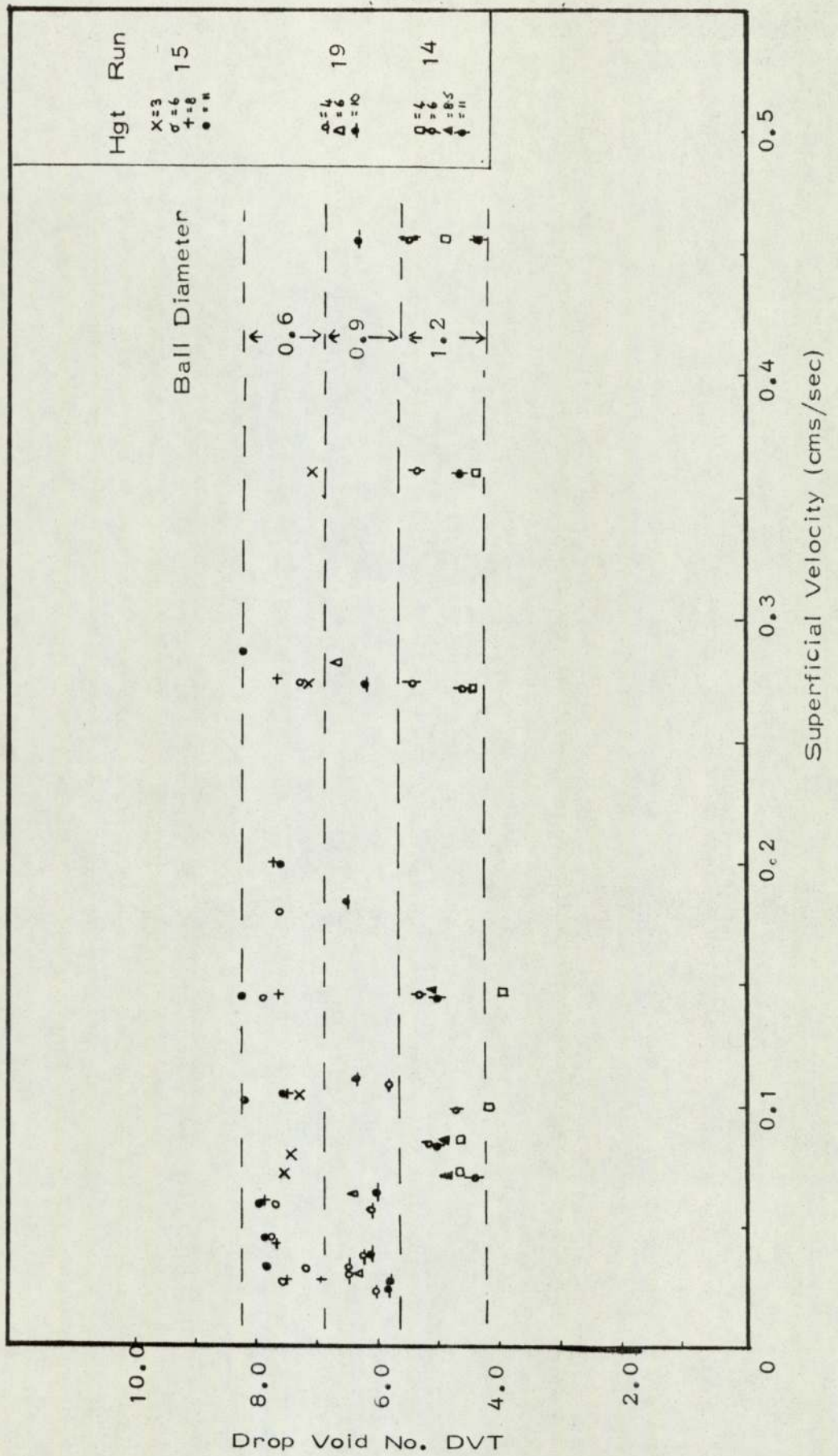




Fig. 9.2.3

RELATIONSHIP OF BED HEIGHT, SUPERFICIAL VELOCITY & BALL DIAMETER WITH DROP-VOID NUMBER (CUBIC)

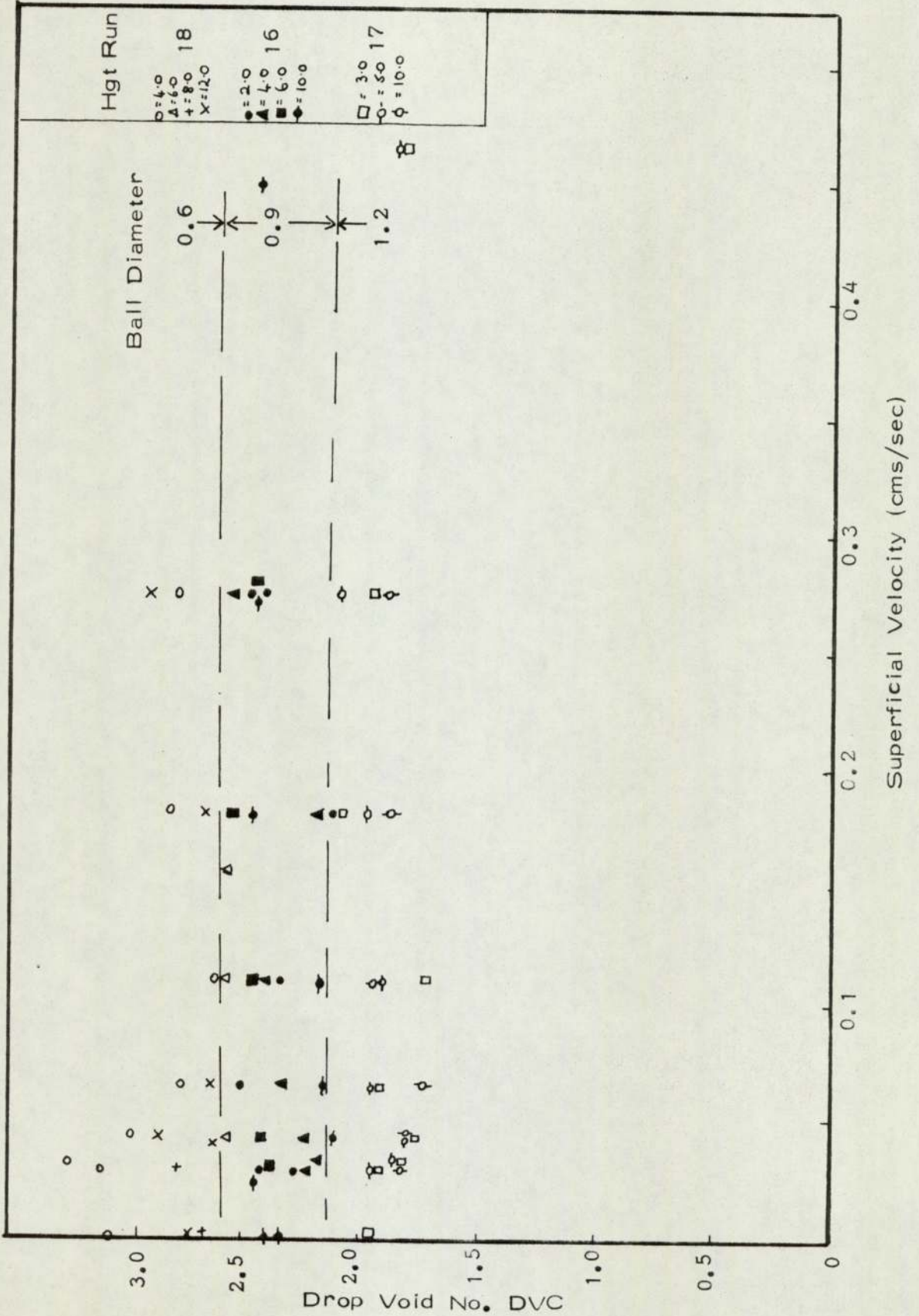


Fig. 9.2.4

RELATIONSHIP OF BED HEIGHT, SUPERFICIAL VELOCITY & BALL DIAMETER WITH DROP-VOID NUMBER (TRIANGULAR)

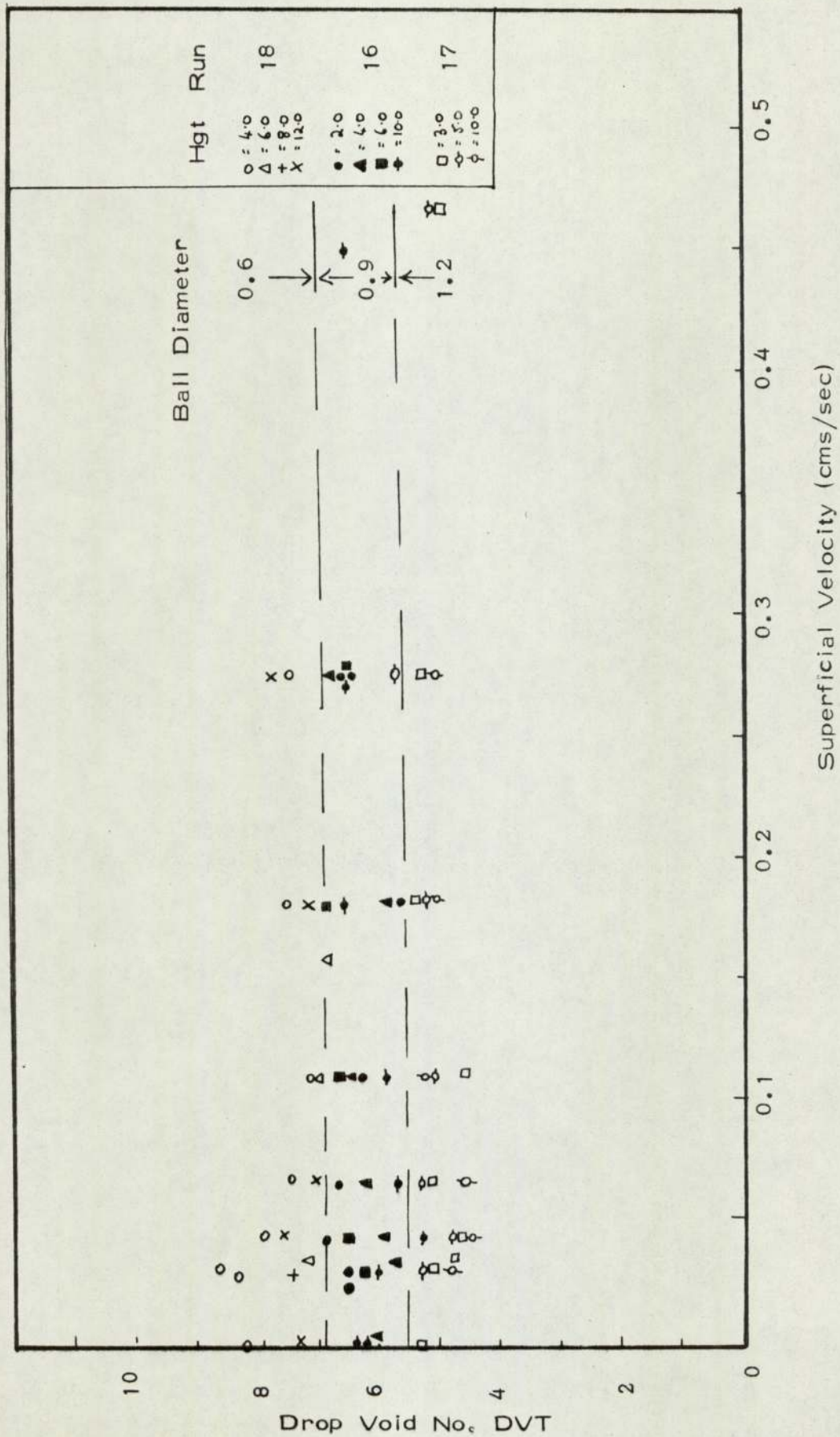




Fig. 9.2.5

RELATIONSHIP OF BED HEIGHT, SUPERFICIAL VELOCITY & BALL DIAMETER WITH DROP-VOID NUMBER (TRIANGULAR)

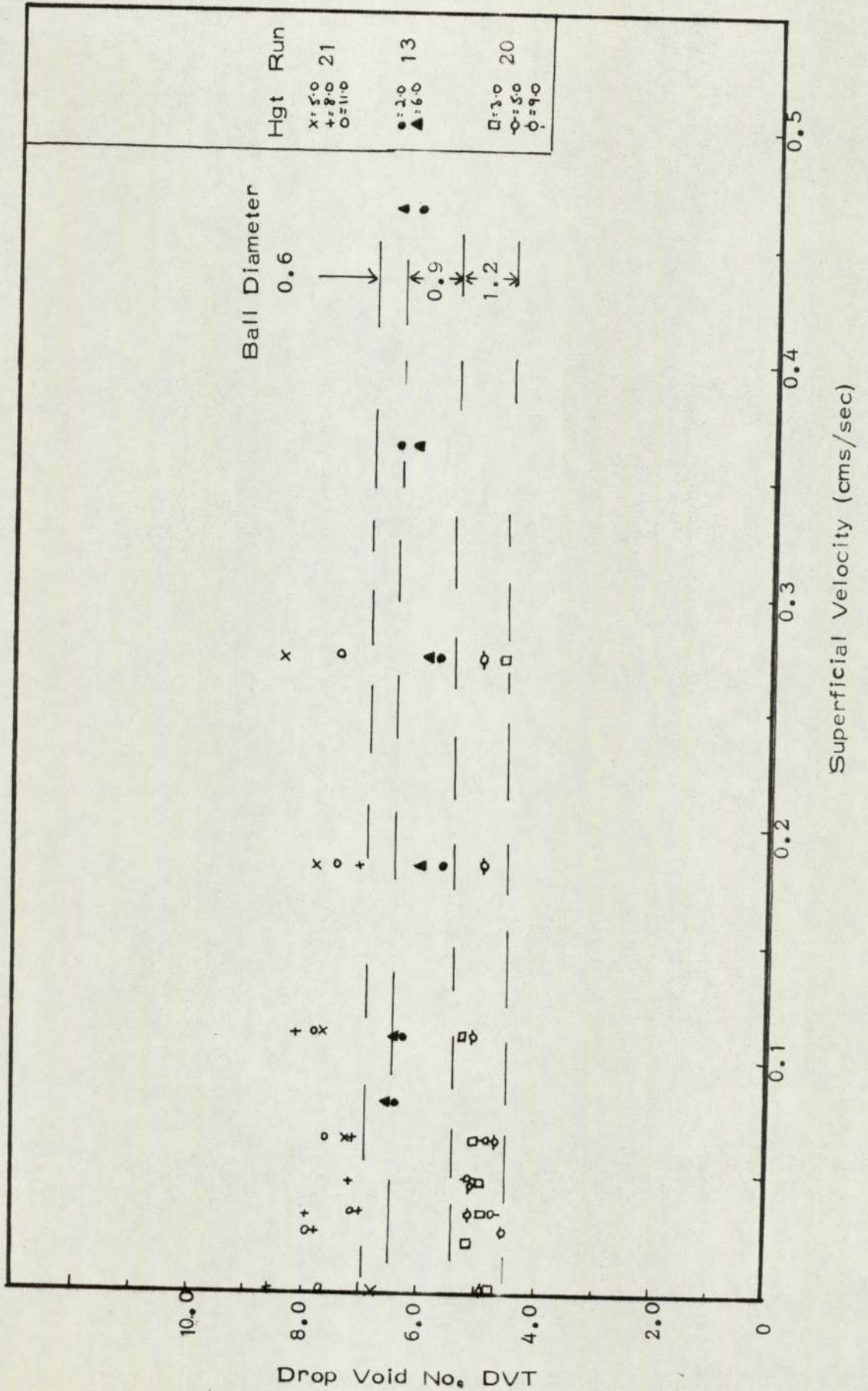


Fig. 9.2.6

RELATIONSHIP OF BED HEIGHT, SUPERFICIAL VELOCITY & BALL DIAMETER WITH DROP-VOID NUMBER (CUBIC)

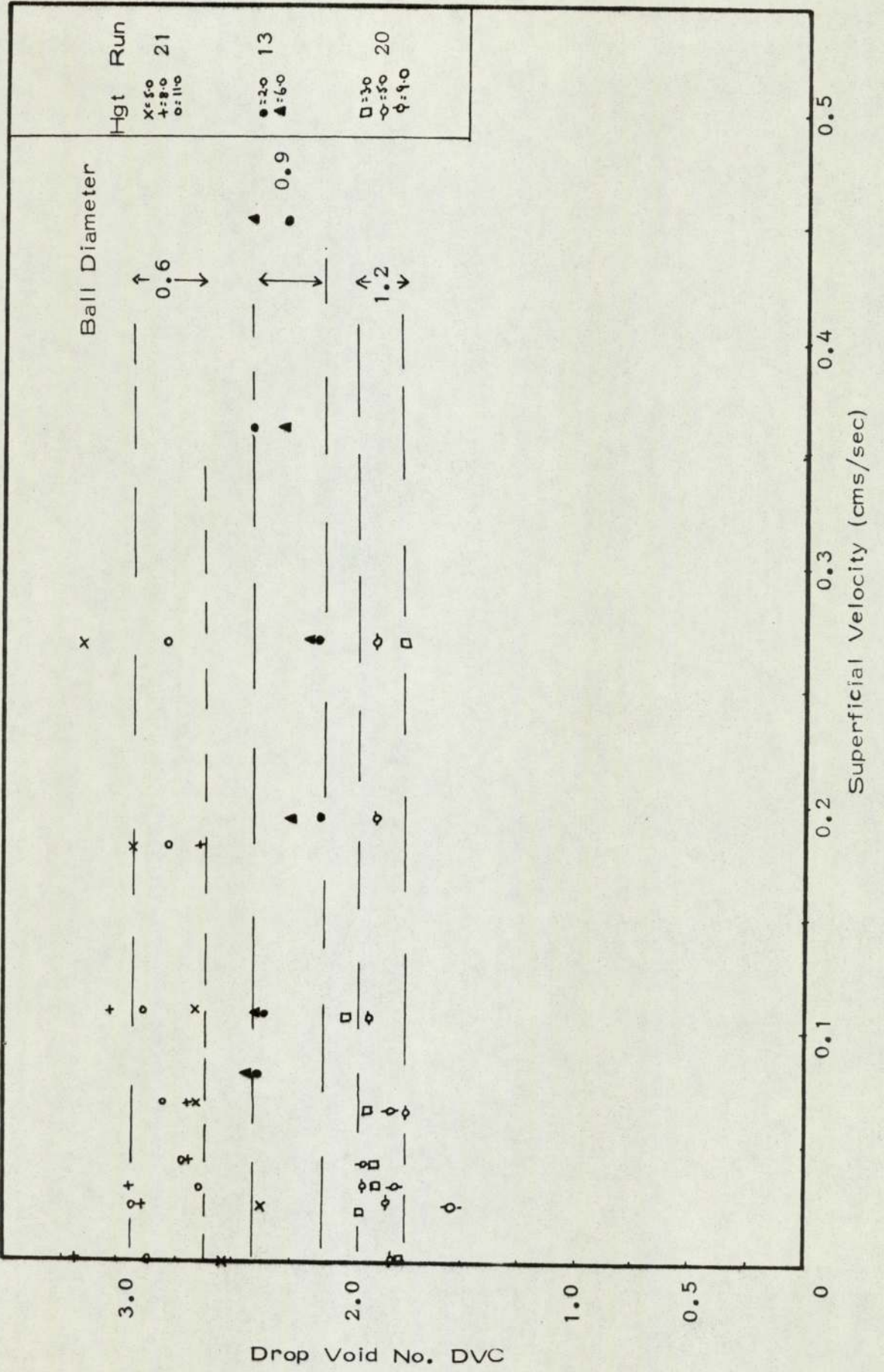




Fig. 9.2.7

RELATIONSHIP OF BED HEIGHT, SUPERFICIAL VELOCITY & BALL DIAMETER WITH DROP-VOID NUMBER (CUBIC)

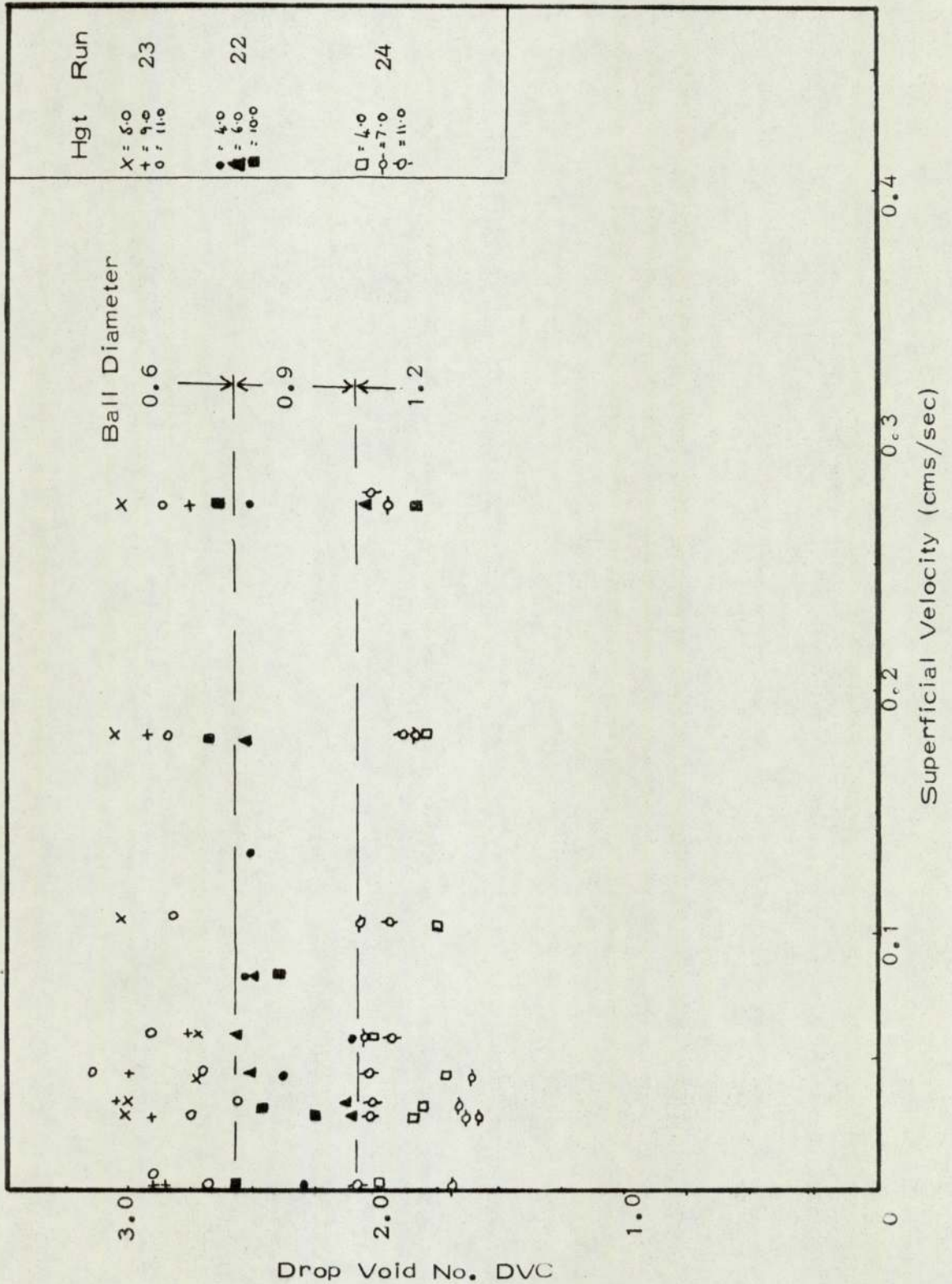
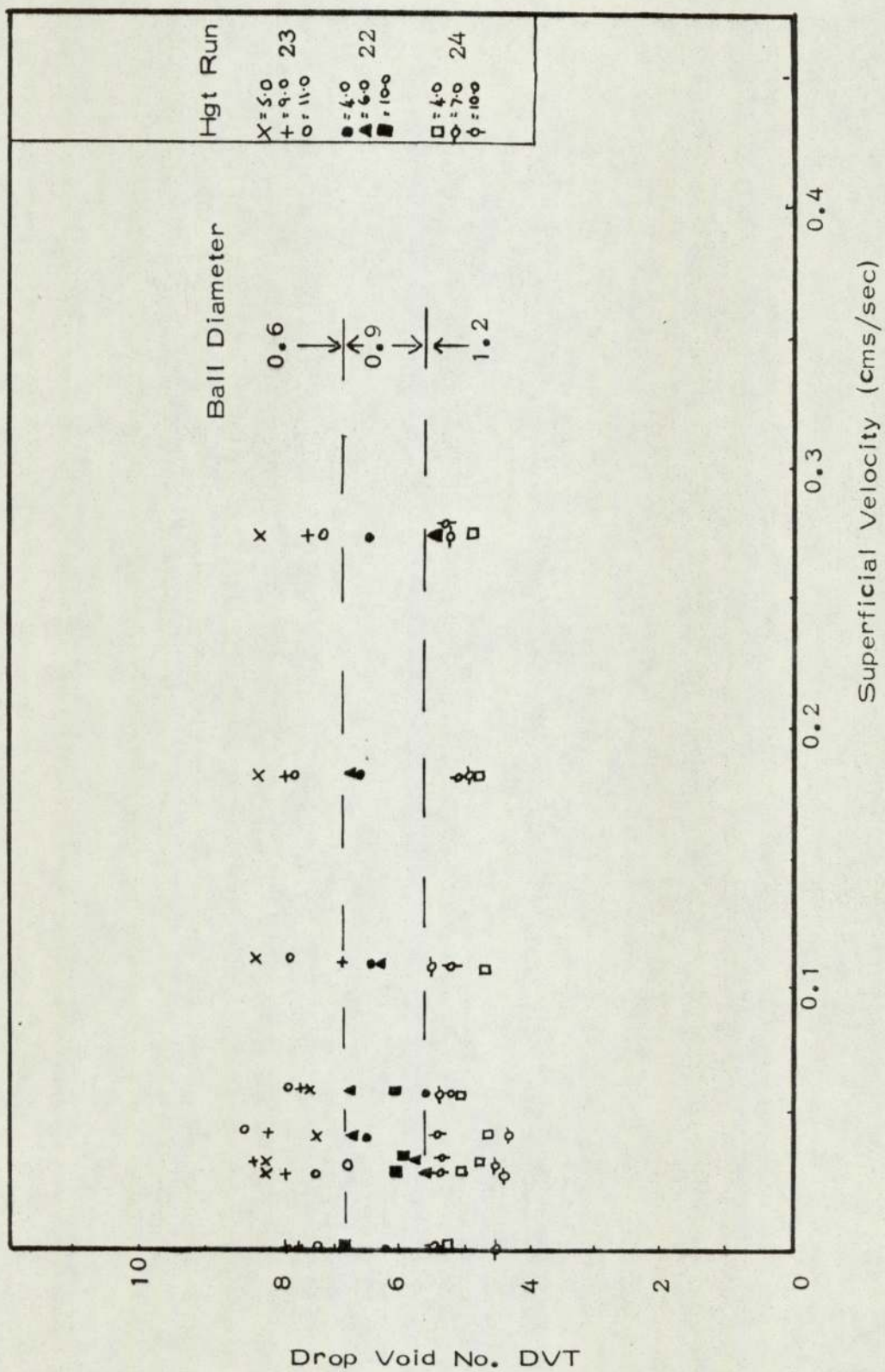


Fig. 9.2.8

RELATIONSHIP OF BED HEIGHT, SUPERFICIAL VELOCITY & BALL DIAMETER WITH DROP-VOID NUMBER (TRIANGULAR)





The average Drop Void Nos. and their standard deviations, given in Table (9.2), were evaluated from the data in Appendix(A.4.1). Each Drop Void No. represents approximately 1800 individual drop measurements for each experiment.

Table 9.2

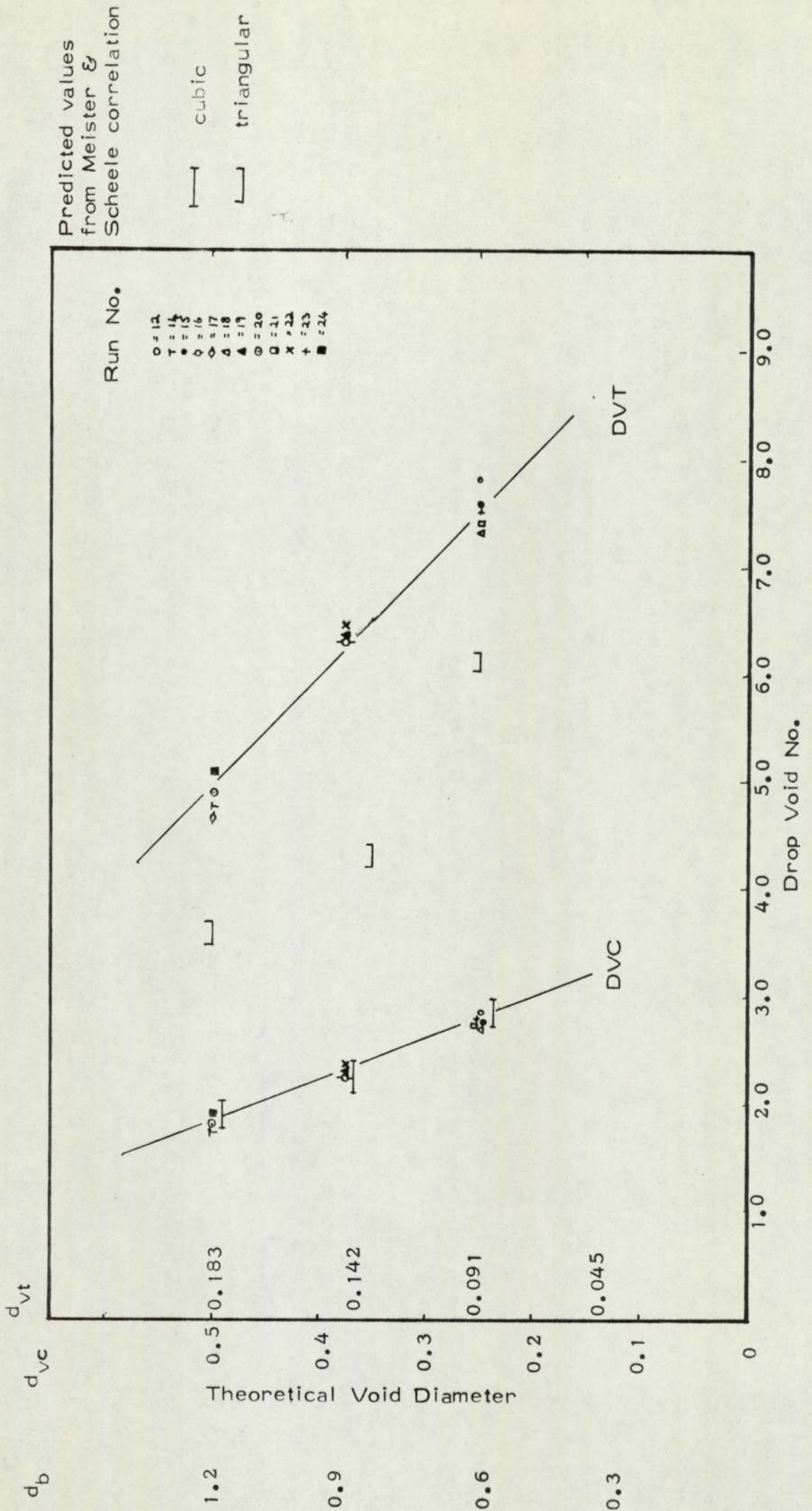
Run	d ball	DVC	st. dev	DVT	st. dev
12	0.6	2.94258	0.164617	7.8849	0.4411
14	1.2	1.79961	0.16303	4.8223	0.4387
15	0.6	2.8413	0.14491	7.6134	0.3883
*16	0.9	2.3652	0.18520	6.3379	0.49653
*17	1.2	1.7535	0.46877	4.6986	1.2561
*18	0.6	2.7573	0.21571	7.3884	0.57803
19	0.9	2.3771	0.12722	6.3697	0.340887
20	1.2	1.8505	0.11593	4.9585	0.310657
21	0.6	2.7643	0.26135	7.40725	0.70031
*22	0.9	2.4317	0.21069	6.5159	0.56456
*23	0.6	2.8702	0.19105	7.69091	0.51193
*24	1.2	1.9199	0.15115	5.1448	0.40502

\* Preferentially wetted packings

The experimental Drop Void Nos., DVC and DVT were plotted against their respective void diameters,  $d_{vc}$  and  $d_{vt}$ , as shown in Fig.(9.2.9). The Drop Void Nos. for each respective ball diameter show good agreement with those obtained from different experimental conditions. From the data presented, it would also appear that a linear relationship exists between the Drop Void No. and void diameter for both cubic and triangular geometries. However, to evaluate which packing geometry is more applicable to the exit layer of the packing, it is necessary to compare the experimental Drop Void Nos. with those obtained from the theory of

Fig. 9.2.2.9

COMPARISON OF EXPERIMENTAL & THEORETICAL DROP-VOID NUMBERS





drop formation at standard nozzles. From the literature on drop formation at flat nozzles and sharp edged orifices, it was concluded that the correlations of Meister and Scheele<sup>(96)</sup> were most suitable for use because:-

- (1) The models were based on a sound rate of momentum balance;
- (2) their work covered the whole range of conditions of drop formation from infinitely slow formation to the break-up of jets;
- (3) their experimental work covered a wide range of physical properties, and the reported agreement between experimental and predicted volumes was within 11%;
- (4) for the systems used in this study, i.e.  $\mu < 10 \text{ cP}$ , their correlations can be solved analytically.

Using the Meister and Scheele correlation Fig(A.5.1 - 3) the theoretical Drop Void Nos. were obtained by evaluating the drop diameter formed at an orifice equivalent to the void diameter described by the cubic and triangular geometries of each ballotini size. The velocity during drop formation was unknown, hence each theoretical drop void number was calculated for the velocity range 2 - 10 cms/sec (i.e. in the sub-jetting region).

When the theoretical values are superimposed on Fig.(9.2.9) it can be seen that the cubic geometry values are in very close agreement with the cubic experimental values, whereas the agreement is poor for the triangular geometry.

It would appear, therefore, that the exit drop diameter is a function of a mean exit packing geometry equivalent to a cubic arrangement of ballotini, where  $k = 0.414$ . For this to be true, the following assumptions must apply:-

- (i) The drop formation mechanism from a void within a cubic ballotini arrangement is the same as that from sharp-edged orifices or standard nozzles.
- (ii) the void diameter of a ballotini geometry can be described by the maximum circle inscribed in the passage of the packing;
- (iii) the dispersed phase flow phenomena through the packing restriction is the same as that characterizing drop formation at a single nozzle or orifice under continuous flow conditions.

Further work was performed to investigate the above assumptions. This encompassed:-

- (A) A single flat nozzle with continuous flow;
- (B) single ballotini orifices with continuous flow conditions;
- (C) single ballotini orifices under drop release conditions.

### 9.3) Single Nozzles

In a parallel study suggested by the author but performed by Jenkinson<sup>(173)</sup>, drop formation at single flat nozzles and single ballotini orifices was investigated. Both experiments were carried out under the condition of drop formation by continuous flow. For single flat nozzles, Jenkinson found good agreement between the experimental values and those predicted by the correlation of Meister and Scheele. For single ballotini nozzles, the void diameter was described using a hydraulic mean diameter ( $d_h$ ):-

$$d_h = \left( \frac{4 \times \text{volume of void filled by the fluid}}{\text{surface area of contact by fluid}} \right) \quad (9.3)$$

For single ballotini nozzles, good agreement was found between predicted and experimental values for  $d_h > 0.54$ . However, for the majority of the results, where  $d_h < 0.54$ , very poor agreement was obtained. This arose because drop formation mechanisms changed below a critical hydraulic mean diameter. No



further information was given, however, several other points in this work merit discussion.

The shape of the curves described by the drop diameter formed at different sized ballotini nozzles<sup>(173)</sup> followed a similar peak to the valley trend, as shown for the packed bed results Fig.(9.1.3). This would suggest that for single nozzles, the drop formation process is very sensitive to effects of the orifice geometry on flow rate.

In a continuous flow operation, the total cross-sectional area of the void would probably act as the orifice, and the drops formed are some function of the void diameter equivalent to the area of the restriction ( $d_v^t$ ). The equations for the void diameter are given below:-

$$\text{Cubic} \quad \text{Void area} = \left( d_b^2 - \pi \frac{d_b^2}{4} \right); \quad d_{vc}^t = \left( 0.274 d_b^2 \right)^{0.5} \quad (9.4)$$

$$\text{Triangular} \quad \text{Void area} = \left( 0.432 - \frac{d_b^2}{8} \right); \quad d_{vt}^t = \left( 0.051 d_b^2 \right)^{0.5} \quad (9.5)$$

Using eqn. (9.4)(9.5) the results reported for single ballotini orifices operating under continuous flow are presented below:-

$d_b$	$d_{vc}^t$	$d_{dj}$	$d_{dm}$	$d_{vt}^t$	$d_{dj}$	$d_{dm}$
1.2	0.625	1.14	1.10	0.272	0.72	0.77
0.9	0.450	0.94	0.95	0.204	-	-
0.6	0.325	0.89	0.86	0.136	0.65	0.62

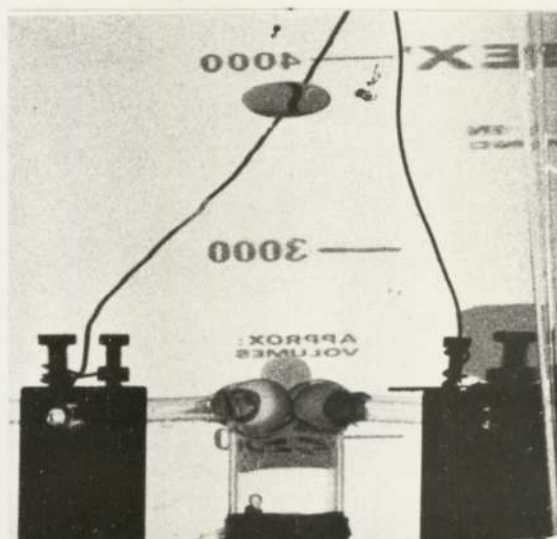
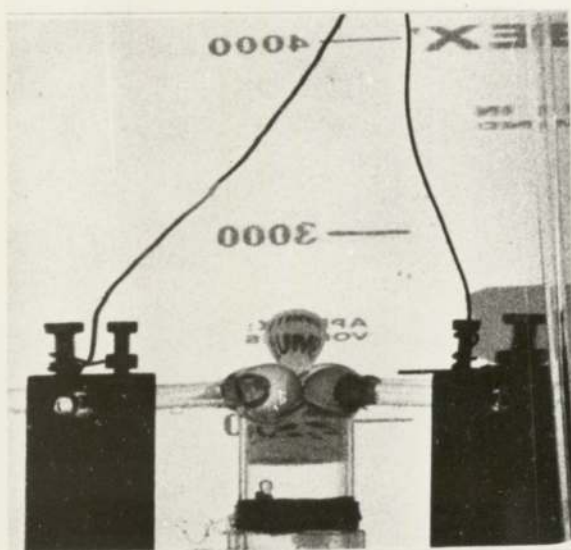
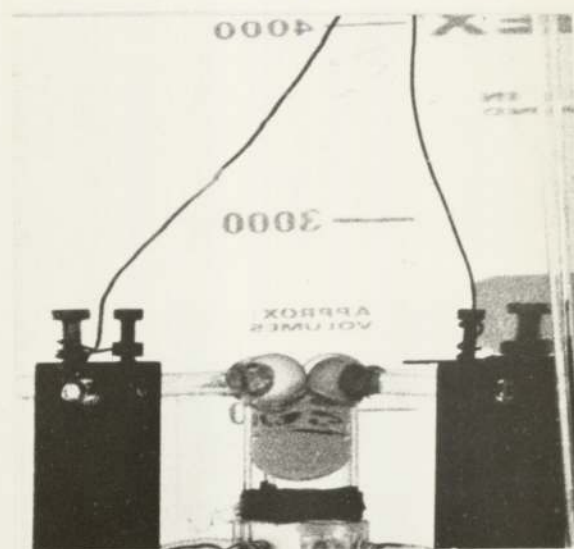
(where j & m refer to drop diameter obtained by Jenkinson<sup>(173)</sup> & Meister<sup>(96)</sup>)

Using void diameters based on the total cross-sectional area available for flow, good agreement between experimental values and theoretical values was obtained.

However, comparison of the actual values for the single

Fig. 9.3

NORMAL EXIT DROP FORMATION





cubic ballotini orifices with those obtained for a packed bed (Table 9.3.1) results in a difference of 10 - 25%.

Table 9.3.1.

$d_b$	Average packed bed - $d_{xt}$	Single Cubic Nozzle - $d_{dj}$
1.2	0.9	1.14
0.9	0.845	0.94
0.6	0.70	0.89

All the experimental evidence suggested that the mechanism of drop formation at a ballotini nozzle was sensitive to the flow conditions present during drop formation. The release mechanism in a packed bed effectively represents a non-steady state, as described in Section (7.3). The retained mass can only break through the restriction when the buoyancy forces are greater than the surface tension forces. On break-through, the stationary held-up mass has to accelerate from a zero velocity to that which is equivalent to the terminal velocity of the resulting drop. At some point during the acceleration period, a drop will form from the balance of the buoyancy, kinetic and surface forces present. The process of drop formation is further complicated by the effect of orifice geometry on the flow into the drop during initial formation and also when the drop has lifted away from the orifice during the detachment period.

The process of drop formation and detachment was investigated using the cubic ballotini orifices employed during the investigation of the inlet drop mechanism - Fig. (9.3) shows a typical sequence of drop retention and release. Studies were made of the release mechanisms and subsequent drop formation process

using cine photography. The velocity of the liquid flowing through the orifice was analysed from the time required for drop formation. In all the systems and orifice sizes investigated, the velocity of the liquid into the drop was found to be below the velocity required for jetting as predicted by Meister and Scheele<sup>(109)</sup>, eqn(3.13).

The theoretical and experimental drop diameter ( $d_{dm}$ ;  $d_{exp}$ ) for single ballotini nozzles, and the average exit drop diameter ( $d_{xt}$ ) from the packed bed studies are given in Table (9.3,3):-

Table 9.3.3

<u>Toluene</u>					
$d_b$	$U_j$	$U_x$	$d_{exp}$	$d_{dm}$	$d_{xt}$
1.2	-	-	-	-	-
0.9	15.2	5.25	0.920	0.90	0.845
0.6	19.0	4.75	0.690	0.74	0.70
<u>Iso Octane</u>					
1.2	-	-	-	-	-
0.9	16.8	7.25	0.73	0.77	-
0.6	25.8	7.85	0.53	0.64	-
<u>Diethyl Carbonate</u>					
1.2	8.0	0.9	1.08	1.06	-
0.9	9.7	1.28	0.94	1.01	-

The theoretical value,  $d_{dm}$  was estimated using the velocity,  $U_x$ , obtained from cine photography analysis, and the void diameter of a cubic geometry, where  $d_v = 0.414 d_b$ . The results show good agreement between the theory of drop formation at standard nozzles and the experimental values obtained from the packed bed and single ballotini orifices, under the release mechanism.

Therefore, it is concluded that:-



- (1) The mean exit packing arrangement of a random packing of spheres is similar to a cubic geometry of ballotini;
- (2) the void diameter of a cubic ballotini geometry can be characterized by  $d_v = 0.414 d_b$ , when under drop release conditions;
- (3) the exit drop diameter formed on break through can be predicted using the Meister and Scheele correlation: where
 
$$d_v = 0.414 d_b$$

#### 9.4) Drop Release Mechanism

Any random packing of spheres will possess a distribution of void diameters. Consequently, for operation involving normal retention-release mechanisms, a distribution of exit drop sizes is to be expected. However, during investigation of drop formation on release from single ballotini orifices, it was observed that in some cases, the overall process was dependent on behaviour below the orifice. Three different modes of drop release were observed:

1. Normal Release: Fig. (9.3). Drop retention and growth by coalescence proceeded until the buoyancy forces exceeded the surface forces, resulting in penetration. Drop growth took place in a regular manner - i.e. each new drop fed into the restriction coalesced with the larger mass of the retained drop. On penetration and release, the drops formed were of even size ( $\pm 0.05$  cms). This mode of drop formation was observed in the majority of cases, and the results were used in Table (9.2).

2. Excess Hydrostatic Head: Fig.(9.4.1). Drop retention and subsequent growth occurred as described in the normal release

mechanism. However, beyond a certain point, additional drops coalesced with each other, but not with the upper retained mass (A). As a result, the lower drop increased in size until it forced the upper drop through the orifice (B). Nevertheless, the total volume retained, i.e. the effective buoyancy forces, much exceeded that required for release under normal conditions. During the initial process of penetration, the lower and upper drops coalesced resulting in a quasi jetting situation, as in Fig.(C - F). The jet may have resulted from the 'kick' associated with the transference of the contents of one drop into the other. Alternatively, the situation of penetration and release may have become unstable owing to excessive hydrostatic forces acting on the orifice. The instabilities imposed during drop formation resulted in secondary droplets (H).

### 3. Release by Coalescence : Figs. 9.4.2 and 9.4.3

The drop retained at the orifice underwent coalescence with the feed drop resulting in premature penetration, owing to the inherent instabilities of film rupture. This situation is similar to that in 'I2' but the total volume was below that required for normal release. Figs.(9.4.2) & (9.4.3) illustrate that the mode of release occurred when coalescence took place, either :-

- (i) Between the lower drop and the retained mass;
- or (ii) Between two lower drops.

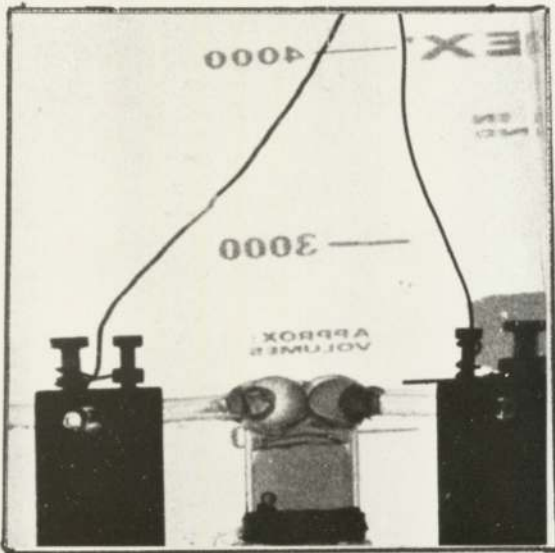
In both cases a single drop was formed and no secondary drops were observed.

The existence of unstable drop release processes compound the difficulties of relating the exit drop sizes to the

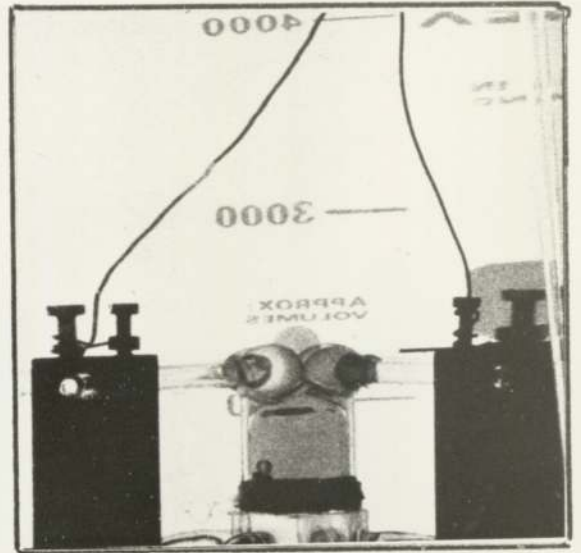


Fig. 9.4.1

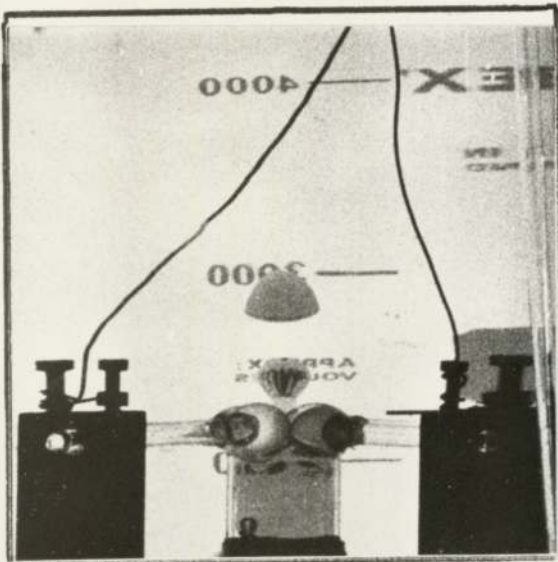
EXIT DROP FORMATION  
UNDER EXCESS HYDROSTATIC HEAD CONDITIONS



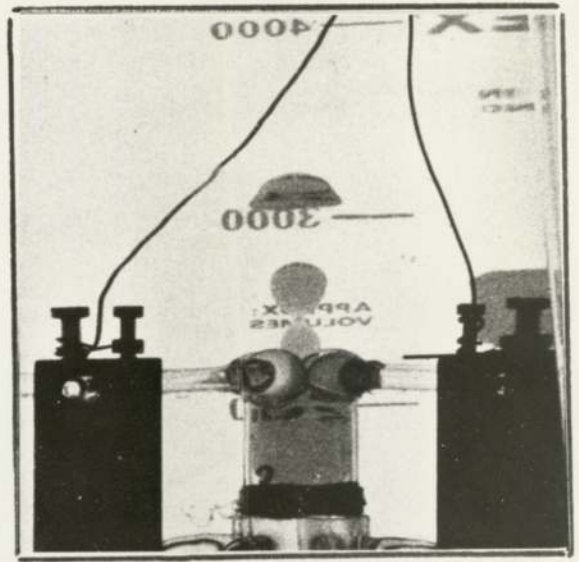
(A) Uncoalesced lower mass



(B) Lower mass forces through penetration of upper mass



(C) Lower and upper mass coalesce

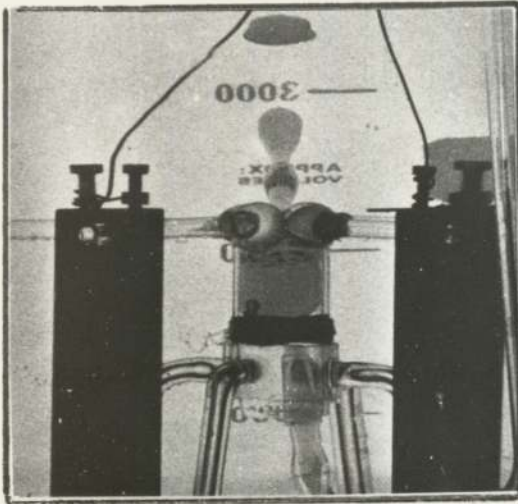


(D) Unstable condition

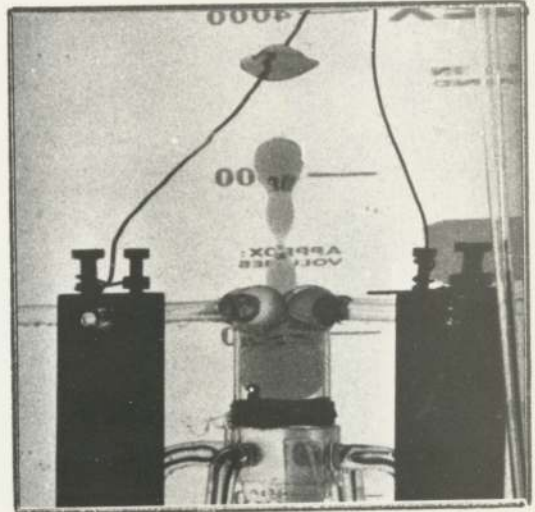
Fig. 9.4.1

(Continued)

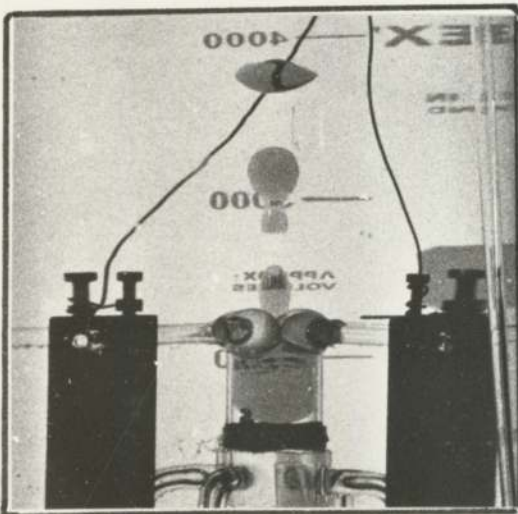
EXIT DROP FORMATION UNDER  
EXCESS HYDROSTATIC HEAD CONDITIONS



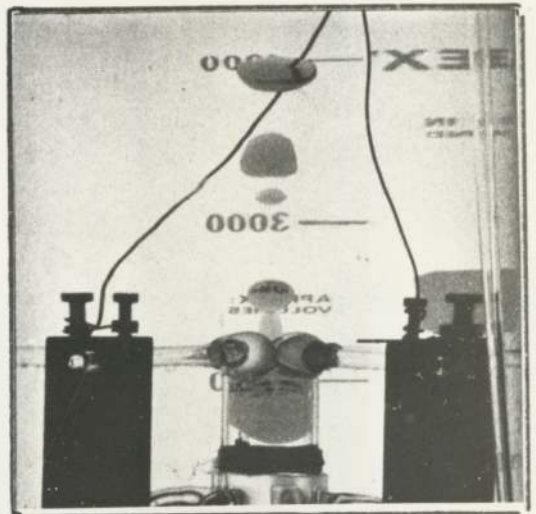
(E) Formation of jet



(F) "Necking" of jet



(G) Jet detachment

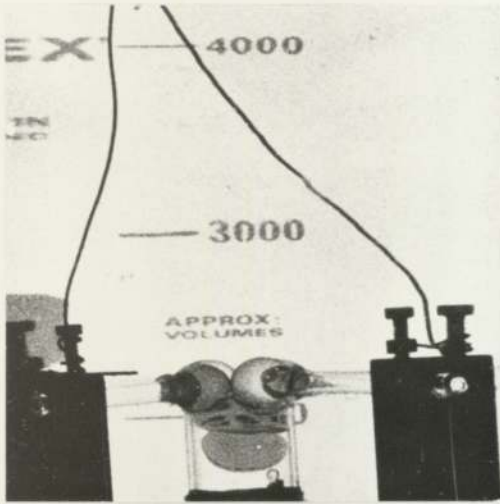


(H) Formation of Secondary Droplet

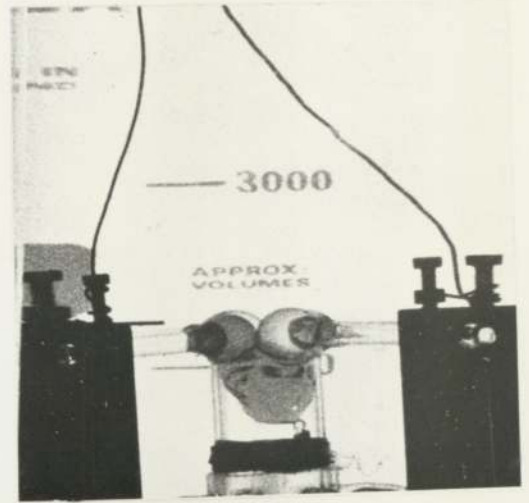


Fig. 9.4.2

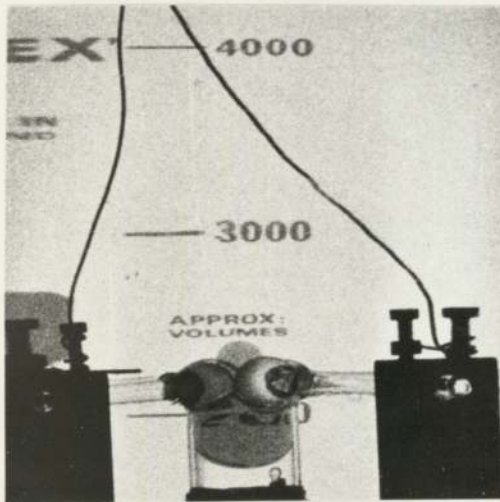
EXIT DROP FORMATION  
PROMOTED BY COALESCENCE



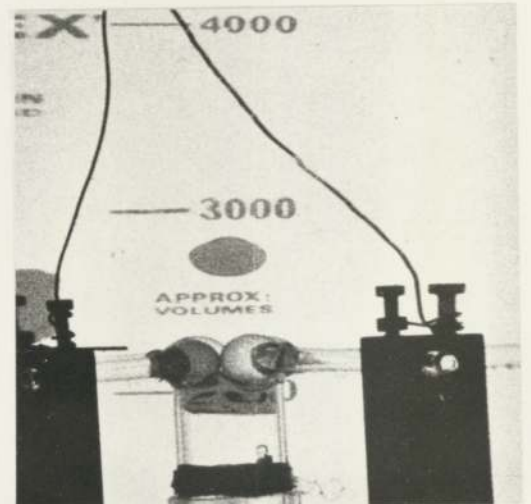
(A) Arrival of Droplet



(B) Coalescence of Droplet



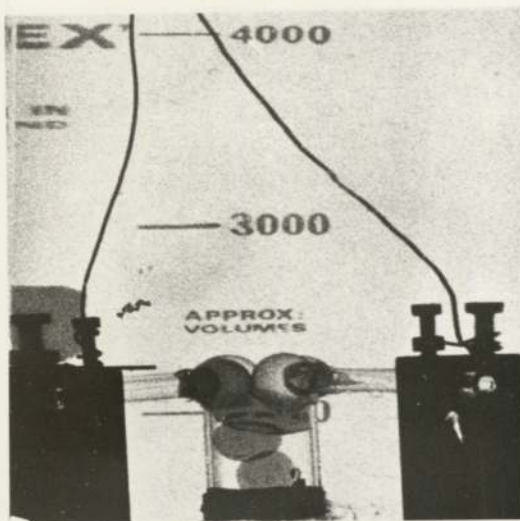
(C) Premature Penetration



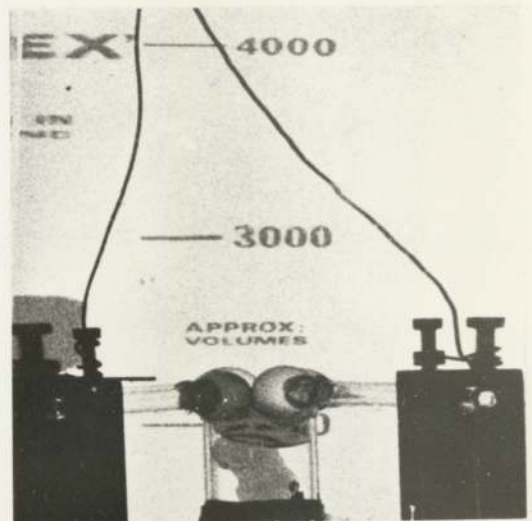
(D) Single Drop Release

Fig. 9.4.3

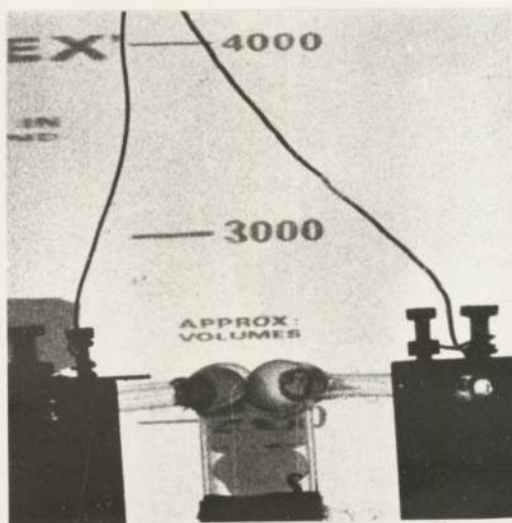
EXIT DROP FORMATION  
PROMOTED BY COALESCENCE



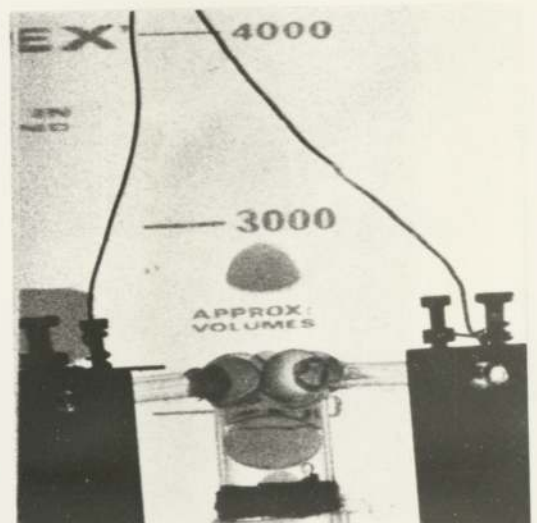
(A) Lower Drops Uncoalesced



(B) Lower Drops Coalesce



(C) Drop Contents Transferring



(D) Penetration and Drop Formation (Lower Drop has not coalesced with Upper Mass)



void size distribution in the exit layer. Drop formation by normal release and jetting was observed for the packed bed, as shown in Figs.(9.4.4 A & B). However, in neither case was it clear which mechanism of release was operating. In Fig(9.4.4.B) the mode of release may have been normal or premature, whilst in Fig.(9.4.4.A) jetting may have been caused by excessive hydrostatic forces, as described in (9.4.2) or breakup of rivulet flow from within the bulk of the packing. In the photograph of jetting, Fig( A ) a neighbouring orifice is shown acting under normal release and the drops formed are larger in size than those produced by jetting.

#### 9.5) Design Considerations

If the bed is operating under total coalescence, the exit drop diameter can be predicted, provided the characteristics of the exit packing layer geometry are known. Unfortunately, it is often difficult to determine the exit packing layer geometry and whether the packing is operating under total coalescence. A more general correlation of the relationship of the exit drop diameter with system parameters has been presented in Section ( II ).

For operation under total coalescence, it has been shown that an increase in the exit drop diameter was obtained with an increase in the exit void diameter. This is of importance in the design of a packed bed, since any increase in the exit drop size represents an increase in operation efficiency. Clearly, however, there is a limit to this technique.

Above a certain size, a rising or falling drop is no longer stable, and break up will result from induced oscillation imposed by the drag forces<sup>(174)(175)</sup>. For a liquid-gas system, break up occurs by the cavity at the rear of the drop penetrating

(175)  
 the drop, resulting in shattering. For liquid-liquid systems, break up has been observed to occur when the frequency of oscillation imposed by the drag forces equals the natural frequency (176) of the drop. This has been represented by the following eqn.:-

$$\left( DE_1 \right)_{crit} = \left[ 1.452 \times 10^{-2} \frac{\sigma}{\Delta\rho} \right]^{0.5}$$

For the system investigated in this study, the maximum drop size which is theoretically stable whilst rising under its own buoyancy force is:-

Continuous Phase	Dispersed Phase	Max. Drop Size (cms)
Water	Diethyl Carbonate	2.6
"	Toluene	1.95
"	Iso-octane	1.6
"	MIBK	0.84

Therefore, in the design of a coalescing aid, the maximum exit drop size must be related to:-

- (i) Drop retention-coalescence and release;
- (ii) Drop formation at the exit packing layer;
- (iii) Maximum stable drop size.

These are valid for non-wetted packings only, and different specifications are predicted for wetted packings. Whilst this study did not extend to wetted packings, Figs. 9.4.4(C & D) show how greater or less separation can be obtained with packings wetted by the dispersed phase. In Fig. 9.4.4(D) half of the exit layer was treated with dichloro-methyl silane to render it wetted. From the wetted packing, large diameter jets formed, but these ruptured to give both large and small drops; in some cases very small

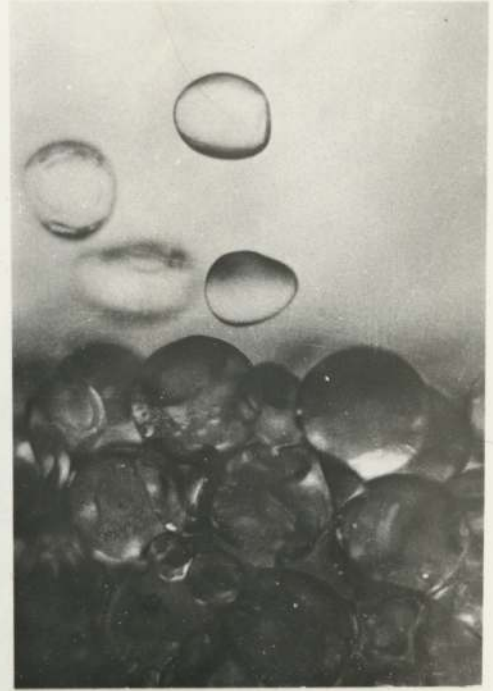


Fig. 9.4.4

EXIT PACKING DROPLET PHENOMENA

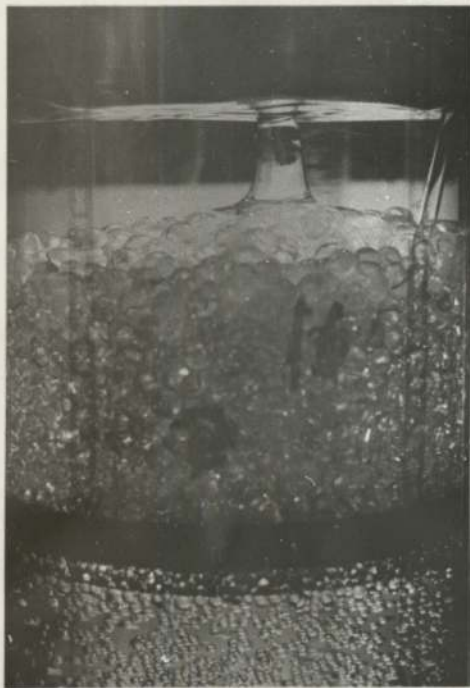


(A) Quasi Jetting



(B) Normal Release

NON-WETTED PACKINGS



(C) Exit Layer Wetted  
(Total Separation)



(D) Half Wetted - Half Non-Wetted  
Illustrating Jetting and  
Secondary Droplet Formation

secondary drops were formed. Drop sizes were more uniform from the non-wetted section and this packing was probably acting as a more efficient separator.

Fig. 9.4.4.(C) demonstrates how the flow characteristics of a wetted packing may be used to maximum advantage, i.e. to achieve total separation. This was obtained by promoting a preferential drain-off point by means of a small apex in the bed height. Thus, only one large jet left the bed. To prevent jet break up, the upper organic water interface was lowered below the length of the jet required for break up. Hence, the coalesced drops leave by one jet which feeds directly into a bulk interface.

#### Concluding remarks on exit drop mechanisms

The work carried out in this chapter has indicated that in non-wetted packings the exit drop dispersion can be related to the geometry of the packing in the exit layer. However, this work was carried out under the induced conditions of total coalescence, i.e., the inlet drop dispersion undergoes retention and growth before release and drop formation occur. Whilst this indicates the maximum drop size possible for the packing, of greater importance is the relationship between the packing geometry and drop retention. Therefore, work was carried out to investigate the prediction of droplet retention in packed beds of mono-sized ballotini.



CHAPTER 10.

DISCUSSION OF RESULTS

Application of Inlet Model to the efficiency of a Packed Bed

## 10.1 Packed Bed Considerations

It has been shown that the drop retention can be predicted with good accuracy if the physical properties of the liquid system and the void diameter are known. In many practical situations, the mean void diameter or, more important, the void size distribution of the packing, is not known. In this study, random packings of mono-sized ballotini were used, as much information exists as to the packing properties of spheres. By using the theoretical approach of the inlet model and a void size distribution, it was hoped to estimate the efficiency of a packed bed by comparing the experimental mean exit drop size with the maximum drop size possible for that packing.

Before discussing the experimental results obtained to test the above hypothesis, it is necessary to introduce a method of determining the geometry of packing. The bulk voidage values of a random packed bed of equal sized ballotini in a 9" column are shown in Table (10.1). Also included in Table (10.1) are the geometric properties of several fundamental packing arrangements, some of which are shown in their different forms.

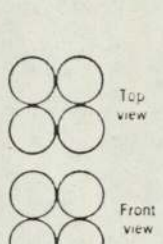
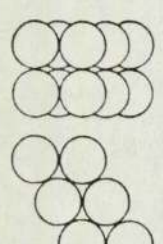
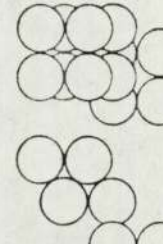
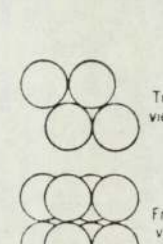
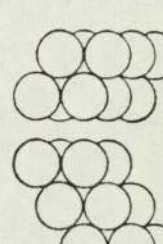
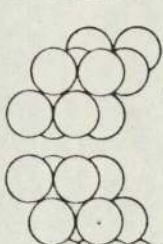
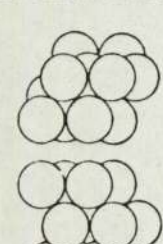
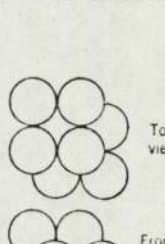
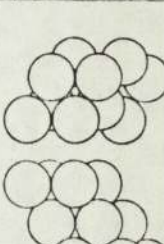
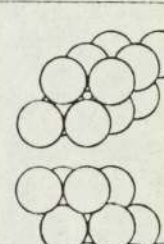
Comparison between the voidage values of the random packed bed with those of the fundamental units of packing indicates that the orthorhombic geometry is likely to be dominant. From Fig. (10.1) it can be seen that several different forms of an orthorhombic packing arrangement exist, but more important, this unit consists of both triangular and cubic geometries. Thus, even in the case of a single packing unit, different characteristics of retention or passage are possible. Moreover, in a random packing arrangement, a greater distribution of void diameters will exist. Whereas no



Table 10.1 PACKING GEOMETRIES OF EQUAL SIZED SPHERES

Name/Coordination No.	$\epsilon$	Pore volume Unit volume	radius inscribed in cavities	radius insc. in passage
Rhombohedral 12	0.2595	0.3505	0.2247 r 0.4142 r	0.1547 r
Spheroidal 10	0.3018	0.4324	0.2910 r	0.2649 r 0.1547 r
Orthorhombic 8	0.3954	0.6540	0.5275 r	0.4142 r 0.1547 r
Body centre cubic 8	0.3198	0.4702	0.2910 r	0.2247 r
Hexagonal extended layers ABAB 8	0.4626	0.8607	0.5275 r 0.8028 r	0.1547 r
Hexagonal extended layers ABCABC 6	0.4626	0.8607	0.8028 r	0.3333 r
Primitive cubic 6	0.4764	0.9099	0.7320 r	0.4142 r

Systematic Arrangement of Spheres and their Porosities

 <p>1 Cubic Porosity 0.476</p>	 <p>2 Orthorhombic (clear passage) Porosity 0.3954</p>	 <p>3 Orthorhombic (blocked passage) Porosity 0.3954</p>	 <p>4 Orthorhombic Porosity 0.3954</p>	 <p>5 Tetragonal Sphenoidal (clear passage) Porosity 0.3019</p>
 <p>6 Tetragonal Sphenoidal (blocked passage 1) Porosity 0.3019</p>	 <p>7 Tetragonal Sphenoidal (blocked passage 2) Porosity 0.3019</p>	 <p>8 Rhombohedral Porosity 0.2595</p>	 <p>9 Rhombohedral (clear passage) Porosity 0.2595</p>	 <p>10 Rhombohedral (blocked passage) Porosity 0.2595</p>

Experimental voidage values of randomly packed beds of ballotini :

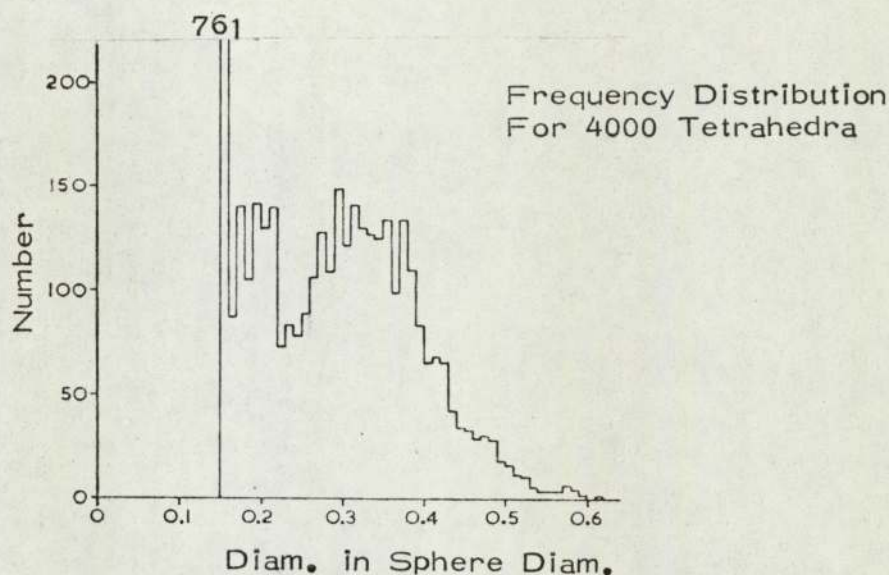
Ballotini	1.2 cms	6" diameter column	9" diameter column
Diameter	0.9 cms	0.42	0.415
	0.6 cms	0.41	0.408
		0.40	0.395

Theoretical Voidage: Cubic = 0.476 Triangular = 0.396



reliable experimental size distribution of random equal size spheres exists, several theoretical approaches have been reported. Mason<sup>(177)</sup> using a random number generator for edge lengths 1.0 - 1.4, obtained the size distribution of the void diameters of a random packing of equal spheres shown in Fig.(10.2).

Fig. 10.2



The median was reported at 0.275 D, but the mode clearly occurs at 0.15 D, where D = diameter of the sphere. The mode value is approximately equal to the geometric relationship of a triangular packing arrangement, i.e.  $d_v = 0.1545 d_b$ . From the histogram it is also seen that 1/5 of all void diameters can be described by the triangular geometry.

The controlling factor for coalescence is that the inlet drop diameter has to be greater than the minimum void diameter. Mason's work has shown that the smallest void in a random packing of spheres is that described by the triangular arrangement. In order to design an experiment to investigate packing efficiencies, it is desirable that the conditions of total coalescence are not obtained. Thus, by using the inlet drop theory of retention, the following inlet drop diameters required for retention are obtained, Table(10.2).



Table 10.2

$d_b$	$d_{vt}$	Inlet drop diameter required for retention (cms)		
		Toluene	Iso-Octane	M.I.B.K.
1.2	0.183	0.315	0.435	NR *
0.9	0.142	0.198	0.224	NR *
0.6	0.091	0.116	0.125	0.181

\* NR = No Retention

To evaluate the accuracy of the inlet model, an inlet drop diameter was chosen which was approximately equal to the minimum drop diameter required for retention with the 0.6 cms diameter ballotini. The same size inlet drop was used with the 0.9 and 1.2 cms, in order to compare the accuracy of the model and also to evaluate the characteristics of packings operating on the limit of drop retention.

The values shown in Table (10.2) suggest that if the assumption of packing geometry and the prediction of the size of drop retained are correct, then for an inlet drop size of 0.1 - 0.16 cms, coalescence is expected within the 0.6 cms ballotini, but the amount of retention and coalescence will decrease with an increase in (i) ballotini diameter, and (ii) physical property number values. The 9" diameter counter-current apparatus described in para. (5.2.2) was used to investigate packing efficiencies. This apparatus can be operated under co-current or counter-current flow conditions. Initial experiments were carried out using only dispersed phase flow as described in Section (5.2.1).

From the theory of drop retention, it can be said that if the forces promoting drop passage are effectively reduced by counter-current flow, then an increase in coalescence is predicted. Therefore, several experiments were carried out to investigate the effects of counter-current flow. The results for dispersed phase flow and counter-current flow are given in Appendix(A.4.2-3) and in Table (10.3).



TABLE 10.3

## RESULTS FROM 9" DIAMETER COLUMN

Run No.	Phys. Property No.	Diameter Packing (cms)	9" Diameter Column				$d_{xt}$ average (cms)	Standard Deviation (cms)	$d_{xt}$ Theoretical (cms)	Packing Efficiency (%)
			DVC	DVT	Distribution	Plate Orifice diam = 0.4 mm				
<u>Dispersed Phase Flow Only - Distribution Plate Orifice diam = 0.4 mm</u>										
2		1.2	0.22147	0.59311		0.110	-	1.0	0.0	
6	2.1	0.9	1.10741	2.96742		0.412	0.134	0.855	40.3	
11		0.6	2.36514	6.33765		0.592	0.0338	0.750	75.5	
<u>9" Column Counter-Current Flow</u>										
24		1.2	0.22874	0.61273		0.114	-	0.88	0.0	
27	2.9	0.9	0.49986	1.33945		0.187	0.0186	0.75	13.4	
30		0.6	1.873313	5.01926		0.469	0.0478	0.66	64.0	
13		1.2	0.22987	0.61518		0.1145	-	0.66	0.0	
16	9.8	0.9	0.39812	1.0669		0.149	0.0247	0.55	8.90	
21		0.6	1.26051	3.37763		0.314	0.066	0.475	57.0	
7		0.9	1.3567	3.6351		0.513	0.161	0.855	53.8	
10	2.1	0.6	2.5145	6.73802		0.628	0.061	0.750	81.1	
30	2.9	0.6	1.86456	4.9963		0.464	0.054	0.66	63.8	
<u>9" Column Counter-Current Flow</u>										
7		0.9	1.3567	3.6351		0.513	0.161	0.855	53.8	
10	2.1	0.6	2.5145	6.73802		0.628	0.061	0.750	81.1	
30	2.9	0.6	1.86456	4.9963		0.464	0.054	0.66	63.8	

\* Inlet dispersion produced from a distributor plate with 0.04 cms diameter orifice



The packing efficiency given in Table(10.3) was defined by the following equation:-

$$\eta = \left[ \frac{d_{xt \text{ mean}} - d_{in}}{d_{xt \text{ theory}} - d_{in}} \right] \times 100 \quad (10.1)$$

where  $d_{xt \text{ theory}}$  is the maximum exit drop size for that packing size. From the previous discussion in Section(9.3), this has been shown to occur under conditions of total coalescence and can be predicted by the correlations of Meister and Scheele, using the equn.  $d_v = 0.414 d_b$ .

The mean inlet drop and outlet drop diameters were obtained from photographs. These were used to determine the Drop Void Numbers, DVC, DVT, and the average exit drop diameter, as described in Section (9.2). The inlet drop sizes were found to be in very good agreement with those obtained by Hitit<sup>(2)</sup> who used the same systems and apparatus.

## 10.2) Discussion of Results

The predicted trends of packing efficiency have been proved to be correct in that the data obtained under packed column operation shows that:-

- (a) Packing efficiency decreases with increase in ball diameter;
- (b) Packing efficiency decreases with increasing buoyancy group number.

The predicted size of drop which would be retained in the minimum void diameter in the triangular geometry is shown in Table (10.2). For the inlet drop size range used in Systems I, II, III - Table(10.3)- it was predicted that coalescence would occur only for the 0.6 cms packing and little or no coalescence would be expected for 0.9 and



1.2 cms diameter packings. This was the case with the noticeable exception of the 0.9 cms packing for Toluene, which had a mean outlet drop size of 0.412 cms. A measure of coalescence taking place is given by the packing efficiency in Table(10.3), and it can be assumed that values  $< 15\%$  represent no coalescence. The surprisingly high packing efficiency for Toluene with the 0.9 cms diameter packing may possibly be explained by the existence of a residence time for drop passage, i.e. drops which are just above the critical point of retention squeeze through the aperture, but time is required for deformation and passage. During the time period of passage, subsequent drops arrive at the same restriction, and some contact is possible. Although the situation is unstable, contact between semi-stationary drops results in some cases in coalescence. Alternatively, it could be suggested that coalescence will take place by dynamic drop-drop collisions, but counter-current results show this not to be so.

For counter-current flow, however, a small increase in packing efficiency was found for a toluene system, and a slight decrease was found for iso-octane. The increases may be real or they could be explained by experimental error. From observations made at the column wall of the interstices of the packing, no drop-drop coalescence was observed under counter-current flow operation. At high dispersed and continuous phase flow rates, the voids were seen to contain large numbers of inlet drops undergoing much swirling and drop-drop collision. However, very little coalescence was seen to take place during the dynamic process existing during 'swirling'. This confirms observations of previous workers<sup>(2,50)</sup> and suggests that the static process of coalescence



described in Section (7.1) is probably the dominant process. The static process has been defined by drop collision with a retained drop in a packing restriction. Under counter-current operation, some coalescence may be possible by drops jostling for priority in the interstices, in a manner similar to that in the drop-squeeze situation, Fig.(7.1). Further experimental work was required to observe the droplet hydrodynamics within the bulk of the packing to substantiate this hypothesis.

#### Packing Efficiency Considerations

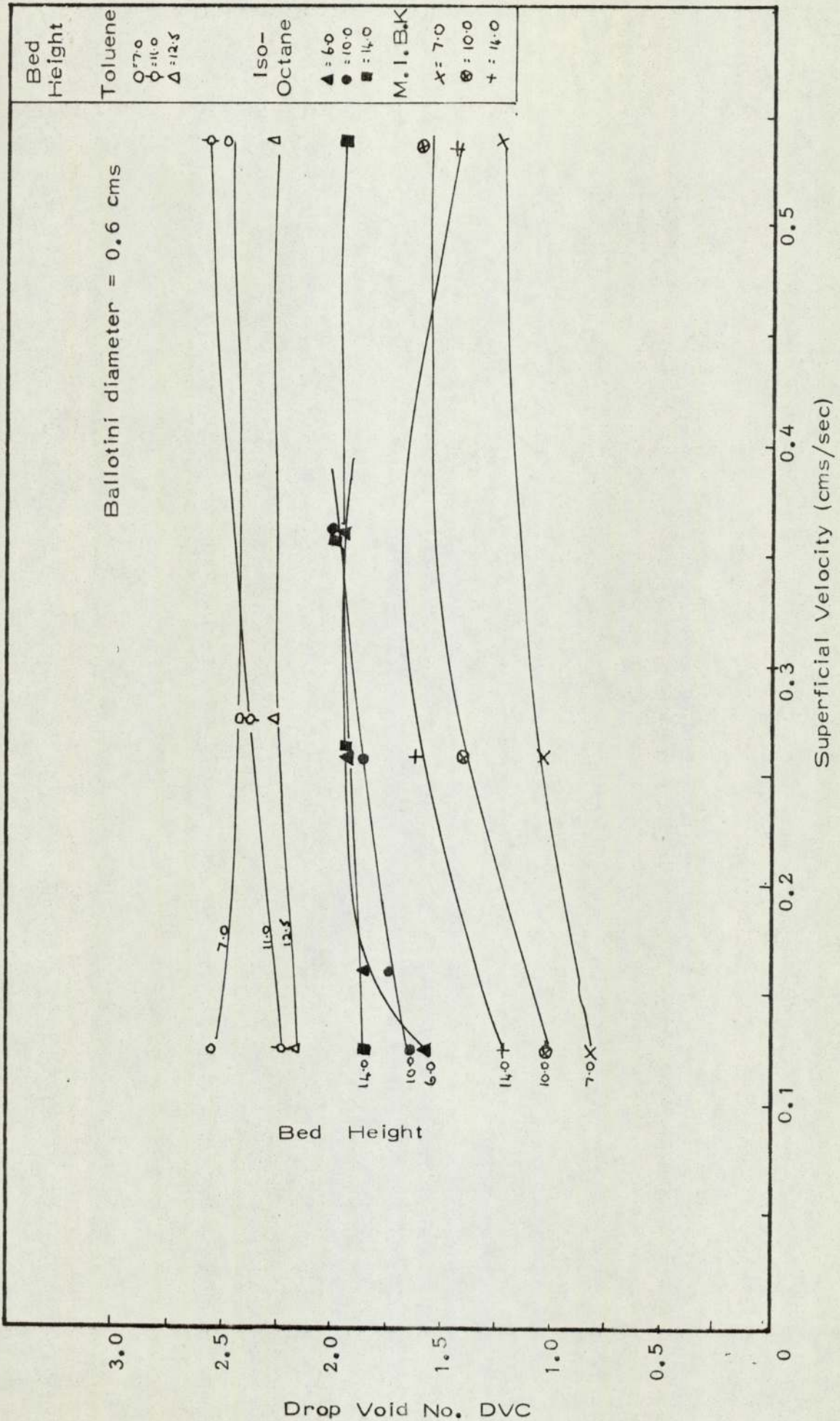
The average exit drop diameter for each run was taken for a range of bed heights and flow rates, and represents approximately 1800 individual drop measurements for each of the single phase flow studies and approximately 5000 for each of the counter-current studies. In this way, some 35,000 drop measurements were obtained for analysis.

A regression analysis carried out on the 9" diameter column results indicated that bed height, continuous and dispersed flow rates had very little effect on the overall correlation - Appendix (A3.6). However, the accuracy of the correlation was only fair, owing to the existence of two distinct processes of retention and release in the packing. The regression analysis has shown that the most important parameter was that of the ballotini diameter. Thus the procedure for averaging all the mean exit drop diameters for one particular ballotini diameter was justified.

The data obtained for  $d_b = 0.6$  cms in the 9" diam. column operating under dispersed phase flow conditions is shown in Fig.(10.3). It can be seen that whilst flow rate has very little effect on the exit drop size, the effect of bed height varies with each of the

Fig. 10.3

VARIATION OF DROP-VOID NUMBER WITH BED HEIGHT  
(9" Diameter Column)





three systems investigated. For M.I.B.K., the exit drop diameter increases with bed height, but the reverse is true for Toluene, but no distinct trend is observed for Iso-octane. This would explain why the regression analysis gave a low coefficient for the bed height. The independence of the exit drop diameter from the bed height for packings operating in the regions studied, i.e.

$d_{in} \approx d_{void\ min}$  is surprising in view of the following considerations.

From previous work, it has been shown that approximately 1/5 of all the voids in a random packing of equal sized spheres are equal to the minimum void diameter. Therefore, in the case of a mono-sized inlet dispersion passing through a packing where retention occurs only in the minimum void diameter, then the probability of drop passage is  $\left(\frac{4}{5}\right)^n$ , where "n" is the number of layers of packing. This assumes no interaction of retained or coalesced drops on voids which would otherwise allow free passage of a drop. This indicates that the probability of passage is related to the packing height, i.e. the no. of packing layers. Therefore, assuming retention only occurs in the minimum void diameter, then the probability of retention can be evaluated as shown in Table(10.4). It can be seen that for the packing heights used in this study, i.e. 7 - 20 cms, a very high probability of retention is predicted; where the probability of retention  $\zeta$  is given by:  $\zeta = 1 - \left(\frac{4}{5}\right)^n$ .

Table 10.4

$\zeta$ Values:	.2	.36	.489	.591	.673	.738	.79	.832	.866	.892
n =	1	2	3	4	5	6	7	8	9	10
$\zeta$ Values:	.9135		.931		.9436		.9558		.9646	
n =	11		12		13		14		15	
$\zeta$ Values:	.9716		.9774		.9819		.9864		.9884	
n =	16		17		18		19		20	

If one packing restriction occurs for every ballotini diameter, then



for a bed height = 9 cms and  $d_p = 0.6$  cms;  $n = 15$ . This implies that 96.46% of all the inlet drops would be retained and coalesced within the bed if  $d_{in} = d_{min \text{ void}}$ . This can be related to the packing efficiencies by consideration of the following example.

Consider 1000 drops of 0.1 cms diameter entering a 0.6 cms ballotini packing; assuming that hold-up occurs only in the voids smaller or equal to the triangular packing arrangement, which constitute 1/5 of the packing void diameters. In these circumstances, the above probability can be applied to demonstrate the relationship between the probability of passage and the efficiency of the packing. For a packing height of 9 cms and 6 cms:-

$n = 15$	Probability of passage=0.0354
	No. of drops passing = 35.4
	No. retained drops = 964.4
$n = 10$	Probability of passage=0.108
	No. of drops passing = 108
	No. retained drops = 892

If It is assumed that all the retained drops coalesce to form a 0.5 cms drop, then for this volume of drop, 125 x 0.1 cms drop are required. Thus, the mean exit drop diameter can be found:

No. & size of drops	Total Volume	Total No. of drops	Mean Exit Drop diam.
$n=15 \quad (7.7 \times 0.5) + (35.4 \times 0.1)$	1.0	43.1	0.285 cm
$n=10 \quad (7.1 \times 0.5) + (108 \times 0.1)$	1.0	115.1	0.205 cm

(In reality, a fraction of a drop does not exist, but its inclusion is for illustrative purposes only).

To relate the mean exit drop  $d_{xt \text{ mean}}$  to the packing efficiency, It is necessary to consider the maximum exit drop diameter possible for that packing and system. This has been defined in



Section (9.3) as column operation under 'total coalescence'. If at total coalescence the 0.5 cms drop is stated as the maximum drop size, then using eqn. (10.1), it is possible to calculate packing efficiency values, viz:-

$$\sum_{\text{or } n = 15; \quad \lambda = \left( \frac{0.285 - 0.1}{0.5 - 0.1} \right) \times 100 = 46.3\%$$

$$\sum_{\text{or } n = 10; \quad \lambda = \left( \frac{0.205 - 0.1}{0.5 - 0.1} \right) \times 100 = 26.2\%$$

Thus, from the worked example, it can be seen that the theory of drop retention and release can be combined with the theory of probability associated with void size distribution to predict the theoretical packing efficiency.

The above example illustrates how the packing efficiency is sensitive to the outlet drop size distribution, particularly with regard to the number and size of the uncoalesced drops. This would indicate a need to measure all the drops in the exit dispersion. However, apart from the time and effort required, several difficulties are inherent in this suggestion.

Exit drop formation has been shown to take place at "active sites" undergoing a cyclic process of retention-growth by coalescence-and release (Sections 8 and 9). Thus, the mean exit drop size evaluated from any one photograph was dependent not only on the local geometric properties of the packing but also on the recorded point in the retention-release cycle. To overcome this difficulty and to obtain a more representative record, the total cross-sectional area of the column was photographed. However for the column diameters used in this study (6-9") problems were encountered with the image definition of small diameter droplets owing to the relationship between magnification, focal plane area and the depth of field. These problems are particularly apparent

when a large distribution of drop diameters is present, i.e. packed bed operation under partial coalescence.

The preceding points illustrate the problems inherent in obtaining an accurate representation of the mean exit drop diameter; not least of which is the effort and time required in manual measurement of the salient drop dimensions. To overcome some of these problems, several techniques were developed to utilize the properties of an Image Analysing Computer (Quantimet 720) to make an automatic assessment of the mean drop size (Chapter 6). The experimental technique involved the use of parallel light to obtain shadowgraphs which were suitable for use on the Quantimet 720. One of the advantages of parallel light is that it eliminates depth of field problems and small drops can be easily observed - this is shown in Fig. (6.2.2.C).

Chapters 8, 9 and 10 have been concerned with isolating and investigating the processes of drop retention and drop release in the bulk of the packing and at the exit layer of the packing. However, a need exists for a general correlation between the exit drop size and the overall system properties. Consequently, an experimental programme was carried out using Shadowgraph Photography to obtain the exit drop diameter for use with a general correlation. This has been described in more detail in Chapter 11.



CHAPTER 11.

DIMENSIONAL ANALYSIS

11.1) Dimensional Analysis

The parameters affecting exit drop size were first correlated by dimensional analysis. The factors that were considered to influence drop coalescence in the packed bed were as follows:-

$d_{xt}$	= the outlet drop size	(L)
$\Delta P$	= pressure drop over the bed	(ML <sup>-2</sup> )
$\rho_d$	= density of dispersed phase	(ML <sup>-3</sup> )
$\Delta \rho$	= density difference	(ML <sup>-3</sup> )
$g$	= gravity	(LT <sup>-2</sup> )
$d_{in}$	= inlet drop size	(L)
$d_b$	= diameter of ball or $d_v$ = diameter of void	(L)
$h_b$	= bed height	(L)
$\gamma$	= interfacial tension	(MT <sup>-2</sup> )
$\mu_d$	= viscosity of dispersed phase	(ML <sup>-1</sup> T <sup>-1</sup> )
$u_d$	= flow rate (superficial velocity)	(LT <sup>-1</sup> )

The Pi-Buckingham method was used to form the dimensionless groups.

Selecting  $\Delta P, u_d, g$ , as the three basic parameters, the following groups were evaluated:-

- $$P, u_d, g, \mu_d = (ML^{-2})^a (LT^{-1})^b (LT^{-2})^c (ML^{-1}T^{-1})^d = 0$$

i.e.  $a = -1$        $b = -1$        $c = 0$        $\left( \frac{\mu_d}{P u_d} \right)$
- $$P, u_d, g, \Delta \rho = (ML^{-2})^a (LT^{-1})^b (LT^{-2})^c (ML^{-3})^d = 0$$

i.e.  $a = -1$        $b = 2$        $c = -1$        $\left( \frac{u_d^2 \Delta \rho}{\Delta P g} \right)$
- $$P, u_d, g, \rho_d = (ML^{-2})^a (LT^{-1})^b (LT^{-2})^c (ML^{-3})^d = 0$$

i.e.  $a = -1$        $b = 2$        $c = -1$        $\left( \frac{u_d^2 \rho_d}{\Delta P g} \right)$
- $$P, u_d, g, \gamma = (ML^{-2})^a (LT^{-1})^b (LT^{-2})^c (MT^{-2})^d = 0$$

i.e.  $a = -1$        $b = -2$        $c = 0$        $\left( \frac{\gamma}{\Delta P u_d^2} \right)$
- $$P, u_d, g, d_{in} = (ML^{-2})^a (LT^{-1})^b (LT^{-2})^c (L)^d = 0$$

i.e.  $a = 0$        $b = -2$        $c = 1$        $\left( \frac{g d_{in}}{u_d^2} \right)$



The parameters  $d_b$ ,  $h_b$ ,  $d_{xt}$  have the same fundamental unit (L).

Hence the following groups result:

$$6) \left( \frac{gd_b}{u_d^2} \right) \quad \text{or} \quad \left( \frac{gd_v}{u_d^2} \right) \quad 7) \left( \frac{gh_b}{u_d^2} \right) \quad 8) \left( \frac{gd_{xt}}{u_d^2} \right)$$

The recurring set of  $\Delta P, u_d, g$  is not the only possible choice, in fact, several sets are suitable, and further analysis would yield different groups to those above. Yet, using the Pi-Buckingham transformation method it is possible to arrive at the same groups.

The term  $\Delta P$ , although difficult to measure, was included because it was considered important in the coalescence process. To eliminate this term and to form more recognizable groups, the standard technique of  $\pi$  transformation was carried out.

Transformation	Group	Name	Description
$\left( \frac{(\pi_1)^4 \pi_3}{(\pi_2)^2 (\pi_4)^2} \right)$	$\left( \frac{\mu^4 \Delta \rho g}{\gamma^3 \rho_d^2} \right)$	Property No.	Effect of surface tension viscosity & acceleration of dispersed phase
$\left( \frac{(\pi_1)^2}{\pi_2 \times \pi_7 \times \pi_6} \right)$	$\left( \frac{\mu d}{(\rho_d h_b \gamma)^{1/2}} \right)$	Ohnersonge No.	$\frac{\text{Viscous forces}}{(\text{Inertia force} \times \text{surface force})^{1/2}}$
$\left( \frac{\pi_3 \times \pi_8}{\pi_2} \right)$	$\left( \frac{d_{in}^2 g \Delta \rho}{u_d^2 \rho_d} \right)$	Expansion No.	$\frac{\text{Buoyancy force}}{\text{Inertia force}}$
$\left( \frac{(\pi_7)^2 \times \pi_3}{\pi_6} \right)$	$\left( \frac{d_{in}^2 g \Delta \rho}{\gamma} \right)$	Bond No.	$\frac{\text{Gravity force}}{\text{Surface tension force}}$
$(\pi_8 / \pi_7)$	$(d_{xt} / d_{in})$	Drop No.	Relation between drop in and drop out
$(\pi_5 / \pi_7)$	$(d_{in} / h_b)$	Height No.	Effect of packing height
$(\pi_5 / \pi_6)$	$(d_{in} / d_v)$	Void No.	Effect of void diameter on drop in
$\left( \frac{\pi_7^3 \times \pi_2 \times \pi_3}{\pi_1^4} \right)$	$\left( \frac{\Delta \rho \rho_d d_{in}^3 g}{\mu d} \right)$	Archimedes No.	$\frac{\text{Inertia force} \times \text{gravity force}}{(\text{viscous forces})}$

Therefore, the final correlation was:-

$$\left( \frac{d_{xt}}{d_{in}} \right) = C \left( \frac{\mu^4 g \Delta \rho}{\gamma^3 \rho_d^2} \right)^a \left( \frac{\mu d}{(\rho_d h_b \gamma)^{1/2}} \right)^b \left( \frac{d_{in} g \Delta \rho}{u_d^2 \rho_d} \right)^c \left( \frac{d_{in}^2 g \Delta \rho}{\gamma} \right)^e \left( \frac{d_{in}}{d_v} \right)^y \left( \frac{d_{in}}{h_b} \right)^x \left( \frac{\Delta \rho \rho_d g d_{in}^3}{\mu^2 d} \right)^z$$



The constants C, a, b, c, e, x, y, z were evaluated using ICL 1905 Statistical Analysis Library Programme - Appendix (A.3.7).

When the experimental data from the inlet and exit drop studies of the packed bed were inserted in equation (11.1) a general correlation of reasonable accuracy could not be obtained - Appx. (A3.5)(A.3.6). This was found to be due to the experimental bias inherent in the above studies. These have been fully discussed in Sections(9)&(10). Therefore, a further experimental study was carried out, based on the factorial analysis of randomized blocks and latin squares, as described by Davis<sup>(190)</sup>.

The 10 parameters in the derived dimensional equation can be grouped into the following sets of variables:

(i)	Physical properties of the liquid	A, B, C, D
(ii)	Dispersed phase flow rates	1, 2, 3, 4
(iii)	Bed heights	1, 2, 3, 4
(iv)	Diameter of ball (or void)	1, 2, 3
(v)	Inlet drop diameter	1, 2, 3

Groups (iv) and (v) can be combined to give the ratio of the ball diameter to inlet drop diameter. For  $d_b = 1.2, 0.9, 0.6$  cms and the inlet drop of 0.1, 0.25, 0.5 cms, the following ratios are determined:

12.0	4.8*	2.4
9.0*	3.6	1.8
6.0	2.4*	1.2*

From previous analysis of experimental results, it has been found that for a ratio  $> 6.0$  little or no coalescence occurs. Therefore, the four ratios of  $d_b/d_{in}$  are biased more to the lower values, viz - 1.2, 2.4, 4.8, 9.0. This approach proved to be justified by further treatment of the experimental results for values of ratio more than 9.0. These values had the effect of making the overall correlation less accurate, the reasons for this are given in Section (11.4).



Thus, the final variables are:

- |     |  |   |
|-----|--|---|
| (1) | System properties  | A, B, C, D  |
| (2) | Dispersed phase flow rates   | 1, 2, 3, 4  |
| (3) | Bed heights  | 1, 2, 3, 4  |
| (4) | $\left( \frac{\text{Ball diameter}}{\text{Inlet drop diameter}} \right)$ | $\bar{a} \quad \bar{\beta} \quad \bar{\gamma} \quad \bar{\delta}$ |

The notation used for the variables represents values across the full range of experimental conditions possible with existing apparatus. To investigate each individual parameter once would have entailed 256 experiments, however, the experimental work was further reduced by formation of 4 x 4 Graeco-Latin Squares, e.g.

No. 1		Flow Rates			
		1	2	3	4
Bed Height	1	A $\bar{a}$	B $\bar{\beta}$	C $\bar{\gamma}$	D $\bar{\delta}$
	2	B $\bar{\gamma}$	A $\bar{\delta}$	D $\bar{a}$	C $\bar{\beta}$
	3	C $\bar{\delta}$	D $\bar{\gamma}$	A $\bar{\beta}$	B $\bar{a}$
	4	D $\bar{\beta}$	C $\bar{a}$	B $\bar{\delta}$	A $\bar{\gamma}$

The numbers and letters are assigned at random to their respective variables, thus producing 16 experimental trials. To improve on the reliability of the correlation, the same variables were used to form four 4 x 4 Graeco-Latin Squares. This represented 64 experimental trials, which was an optimization of the amount of experimental work required and the parameters to be investigated. The experimental work was undertaken in the manner described earlier, and the data is presented in Appendix (A.4.4). The analysis of the mean diameter was accomplished using Shadowgraph photography and the image analysing computer, as described in Section (6.2) and (6.3).

The analysis of the variance of the experimental results was included in the evaluation of the equation (11.1), using an ICL 1905 Statistical Analysis Library Package<sup>(193)</sup>. The solution was based on a multiple regression analysis, which can be described

by the following stages:

- A) Formation of the observation matrix and subsequent transformation matrix;
- B) Linearization of the transformation matrix by natural logs;
- C) Computation of the arithmetic mean, variance/standard deviation, maximum and minimum values of each variable;
- D) Computation of the cross product, co-variance and correlation matrix;
- E) Evaluation of the normalized matrix;
- F) Print out of the overall coefficient, the coefficient of each group and the intercept term.

### 11.2) Results and Correlations

For equation (11.1) the following coefficients were evaluated:

$$a = -0.198, b = 0, e = 0, x = -0.019, y = 0.345, z = -0.381$$

Thus, equation (11.1) becomes:-

$$\left(\frac{d_{xt}}{d_{in}}\right) = C \left(\frac{g \mu_d^4 \Delta p}{\rho_d^2 \gamma^3}\right)^{-0.198} \left(\frac{d_{in}}{h_b}\right)^{-0.019} \left(\frac{d_{in}}{d_v}\right)^{0.345} \left(\frac{\rho_d g d_{in}^3 \Delta p}{\mu_d^2}\right)^{-0.381}$$

$$\text{where } C = 0.9648$$

Summation of the individual parameters in the above equation gives:-

$d_{xt}$	=	+1.0	$\mu_d$	=	+0.030
$g$	=	-0.579	$d_{in}$	=	+0.173
$\Delta p$	=	-0.579	$u_d$	=	0.0
$\gamma$	=	+0.596	$d_v$	=	-0.345
$\rho_d$	=	+0.017	$h_b$	=	+0.019

It was assumed that  $\mu_d$ ,  $h_b$  and  $\rho_d$  have very little effect on the overall equation, thus, on rearrangement of the above terms, the following relationship was obtained:-

$$\text{DROP No.} \propto (\text{BOND No.})^{-0.58} (\text{VOID No.})^{0.345}$$



Repeating the regression analysis on the Bond and Void Nos. the following relationship was found:

$$\left(\frac{d_{xt}}{d_{in}}\right) = 0.875 \left(\frac{\gamma}{d_{in}^2 \Delta \rho g}\right)^{0.575} \left(\frac{d_{in}}{d_v}\right)^{0.343} \quad (11.2)$$

### 11.3) Relationship of individual parameters to the exit drop size

By close inspection of equation (11.2) the following points can be made:

- I)  $d_{xt} \propto (\gamma)^{0.575}$  i.e. when the interfacial tension increases, the exit drop size increases. It has been shown that the criteria for coalescence is retention of droplets within the void, thus the above relationship is to be expected from theoretical considerations. As the surface forces increase, the drop is less able to deform, so passage through the restriction is less likely, thus increasing the probability of retention.
- II)  $d_{xt} \propto (\frac{1}{\Delta \rho g})^{0.575}$  i.e. when the buoyancy forces increase, the exit drop size decreases. As the buoyancy force increases, consequently the force pushing the drop through a restriction also increases. Thus the probability for retention is smaller and <sup>less</sup> coalescence will occur.

Points (I) and (II) can be combined to give:  $d_{xt} \propto \left(\frac{\gamma}{\Delta \rho g}\right)^{0.575}$

which is the reciprocal of the physical property group used in the inlet drop theory for coalescence within a packed bed (8.1). The controlling factor in the mechanism of coalescence within a packed bed has been shown to be the point of initial drop retention, which increases with decreasing values of the group  $(\Delta \rho g / 2 \gamma)$ . Thus the relationship found by the empirical approach of a dimensional analysis is in direct agreement with the theoretical consideration of drop retention.



This study has previously shown that the exit drop size is a function of two distinct processes. The first process is that of drop retention and coalescence; the second is the process of drop formation and release from the exit of the bed. In many correlations<sup>(96)(94)(98)</sup> given for the drop formation at standard nozzles, the drop size is shown to increase with an increase in  $(Y / \Delta \rho g)$ . Thus the relationship found in the dimensional analysis is in direct agreement with the theory of both the inlet and outlet mechanisms operating in a packed bed coalescer.

- III)  $d_{xt}$  is independent of  $u_d, h_b$  and  $\mu_d$ : equation (11.1). The independence of  $d_{xt}$  from viscosity was to be expected as only a small range of viscosities were investigated (0.0051 - 0.0082 poises). Thus, care must be taken when applying the equation (11.1) to systems outside the range of parameters used to evaluate the above correlations. This can be illustrated by considering the droplet hydrodynamics of a viscous system. From the Inlet theory it can be suggested that an increase in the viscosity of either phase would increase drag forces, hence reducing the overall forces promoting droplet passage. Therefore, an increase in drop retention and coalescence is expected for an increase in viscosity. Similarly, this effect of  $\mu_d$  with  $d_{xt}$  is in accordance with the work of Meister and Scheele<sup>(96)</sup> in their work on drop formation at single nozzles. Their correlations show that the drop size formed at a standard nozzle increase as the viscous forces increase.

It is of interest to note that in this study of coalescence in packed beds, the relation between  $Y, \Delta \rho, \mu_d$  and coalescence - (i.e. the exit drop size) is in direct disagreement with the effect of these parameters on the coalescence times of single drops. This illustrates the difficulties which can be experienced when applying the characteristics of single drop behaviour to more



complex macroscopic situations.<sup>(2)</sup>

The independence of  $d_{xt}$  with  $u_d$  and  $h_b$  supports the assumptions made in the 6<sup>th</sup> column co-current studies in the derivation of the Drop-Void Nos. (9.2). It was initially suspected that the exit drop formation process from a packed bed was analogous to that at a standard nozzle, where  $d_{xt}$  increases with velocity. However, from the studies of single ballotini under drop release, it was found that the orifice velocity was a function of the hydrostatic head and the physical properties of the system, and as such was independent of superficial velocity associated with dispersed flow rates.

The independence of  $d_{xt}$  from bed height,  $h$ , is surprising in view of the probability theory of drop retention (10.3). However, within the limits of the experimental Graeco-Latin factorial analysis, the above relationship is closely dependent on the experimental conditions. This fact is more clearly explained by the following relationships.

$$\text{IV) } d_{xt} \propto \left(\frac{1}{d_v}\right)^{0.343} \quad \text{and} \quad d_{xt} \propto (d_{in})^{0.193}$$

It has been shown that the behaviour of a packed bed is a function of two distinct processes which may augment or oppose each other. This being the case, one, both or neither of these processes may be operating at a given condition in the bed. This is shown in the following table, which indicates the effect of  $d_{in}$  with  $d_v$  on  $d_{xt}$ .

$d_{in}$ (relative)	Coalescence Level	Relationship with $d_{xt}$	Theory	No. of processes operating
1) $< d_v \min$	None	$d_{xt} = d_{in}$	Inlet	(0)
2) $d_v \min \leftrightarrow d_v \max$	Partial	$d_{xt} \propto (h) \left(\frac{1}{d_v}\right) (d_{in})$	Inlet Outlet	(2)
3) $> d_v \max$	Total	$d_{xt} \propto (d_v)$	Outlet	(1)

Under the factorial experimental approach, one would not expect the dimensional analysis leading to equation (11.1) to be an accurate representation of the results. Indeed, the most suitable approach under these conditions would be to use a non-linear sum of squares minimization procedure, based upon some suitable model for the different processes.

#### 11.4) Accuracy of General Correlations

The data and output associated with the regression analysis is shown in Appx. (A.3.7) & (A.4.5). The overall coefficient, which was a measure of the fit of the data to the correlations (11.1) and (11.2) was very close. For the original correlation of 8 groups, the overall coefficient was 0.944, whereas for the simplified 3 group analysis, it was 0.939. This would indicate that there was only a small loss of accuracy associated with the procedure of simplification.

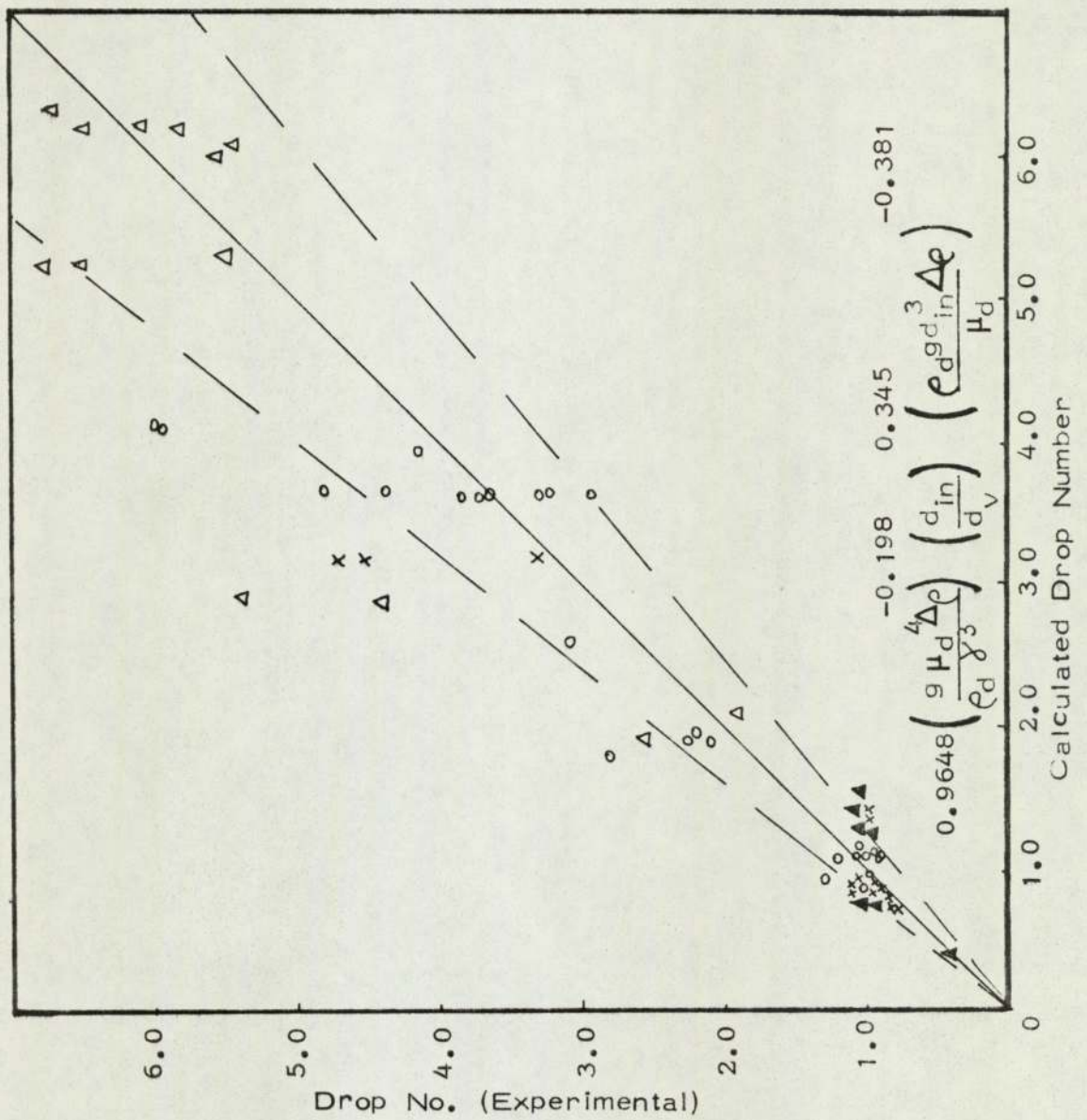
Fig. (11.4) shows the experimental and predicted values of the Drop No. (eqn. 11.1). Whereas the average error was approximately 20%, several points lie well beyond this region.

The reason for the spread of results is that several distinct processes are taking place within the bed. Drop No. values approximately equal to 1.0 indicate that the inlet drop size does not change on passage through the bed. However, this does not necessarily mean that no coalescence has taken place. For instance, if a large drop enters a packing with small apertures, then drop retention and coalescence can occur, but the exit drop size, which is determined by the drop formation mechanism at the exit void diameter, may be equal to the inlet drop size - thus, the Drop Void No. = 1.0. Conversely, values of the Drop No.  $> 1.0$



Fig. 11.4

GENERAL CORRELATION OBTAINED FROM DIMENSIONAL ANALYSIS EVALUATED USING THE I.C.L. STATISTICAL PACKAGE:- LINEAR REGRESSION WITH EIGHT GROUPS



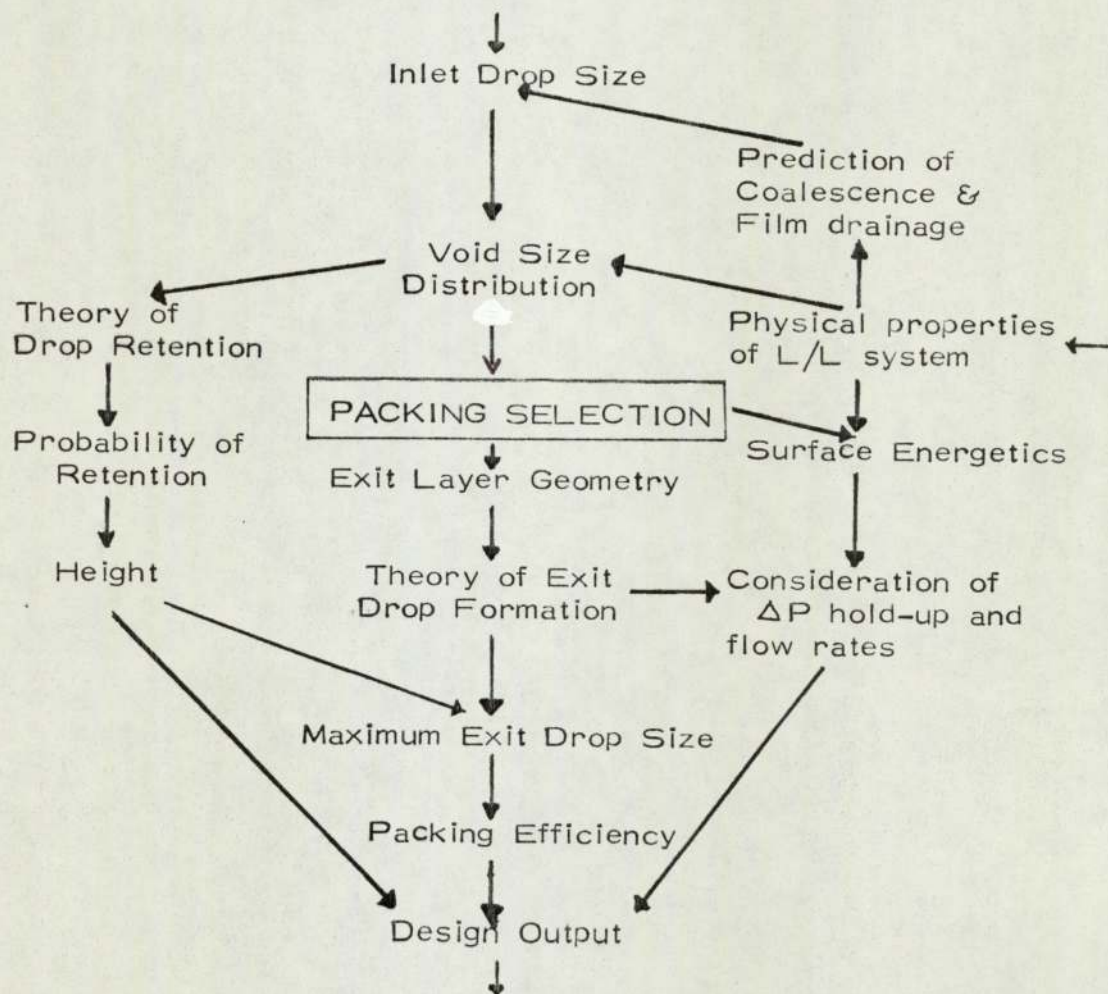
- Toluene
- × Iso-Octane
- ▲ M.I.B.K.
- △ Diethyl Carbonate

suggest that the inlet drop size has increased, but in actual fact the packing may be operating anywhere in the range of partial to total coalescence.

In retrospect, the correlations given by dimensional analysis are a good indication of the overall behaviour of a packed bed, but any conclusions drawn must be related to both the inlet and outlet studies as detailed in Sections 8, 9 and 10.

The general correlation may be used to obtain an initial estimate of the "separating" properties of a packed bed coalescer, however, the following design flow sheet is proposed to enable a more systematic evaluation of the specifications required for design.

#### DESIGN CONSIDERATIONS FOR A PACKED BED COALESCER





## CONCLUSIONS

The main conclusions drawn from this investigation are as follows:-

1. The use of a packed bed of equal sized glass spheres facilitated a fundamental analysis of the relationship between packing geometry, droplet hydrodynamics and the coalescence mechanisms of mono-sized primary dispersions.
2. A novel experimental technique has been developed to obtain the exit drop size distribution. This involved the use of a parallel light source to obtain a shadowgraph which could be analysed automatically on an Image Analysing Computer.
3. Two distinct processes of droplet behaviour occur within non-wetted packings. In the first, droplets enter and pass through the packing until they meet a restriction at which droplet retention and subsequent coalescence occur. The second process is that of drop formation at the exit of the packing, which is related to the release mechanisms which occur after the retained droplets have grown by coalescence.
4. A mathematical model has been developed to relate the buoyancy and surface forces in terms of drop size and shape in the aperture of a packing element. The roots of the equation represent the point at which the drop is in equilibrium at the critical point of retention and passage. The range of drop diameters between the two roots represents sizes which will not pass through the packing restriction.
5. For non-wetted packed bed operation, the limiting criteria for coalescence is droplet retention within the voids of the packing. For random non-wetted packings of equal sized spheres, the



limiting void diameter was found to be that described by a triangular packing geometry where  $d_v = 0.185 d_b$ .

6. Following complete coalescence within the bulk of the packing, the drop sizes in the exit dispersion are dependent on the release mechanisms at the exit layer of the bed. For non-wetted packings of equal sized spheres, the mean exit drop diameter formed on release could be predicted using the correlations of Meister and Scheele, where the mean exit packing void diameter was equivalent to that described by the cubic geometry, i.e.

$$d_v = 0.414 d_b.$$

7. A definition of packing efficiency was proposed by equating the experimental mean exit drop size with the theory of droplet release and the probability of droplet retention. This enabled a quantitative comparison to be made of the theoretical and experimental limitations of a packed bed as a coalescing aid.

8. A general correlation between the exit drop size and the system properties was obtained from a Greco-Latin factorial experimental programme using a linear multiple regression on a dimensional analysis.

9. Column operation under counter-current flow indicated that very little drop-drop coalescence took place within the bed. Since drop growth occurs by retention and impaction then the predominant mechanism of coalescence has been likened to the static situation of that in drop-interface coalescence.

Conclusions 1 - 9 identify the steps required for the design of a packed bed coalescer. However, further investigation is required which has been specified in the recommendations.



## RECOMMENDATIONS FOR FURTHER WORK

1. During this study observation of droplet behaviour within the packing was aided by the use of light-emitting dyes. This technique, whilst relatively successful, can be improved upon by using a matching refractive index procedure, where the optical properties of glass ballotini are used to their best advantage. This would entail matching the refractive index with both liquid phases or alternatively with the continuous phase only. In the first case, photo-sensitive dyes could be used to identify local hydrodynamic behaviour in a manner similar to that described by Allak<sup>(36)</sup>. In the second case, fluorescing or scintillating dyes could be used in the absence of external light sources to improve the opacity of the bed.
2. The mathematical model given in Section 7, and the general correlation in Section 11, can be further investigated using systems with more extreme physical properties, particularly with regard to viscosity of both the continuous and dispersed phase.
3. A study is recommended to investigate smaller inlet drop sizes in relationship to the geometry of the packing. Fundamental analysis necessitated that a mono-sized inlet dispersion be passed through the packing. During this study, a technique was developed which enabled dispersions of diameters much below that formed at conventional distributor plates to be produced; i.e. in the range 100-1000  $\mu$  m. Whilst this work is still in the development stage, it would appear possible for electron-micromeshes, supplied by E.M.I., to be used to form mono-sized dispersions with diameters in the secondary dispersion range. Thus, an investigation is recommended

with decreasing drop diameters to study the droplet hydrodynamic and coalescence mechanisms within packed beds over the transition range between primary and secondary dispersions.

4. The geometry of the packing and the relationship between the drop size and the aperture is important in predicting retention and coalescence. Thus it is suggested that a study be made relating the sphericity factor and the voidage values of more conventional packings to that of spherical particles. This would allow the application of the model to predict drop retention and hence serve as a guide to practical coalescer or extraction column packing performance.

5. The mathematical model to predict the point of retention and release was based on several assumptions which require further treatment; that is, an idealized drop profile, drag forces and complete non-wetting. Of particular importance is the assumption of complete non-wetting. It has been shown in Appendix (1) that the contact angle can be related to the buoyancy force required for drop release. Thus, information on hold-up and pressure drops could be obtained by relating the work carried out in this study to that of a quantitative analysis of the surface energetics.



## APPENDIX A.1

### CONSIDERATIONS OF SURFACE ENERGETICS

	Page
1) Surface energy and the upper limit of the Inlet Model	1
2) Theoretical approach to predict contact angles	IV
3) Evaluation of contact angle and surface tension	VII
(1) Interpretation of the graphs of Hartland and Hartley	
(2) Initial evaluation of graphs	
(3) Experimental programme and discussion	
4) Conclusions	XIX

#### Graphs

Fig. A.1.1	Evaluation of contact angle from drop dimensions
Fig. A1.2	Evaluation of surface tension values from drop dimensions
Fig. A1.3	Evaluation of contact angles from drop dimensions( $5^{\circ}$ - $20^{\circ}$ )
Fig. A1.4	Evaluation of contact angle when $\theta_c < 10^{\circ}$
Fig. A1.5	Evaluation of surface tension when $\theta_c > 90^{\circ}$

#### Tables

	Experimental data and evaluated parameters
A1.2	Contact angle analysis of surface preparation
A1.3	Surface tension analysis of surface preparation
A1.4	Properties of glass specimens
A1.5	Contact angle analysis of surface composition
A1.6	Surface tension analysis of surface composition
A1.7	Comparison of Staicopolous' nomographs with Hartland's graphical presentation

### A.1) Surface Energetics

The relationship between the surface energetics of liquid-liquid dispersions and packed beds has received little attention, except in the extreme conditions of complete non-wetting and wetting. While significant practical advantages have been obtained by the selection of coalescing aids with surfaces preferentially wetted by the dispersed phase, the surface energetics have not been treated quantitatively. This study was restricted to non-wetted packings and a model has been developed to predict the conditions under which drop retention or drop passage can occur. From the pressure balance eqn(7.9) the two roots were found to be real, and these correspond to the minimum and maximum drop diameter which will be retained under a given set of conditions. Experimental studies showed that whilst the lower root was in good agreement with theory, the upper root, i.e. the point at which passage occurs after retention and consequent growth by coalescence, was in most cases much lower than predicted.

The mechanism of drop passage after retention was described by considering the position of the advancing interface with respect to the minimum diameter of the void. When the diameter of the advancing interface was equal to the minimum void diameter it was assumed, from surface area considerations, that spontaneous passage would occur for any further penetration. In this sense, the behaviour of large drops is closely related to the break-through phenomena associated with continuous flow of mercury in porosimetry studies.

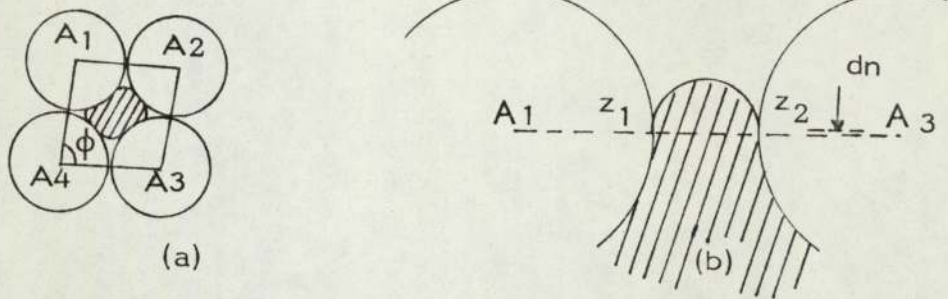
Considerable work has been carried out to quantify the above phenomena and the work of Mayer and Stowe<sup>(56)</sup> is presented to illustrate how Young's equations can be applied to the droplet



hydrodynamics within a non-wetted packed bed.

Mayer and Stowe considered the case of an advancing interface in a restriction of equal sized spheres - Fig.A.1(a) & (b).

Fig. A.1



$$\phi = \text{packing angle} \left[ \frac{\pi}{2} + \frac{\pi}{3} \right]$$

For a non-wetted fluid, only a portion of the mercury perimeter,  $L$ , is in contact with the spheres, and:

$$L = L_{lv} + L_{ls} \quad \text{where the subscripts, l, s and v refer to the liquid, solid and vapor respectively} \quad (\text{A.1})$$

At the position of beak-through, Fig(A.1 (b)) the work associated with infinitesimal changes in the surface is equal to the net change in surface energies. This work is given by:

$$PdV = \sigma_{lv} dS_{lv} + \sigma_{ls} dS_{ls} + \sigma_{sv} dS_{sv} \quad (\text{A.2})$$

For a further intrusion in a void space by an infinitesimal distance  $d_n$ , the change of advancing interface will be negligible and only the incremental changes in surface and volume need be considered, i.e. -

$$dV = Adn \quad (\text{A.3})$$

$$dS_{lv} = L_{lv} dn \quad (\text{A.4})$$

$$dS_{ls} = -dS_{sv} = L_{ls} dn \quad (\text{A.5})$$

where  $A$  represents the mercury cross sectional area, and  $L$  its perimeter.

On substitution of (A.3) (A.4) (A.5) into (A.2) and making use of Young's eqn:-

$$\sigma_{sv} - \sigma_{ls} = \sigma_{lv} \cos \theta_c \quad (\text{A.6})$$

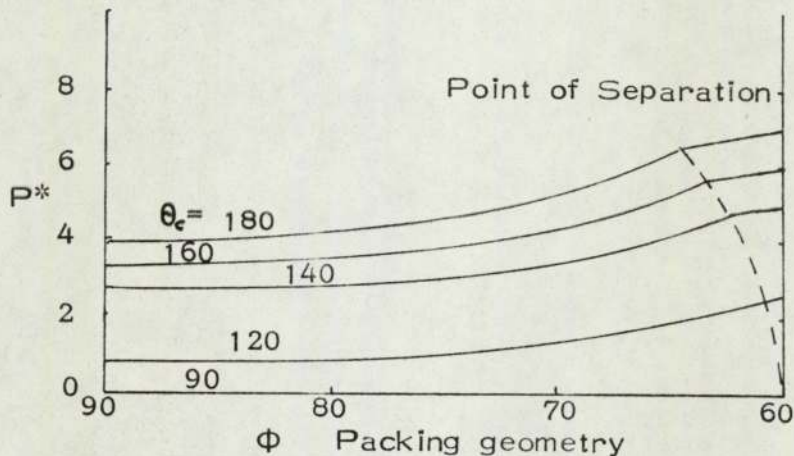
the following eqn. results for the break-through pressure of any packing configuration between  $\phi = 90^\circ - 60^\circ$  (cubic and triangular geometries)

$$P = \sigma_{lv} \frac{L^1}{A} \quad (\text{A.7})$$

where 
$$L^1 = L_{lv} - L_{ls} \cos \theta_c \quad (\text{A.8})$$

To solve this equation,  $L_{lv}$  was evaluated from a geometric construction for a range of contact angles  $\theta_c$ . Over a range of parameters, Mayer and Stowe presented the graphical relationship shown in Fig A1(c) to relate the break-through pressure,  $P$ ,<sup>\*</sup> packing geometry,  $\phi$ , and contact angle  $\theta_c$ .

Fig. A1(c)



The major drawback with this work is that the contact angle,  $\theta_c$ , must be known before  $L^1$  can be evaluated for a solution of eqn(A.7). For the real situation of an advancing interface in a toroidal packing restriction, evaluation of  $\theta_c$  would be extremely difficult, if not impossible.

However, in Mayer & Stowe's work, it was suggested that an approach similar to that used in figures of 'revolution' be



used to obtain the necessary boundary condition of the contact angle,  $\theta_c$ . Therefore, an initial attempt has been made to determine the applicability of the theory which predicts contact angles from figures of revolution. In many cases it is impossible to compare contact angles predicted from the theory with experimental values, owing to the difficulties inherent in measuring the latter. However, in the case of a sessile drop, the contact angle can be 'easily' measured. Therefore, an experimental study was carried out to compare the experimental contact angle with that predicted from the dimensions of a sessile drop.

#### Theoretical approach to determine contact angles

Contact angles are important for the shape of liquid surfaces and their motion relative to solids. These are often related to capillary pressure in their prediction of drop profiles. For instance, the differential equation of a meniscus is determined by the capillary pressure and gravitation, but the boundary condition depends on the magnitude of  $\theta_c$ , the contact angle. Likewise, the determination of the important thermodynamic property of surface tension by all existing methods relies on the analysis of interfacial shapes.

Experience has shown that the knowledge of contact angles is much less reliable than one would suppose. Measurement of a contact angle is relatively easy, but repetition of the test may afford markedly differing results.

A starting point towards the solution for contact angle and surface tension from the dimensions of a sessile drop is provided by Laplace's Law<sup>(119)</sup> which relates the pressure difference across an interface to the curvatures of the interface and the interfacial

tension:

$$\Delta P = \gamma \left( \frac{1}{R_1} + \frac{1}{R_2} \right) \quad (\text{A.9})$$

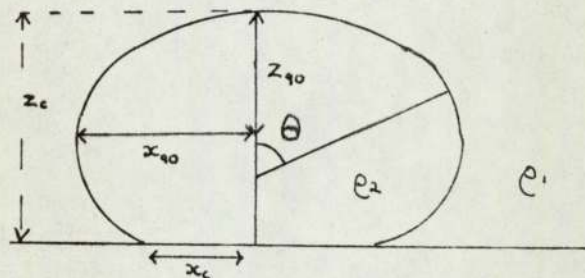
where  $\Delta P$  is the excess pressure inside the fluid interface,  $R_1$  and  $R_2$  are the principal radii of curvature of the interface and  $\gamma$  is the interfacial tension.

This equation generally leads to a second order differential equation, from which, in principle at least, it is possible to calculate the equilibrium shape of any curved surface between two fluids. When the principal radii of curvature are both finite but unequal as in the case of a sessile drop resting on a solid surface, solution must be obtained by numerical integration of eqn(A.9).

A.2.1) Analysis of the Meniscus meeting the Axis of Revolution

Fig. A1(d) shows a drop  $\rho_2$  in a surrounding fluid  $\rho_1$ , resting on a horizontal plate. The angle  $\Theta$  varies from  $0^\circ$  at the origin, i.e. the top of the drop, to  $180^\circ$  at the plate.

Fig. A1(d)



Laplace's equations can be written as:-

$$\left( \frac{1}{R} + \frac{1}{R_2} \right) = \frac{2\gamma}{b} + (\rho_2 - \rho_1) g z_c \quad (\text{A.10})$$

where  $b$  is the radius of curvature.

Multiplying by  $|b|$ , which serves as a unit of length, and

dividing by  $\gamma$  yields:-

$$\left( \frac{b}{R_1} + \frac{b}{R_2} \right) = 2 + \beta \left( \frac{z_c}{b} \right) \quad (\text{A.11})$$

where  $\beta = cb^2$  which is a positive dimensionless parameter which determines the shape.



For the curvature of the interface, one can either use the form:-

$$\left( \frac{1}{R_1} + \frac{1}{R_2} \right) = \left( \frac{d(x \sin \theta)}{x dx} \right) \quad (\text{A.12})$$

or

$$\left( \frac{1}{R_1} + \frac{1}{R_2} \right) = \frac{d^2 z / dx^2}{1 + (dz / dx)^2} \times \left[ 1 + (dz / dx)^2 \right]^{1/2} \quad (\text{A.13})$$

The problem was first solved by Bashforth & Adams<sup>(13)</sup> in 1881, who calculated the profile by numerical integration of eqn (A.11). They tabulated  $x/b$ ,  $z/b$ , for a large number of  $\beta$  values at intervals of  $5^\circ$  for  $\theta_c$  between  $0^\circ$  and  $180^\circ$ . In addition, numerical values were given for  $V_\theta / b^3$  where  $V_\theta$  is the volume of the drop between the origin and a horizontal profile,  $z$ , corresponding to  $\theta$ . Using the equation:-

$$\frac{V_\theta}{b^3} = \pi (x/b)^2 \left[ 2 - \frac{2 \sin \theta + \beta z_c}{x/b} \right] \quad (\text{A.14})$$

and the original Bashforth & Adams' tables, the volume can also be calculated.

However, although the physical properties of the drop are generally known, and the volume can readily be determined, the radius of curvature  $|b|$  at the apex, is difficult to measure.

The correct value of  $|b|$  is usually obtained after 3 cycles of approximation; application to further cycles is reported to produce negligible change. In spite of this reiterative procedure, the work of Bashforth & Adams has been considerably used. For example, Sugden<sup>(120)</sup> used Bashforth & Adams' tables to analyze the problem of capillary rise, whilst Blaisdell<sup>(178)</sup> extended the value  $\beta$  past that calculated previously. In a similar approach, Staicopolus<sup>(121-123)</sup> obtained a digital computer solution from which he developed empirical equations and nomographs, permitting the computation of contact angles and surface tension. Parvatikar<sup>(124)</sup> used the tables of Bashforth & Adams to develop tables relating  $(R)_r = R$  and  $VR^3$ , where  $R$  is the maximum drop radius to the contact angle. Parvatikar



also presented a comparison of this method with those of Bashforth & Adams and Staicopolous. Other empirical solutions have been proposed by Mack and Lee<sup>(125)</sup> with which the contact angle can be computed. Various works have considered very small or very large drops, and used the criteria of near-spherical shape or maximum height to compute values of surface tension and contact angle. These depend greatly on the drop size considered.

In this study, the theory presented by Hartland and the computed data of Hartley<sup>(126)</sup> was used to evaluate the contact angles and surface tension of sessile drops on plane solid surfaces. However, this work was of a purely theoretical nature, and this experimental study was carried out in conjunction with the above authors to investigate its accuracy.

### A.3) Evaluation of Contact Angle & Surface Tension using the Graphical Presentation of Hartland & Hartley

The numerical integration of the second order differential equation describing the profile of a sessile drop was carried out by Hartland and Hartley<sup>(126)</sup> using the Runga Kutta method. To facilitate easy reference, the derived data was presented in graphical form as given in Figs(A 1.1 and A1.2). Experimental values of the drop height,  $z_c$ , drop radius,  $x_c$  and drop volume  $v$ , were obtained by the method described earlier (5.3.3) and used with Figs.(A1.1 and A1.2) to find the contact angle and surface tension respectively. To evaluate the accuracy of this method, the calculated values were compared to the values measured directly during the experiment and also to those reported in the literature. The evaluation of the surface tension was carried out simultaneously with the contact angle determination, owing to the inherent unreliability of



contact angles as a reference point. Contact angles, although relatively easy to measure, are notorious for the markedly differing values obtained on repetition of the test. Therefore, to obtain a more reliable estimate of the accuracy of a graphical presentation to the solution of drop profiles, the calculated values of surface tension were compared to those obtained experimentally, which have been reported in the literature.

### A.3.1) Use of the graphs

#### (a) Contact angles

Fig (A1.1) is presented with axis' in the dimensionless terms,  $X$ ,  $Z$  and  $V$  where:

$$\bar{X} = x_c \left[ \sqrt{c} \right] \quad \bar{Z} = z_c \left[ \sqrt{c} \right] \quad \bar{V} = v \left[ \frac{3}{2} \sqrt{c} \right] \quad \text{where } c = \left( \frac{\Delta \rho g}{\gamma} \right)$$

The values  $x_c$ ,  $z_c$  and  $v$ , which are measured directly from enlarged negatives using the P.C.D. digital reader, (Fig. 5.3.3.C) are thus used to evaluate  $\theta_c$  between  $180^\circ - 20^\circ$  (For purposes of notation  $x_c, z_c, v$  or  $v$  will be notated by  $X, Z$  or  $V$ ) Fig (A1.3) shows a plot of  $X/Z$  versus  $V^{1/3}/Z$  for the values between  $20^\circ$  and  $5^\circ$ . It is noticed that for values of  $\theta_c < 5^\circ$ , extrapolation from the graph is impossible. Therefore, an alternative presentation of  $\theta_c$  as a function of drop dimensions<sup>(126)</sup> is presented, Fig.(A1.4). For low values of  $\theta_c$  it was found that  $\bar{X}$  is a unique function of  $\sin \theta_c / \bar{Z}$  consequently data for the  $5^\circ$  range was used to evaluate Fig.(A1.4). To confirm this relationship, several values of  $\bar{X}$  and  $\bar{Z}$  from the  $10^\circ$  range were evaluated and these were found to fall on the curve given by the  $5^\circ$  data. As a further check, the limiting relationship for a 2 dimensional drop,

given by: 
$$\sin \theta_c = \frac{Z(\bar{1} - 1) X e^{-X}}{((\bar{1} - X - 1) e^{-X})}$$

was evaluated for appropriate values of  $X$  and  $Z$ .

Using a table of modified Bessel Functions<sup>(179)</sup>, the corresponding  $\theta_c$  values; were found to be within  $\pm 4\%$  of those evaluated directly from Fig.(A1.4).

(b) Surface Tension :- Denoted as  $\gamma$  or  $\sigma$

Using the dimensions  $x_c$ ,  $z_c$  and the drop volume  $v$ , the surface tension can be determined from Fig.(A1.2); where the evaluated term  $\bar{Z} = z_c (\rho g/r)^{1/2}$ . Unfortunately, this graph suffers from the fact that the parameter  $Z/V^{1/3}$  is almost vertical and for very small changes in  $\frac{X}{V^{1/3}}$  a large change occurs in the Z value. Obviously, interpolation errors are high, and the advantages of this graph are questionable. An exhaustive search was carried out to find a suitable alternative but no better presentation was found. However, Hartley suggested that a plot of  $\frac{Z_{\theta_c}}{X_{90}}$  versus  $X_{90}$  could be used to evaluate the surface tension for a drop with a contact angle  $> 90^\circ$ . This is shown in Fig.(A1.5) where  $Z_{\theta_c}$  has been evaluated at  $\theta_c = 160^\circ$ ,  $140^\circ$  and  $110^\circ$ . The disadvantages of this graph are:

(i) the contact angle needs to be known

(ii) the upper part of the curve, at high  $\frac{Z_{\theta_c}}{X_{90}}$  values is flat.

Nevertheless, as no suitable alternative exists, this graph was the best means available for evaluating  $\theta_c$  values from drop dimensions.

### A.3.2) Initial Evaluation of Graphical Solution

An experimental study was carried out using sessile drops of mercury and water on cleaned microscope slides as described in Section (5.3). It was noticed that a large distribution of values were obtained for both  $\theta_c$  and  $\sigma$ . An investigation into the causes produced the general conclusion that the graphical solutions were very sensitive to error - (this has been described in more



detail in (A.3.3.4). ) Errors were found to exist in the use of a syringe needle as a measure of magnification, and more importantly in the volume determination. The volume determination was carried out by direct reading of the vernier scale on the syringe. This was graduated in 0.001 ml intervals, and further approximation to the next decimal point was possible. However, it was found from direct weighing that errors arose due to evaporation, slack in the barrel and piston movement and from the residual volume left at the needle tip on drop detachment. The magnitude of these errors was found to be dependent on the individual experimental conditions and as such was difficult to quantify accurately. To overcome this problem, the drop volume was determined by direct weighing to 0.0001 g.

### A.3.3) Experimental Programme

The bulk of this report has been concerned with dispersions in non-wetted packings where  $\theta_c > 90^\circ$ . Consequently, studies were carried out using a mercury-air-glass system, where  $\theta_{c,ls} > 90^\circ$ . Several tests were performed on a liquid-liquid-solid system, but the problems inherent in accurate volume determinations prevented any meaningful analysis.

For liquid-gas-solid systems, the volume determination was carried out by transferring the slide and the drop to a balance where the weight could be determined with an accuracy to 0.0001 g. However, for a L-L-S system, this approach was not possible, and the weight was determined using a top pan Mettler balance as shown in Fig. 5.3.3(b). The digital display unit used in conjunction with the balance only gave weights in grammes to the 3rd decimal place. Furthermore, in practice it was found that the value indicated by the 3rd

decimal place was subject to much fluctuation, owing to the magnitude of the weight of the total apparatus.

Investigation into the relationship between measured and calculated values of  $\theta_c$  and  $\sigma$  was carried out simultaneously with observation of contact angles with the following:

- (1) Surface cleaning and surface preparation;
- (2) Surface composition and drop volume;
- (3) Drop detachment mechanisms.

#### A.3.3 (1) Surface cleaning and surface preparation

Unused glass microscope slides were cleaned by various methods in acidified dichromate solutions, surfactants and organic vapours. The method of each respective treatment is given in Table(A1.1). To investigate the effect of surface roughness, two slides were artificially roughened before being cleaned by the acid treatment and that of the surfactant. As a comparative test, an uncleaned slide was used to determine what effect, if any, there is in cleaning the slide prior to use. After the above preparation procedures, all slides were ultimately rinsed three times in triple distilled water, using ultrasonification. The drop dimensions and the evaluated  $\theta_c$  and  $\sigma$  values are given in Tables(A1.2) and (A1.3); but the mean values of  $\theta_c$  and the spread of experimental angles  $d\theta_{ce}$ , calculated angles  $d\theta_c$ , and the maximum difference  $d\theta_m$  are summarized in Table(A1.1).

The results indicate that cleaning by the surfactant method using R.B.S. Concentrate (a laboratory detergent) was the most desirable if reproducible experimental results were required. Surface preparation with acidified chromate solution was found to give the largest error, with the exception of (10-12)\* which had been artificially roughened.



Table A1.1

No.	Treatment	Time	Spread			Contact Angle <sup>o</sup>		Average % Difference
			$d\theta_c$	$d\theta_e$	$d\theta_m$	$\theta_c$	$\theta_e$	
1-3*	Surfactant (R.B.S.)	3 days	5.0	7.0	10.0	152	148	2.75
4-6	"	"	3.0	3.5	2.5	141	140	0.75
7-9	Saturated Acid	"	9.0	2.5	19.0	144	132	5.6
10-12*	"	"	0.0	2.5	2.0	165	163	1.0
13-15	Acid dilute	"	18.0	4.0	23.0	145	141	7.0
16-18	Acid fresh	2 mins	7.0	4.0	11.0	147	141	3.8
19-21	Soap Powder	2 hrs	6.0	7.0	15.0	147	139	5.4
22-24	Iso-Proponal Vapour	4 hrs	6.0	2.0	4.0	143	140	2.1
25-27	Uncleaned	-	3.0	2.0	8.0	146	141	3.7

\* - Artificially roughened slides

Values given are the arithmetical average for 3 drops volume of 5, 10 and 20  $\mu$ l

A higher contact angle was found for both artificially roughened slides than for an unroughened slide cleaned by any method. This is to be expected, but in the case of nos. 10-12, the contact angle was extremely difficult to measure, and four different operators recorded values from 155<sup>o</sup> to 170<sup>o</sup>; thus indicating the human element in the measurement of contact angles. It may be fortuitous that the spread of values is very low for Nos. 10-12, but in the author's opinion, this result is not conclusive. Surprisingly, the various cleaning procedures, including the uncleaned slide, had a relatively small effect on the contact angle. Considering the spread of values in each individual treatment, it is difficult to say for certain how the cleaning

procedures effect the contact angle. However, fair agreement was obtained between calculated and measured values of the contact angle. This was not so for surface tension values Table(A1.3). A spread of values between 690 - 290 dynes/cms was obtained, however, it was interesting to note that the arithmetical mean was 450 dynes/cms, which is very close to the literature value of  $460 \pm 5$  dynes/cms.

#### A.3.3 (2) Surface Composition of glass and effect of drop volume

The above experiment was carried out with relatively small drop volumes, 5 - 20  $\mu$  l, therefore, to investigate the effect of drop volume, a study was carried out using volumes in the range 1 - 200  $\mu$  litres. In previous experiments, it was observed that the contact angle was dependent on the mechanism of drop placement on the slide. Therefore, during the study of drop volumes, two techniques of drop placement were employed. The effect of drop volume was investigated by incremental build-up of the original drop on the slide, by adding given volumes of mercury. Thus, the original drop is deposited in a manner denoted by "single deposition" whilst that of subsequent drops obtained by addition has been denoted by "incremental build up".

The study of drop volume and drop placement was carried out on glass specimens of different composition which had been ground and polished to a high degree of flatness. Quartz, pyrex and high quality general purpose glass were used, and the specifications are given in Table(A1.4). The glass specimens were soaked in R.B.S. surfactant and then washed three times in triple distilled water with gentle ultrasonification.

The experimental data and calculated values are shown in Tables (A1.5) and (A1.6). For all the glass specimens, the contact



angle decreased as the volume increased. Furthermore, a distinct trend existed for the change in drop placement technique. From the calculated values, it can be seen that a large change occurs between the contact angle obtained from single deposition and that of the first drop by incremental build up. This effect is more prominent for the calculated values than for the experimental values, however, the effect of contact angle with volume is in agreement with that of other authors<sup>(177)(180)</sup>. Much debate and controversy exists as to whether a drop can have more than one stable contact angle and no conclusive evidence is available to substantiate the effect of drop volume. The measured effect of the contact angle with drop volume may be a fundamental characteristic of wetting or alternatively, hysteresis and experimental technique may explain this phenomena. To investigate the mechanism of drop placement, a cine film was taken and the observations are discussed in Section (A.3.3.5).

From the results, it can be seen that the surfaces of differing composition have varying average contact angle values. For general purpose glass, pyrex and quartz, the contact angle for single deposits was  $144^{\circ}$ ,  $140^{\circ}$ ,  $134^{\circ}$ , whilst for incremental build up, the average value was  $136^{\circ}$ ,  $133^{\circ}$  and  $128^{\circ}$  respectively.

The values obtained for the surface tension are shown in Table(A1.6) and again it is noticed that the arithmetical mean is close to the literature value - i.e. 460 dynes/cms, whereas the average experimental  $\sigma = 451.02$  dynes/cms. However, a range of  $\sigma$  values of between 195-670 dynes/cms was obtained. This would seem to suggest that the errors in analysis were random and not biased in any systematic way.

### A.3.3(3) Error Analysis

In order to determine whether the error is experimental (including interpolation errors) or analytical, the drop dimensions obtained in Tables(A1.5) and(A1.6) were used to evaluate  $\theta_c$  and  $\sigma$  using the nomographs of Staicopolous. The (121-123) nomographs of Staicopolous are presented such that  $\theta_c$  and  $\sigma$  can be evaluated from either x or z dimensions only. Therefore, the results presented in Table(A1.7) denoted as  $\theta_{xS}$ ,  $\theta_{zS}$ ,  $\sigma_{xS}$ ,  $\sigma_{zS}$ , refer to the respective values obtained from the nomographs of Staicopolous for the x and z coordinates only. Similarly, refer to values derived from Hartland's graphs.

From inspection of the surface tension values, it can be seen that both solutions are sensitive to errors, but not in a regular manner. For example, No. 1 has a value of  $\sigma_h = 251$  dynes/cms, whereas  $\sigma_{xS}$  and  $\sigma_{zS}$  are 433 & 436 dynes/cms respectively. The converse is the case for No. 3, where  $\sigma_h = 460$  and  $\sigma_{xS}$  and  $\sigma_{zS} = 712$  and 726 dynes/cms respectively. Whilst agreement between Staicopolous' and Hartland's solutions is not very good, the two methods of Staicopolous, i.e. x and z coordinates, give surface tension values which are in good agreement.

In the evaluation of  $\theta_c$  a considerable difference in the value of the contact angle is found from Staicopolous' nomographs, depending on whether x or z dimensions are used. Generally it can be observed that the contact angle evaluated from Hartland's graph always falls within  $\pm 4^\circ$  of one of the values derived from Staicopolous' nomographs. Clearly, however, these results must be viewed with some reservations, as no definite conclusion can be made to indicate the source of errors.



### A.3.3(4) Interpolation and experimental errors

To identify how sensitive Hartland's graphs are to experimental error, the dimensions recorded for a large and small drop, given by Nos. 8 and 13 in Tables(A1.5) and(A1.6) were investigated.

Taking the values of No. 8 for a relatively large drop, and evaluating  $\sigma$  which is a more reliable parameter than i.e.

No.	$x_{90}$	$Z / x_{90}$	$\bar{x}_{90}$	$\sigma$	Volume
8	0.5070	0.6930	2.55	521.87	199.18 $\mu$ l

For a theoretical value of the surface tension,  $\sigma_{\text{theory}}$ , equal to that of the literature value, i.e. 460 dynes/cms, then for a theoretical  $\bar{x}_{90}$ , it can be shown that  $x_{90} = 0.5125$ . This represents a difference in  $x_{90}$  equal to 1.073%. In real terms, this can be related to the actual technique used for determining drop dimensions on the PCD digital reader. This instrument has the capacity of measuring accurately to 0.0001 cms, however, the sensitized marker device has to be positioned exactly on the drop profile for this accuracy to be valid. For an enlarged image of the drop equal to approximately 20 cms, an error of 1.073% in measuring  $x_{90}$  represents a physical error of 1 mm at each point of measurement. This would seem to be a result not entirely of the limitation of human ability, but also of the fact that photographically, the drop interface is not clearly defined, owing to the depth of field problems at high magnification. Similarly, clarity is reduced owing to the high magnification by the camera lens and the projection device as well as the grain of the film and ground glass screen used for measuring drop dimensions.

Alternatively, a small drop has been analysed in a similar manner as above for No. 13 Table(A1.6):-

No.	$x_{90}$	$Z_{\theta}/x_{90}$	$\bar{X}_{90}$	$\sigma$	Volume
13	0.0706	1.4886	0.58	195.6	1.2782 l

For the above data, it can be seen from Fig.(A1.5) that the value of  $Z_{\theta}/x_{90}$  equal to 1.4886 falls on the horizontal region of the curve, thus error in interpolation is expected to be high. However, for  $\sigma_{\text{theory}} = 460$  dynes/cms,  $\bar{X}_{90}$  would need to be 0.38, which is a large error in spite of inaccuracies in interpolation. However, in this region, an error of 0.1 in  $Z_{\theta}/x_{90}$  (i.e. 1.58 - 1.48) can be obtained by a difference of 0.003 in the measurement of  $x_{90}$ . This results in an error of 250 dynes/cms in the surface tension value. The above error analysis indicates the sensitivity of surface tension values to small errors in determining drop dimensions. The same effect is found for contact angles, but it is difficult to quantify this, owing to the experimental difficulties in accurately measuring angles  $> 90^{\circ}$ .

Whilst experimental and interpolation errors exist, of no less importance are the "wetting" effects at the solid-liquid-vapour interface during drop detachment. To investigate this, high speed photography was carried out using a Locam cine camera at 100 frames/second.

#### A.3.3.(5) Analysis of the drop detachment mechanisms and vibrational effects on contact angles and drop dimensions

The film<sup>(126)</sup> obtained illustrated the extremes of drop deposition, either by impaction or adhesion; that is, the drop can be placed on the surface by two methods:-

- (1) A drop which had grown at the needle tip was allowed to fall on to the glass slide by reason of its own weight. The resulting deformation on impact was thus filmed.





- (2) The drop which had formed at the needle tip was allowed to come into contact with the solid surface before detachment had occurred. The drop was increased in size, then the needle withdrawn by raising the syringe. The resultant deformation and detachment was filmed in the manner described above.

Two very important observations were made. Firstly, in both detachment mechanisms it was difficult to say whether the drop had an advancing or receding angle. For instance, on impact, the drop flattens then contracts; this behaviour was repeated several times with decreasing amplitude. Initially the mercury spread across the solid surface with a true advancing interface - where an advancing interface is that defined by movement into a previously dry area. On retraction, the interface recedes, possibly leaving an adsorbed layer, and in this sense the interface is receding over a previously 'wetted' area. The above definitions hold true in the first cycle of drop deformation. However, in subsequent oscillations of the drop profile, the interface which advances does so over a previously wetted area - hence the above definition does not hold true.

Likewise, in the second mechanism of drop deposition a similar process was observed on withdrawal of the needle from the drop. Although the drop had grown with a true advancing angle, on withdrawal of the needle, the interface was pulled upwards by the adhesion forces acting at the needle tip. This resulted in distortion of the drop profile and the drop contracted at the base. When the needle detached itself from the drop, the shape returned to the equilibrium position by a series of oscillations, involving advancing and receding interfaces. Without further experimentation, it is difficult to say what effect this stretching and snapping had on



surface wetting, adsorption and ultimately, the contact angle.

The second interesting observation was that concerning vibration of the drop profile. Both mechanisms of drop detachment produced oscillations of the drop profile, but these were generally damped out very quickly; whereas external vibrations within the building imparted a continuous effect.

From the film, it was observed that vibrations caused the drop to distort in both the horizontal and vertical planes. Furthermore, an increase of one axis obviously resulted in a decrease of the other axis, thus increasing the net effect in calculation. From measurements taken it was found that, whilst a maximum difference in  $x_{90}$  and  $z$  was only 0.0068 and 0.0079 cms respectively, this had the effect of a surface tension value differing by 102 dynes/cms. This result obviously indicates the importance of vibrational effects in the sensitivity of the graphical method to predict surface tension from the dimensions of a sessile drop. Although it is strongly recommended that the vibrational effects should be minimized in further work, it is recognized that this effect is probably more evident with a mercury-air system owing to the inherently high density and surface tension values of this system.

#### A.4) Conclusions

The contact angles obtained from drop dimensions are in reasonable agreement with those recorded experimentally and with those reported in the literature.

It was found that for mercury there is a decrease in the contact angle with increasing drop volume. However, the value of  $\theta_c$  was found to depend on how the drop was placed on the surface, and the composition of the glass. The latter points indicate that



some standardization is required in the experimental procedure of surface preparation and drop deposition. Similarly, results regarding the contact angle need to be specified as to composition of the surface, purity of the phases and form of the angle measured.

The surface tension values for mercury have a random scatter around a mean value of 450 dynes/cms. Although the distribution of values covers a range of  $\pm 250$  dynes/cms, the average value compares well with the literature value of 460 dynes/cms. Whilst mercury is noted for its sensitivity to contamination, it is thought that the distribution is due to small errors in measurement of drop dimensions. Errors have been identified from several sources, viz. magnification, vibrational effects, measurement of drop dimensions and interpolation from the graphs.

The evaluation of the contact angles and surface tension values from a graphical presentation has the advantage of being both quick and easy to use. The main disadvantages lie in the fact that the graphs are extremely sensitive to small errors, and that often interpolation is very difficult.

Finally, in view of the above observations, it was concluded that many difficulties will arise in attempting to apply equations for figures of revolution to the configuration at the position of breakthrough, as described by Mayer and Stowe. Due to the complexly curved nature of the interface at the liquid vapour surface shown in Fig. (A1.a) the relationship between  $R_1$ ,  $R_2$  and  $x$ ,  $z$ , would be extremely difficult, if not impossible, to define. Thus, it is concluded that contact angles should either be determined experimentally or by a reiterative procedure of comparison of the calculated and experimental values of breakthrough pressure.



Fig. A1.1  
EVALUATION OF CONTACT ANGLE FROM DROP DIMENSIONS

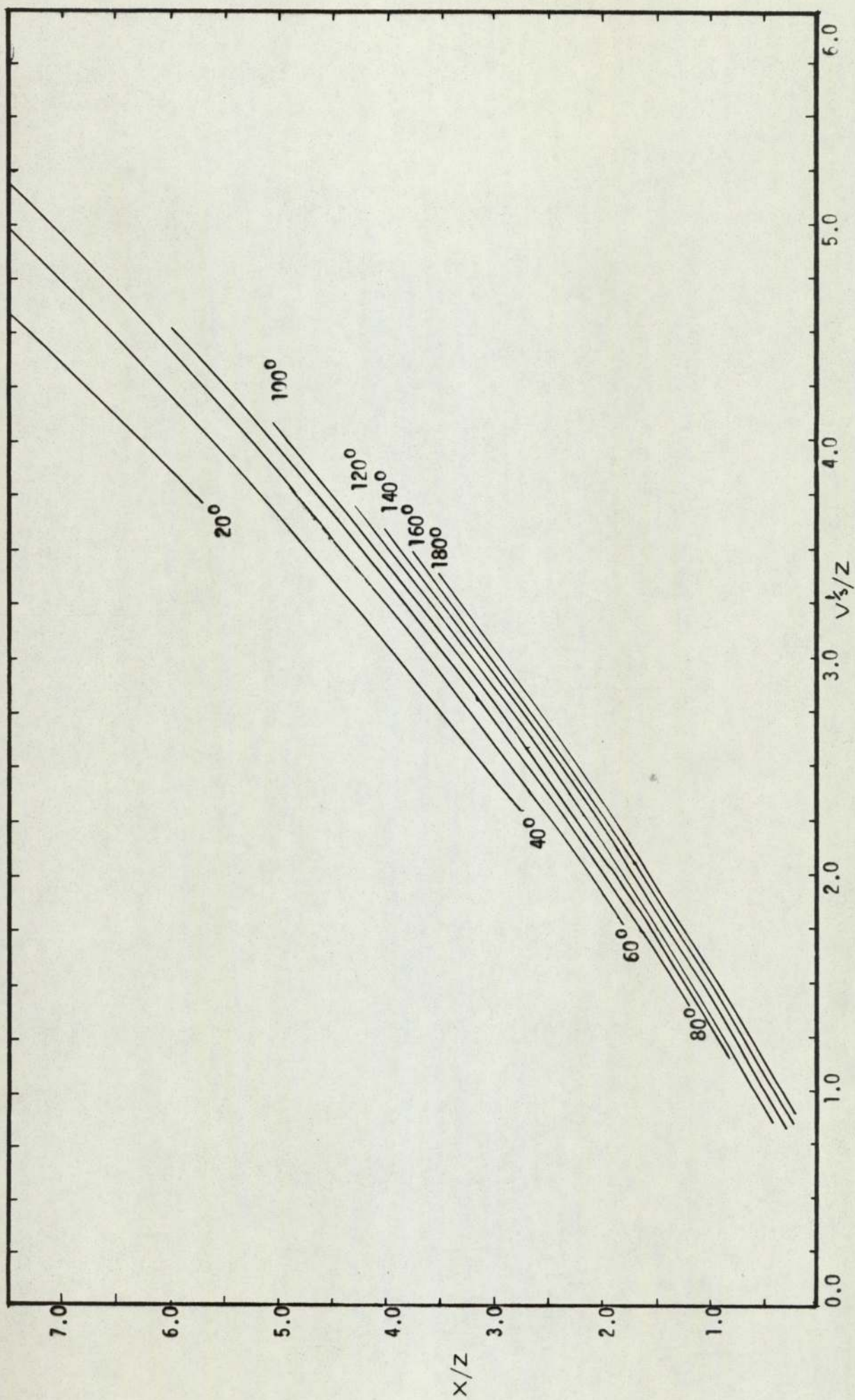


Fig. A1.2

EVALUATION OF SURFACE TENSION VALUES FROM DROP DIMENSIONS

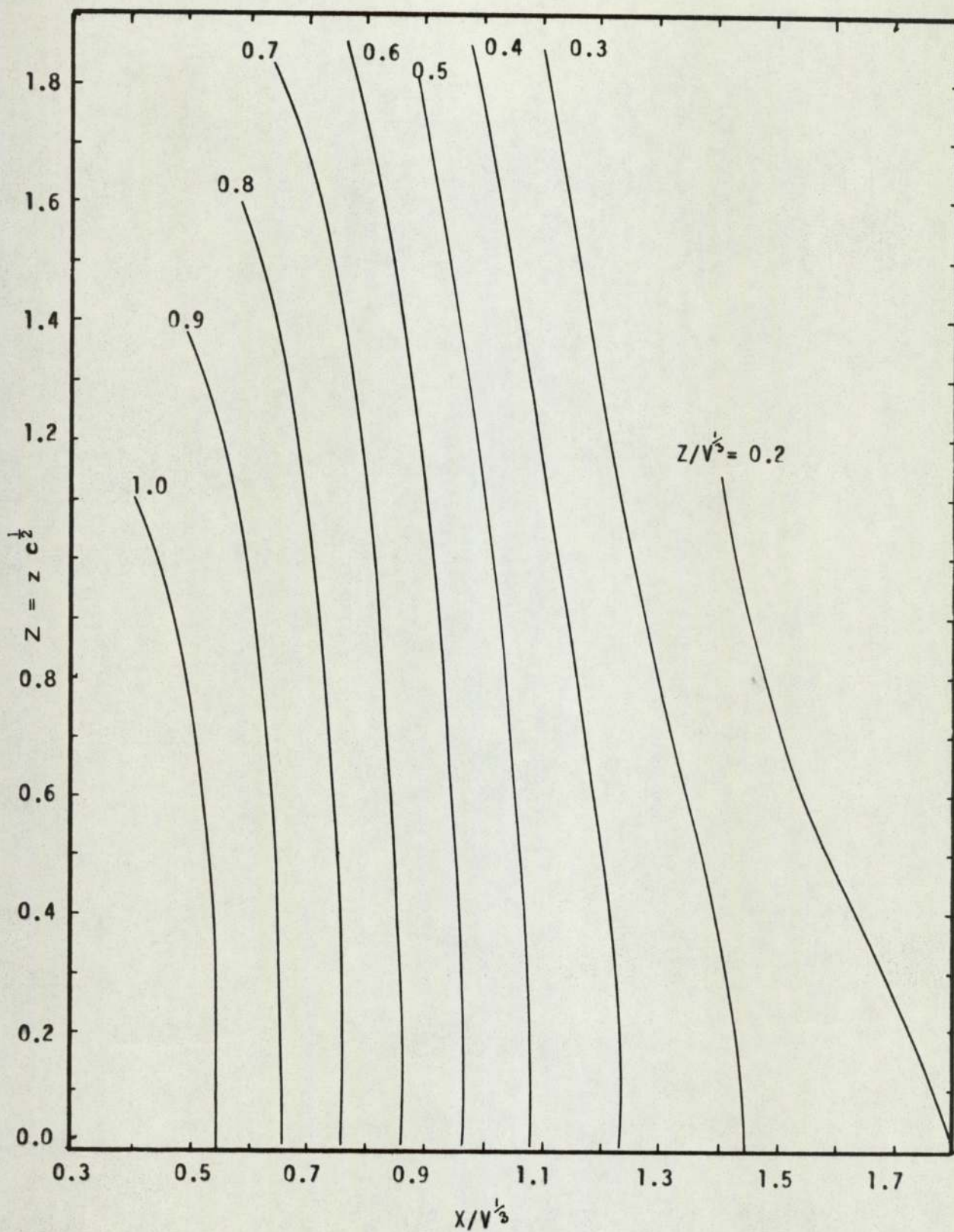




Fig. A1.3

EVALUATION OF CONTACT ANGLE FROM DROP DIMENSIONS

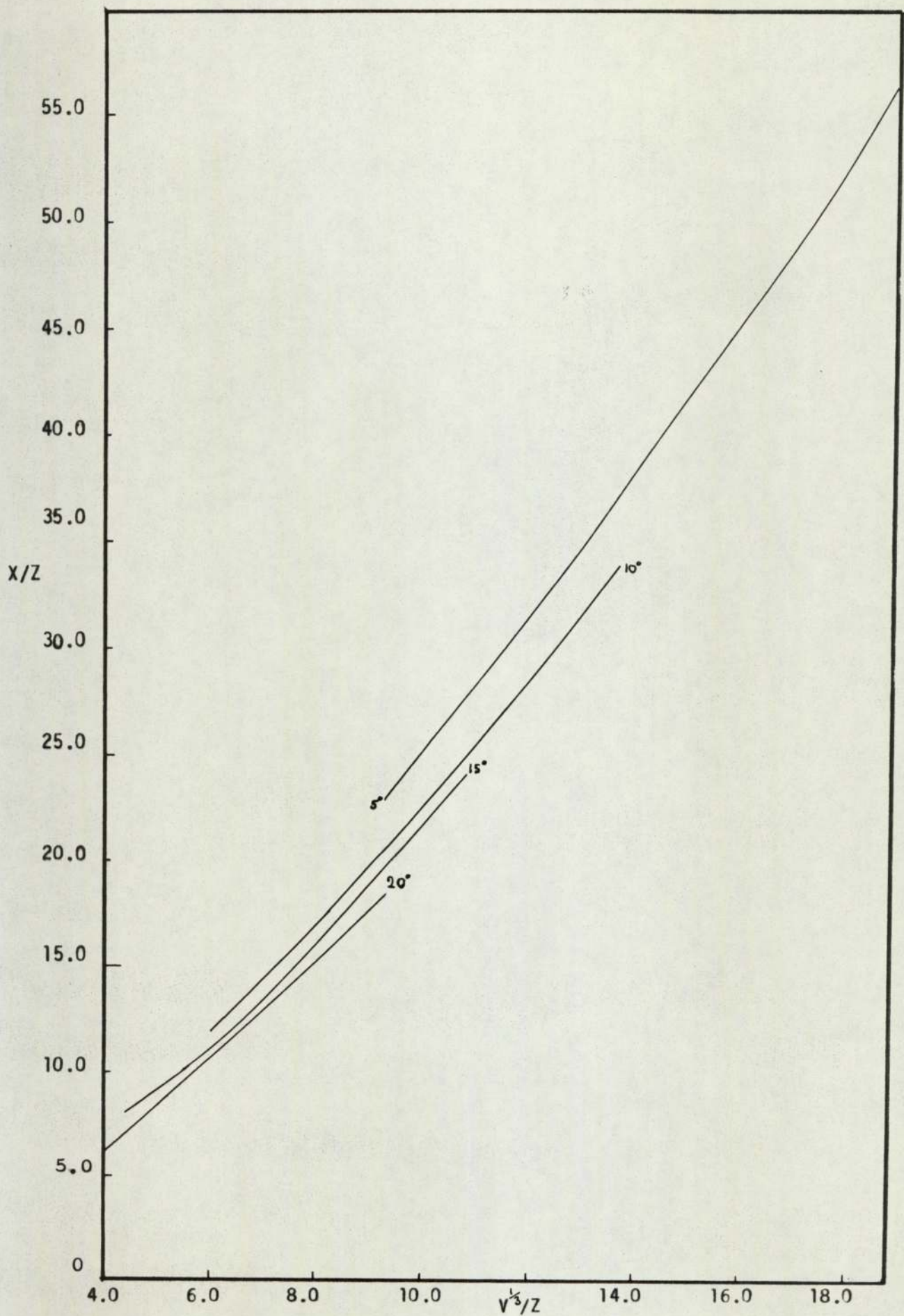


Fig. A1.4 EVALUATION OF CONTACT ANGLE  
WHEN  $\theta_c < 10^\circ$

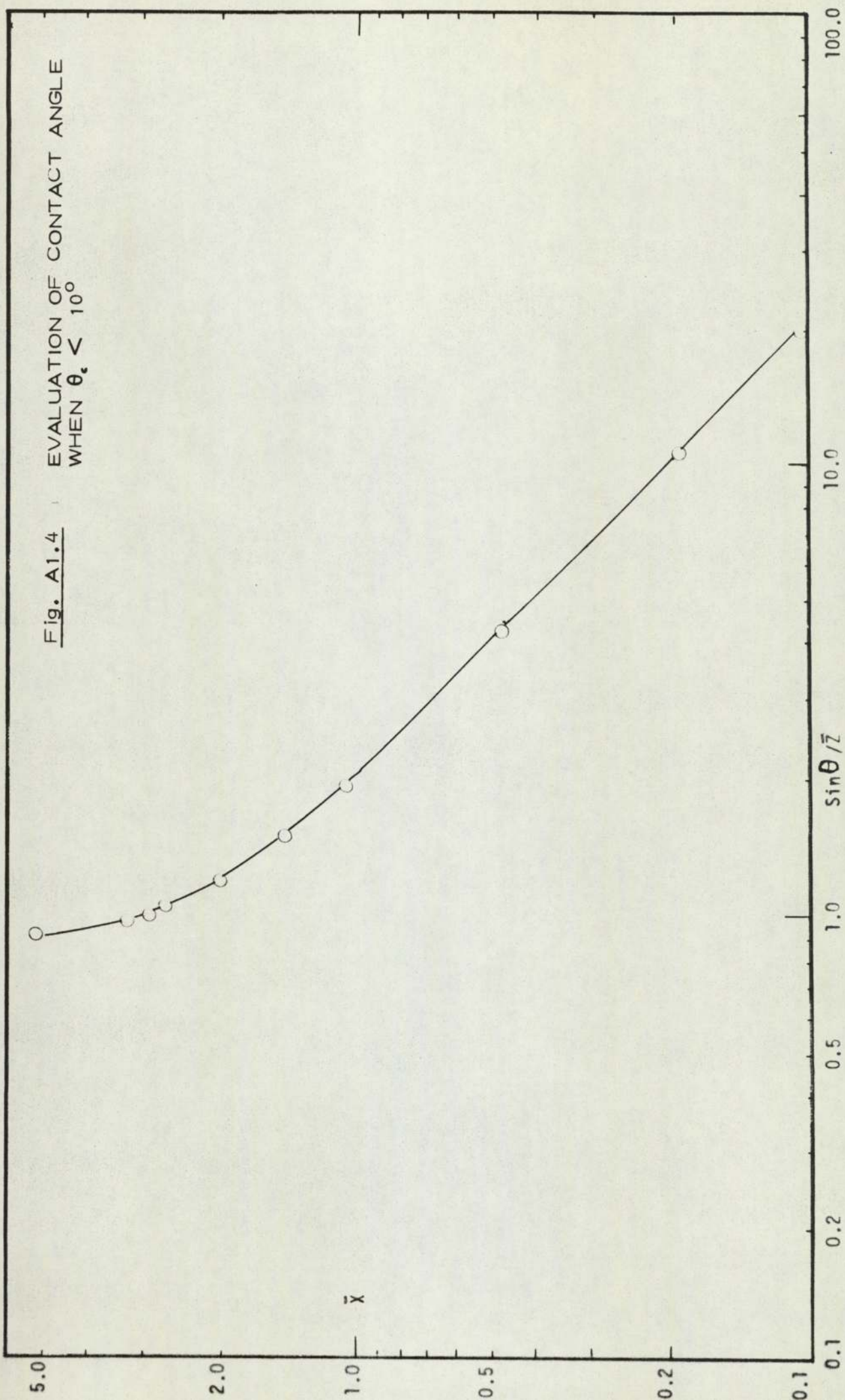




Fig. A1.5

DETERMINATION OF SURFACE TENSION  
USING DIMENSIONS OF DROPS WITH  
CONTACT ANGLES  $\theta_c > 90^\circ$

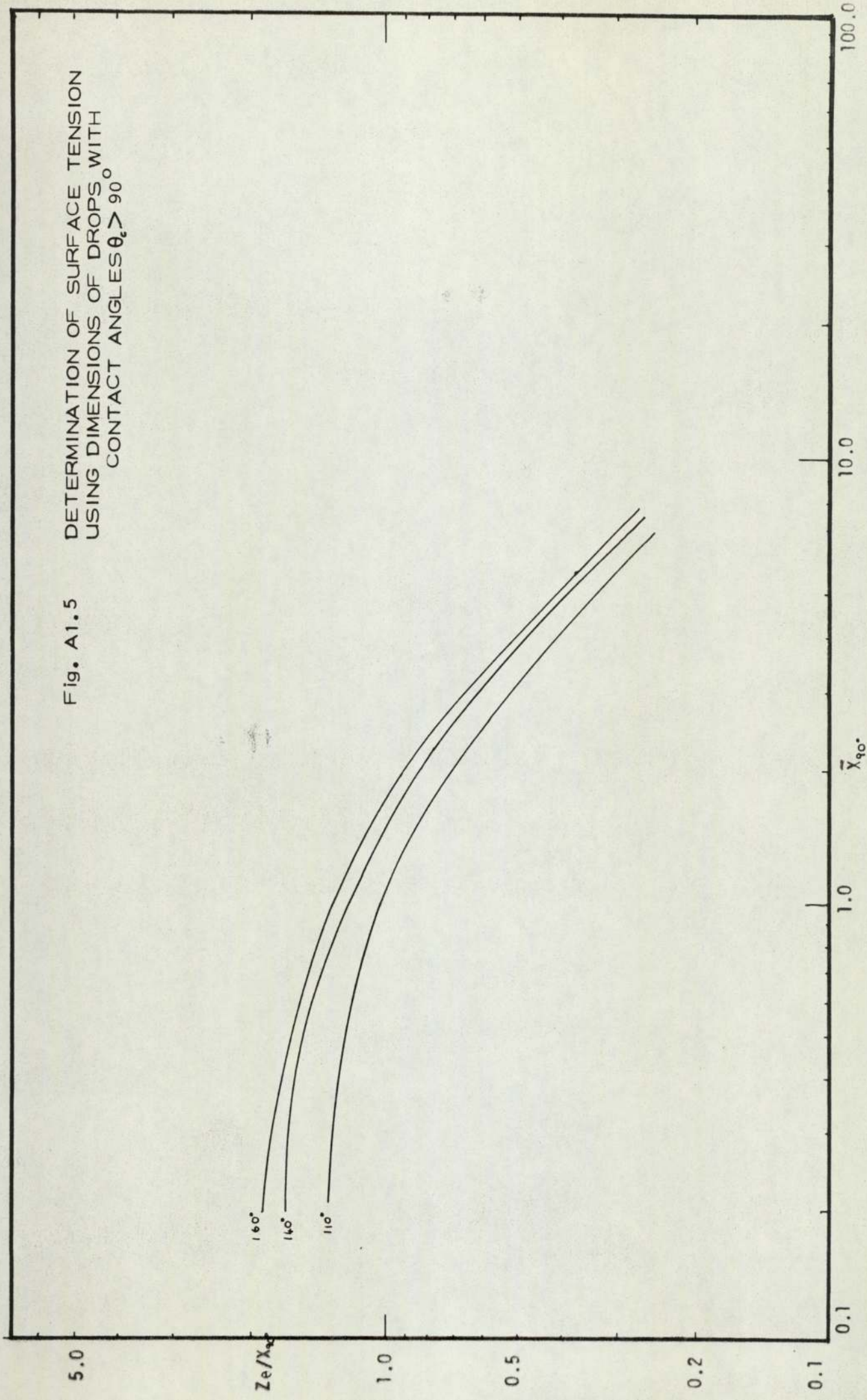


Table A1.2

## Analysis of Surface Preparation - Mercury on Glass

No.	Z	$x_c$	$x_{90}$	$\frac{x_c}{Z}$	Wgt.	$V^{\frac{1}{3}}$	$\frac{1}{V^{\frac{1}{3}}}$	$\frac{W}{V}$ approx.	$W$ exp.
1	.1853	.0704	.1169	.3799	.0676	.17126	.9314	150	152
2	2080	1014	1463	486	1362	21632	1.04		
3	2440	1425	1890	5840	-	-		148	
4	1717	0895	1166	5206	0722	17507	1.01962	140	138
5	1980	1128	1462	5697	1395	21805	1.1013	140	140
6	2370	1519	1951	6409	2691	27144	1.1453	143	141.5
7	1659	0901	1116	5431	0700	17327	1.0444	141	131.5
8	1934	1162	1443	6008	1290	21243	1.098	141	131.0
9	2218	1539	1888	6939	2616	2688	1.2123	150	134.0
10	1782	0633	1140	3552	0699	17318	0.9719	165	162
11	2055	0876	1383	4263	1344	21536	1.0479	165	163
12	2424	1204	1845	4967	2667	37063	1.116	165	164.5
13	1775	0857	1177	4828	0786	18009	1.0146	151	142.0
14	2043	1159	1479	5673	1350	21567	1.0556	161	138
15	2380	1520	1937	6386	2693	2715	1.1408	143	142
16	1737	0847	1174	4876	0710	17409	1.002	143	142
17	1996	1106	1452	5541	1373	21689	1.0866	150	139
18	2355	1531	1923	6501	2709	27203	1.155	147	143
19	1693	0822	1144	4584	0714	17442	0.9718	146	142
20	1972	1130	1425	5130	1320	21406	1.0855	146	135
21	2327	1530	1908	6584	2360	27374	1.1763	150	140
22	1664	0799	1130	4802	0700	17327	1.0413	139	139
23	2053	1117	1483	5441	1389	21773	1.0605	145	141
24	2362	1519	1801	6409	2667	27062	1.1457	144	140
25	1765	0804	1158	4555	0691	17253	0.9775	145	142
26	1985	1014	1388	5108	1164	20527	1.0341	148	140
27	2420	1532	1946	-	-	-	-	-	-

Volume  $\approx$  5, 10, 20  $\mu$ l



Table A1.3

## Analysis of Surface Preparation - Mercury on Glas

No.	Frame No.	$\bar{z}/x_{90}$	$x_{90}$	$\bar{X}_{90}$	$\sigma$ dyes/cm
1	9	1.5851	.1169	.540	691.6
2	10	1.4217	.1463	.83	410.16
3	11	1.2910	.1890	1.05	427.73
4	12	1.4725	.1166	.62	666.9
5	13	1.354	.1462	.28	463.6
6	14	1.2147	.1951	1.05	455.79
7	15	1.4865	.1116	.61	441.87
8	16	1.3402	.1643	.80	429.518
9	17	1.1747	.1888	1.22	316.16
10	18	1.563	.1140	.75	350.14
11	19	1.483	.1383	.8	395.68
12	20	1.313	.1845	1.25	289.16
13	21	1.502	.1177	.65	432.66
14	22	1.381	.1479	.74	527.35
15	23	1.228	.1931	1.05	449.27
16	24	1.479	.1174	.64	444.227
17	25	1.374	.1452	.84	394.46
18	26	1.225	.1423	1.05	442.601
19	27	1.479	.1144	.65	408.53
20	28	1.383	.1425	.82	398.68
21	29	1.2196	.1908	1.1	391.192
22	30	1.4725	.1130	.62	438.535
23	31	1.384	.1483	.80	453.66
24	32	1.3114	.1801	.9	528.65
25	33	1.524	.1158	.60	491.769
26	34	1.430	.1388	.26	440.332
27	35	1.2435	.1946	-	-
28	36	-	-	-	-

Table A1.4

WISAG, Oerlikonerstrasse 88  
8057 Zürich (Switzerland)

---

1. Pure transparent quartz glass plate ground and polished	Herasil 111 Diameter : 4 cm Thickness : 3 mm
2. Pure transparent quartz glass plate ground and polished	Herasil 11 Diameter : 4 cm Thickness : 3 mm
3. Pure transparent quartz glass plate ground and polished	Herasil I Diameter : 3.5 cm Thickness : 2 mm

ORIEL OPTIK GmbH  
Mecklenburgerstrasse 27  
61 Darmstadt (Germany)

---

4. General purpose high quality flat plate glass A-45 - 102-0	
Circular	Diameter : 5 cm Thickness : 6 mm
5. General purpose high quality flat plate glass A-45 - 302-0	
Square	Side : 5 cm Thickness : 6 mm
6. One side polished Pyrex first surface flat reflector 1/4 $\lambda$ flat, uncoated	A-33 - 242-00 Diameter : 2.54 cm Thickness : 6.4 mm



Table A1.5

No. Frame No.	Wgt	Vol. $\mu\text{l}$	$\frac{1}{\sqrt{3}}$	$\frac{y}{z}$	$x_c$	z	$\frac{x_c}{z}$	$\theta$ calc.	$\theta$ Exp.
1	5	0.0197	1.464	.1175	1.9964	0.0590	.1139	0.51799	137-140
2	6	0.1119	8.315	.2025	1.0885	0.1125	.1867	0.6025	140-138-136
3	7	0.5213	38.7	.3383	1.2870	0.2236	.2629	0.8505	130-132-132
4	8	2.0283	150.73	.53219	1.6815	0.4156	.3165	1.3131	130-127
5	9	0.0326	2.42	.1343	0.9711	0.0613	.1383	0.4425	148-145-140
6	10	0.2513	18.67	.2653	1.1406	0.1548	.2326	0.6655	138-140-140
7	11	0.5489	40.792	.3442	1.2725	0.2222	.2705	0.8215	132-130-134
8	12	2.6803	199.18	.58401	1.6619	0.4685	.3514	1.3332	120-130-134
9	14	0.0098	0.7282	.0899	0.9865	0.0447	.0912	0.49013	140-138-139
10	15	0.0859	6.383	.18506	1.0516	0.1020	.1764	0.57833	132-134-126
11	16	0.4070	30.24	.31157	1.2743	0.2062	.2445	0.8433	127-136-129
12	17	1.3833	102.8	.4684	1.4801	0.3406	.3165	1.076	130-136-132
13	23	0.0172	1.2782	.10852	1.0326	0.0585	.1051	0.5577	137-134-138
14	24	0.1203	8.9402	.20754	1.1328	1.309	.1832	0.7145	120-117-118
15	25	0.5552	41.6	.34550	1.3224	.2389	.2614	0.9139	120-120-124
16	26	1.9902	47.904	.52884	1.6317	.4138	.3241	1.2767	125-130-124
17	28	0.0325	2.4152	.13417	1.6095	.0687	.1329	0.51693	140-136-140
18	19	0.2297	17.0704	.25748	1.1614	.1600	.2213	0.72169	128-128-130
19	30	0.7052	52.407	.37422	1.3598	.2625	.2352	0.95385	123-127-121
20	31	-	-	-	-	-	-	-	-
21	33	0.0250	1.8579	.12293	1.0409	.0687	.1181	0.5817	128-135-124
22	34	0.2089	15.524	.24946	1.18005	.1590	.2114	0.75212	123-120-127
23	35	0.7821	58.122	.38736	1.34502	.2772	.2880	0.9625	118-120-122
24	36	1.6534	122.874	.49714	1.60112	.3874	.3105	1.2476	121-120-120

Mercury on special glass plates

- 1- 4 Pure quartz, ground polished Heraeus III
- 5- 8 General purpose high quality glass
- 9-12 Pyrex - polished  $1/4 \lambda$  flat uncoated
- 13-16 Pure quartz, ground polished Heraeus I
- 17-20 General purpose high quality glass
- 21-24 Pure quartz, ground polished Heraeus III.

Table A1.6

Mercury on Special Glass Plates

No.	$x_{90}$	$\frac{Z}{x_{90}}$	$\bar{x}_{90}$	$\sigma$
1	0.0745	1.5288	0.54	251.27
2	0.1389	1.3441	0.95	282.219
3	0.2504	1.0499	1.34	460.98
4	0.4454	0.7105	2.4	454.68
5	0.0861	1.6062	0.44	505.51
6	0.1846	1.26002	0.94	509.139
7	0.2525	1.0712	1.3	498.04
8	0.5070	0.69309	2.55	521.8729
9	0.0598	1.5250	0.56	
10	0.1236	1.4247	0.60	560.226
11	0.2303	1.06165	1.30	414.314
12	0.3742	1.8458	1.95	486.146
13	0.0706	1.4886	0.58	195.6
14	0.1456	1.2582	0.75	497.54
15	0.2594	1.0077	1.15	671.69
16	0.4400	0.73659	2.38	451.21
17	0.0878	1.5136	0.53	362.27
18	0.1830	1.2114	0.95	489.81
19	0.2852	0.96493	1.50	477.25
20	0.0819	1.4420	0.58	263.23
21	0.1766	1.19705	0.94	465.966
22	0.3010	0.9568	1.40	610.24
23	0.4098	0.7576	2.1	502.729
			Average	$\approx$ 451.02



Table A1.7

Using Staicopolus<sup>1</sup> Nomographs to determine Surface Tension and Contact Angle

Using Results from Film 7 :  
Remeasured Values.

No. Frame	$x_c$	$x_{90}$	$z$	$z_{90}$	$\frac{x_{90}}{z_{90}}$	$(\frac{x}{b})_{90}$	$(\frac{y}{b})_{90}$	$h_x$	$h_z$	$\beta$
1 5	0.0594	0.753	0.1168	.0733	1.0273	0.98	0.95	.0768	.0722	0.1
3 7	0.2240	0.2497	0.2635	.1908	1.3088	0.76	0.575	.3285	.3318	2.0
10 15	0.1031	0.1245	0.1776	.1138	1.094	0.935	0.865	.1332	.1316	0.4
24 36	0.3864	0.4088	0.3617	.2359	2.222	0.320	0.150	1.36	1.572	103.0
11 16	0.2054	0.2295	0.2477	.1860	1.2472	0.820	0.65	.2836	.283	1.9

	$\sigma_{x_s}$	$\sigma_{z_s}$	$\sigma_H$
1 5	433.006	436.63	251.87
3 7	712.53	726.509	460.98
10 15	522.24	507.772	560.226
24 36	209.2	317.5	502.729
11 16	540.14	542.5	414.314

$\frac{z}{b}$	$\frac{z/b}{z/b_{90}}$	$\theta_{z_z}$	$\theta_H$	$\theta_{s_x}$	$(\frac{x_c}{b})$	$(\frac{x_c}{b}) / (\frac{x_c}{b})_{90}$
1.55	1.592	129	137	136	0.7734	0.78918
0.794	1.381	126.7	130	142	0.6818	0.897
1.346	1.556	133.5	132	110	0.774	0.8278
0.2301	1.533	-	121	125	0.284	0.8875
0.875	1.346	124.0	127	110	0.7268	0.8944

APPENDIX 2.

PHYSICAL PROPERTIES OF LIQUID-LIQUID SYSTEMS



APPENDIX 2.

PHYSICAL PROPERTIES OF LIQUID-LIQUID SYSTEMS

The following physical properties have been taken from International Critical Tables, except interfacial tensions which have been measured with a Du Nuoy Tensiometer.

---

Interfacial tension - Dynes/cm

<u>System</u>		Temperature
Toluene - water	35.9	23°C
M.I.B.K. - water	9.8	22°C
Isooctane - water	51.1	23°C
Diethyl carbonate - water	13.1	22°C

---

Viscosity - centipoise

Toluene	0.58	20.6°C
M.I.B.K.	0.62	21.3°C
Isooctane	0.51	25°C
Diethyl carbonate	0.82	25°C

---

Density - gm/cc.

Liquid

Toluene	0.864	20°C
M.I.B.K.	0.80	20°C
Isooctane	0.693	20°C
Diethyl carbonate	0.976	20°C

---

### APPENDIX 3.

#### COMPUTER PROGRAMMES

- A.3.1 Evaluation of exit drop diameter (UAFORTRAN)
- A.3.2 Evaluation of exit drop diameter (Basic)
- A.3.3 Drop dimension "sort" procedure  
Typical output of data
- A.3.4 Inlet drop model
- A.3.5 Regression Analysis (Total Coalescence)
- A.3.6 Regression Analysis (Partial Coalescence)
- A.3.7 Regression Analysis (Command Statements)  
Output from Regression Analysis (Dimensionless Groups)  
Correlation matrix and means for Regression Analysis
- A.3.8 Regression Analysis (Simplified 3 Groups)  
Output of observation matrix and correlation matrix



## Programme to Evaluate Exit Drop Diameter Using UAFORTRAN

```

0012          PAGE 1
0013          READ FROM (CB)
0001          PAGE 2
0002          NALTER STEAM
0003          DIMENSION A(100), B(100)
0004          COMMON NOP, DSMEAN, DVMEAN, DS(100), DV(100), SSCF
0005          READ(1,10) PI
0006          10 FORMAT(=0.0)
0007          READ(1,11) ND
0008          11 FORMAT(10)
0009          DO 100 J = 1,ND
0010          READ(1,11) NF
0011          READ(1,12) NOR, NUB, NOP, RMAG, DIAB, FLOWR, HBED
0012          12 FORMAT(510, 4F0.0)
0013          READ(1,13) (A(K), K = 1,NOP)
0014          READ(1,13) (B(K), K = 1,NOP)
0015          13 FORMAT(100F0.0)
0016          CALL SORT (A,NOP)
0017          CALL SORT (B,NOP)
0018          SSQ = 0.0
0019          SCUBE = 0.0
0020          DO 50 I = 1, NOP
0021          A(I) = A(I)/RMAG
0022          B(I) = B(I)/RMAG
0023          IF(A(I) GT B(I)) GOTO 29
0024          DS(I) = A(I)
0025          DV(I) = A(I)
0026          GOTO 49
0027          29 F = SQRT((A(I)+A(I)-B(I)+B(I))/(A(I)+A(I)))
0028          DS(I) = SQRT(A(I)+A(I)/2.0 + B(I)+B(I)/(4.0+PI)*ALOG((1.0+F)/(1.0-
0029          1.F)))
0030          DV(I) = (A(I)+A(I)+B(I))*+(1.0/3.0)
0031          49 SSQ = SSQ + DS(I)*DS(I)
0032          SCUBE = SCUBE + (DV(I))*+3.0
0033          50 CONTINUE
0034          DSMEAN = SQRT(SSQ/NOP)
0035          DVMEAN = (SCUBE/NOP)*+(1.0/3.0)
0036          SUPV = FLOWR/(15.0*PI*15.25*15.24)*(1000.0)
0037          CALL SLIMIT
0038          DT = 0.1548*DIAB
0039          DC = 0.4140*DIAB
0040          DST = DSMEAN/DT
0041          DSC = DVMEAN/DC
0042          WRITE(2,72)NF, NOR,HBED,SUPV,DSMEAN,DST,DSC,DIAB,SSCF
0043          72 FORMAT(111,15,F8.1,F9.4,F8.5,F8.5,F6.3,F6.3,F5.2,F7.4)
0044          100 CONTINUE
0045          STOP
0046          END

```

END OF SEGMENT, LENGTH 437, NAME ST/FAN

```

0047          SUBROUTINE SLIMIT
0048          COMMON NOP, DSMEAN, DVMEAN, DS(100), DV(100), SSCF
0049          SVDEV = 0.0
0050          SSDEV = 0.0
0051          DO 110 I = 1,NOP
0052          SVDEV = SVDEV + (DVMEAN-DV(I))*(DVMEAN-DV(I))
0053          SSDEV = SSDEV + (DSMEAN-DS(I))*(DSMEAN-DS(I))
0054          110 CONTINUE
0055          SVDEV = SQRT(SVDEV/(NOP-1))
0056          SSDEV = SQRT(SSDEV/(NOP-1))
0057          SVCF = 1.96*SVDEV/SQRT(FLOAT(NOP))
0058          SSCF = 1.96*SSDEV/SQRT(FLOAT(NOP))
0059          RETURN
0060          END

```

END OF SEGMENT, LENGTH 125, NAME SLIMIT

```

0061          SUBROUTINE SORT (X,N0)
0062          DIMENSION X(100)
0063          DO 51 K=1,N0-1
0064          DO 51 N=K+1,N0
0065          IF(X(K) GT X(N)) GOTO 51
0066          DM=X(K)
0067          X(K)=X(N)
0068          X(N)=DM
0069          51 CONTINUE
0070          RETURN
0071          END

```



## APPENDIX A.3.2

## Programme to Evaluate Exit Drop Diameter Using Honeywell

```

10  REM      SIZEANALYSIS
20  DIM A(100),B(100),D(100),T(100)
40  FOR N1=1,100
50  INPUT F1,F2,R
60  S1=0
70  S2=0
80  FOR I=1,1000
90  INPUT A(I),B(I)
100 IF A(I)=1000.GOTO 120
110 NEXT I
120 N=I-1
130 FOR I=1,N
140 A(I)=A(I)/R
150 B(I)=B(I)/R
151 IF B(I)<=A(I) GOTO 155
152 X=B(I)
153 B(I)=A(I)
154 A(I)=X
155 IF A(I)<>B(I) GOTO 160
156 D(I)=A(I)
157 T(I)=A(I)
158 GOTO 190
160 E=SQR((A(I)*A(I)-B(I)*B(I))/(A(I)*A(I)))
170 D(I)=SQR(A(I)*A(I)/2+B(I)*B(I)/(4*E)*LOG((1+E)/(1-E)))
180 T(I)=(A(I)*A(I)*B(I))1/3
190 S1=S1+D(I)*D(I)
200 S2=S2+(T(I))1/3
210 NEXT I
220 D3=SQR(S1/N)
230 D4=(S2/N)1/3
240 PRINT "FILM NUMBER = ",F1
250 PRINT "FRAME NUMBER=",F2
260 PRINT "RMAG          = ",R
270 PRINT "      I                DS(I)          DV(I)"
280 FOR I=1,N
290 PRINT I,D(I),T(I)
300 NEXT I
310 PRINT "DS MEAN = ",D3
320 PRINT "DV MEAN = ",D4
330 PRINT " N = ",N
335 GOSUB 400
340 NEXT N1
350 STOP
400 REM  SUBROUTINE SLIMIT
410 S5=0
420 S6=0
430 FOR I=1,N
440 S5=S5+(D3-D(I))*(D3-D(I))
450 S6=S6+(D4-T(I))*(D4-T(I))
460 NEXT I
470 S5=SQR(S5/(N-1))
480 S6=SQR(S6/(N-1))
490 S7=1.96*S5/SQR(N)
500 S8=1.96*S6/SQR(N)
510 PRINT "AREA 95% CONFIDENCE SPREAD = ",S7
520 PRINT "VOLUME 95% CONFIDENCE SPREAD = ",S8
530 RETURN

```



### APPENDIX A.3.3

Programme to "Sort" Drop Dimensions Obtained From  
Image Analysing Computer for use with Appendix (A.3.2)

```
10  REM          PROGRAM TO SORT NUMBERS
15  DIM X(100),Y(100),A(100),B(100),C(100)
20  INPUT F1,R1,R2
30  N1=1
40  INPUT D,N
50  IF D=1000 THEN 100
60  FOR I=N1,N1+N-1
70  X(I)=D
80  NEXT I
90  N1=N1+N
95  GOTO 40
100 N2=1
110 INPUT D,N
120 IF D=1000 THEN 200
121 L=N2+N-1
130 FOR I=N2,L
140 Y(I)=D
150 NEXT I
160 N2=N2+N
170 GOTO 110
200 FOR I=1,N1
210 X(I)=X(I)*.4
211 X(I)=X(I)+.15
215 Y(I)=Y(I)*.4
216 Y(I)=Y(I)+.15
220 NEXT I
225 IF N1<N2 THEN N3=N1: GOTO 240
230 N3=N2
240 FOR I=1,N3-1
250 FOR J=I+1,N3
260 IF X(I)>X(J) GOTO 300
270 Z=X(I)
280 X(I)=X(J)
290 X(J)=Z
300 IF Y(I)>Y(J) GOTO 340
310 Z=Y(I)
320 Y(I)=Y(J)
330 Y(J)=Z
340 NEXT J
350 NEXT I
360 PRINT R2
370 PRINT N3
380 PRINT F1
381 PRINT R1
390 FOR I=1,N3
400 PRINT X(I)
401 PRINT Y(I)
410 NEXT I
420 GOTO 20
430 END
```



contd. APPENDIX A.3.3

Typical Output of Data Following "Sort" Routine(Appx.A.3.3)  
and Size Analysis (Appx. A.3.2)

RUN NUMBER =	1.18	
FILM NUMBER =	1.18	
RMAG =	.46	
I	DS(I)	DV(I)
1	.839791	.83324
2	.858401	.844535
3	.685603	.671746
4	.49333	.493314
5	.436052	.435939
6	.337862	.337537
7	.337862	.337537
8	.337862	.337537
9	.337862	.337537
10	.337862	.337537
11	.350313	.343472
12	.350313	.343472
13	.350313	.343472
14	.350313	.343472
15	.283525	.282805
16	.283525	.282805
17	.283525	.282805
18	.283525	.282805
19	.283525	.282805
20	.252235	.243252
21	.221822	.217615
22	.221822	.217615
23	.221822	.217615
24	.221822	.217615
25	.221822	.217615
26	.173227	.173044
27	.173227	.173044
28	.173227	.173044
29	.157577	.154635
30	.157577	.154635
31	.157577	.154635
32	.157577	.154635
33	.157577	.154635
34	.157577	.154635
35	.133297	.132733
DS MEAN =	.36624	
DV MEAN =	.415202	
N =	35	
AREA 95% CONFIDENCE SPREAD =		.630709E-01
VOLUME 95% CONFIDENCE SPREAD =		.691418E-01



## APPENDIX A.3.4

### INLET DROP MODEL

Programme to find Equilibrium Point of a drop passing through an orifice

```

1  REM          ANALYSIS OF PRESSURE BALANCE
5  P1=3.14159
10 FOR D=.9,1.5,.3
11 FOR I=1,8
12 PRINT
13 NEXT I
14 N=0
15 D1=D
16 PRINT "DIAMETER OF SPHERE ";D1
20 D2=.1543*D
21 PRINT "MINIMUM VOID DIAMETER";D2: PRINT
22 PRINT " DROP DIA.",TAB(15),"BOUYANCY NO.";
23 PRINT TAB(32),"CHI",TAB(45),"F VALUE";
24 PRINT TAB(53),"PREDICTION"
25 FOR P=3.5,.5,-.5
27 M1=0
28 M2=0
29 FOR S2=.5,3.5,.5
31 M2=M2+1
32 IF M1>.5 GOTO 34
33 S=S2
34 IF S2<D2 THEN F2=1: GOTO 460
40 D5=S+3
44 Q=0
45 J=0
46 REM  EVALUATION OF DROP DIMENSIONS
50 X=J*P1/180
51 R1=(D1*(1-COS(X))+D2)/(2*COS(X))
52 B=(1-SIN(X))*(2*COS(X)*COS(X)+2-2*SIN(X))
53 R3=R1*R1*R1
54 W=(R1*COS(X))+2
55 L=5
56 IF J<1 THEN L=1
60 K=1
63 Z=Q*P1/180
70 R2=(D1*(1-COS(Z))+D2)/(2*COS(Z))
80 R4=R2*R2*R2
85 A=(2+2*SIN(Z)+COS(Z)*COS(Z)*SIN(Z))
95 C=W+(R1*R2*COS(X)*COS(Z))+(R2*COS(Z))+2
100 C=C*D1
110 D9=(D5-2*R4*A-R3*B)/C
115 D3=D9+SIN(X)

```



contd. APPENDIX A.3.4

```

116 REM EVALUATION OF ANGLE "CHI"
120 IF ABS(L)<.1E-01 THEN 200
125 IF K<0 THEN 135
130 IF (D3-SIN(Z))<0 THEN L=-L/2:K=-1: GOTO 140
131 GOTO 140
135 IF (D3-SIN(Z))>0 THEN L=-L/2:K=1
140 Q=Q+L
145 GOTO 63
200 H=(.5*(D1+D2)*(TAN(Z)))-(.5*(D1+D2)*(TAN(X)-1/(COS(X))))
210 H=H+R2+D2/2
211 REM SOLUTION OF PRESSURE BALANCE OVER DROP
220 F=H*P-(R2-R1)/(R2*R1)
221 IF M1>.5 GOTO 300
225 IF F<0 THEN F1=0
226 IF F>0 THEN F1=1
223 IF M2>1.5 GOTO 235
230 GOSUB 570
231 F2=F1
233 GOTO 460
235 IF F2=F1 GOTO 230
236 F2=F1
233 M1=1
242 S=S-.45
243 GOTO 40
300 GOSUB 570
301 M1=M1+1
302 S=S+.5E-01
304 IF M1>9.5 GOTO 322
306 GOTO 40
322 M1=0
460 NEXT S2
470 NEXT P
474 NEXT D
480 EXIT
481 REM SUBROUTINE FOR PRINT-OUT
500 FOR I=1,15
510 PRINT
520 NEXT I
521 PRINT "DIAMETER OF SPHERE ";D1
522 D2=.1543*D
523 PRINT "MINIMUM VOID DIAMETER";D2: PRINT
530 PRINT "DROP DIA.",TAB(19),"BOUYANCY NO.";
540 PRINT TAB(30),"CHI",TAB(44),"F VALUE";
550 PRINT TAB(53),"PREDICTION"
551 N=0
560 RETURN
570 PRINT S,P,Q,F;
571 IF F>0 THEN PRINT TAB(60),"PASSAGE"
572 IF F<0 THEN PRINT TAB(60),"HOLD-UP"
574 N=N+1
575 IF N>48 THEN GOSUB 500
578 RETURN
600 END

```



APPENDIX A.3.5

Output Data From Regression Analysis - 6" Diameter Column  
Operating Under "Total Coalescence"

REGRESSION ANALYSIS      COVA      MATRIX?      CUT OFF PARAMETER      .100000E- 5

DEPENDENT VARIABLE      DROPXT      DEGREES OF FREEDOM      307

INDEPENDENT VARIABLES AT SIGNIFICANT LEVEL      99.00 %

PACKHT      DIABAL      DROPIN      SUPVEL

VARIABLES      IN THE REGRESSION SET

VAR NAME	REGRESSION COEFF	STANDARD ERROR	CONFIDENCE INTERVAL	T STAT	PART CORR	MULTIPLE CORRELATION	F S S
PACKHT	0.0198939	.172355E- 1		1.15	0.07	0.508	.918076E 1
DIABAL	0.2952657	.377158E- 1		7.83	0.41	0.338	.109662E 2
DROPIN	0.0273863	.159853E 0		2.05	-0.12	0.502	.926508E 1
SUPVEL	0.0200287	.112682E- 1		1.78	0.10	0.504	.923516E 1

VARIABLES NOT IN THE REGRESSION SET

VAR NAME	T STAT	PART CORR	MULTIPLE CORRELATION	F S S
F.S.S.				
RESIDUAL ERROR				
MULT CORR				
INTERCEPT TERM				

F.S.S.      .914109F 1

RESIDUAL ERROR      .172556F 0

MULT CORR      0.512

INTERCEPT TERM      -      0.2627592



REGRESSION ANALYSIS COVA MATRIX2 CUT OFF PARAMETER .100000E-5  
 DEPENDENT VARIABLE DROPTX DEGREES OF FREEDOM 85

INDEPENDENT VARIABLES AT SIGNIFICANT LEVEL 99.00 %

DROPIN DIABAL PACKHT SUPVEL

VARIABLES IN THE REGRESSION SET

VAR NAME	REGRESSION COEFF	STANDARD ERROR	CONFIDENCE INTERVAL	T STAT	PART CORR	MULTIPLE CORRELATION	E S S
DROPIN	0.0860978	.177398E 0		0.49	0.00	0.780	.812221E 0
DIABAL	0.4094000	.517174E- 1		7.92	0.60	0.568	.140714E 1
PACKHT	0.0392894	.172684E- 1		2.28	0.24	0.766	.859306E 0
SUPVEL	0.0107738	.185994E- 1		0.58	0.06	0.780	.813174E 0

VARIABLES NOT IN THE REGRESSION SET

VAR NAME	T STAT	PART CORR	MULTIPLE CORRELATION	E S S
E.S.S.				.809977E 0
RESIDUAL ERROR				.976173E- 1
MULT CORR		0.781		
INTERCEPT TERM				0.5277150



APPENDIX A.3.7

Command Statements For Use With ICL Statistical Package  
(Linear Regression Analysis - 8 Dimensionless Groups)

```

10/45/05      24/09/74      ICL 1900 STATISTICAL ANALYSIS      XDS5/
PROBLEM NAME IS MULTRG
DATA ON CARDS
OUTPUT FILE NAME IS      ICL STATFILE
      REEL SEQUENCE NUMBER IS
      FILE GENERATION NUMBER IS
      RETENTION PERIOD IS
OBSERVATION MATRIX      MATRX1
WEIGHTS ARE NOT USED
COL NAMES      MATRX1
      DENDIS
      DENDIF
      GRAVIT
      DROPIN
      DROPXT
      DIABAL
      PACKHT
      INTTEN
      VISDIS
      SUPVEL
NUMBER OF COL NAMES IS      10
MATRIX      10      MATRX1
TRANSFORMATIONS      MATRX1      CHANGE      MATRX3
  BONDNO = ((DROPIN**2.0)*GRAVIT*DENDIF)/(INTTEN)
  DROPNO = (DROPXT/DROPIN)
  VOIDNO = (DROPIN/(DIABAL*2.5))
  HGHTNO = (DROPIN/PACKHT)
  PROPNO = ((GRAVIT*(VISDIS**4.0)*DENDIF)/((DENDIS**2.0)*(INTTEN**5.0))
  OHNGNO = (VISDIS/((DENDIS*PACKHT*INTTEN)**0.5))
  EXPNNO = ((GRAVIT*DROPNO*DENDIF)/((SUPVEL**2.0)*DENDIS))
  ARCHNO = (((DROPIN**3.0)*GRAVIT*DENDIF*DENDIS)/(VISDIS**4.0))
NUMBER OF TRANSFORMATIONS      0008
TRANSFORMATIONS      MATRX3      CHANGE      MATRX2
  BONDNO = ALOG(BONDNO)
  DROPNO = ALOG(DROPNO)
  VOIDNO = ALOG(VOIDNO)
  ARCHNO = ALOG(ARCHNO)
  EXPNNO =ALOG(EXPNNO)
  OHNGNO = ALOG(OHNGNO)
  PROPNO = ALOG(PROPNO)
  HGHTNO = ALOG(HGHTNO)
NUMBER OF TRANSFORMATIONS      0008
CROSS PRODUCT      MATRX2
NUMBER OF OBSERVATIONS IN CROSS PRODUCT IS      62
COVARIANCE      MATRX2
CORRELATION      MATRX2
PRINT MEANS      MATRX1      LP      S

```



Output from Regression Analysis - Dimensional Analysis  
Using 8 Groups derived by Pi-Buckingham Method

XDS3/22

10/52/37 24/09/74 ICL 1900 STATISTICAL ANALYSIS

REGRESSION ANALYSIS COVA MATRX2 CUT OFF PARAMETER .100000E- 5

DEPENDENT VARIABLE DROPNO DEGREES OF FREEDOM 56

INDEPENDENT VARIABLES AT SIGNIFICANT LEVEL 99.00 %

BONDNO VOIDNO ARCHNO EXPNO OHMGNO PROPNO HGHTNO

VARIABLES IN THE REGRESSION SET

VAR NAME	REGRESSION COEFF	STANDARD ERROR	CONFIDENCE INTERVAL	T STAT	PART CORR	MULTIPLE CORRELATION	E S S
VOIDNO	0.3453257	.873242E- 1		3.95	0.47	0.927	.575428E 1
ARCHNO -	0.3811065	.281720E- 1		13.53	-0.88	0.730	.191977E 2
EXPNO	0.0008268	.288914E- 1		0.03	0.00	0.944	.449822E 1
PROPNO -	0.1482224	.294349E- 1		6.73	-0.67	0.896	.814069E 1
HGHTNO -	0.0188588	.427181E- 1		0.44	-0.06	0.944	.451381E 1

VARIABLES NOT IN THE REGRESSION SET

VAR NAME	T STAT	PART CORR	MULTIPLE CORRELATION	E S S
BONDNO	0.00		0.944	.449815E 1
OHMGNO	0.00		0.944	.449815E 1

E.S.S. .449815E 1

RESIDUAL ERROR .283415E 0

MULT CORR 0.944

INTERCEPT TERM - 0.0358272

VARIABLE BONDNO NOT INCLUDED IN SET, PIVOT -.436558E-10 < CUT OFF

VARIABLE OHMGNO NOT INCLUDED IN SET, PIVOT -.135879E- 8 < CUT OFF



CORRELATION MATRIX

	10/52/03	24/09/74	ICL	1900 STATISTICAL ANALYSIS	XDS3/22			
BONDNO	1							
DROPN0	-.925636E 0	1						
VOIDNO	.838741E 0	-.676840E 0	1					
ARCHNO	.959084E 0	-.871475E 0	0	1				
EXPNNO	-.235135E 0	.237067E 0	0	-.138612E 0	1			
OHNGNO	-.349161E 0	.291042E 0	0	-.327073E 0	-.467626E 0	1		
PROPN0	-.197235E 0	.126176E 0	0	-.307197E 0	-.468731E 0	-.409770E 0	1	
HGHTNO	.557054E 0	-.506110E 0	0	.536599E 0	.605984E 0	.200798E 0	.200798E 0	1

CORRELATION MATRIX 10/52/32 24/09/74 ICL 1900 STATISTICAL ANALYSIS XDS3/22

REGRESSION ANALYSIS

	PROPN0	HGHTNO	COVA
BONDNO	-.197235E 0	.557054E 0	0
DROPN0	.126176E 0	-.506110E 0	0
VOIDNO	-.307197E 0	.536599E 0	0
ARCHNO	-.468731E 0	.605984E 0	0
EXPNNO	-.409770E 0	.200798E 0	0
OHNGNO	.528532E 0	-.328392E 0	0
PROPN0	.100000E 1	-.358218E 0	0
HGHTNO	-.358218E 0	.100000E 1	1

MATRIX 10/52/00 24/09/74 ICL 1900 STATISTICAL ANALYSIS XDS3/22

PRINT CORRELATION MATRIX2

	MEAN	MINIMUM VALUE	MAXIMUM VALUE	STANDARD DEVIATION
CONST	.100000E 1			
BONDNO	-.178282E 1	-.401881E 1	.161056E 1	.171577E 1
DROPN0	.762287E 0	-.901404E 0	.207317E 0	.821439E 0
VOIDNO	-.140526E 1	-.248491E 1	-.182322E 0	.794906E 0
ARCHNO	.992320E 1	.583417E 1	.138186E 1	.285289E 1
EXPNNO	.142709E 2	.826659E 1	.150284E 2	.155355E 1
OHNGNO	-.746637E 1	-.862979E 1	-.631556E 1	.554197E 0
PROPN0	-.251949E 2	-.264742E 2	-.214544E 2	.164784E 1
HGHTNO	-.322671E 1	-.329832E 1	-.138629E 1	.115702E 1



APPENDIX A.3.8

Output From Regression Analysis - Simplified Dimensional Analysis

19/34/33 19/09/74 ICL 1900 STATISTICAL ANALYSIS XDS3/22

REGRESSION ANALYSIS COVA MATRIX2 CUT OFF PARAMETER .100000E-3

DEPENDENT VARIABLE DRODNO DEGREES OF FREEDOM 57

INDEPENDENT VARIABLES AT SIGNIFICANT LEVEL 99.00 %

BONDNO VOIDNO

VARIABLES IN THE REGRESSION SET

1

VAR NAME	REGRESSION COEFF	STANDARD ERROR	CONFIDENCE INTERVAL	T STAT	PART CORR	MULTIPLE CORRELATION	F S S
----------	------------------	----------------	---------------------	--------	-----------	----------------------	-------

BONDNO	0.5749065	.404095E-1		14.25	-0.88	0.687	.204720E 2
--------	-----------	------------	--	-------	-------	-------	------------

VOIDNO	0.3424532	.850165E-1		4.03	0.47	0.921	.577882E 1
--------	-----------	------------	--	------	------	-------	------------

VARIABLES NOT IN THE REGRESSION SET

VAR NAME	T STAT	PART CORR	MULTIPLE CORRELATION	F S S
----------	--------	-----------	----------------------	-------

E.S.S.	.449834E 1			
--------	------------	--	--	--

RESIDUAL ERROR	.280924E 0			
----------------	------------	--	--	--

MULT CORR	0.939			
-----------	-------	--	--	--

INTERCEPT TERM	0.2168556			
----------------	-----------	--	--	--



MATRIX	MATRIX1	MEAN	MINIMUM VALUE	MAXIMUM VALUE	STANDARD DEVIATION
	CONST	.10000E 1			
	DENDIS	.856267E 0	.693000E 0	.976000E 0	.101627E 0
	DENDIF	.163753E 0	.240000E-1	.507000E 0	.101627E 0
	GRAVIT	.981100E 3	.981100E 3	.981100E 3	.996551E-2
	DROPIN	.266667E 0	.100000E 0	.500000E 0	.182883E 0
	DROPT	.476553E 0	.100000E 0	.110000E 1	.204560E 0
	DIAGAL	.548000E 0	.240000E 0	.480000E 0	.165265E 0
	PACKHT	.765000E 1	.100000E 1	.230000E 2	.692395E 1
	INTTEN	.324033E 2	.980000E 1	.511000E 2	.152985E 2
	VISDIS	.617353E-2	.510000E-2	.820000E-2	.112985E-2
	SUPVEL	.501350E-1	.166000E-1	.250000E 0	.524995E-1
	PRINT MEANS		MATRIX2 LP S		

19/34/24 . 19/09/74 ICL 1900 STATISTICAL ANALYSIS XDS3/22

MATRIX	MATRIX2	MEAN	MINIMUM VALUE	MAXIMUM VALUE	STANDARD DEVIATION
	CONST	.100000E 1			
	BONDNO	-.170829E 1	-.401881E 1	.161055E 1	.169367E 1
	DROPNO	.722136E 0	-.901402E 0	.207317E 1	.304087E 0
	VOIDNO	-.159258E 1	-.248491E 1	-.182322E 0	.805024E 0
	PRINT CORRELATION		MATRIX2 LP		

19/34/27 19/09/74 ICL 1900 STATISTICAL ANALYSIS XDS3/22

CORRELATION MATRIX	MATRIX2	BONDNO	DROPNO	VOIDNO
	BONDNO	.100000E 1	-.921147E 0	.845244E 0
	DROPNO	-.921147E 0	.100000E 1	-.680668E 0
	VOIDNO	.845244E 0	-.680668E 0	.100000E 1
	REGRESSION ANALYSIS		MATRIX2	COVA



APPENDIX 4.

EXPERIMENTAL DATA

- A.4.1 6" Diameter Column - Dispersed phase flow only
- A.4.2 9" Diameter Column - Dispersed phase flow only
- A.4.3 9" Diameter Column - Counter-current flow
- A.4.4 6" Diameter Column - Dispersed phase flow only  
(Graeco-Latin factorial experimental analysis -  
Exit drop diameter evaluated from Shadowgraphs  
using Quantimet 720)
- A.4.5 Output data of Inlet model for triangular geometry



APPENDIX A.4.1

DATA OBTAINED FROM 6" DIAMETER COLUMN

Dispersed Phase Flow Only

contd. APPENDIX A.4.1

Run	No.	h	$u_d$	$d_{xt}$	DVT	DVC	$d_b$	C.L.
o	1	1.5	0.0538	1.070	5.759	2.155	1.20	0.2545
o	2	1.5	0.0603	1.023	5.504	2.056	1.20	0.1624
o	3	1.5	0.1141	1.530	6.235	3.079	1.20	0.4461
o	4	1.5	0.1917	1.327	7.145	2.672	1.20	0.3026
o	5	4.0	0.0237	1.021	5.660	2.116	1.20	0.1961
o	6	4.0	0.0603	0.969	5.217	1.951	1.20	0.1020
o	7	4.0	0.1141	0.926	5.360	2.004	1.20	0.1232
o	8	4.0	0.1917	0.969	5.522	1.990	1.20	0.1452
o	10	1.5	0.0237	1.001	5.589	2.015	1.20	0.1602
o	11	1.5	0.1141	1.022	5.504	2.056	1.20	0.1493
o	12	10.5	0.0529	1.027	5.527	2.066	1.20	0.1406
o	13	10.5	0.0603	1.004	5.404	2.020	1.20	0.1279
o	14	10.5	0.1141	0.966	5.510	1.986	1.20	0.1241
o	13	0.0	0.1150	0.657	3.429	1.282	1.20	0.0820
o	14	2.0	0.1150	0.769	4.140	1.546	1.20	0.2116
o	15	2.0	0.2557	1.300	7.001	2.618	1.20	0.5305
o	16	2.0	0.4565	1.003	5.401	2.019	1.20	0.2022
o	17	6.5	0.1150	1.016	5.470	2.045	1.20	0.1794
o	18	6.5	0.2557	1.021	5.496	2.055	1.20	0.1244
o	19	6.5	0.4565	1.013	5.452	2.039	1.20	0.1264
o	20	10.5	0.1150	0.952	5.018	1.876	1.20	0.1516
y	1	10.5	0.1436	0.986	5.508	1.985	1.20	0.2042
y	2	10.5	0.2739	0.910	4.900	1.852	1.20	0.1564
y	3	10.5	0.3698	1.351	7.271	2.719	1.20	0.2960
y	4	10.5	0.4565	1.056	5.686	2.126	1.20	0.1415
y	5	10.5	0.5478	1.074	5.611	2.175	1.20	0.1401
y	6	16.0	0.0000	1.026	5.525	2.066	1.20	0.1446
y	7	16.0	0.1141	0.974	5.243	1.961	1.20	0.1610
y	8	16.0	0.1936	1.105	5.955	2.219	1.20	0.1420
y	9	16.0	0.2739	1.596	8.590	3.212	1.20	0.5616
y	10	16.0	0.3926	0.922	4.963	1.856	1.20	0.1442
y	11	16.0	0.4565	1.045	5.625	2.105	1.20	0.1525
y	12	15.0	0.1141	0.968	5.520	1.989	1.20	0.1586
y	13	15.0	0.2739	1.082	5.622	2.177	1.20	0.1411
y	14	15.0	0.4565	1.061	5.709	2.155	1.20	0.1065
y	15	16.0	0.1141	1.506	7.031	2.629	1.20	0.2991
y	16	16.0	0.2739	1.302	7.006	2.620	1.20	0.2664
y	17	16.0	0.4565	1.289	6.941	2.595	1.20	0.2456
10	9	2.0	0.2812	1.169	8.589	3.157	0.90	0.1551
10	10	2.0	0.4602	1.325	9.515	3.557	0.90	0.2025
10	11	2.0	0.1169	1.167	8.575	3.152	0.90	0.2055
10	12	5.0	0.2739	1.179	8.460	3.165	0.90	0.1189
10	13	5.0	0.4565	1.353	9.710	3.651	0.90	0.1656
10	14	7.0	0.1169	1.099	7.890	2.956	0.90	0.1255
10	16	7.0	0.1917	1.198	7.953	2.974	0.90	0.1456
10	17	7.0	0.2739	1.282	9.202	3.441	0.90	0.1762
10	18	7.0	0.3698	1.155	8.150	3.040	0.90	0.1565
12	5	5.5	0.3698	0.770	8.291	3.100	0.60	0.0565
12	6	5.5	0.4565	0.856	9.004	3.367	0.60	0.0655
12	7	5.5	0.5296	0.728	7.634	2.929	0.60	0.0646
12	8	6.0	0.1169	0.717	7.718	2.886	0.60	0.0465
12	9	6.0	0.2739	0.680	7.525	2.739	0.60	0.0757
12	10	6.0	0.3698	0.717	7.725	2.888	0.60	0.0712
12	11	6.0	0.1169	0.698	7.514	2.810	0.60	0.0474
12	12	6.0	0.2739	0.712	7.665	2.866	0.60	0.0447
12	13	6.0	0.4565	0.741	7.781	2.984	0.60	0.0755



contd. APPENDIX A.4.1

Run	No.	h	$u_d$	$d_{xt}$	DVT	DVC	$d_b$	C.L.
12	14	10.0	0.1169	0.701	7.551	2.823	0.50	0.0622
12	15	10.0	0.2739	0.782	8.423	3.150	0.50	0.0910
12	16	10.0	0.4565	0.788	8.486	3.173	0.50	0.0980
12	17	12.0	0.1169	0.711	7.653	2.862	0.50	0.0652
12	18	12.0	0.2739	0.711	7.653	2.861	0.50	0.0604
12	19	12.0	0.4565	0.715	7.693	2.877	0.50	0.0566
12	20	12.0	0.5478	0.688	7.406	2.769	0.50	0.0915
13	6	2.0	0.0822	0.903	6.482	2.424	0.90	0.1197
13	7	2.0	0.1696	0.877	6.295	2.354	0.90	0.0907
13	8	2.0	0.1917	0.789	5.662	2.117	0.90	0.0671
13	9	2.0	0.2739	0.799	5.738	2.140	0.90	0.0695
13	10	2.0	0.3652	0.908	6.517	2.457	0.90	0.1112
13	11	2.0	0.4565	0.851	6.107	2.283	0.90	0.0653
13	12	6.0	0.0622	0.904	6.485	2.425	0.90	0.1095
13	13	6.0	0.1096	0.877	6.297	2.354	0.90	0.1354
13	14	6.0	0.1917	0.829	5.947	2.224	0.90	0.0940
13	15	6.0	0.2739	0.812	5.627	2.179	0.90	0.0571
13	16	6.0	0.3652	0.852	6.115	2.287	0.90	0.0808
13	17	6.0	0.4565	0.918	6.586	2.462	0.90	0.1229
14	7	4.0	0.0730	0.850	4.576	1.711	1.20	0.0751
14	8	4.0	0.0622	0.851	4.579	1.712	1.20	0.0911
14	9	4.0	0.1004	0.766	4.125	1.542	1.20	0.0675
14	10	4.0	0.1461	0.757	3.970	1.484	1.20	0.1510
14	11	4.0	0.2739	0.837	4.508	1.686	1.20	0.1511
14	12	4.0	0.3652	0.799	4.503	1.609	1.20	0.0767
14	13	4.0	0.4565	0.911	4.904	1.854	1.20	0.1165
14	14	6.0	0.0730	0.821	4.420	1.655	1.20	0.1911
14	15	6.0	0.0622	0.971	5.226	1.954	1.20	0.1412
14	16	6.0	0.1004	0.666	4.769	1.783	1.20	0.1290
14	17	6.0	0.1461	0.992	5.538	1.996	1.20	0.1747
14	18	6.0	0.2739	0.871	4.687	1.755	1.20	0.0662
14	19	6.0	0.3652	1.008	5.428	2.056	1.20	0.1565
14	20	8.5	0.0730	0.913	4.913	1.837	1.20	0.1905
14	21	8.5	0.0622	0.913	4.917	1.839	1.20	0.1525
14	22	8.5	0.1004	1.050	5.652	2.115	1.20	0.2751
14	23	8.5	0.1461	0.991	5.536	1.995	1.20	0.1097
14	27	11.0	0.0622	0.956	5.146	1.924	1.20	0.1119
14	28	11.0	0.1461	0.944	5.082	1.900	1.20	0.1056
14	29	11.0	0.3652	0.865	4.762	1.781	1.20	0.1209
14	30	11.0	0.4565	0.823	4.432	1.657	1.20	0.1042
15	2	3.0	0.0730	0.706	7.599	2.841	0.50	0.0725
15	3	3.0	0.0822	0.687	7.402	2.766	0.50	0.0677
15	4	3.0	0.1004	0.675	7.480	2.797	0.50	0.0615
15	5	3.0	0.1461	0.664	7.561	2.752	0.50	0.0612
15	6	3.0	0.2739	0.659	7.098	2.654	0.50	0.0754
15	7	3.0	0.3652	0.663	7.140	2.670	0.50	0.1025
15	8	3.0	0.5022	0.650	6.995	2.616	0.50	0.0901
15	9	6.0	0.0274	0.712	7.662	2.865	0.50	0.0655
15	10	6.0	0.0320	0.672	7.231	2.704	0.50	0.0614
15	11	6.0	0.0475	0.756	7.928	2.964	0.50	0.1087
15	12	6.0	0.0730	0.677	7.500	2.804	0.50	0.0785
15	13	6.0	0.1096	0.763	8.212	3.071	0.50	0.0716
15	14	6.0	0.1461	0.754	7.900	2.954	0.50	0.0799
15	15	6.0	0.1626	0.709	7.629	2.853	0.50	0.0726
15	16	6.0	0.2739	0.666	7.587	2.762	0.50	0.0751
15	17	6.0	0.0274	0.705	7.587	2.837	0.50	0.1151
15	18	8.0	0.0365	0.663	7.134	2.667	0.50	0.0944
15	19	8.0	0.0457	0.712	7.667	2.867	0.50	0.0716



contd. APPENDIX A.4.1

Run	No.	h	$u_d$	$d_{xt}$	DVT	DVC	$d_b$	C.L.
15	20	8.0	0.0730	0.733	7.896	2.952	0.60	0.0450
15	21	8.0	0.1096	0.695	7.478	2.796	0.60	0.0669
15	22	8.0	0.1461	0.718	7.734	2.842	0.60	0.0727
15	23	8.0	0.2009	0.729	7.844	2.935	0.60	0.0804
15	26	8.0	0.2739	0.710	7.647	2.859	0.60	0.0831
15	25	11.0	0.0274	0.705	7.589	2.850	0.60	0.0476
15	26	11.0	0.0365	0.740	7.971	2.981	0.60	0.0510
15	27	11.0	0.0457	0.728	7.641	2.932	0.60	0.0745
15	28	11.0	0.0730	0.733	7.689	2.950	0.60	0.0750
15	29	11.0	0.1096	0.695	7.479	2.797	0.60	0.0764
15	32	11.0	0.2739	0.714	8.554	3.116	0.60	0.0912
16	2	2.0	0.0274	0.911	6.539	2.445	0.90	0.0614
16	3	2.0	0.0274	0.924	6.633	2.480	0.90	0.0470
16	4	2.0	0.0411	0.971	6.969	2.600	0.90	0.0720
16	5	2.0	0.0657	0.937	6.725	2.515	0.90	0.1257
16	5	2.0	0.1096	0.874	6.272	2.345	0.90	0.0826
16	6	2.0	0.1808	0.791	5.681	2.124	0.90	0.0716
16	7	2.0	0.2757	0.928	6.659	2.490	0.90	0.1177
16	8	2.0	0.2757	0.903	6.478	2.422	0.90	0.1225
16	9	4.0	0.0274	0.827	5.939	2.221	0.90	0.1327
16	10	4.0	0.0501	0.814	5.840	2.184	0.90	0.1352
16	11	4.0	0.0411	0.831	5.964	2.230	0.90	0.0768
16	12	4.0	0.0657	0.873	6.267	2.343	0.90	0.1501
16	13	4.0	0.1096	0.895	6.427	2.403	0.90	0.1521
16	14	4.0	0.1808	0.820	5.882	2.199	0.90	0.0951
16	15	4.0	0.2757	0.955	6.657	2.564	0.90	0.2148
16	16	6.0	0.0274	0.873	6.267	2.343	0.90	0.1337
16	17	6.0	0.0501	1.020	7.520	2.737	0.90	0.1172
16	18	6.0	0.0411	0.918	6.586	2.463	0.90	0.0993
16	17	6.0	0.0657	0.929	6.669	2.493	0.90	0.1352
16	20	6.0	0.1096	0.895	6.421	2.401	0.90	0.1030
16	21	6.0	0.1808	0.933	6.638	2.557	0.90	0.1276
16	22	6.0	0.2757	0.922	6.618	2.475	0.90	0.1191
16	23	8.0	0.0274	0.850	6.098	2.280	0.90	0.1345
16	24	8.0	0.0501	0.713	5.117	1.913	0.90	0.0715
16	25	8.0	0.0411	0.756	5.286	1.976	0.90	0.0592
16	25	8.0	0.0657	0.807	5.792	2.166	0.90	0.1164
16	26	8.0	0.1096	0.809	5.609	2.172	0.90	0.0979
16	27	8.0	0.1808	0.923	6.622	2.476	0.90	0.1709
16	28	8.0	0.2757	0.910	6.535	2.445	0.90	0.1250
16	29	8.0	0.4492	0.919	6.599	2.467	0.90	0.1523
16	30	8.0	0.0000	0.861	6.177	2.510	0.90	0.1020
16	31	8.0	0.0000	0.714	5.557	2.078	0.90	0.1334
16	32	8.0	0.0000	1.006	7.224	2.701	0.90	0.1983
16	33	8.0	0.0000	0.893	6.407	2.396	0.90	0.1293
16	34	8.0	0.0000	0.880	6.318	2.363	0.90	0.1190
17	3	1.5	0.0501	0.362	1.947	0.728	1.20	0.0696
17	4	1.5	0.0411	0.600	3.553	1.328	1.20	0.2472
17	5	1.5	0.0657	0.603	3.678	1.375	1.20	0.2076
17	6	1.5	0.1077	0.716	4.177	1.562	1.20	0.2670
17	7	1.5	0.1808	0.732	3.942	1.474	1.20	0.2060
17	8	1.5	0.2757	0.718	3.666	1.445	1.20	0.1879
17	9	1.5	0.4657	0.922	4.963	1.850	1.20	0.1884
17	10	1.5	0.0000	0.980	5.276	1.973	1.20	0.1945
17	11	3.0	0.0256	0.954	5.134	1.920	1.20	0.2029
17	12	3.0	0.0501	0.904	4.864	1.819	1.20	0.1763
17	13	3.0	0.0411	0.878	4.726	1.767	1.20	0.1617



contd. APPENDIX A.4.1

Run	No.	h	$u_d$	$d_{xt}$	DVT	DVC	$d_b$	C.L.
17	14	5.0	0.0657	0.955	5.140	1.922	1.20	0.1787
17	15	5.0	0.1077	0.852	4.586	1.715	1.20	0.1004
17	16	5.0	0.1808	1.050	5.544	2.073	1.20	0.2157
17	17	5.0	0.2757	0.972	5.233	1.957	1.20	0.1453
17	18	5.0	0.4657	0.928	4.995	1.866	1.20	0.1107
17	19	5.0	0.0000	0.992	5.343	1.996	1.20	0.1241
17	20	5.0	0.0256	0.958	5.155	1.929	1.20	0.1633
17	21	5.0	0.0501	0.926	4.987	1.865	1.20	0.1119
17	22	5.0	0.0411	0.888	4.778	1.787	1.20	0.1206
17	23	5.0	0.0657	0.951	5.283	1.975	1.20	0.1436
17	24	5.0	0.1077	0.947	5.096	1.905	1.20	0.1379
17	25	5.0	0.1808	0.991	5.336	1.993	1.20	0.1981
17	26	5.0	0.2757	1.041	5.604	2.093	1.20	0.1948
17	27	5.0	0.4657	0.934	5.026	1.879	1.20	0.1661
17	28	5.0	0.0000	1.127	6.065	2.266	1.20	0.1669
17	29	10.0	0.0256	0.908	4.685	1.827	1.20	0.0772
17	30	10.0	0.0501	0.868	4.674	1.746	1.20	0.0986
17	31	10.0	0.0411	0.902	4.857	1.816	1.20	0.1036
17	32	10.0	0.0657	0.857	4.613	1.723	1.20	0.0954
17	33	10.0	0.1077	0.961	5.174	1.933	1.20	0.1276
17	34	10.0	0.1808	0.932	5.017	1.876	1.20	0.1373
17	35	10.0	0.2757	0.942	5.070	1.896	1.20	0.1644
18	1	2.0	0.0501	0.687	3.698	1.383	1.20	0.2023
18	2	2.0	0.0411	0.736	3.962	1.481	1.20	0.2486
18	3	2.0	0.0657	0.622	3.347	1.251	1.20	0.1697
18	4	2.0	0.2757	0.986	5.306	1.984	1.20	0.2333
18	5	4.0	0.0256	0.776	8.357	3.123	0.60	0.1987
18	6	4.0	0.0501	0.810	8.718	3.260	0.60	0.1354
18	7	4.0	0.0411	0.740	7.967	2.979	0.60	0.1043
18	8	4.0	0.0657	0.686	7.386	2.762	0.60	0.0866
18	9	4.0	0.1077	0.660	7.105	2.657	0.60	0.0629
18	10	4.0	0.1780	0.701	7.343	2.820	0.60	0.0624
18	11	4.0	0.2757	0.694	7.471	2.793	0.60	0.0604
18	12	4.0	0.0000	0.767	8.258	3.086	0.60	0.0940
18	13	6.0	0.0501	0.635	6.641	2.556	0.60	0.0970
18	14	6.0	0.0411	0.637	6.654	2.563	0.60	0.1094
18	15	6.0	0.1370	0.636	6.647	2.560	0.60	0.1094
18	16	6.0	0.1077	0.645	6.947	2.598	0.60	0.0976
18	25	8.0	0.2757	0.688	7.413	2.772	0.60	0.0744
18	26	8.0	0.0000	0.664	7.150	2.673	0.60	0.1023
18	27	12.0	0.0501	0.614	6.606	2.470	0.60	0.0373
18	28	12.0	0.0411	0.712	7.666	2.867	0.60	0.1241
18	29	12.0	0.0657	0.654	7.040	2.632	0.60	0.0330
18	30	12.0	0.1077	0.597	6.428	2.404	0.60	0.0693
18	31	12.0	0.1808	0.666	7.168	2.680	0.60	0.0749
18	32	12.0	0.2757	0.724	7.799	2.916	0.60	0.0893
18	33	12.0	0.0000	0.677	7.293	2.727	0.60	0.0313



contd. APPENDIX A.4.1

Run	No.	h	$u_d$	$d_{xt}$	DVT	DVC	$d_b$	C.L.
19	1	4.0	0.0256	0.859	6.024	2.252	0.90	0.0831
19	2	4.0	0.0329	0.909	6.223	2.439	0.90	0.0843
19	3	4.0	0.0411	0.863	6.193	2.316	0.90	0.1422
19	4	4.0	0.0657	0.859	6.023	2.252	0.90	0.0844
19	5	4.0	0.1096	0.820	5.864	2.200	0.90	0.0656
19	6	4.0	0.1826	0.477	3.424	1.280	0.90	0.1158
19	7	4.0	0.2785	0.849	6.434	2.413	0.90	0.1243
19	8	4.0	0.4565	0.908	6.517	2.437	0.90	0.1369
19	9	4.0	0.0000	0.843	5.906	2.206	0.90	0.0927
19	10	4.0	0.0000	0.808	5.798	2.168	0.90	0.0859
19	11	6.0	0.0256	0.971	6.970	2.606	0.90	0.1904
19	12	6.0	0.0329	0.887	6.564	2.379	0.90	0.1103
19	13	6.0	0.0411	0.949	6.808	2.546	0.90	0.1754
19	14	6.0	0.0657	0.916	6.575	2.459	0.90	0.1704
19	15	6.0	0.1096	0.913	6.550	2.449	0.90	0.1293
19	16	6.0	0.1826	0.979	7.029	2.626	0.90	0.2463
19	17	6.0	0.2785	0.945	6.785	2.537	0.90	0.1160
20	1	10.0	0.0256	0.813	5.836	2.183	0.90	0.0726
20	2	10.0	0.0329	0.906	6.304	2.432	0.90	0.1106
20	3	10.0	0.0411	0.864	6.200	2.316	0.90	0.0801
20	4	10.0	0.0657	0.849	6.097	2.280	0.90	0.1213
20	5	10.0	0.1096	0.895	6.426	2.403	0.90	0.1317
20	6	10.0	0.1826	0.909	6.527	2.441	0.90	0.1113
20	7	10.0	0.2739	0.871	6.251	2.337	0.90	0.1380
20	8	10.0	0.4565	0.852	6.331	2.367	0.90	0.1190
20	9	3.0	0.0247	0.939	5.162	1.930	1.20	0.1181
20	10	3.0	0.0329	0.919	4.949	1.851	1.20	0.2317
20	11	3.0	0.0411	0.973	4.971	1.859	1.20	0.1564
20	12	3.0	0.0657	0.949	5.108	1.910	1.20	0.2167
20	13	3.0	0.1096	1.000	5.263	2.013	1.20	0.1960
20	14	3.0	0.1826	1.043	5.615	2.100	1.20	0.1776
20	15	3.0	0.2739	0.868	4.675	1.748	1.20	0.1309
20	16	3.0	0.0000	0.883	4.753	1.777	1.20	0.1213
20	17	5.0	0.0256	0.848	4.567	1.708	1.20	0.1256
20	18	5.0	0.0329	0.965	5.194	1.942	1.20	0.1326
20	19	5.0	0.0411	0.941	5.065	1.894	1.20	0.1499
20	20	5.0	0.0657	0.858	4.618	1.727	1.20	0.1113
20	21	5.0	0.1096	0.945	5.086	1.902	1.20	0.1400
20	22	5.0	0.1826	0.914	4.921	1.840	1.20	0.1654
20	23	5.0	0.2739	0.937	5.042	1.885	1.20	0.1112
20	24	5.0	0.0000	0.880	4.736	1.771	1.20	0.1372
20	25	9.0	0.0256	0.775	4.172	1.530	1.20	0.0781
20	26	9.0	0.0329	0.893	4.605	1.797	1.20	0.0912
20	27	9.0	0.0411	0.944	5.079	1.899	1.20	0.1411
20	29	9.0	0.0657	0.903	4.661	1.816	1.20	0.1331
21	1	3.0	0.0256	1.098	11.025	4.421	0.60	0.2499
21	2	3.0	0.0329	1.046	11.258	4.209	0.60	0.2413
21	3	3.0	0.0329	1.022	11.008	4.116	0.60	0.2030
21	4	3.0	0.0411	0.964	10.379	3.881	0.60	0.2192
21	5	3.0	0.0657	0.975	10.499	3.926	0.60	0.1310
21	6	3.0	0.1096	1.030	11.087	4.143	0.60	0.1887
21	7	3.0	0.1826	0.936	10.074	3.767	0.60	0.1124
21	8	3.0	0.2739	0.864	9.300	3.476	0.60	0.1300
21	9	3.0	0.0000	1.044	11.241	4.203	0.60	0.1893
21	10	3.0	0.0256	0.588	6.330	2.367	0.60	0.0364
21	11	3.0	0.0274	0.520	5.003	2.093	0.60	0.0336



contd. APPENDIX A.4.1

Run	No.	h	$u_d$	$d_{xt}$	DVT	DVC	$d_b$	C.L.
21	12	5.0	0.0411	0.568	6.718	2.280	0.60	0.0866
21	13	5.0	0.0657	0.666	7.169	2.600	0.60	0.0975
21	14	5.0	0.1096	0.718	7.720	2.809	0.60	0.0874
21	15	5.0	0.1826	0.751	7.869	2.942	0.60	0.0967
21	16	5.0	0.2739	0.787	8.469	3.167	0.60	0.1190
21	17	5.0	0.0000	0.651	6.797	2.541	0.60	0.1597
21	18	8.0	0.0256	0.724	7.799	2.916	0.60	0.1224
21	19	8.0	0.0329	0.756	7.925	2.963	0.60	0.1150
21	20	8.0	0.0411	0.668	7.189	2.688	0.60	0.0854
21	21	8.0	0.0657	0.600	7.767	2.657	0.60	0.0947
21	22	8.0	0.1096	0.759	8.173	3.050	0.60	0.1150
21	23	8.0	0.1826	0.656	7.061	2.640	0.60	0.0821
21	24	8.0	0.0000	0.890	8.610	3.220	0.60	0.1500
21	25	11.0	0.0256	0.729	7.046	2.934	0.60	0.0821
21	26	11.0	0.0329	0.652	7.015	2.625	0.60	0.1025
21	27	11.0	0.0411	0.675	7.263	2.716	0.60	0.0652
21	28	11.0	0.0657	0.703	7.572	2.831	0.60	0.0709
21	29	11.0	0.1096	0.720	7.750	2.900	0.60	0.0715
21	30	11.0	0.1826	0.692	7.450	2.780	0.60	0.0859
21	31	11.0	0.2739	0.695	7.484	2.798	0.60	0.0877
21	32	11.0	0.0000	0.717	7.721	2.887	0.60	0.0604
22	1	2.0	0.0256	0.838	6.015	2.249	0.90	0.1054
22	2	2.0	0.0329	0.800	6.216	2.324	0.90	0.1151
22	3	2.0	0.0411	0.892	6.404	2.395	0.90	0.1248
22	4	2.0	0.0657	0.992	7.121	2.662	0.90	0.0961
22	5	2.0	0.1096	0.957	6.070	2.569	0.90	0.1359
22	0	4.0	0.0329	0.934	6.703	2.500	0.90	0.1512
22	11	4.0	0.0411	0.928	6.650	2.489	0.90	0.1332
22	12	4.0	0.0639	0.767	5.651	2.113	0.90	0.1390
22	13	4.0	0.1096	0.955	6.856	2.564	0.90	0.1293
22	14	4.0	0.1826	0.949	6.812	2.547	0.90	0.1059
22	15	4.0	0.2739	0.914	6.563	2.454	0.90	0.1354
22	16	4.0	0.0000	0.871	6.252	2.338	0.90	0.1430
22	17	6.0	0.0256	0.783	5.621	2.102	0.90	0.1008
22	18	6.0	0.0329	0.807	5.794	2.167	0.90	0.1252
22	19	6.0	0.0411	0.950	6.816	2.549	0.90	0.1475
22	20	6.0	0.0657	0.951	6.827	2.553	0.90	0.1355
22	21	6.0	0.1096	0.947	6.799	2.542	0.90	0.1462
22	22	6.0	0.1826	0.943	6.766	2.530	0.90	0.1522
22	23	6.0	0.2739	0.765	5.489	2.052	0.90	0.1178
22	24	10.0	0.0256	0.847	6.078	2.273	0.90	0.1484
22	25	10.0	0.0292	0.850	5.955	2.227	0.90	0.0909
22	26	10.0	0.0411	1.015	7.286	2.724	0.90	0.2443
22	27	10.0	0.0657	0.850	6.102	2.262	0.90	0.1608
22	28	10.0	0.1096	0.897	6.441	2.409	0.90	0.1970
22	29	10.0	0.1826	1.003	7.402	2.693	0.90	0.2196
22	30	10.0	0.2739	1.074	7.707	2.882	0.90	0.2410
22	31	10.0	0.0000	0.971	6.968	2.605	0.90	0.2100
23	1	3.0	0.0256	0.942	10.144	3.793	0.60	0.2439
23	2	3.0	0.0329	0.990	10.662	3.987	0.60	0.1850
23	3	3.0	0.0411	0.980	10.549	3.945	0.60	0.2306
23	4	3.0	0.0657	0.962	10.353	3.871	0.60	0.2127
23	5	3.0	0.1096	1.062	11.429	4.274	0.60	0.1433
23	6	3.0	0.1826	0.871	9.574	3.505	0.60	0.1051
23	7	3.0	0.2739	0.952	10.254	3.834	0.60	0.1410
23	8	3.0	0.0000	0.912	9.616	3.670	0.60	0.0754
23	9	5.0	0.0256	0.746	8.033	3.004	0.60	0.1615



APPENDIX A.4.1

Run	No.	h	$u_d$	$d_{xt}$	DVT	DVC	$d_b$	C.L.
23	10	5.0	0.0329	0.749	8.068	3.017	0.60	0.0672
23	11	5.0	0.0411	0.671	7.228	2.703	0.60	0.0409
23	12	5.0	0.0657	0.662	7.343	2.740	0.60	0.0720
23	13	5.0	0.1096	0.764	8.222	3.074	0.60	0.1154
23	14	5.0	0.1826	0.766	8.243	3.082	0.60	0.1443
23	15	5.0	0.2739	0.761	8.169	3.067	0.60	0.1243
23	16	5.0	0.0000	0.567	6.323	2.364	0.60	0.0649
23	17	5.0	0.0000	0.639	7.097	2.654	0.60	0.1024
23	18	9.0	0.0256	0.750	7.657	2.936	0.60	0.1120
23	19	9.0	0.0329	0.764	8.224	3.073	0.60	0.1143
23	20	9.0	0.0411	0.750	8.075	3.019	0.60	0.1067
23	21	9.0	0.0657	0.693	7.456	2.788	0.60	0.0948
23	22	9.0	0.1096	0.639	6.876	2.571	0.60	0.1111
23	23	9.0	0.1826	0.728	7.637	2.930	0.60	0.1000
23	24	9.0	0.2739	0.691	7.442	2.763	0.60	0.1144
23	25	9.0	0.0000	0.716	7.714	2.884	0.60	0.0867
23	26	9.0	0.0000	0.749	7.645	2.933	0.60	0.0810
23	26	9.0	0.0000	0.741	7.757	2.901	0.60	0.0953
23	27	11.0	0.0256	0.665	7.376	2.756	0.60	0.1074
23	28	11.0	0.0329	0.639	6.881	2.573	0.60	0.0390
23	29	11.0	0.0411	0.789	8.491	3.173	0.60	0.0706
23	30	11.0	0.0657	0.726	7.612	2.921	0.60	0.0332
23	31	11.0	0.1096	0.715	7.703	2.880	0.60	0.1042
23	32	11.0	0.1826	0.714	7.639	2.873	0.60	0.0673
23	33	11.0	0.2739	0.660	7.104	2.656	0.60	0.0836
23	34	11.0	0.0000	0.670	7.214	2.697	0.60	0.0420
23	35	11.0	0.0000	0.730	7.862	2.940	0.60	0.0668
24	1	4.0	0.0256	0.940	5.061	1.892	1.20	0.1674
24	2	4.0	0.0329	0.905	4.671	1.821	1.20	0.1343
24	3	4.0	0.0411	0.864	4.633	1.740	1.20	0.1364
24	4	4.0	0.0657	1.025	5.317	2.063	1.20	0.2320
24	5	4.0	0.1096	0.867	4.774	1.785	1.20	0.1343
24	6	4.0	0.1826	0.906	4.675	1.823	1.20	0.1200
24	7	4.0	0.2739	0.919	4.950	1.851	1.20	0.1613
24	8	4.0	0.0000	0.999	5.379	2.011	1.20	0.1702
24	9	7.0	0.0256	0.820	4.416	1.651	1.20	0.1083
24	10	7.0	0.0329	0.826	4.302	1.684	1.20	0.0661
24	11	7.0	0.0411	0.807	4.342	1.624	1.20	0.1290
24	12	7.0	0.0657	1.016	5.471	2.046	1.20	0.2637
24	13	7.0	0.1096	1.034	5.368	2.062	1.20	0.1786
24	14	7.0	0.1826	0.919	4.950	1.851	1.20	0.0939
24	15	7.0	0.2739	0.981	5.283	1.973	1.20	0.1366
24	16	7.0	0.0000	0.846	4.356	1.704	1.20	0.1363
24	17	10.0	0.0256	1.019	5.486	2.031	1.20	0.2416
24	18	10.0	0.0329	1.007	5.421	2.027	1.20	0.1682
24	19	10.0	0.0411	1.023	5.310	2.060	1.20	0.1704
24	20	10.0	0.0657	0.974	5.243	1.960	1.20	0.1393
24	21	10.0	0.1096	0.987	5.311	1.986	1.20	0.0999
24	22	10.0	0.1826	0.950	5.116	1.913	1.20	0.1423
24	23	10.0	0.2739	1.017	5.475	2.047	1.20	0.1661
24	24	10.0	0.0000	1.032	5.661	2.117	1.20	0.1228
24	25	10.0	0.0000	0.989	5.321	1.990	1.20	0.2386
24	26	10.0	0.0000	1.078	5.601	2.169	1.20	0.1777



ontd. APPENDIX A.4.1

Run	No.	h	$u_d$	$d_{xt}$	DST	DSC	$d_b$	C.L.
6	1	1.5	0.0338	1.065	5.731	2.143	1.20	0.2435
6	2	1.5	0.0603	1.040	5.599	2.094	1.20	0.1772
6	3	1.5	0.1141	1.514	8.132	3.048	1.20	0.5285
6	4	1.5	0.1917	1.372	7.387	2.762	1.20	0.3879
6	5	4.0	0.0237	1.068	5.747	2.149	1.20	0.2169
6	6	4.0	0.0603	1.002	5.596	2.018	1.20	0.1139
6	7	4.0	0.1141	1.006	5.418	2.026	1.20	0.1297
6	8	4.0	0.1917	0.988	5.318	1.987	1.20	0.1490
6	10	1.5	0.0237	1.001	5.590	2.015	1.20	0.1834
6	11	1.5	0.1141	1.031	5.551	2.075	1.20	0.1545
6	12	10.5	0.0329	1.063	5.721	2.159	1.20	0.1560
6	13	10.5	0.0603	1.019	5.487	2.052	1.20	0.1500
6	14	10.5	0.1141	1.003	5.400	2.019	1.20	0.1505
6	13	0.0	0.1150	0.637	3.429	1.282	1.20	0.0645
6	14	2.0	0.1150	0.688	3.705	1.385	1.20	0.2027
6	15	2.0	0.2557	1.252	6.034	2.480	1.20	0.5274
6	16	2.0	0.4565	0.979	5.272	1.971	1.20	0.2155
6	17	6.5	0.1150	1.059	5.098	2.131	1.20	0.1659
6	18	6.5	0.2557	1.018	5.478	2.048	1.20	0.1591
6	19	6.5	0.4565	1.014	5.460	2.042	1.20	0.1225
6	20	10.5	0.1150	0.940	5.058	1.891	1.20	0.1628
9	1	10.5	0.1936	0.952	5.127	1.917	1.20	0.2115
9	2	10.5	0.2739	0.907	4.882	1.825	1.20	0.1559
9	3	10.5	0.3698	1.351	7.275	2.720	1.20	0.5571
9	4	10.5	0.4565	1.050	5.050	2.115	1.20	0.1409
9	5	10.5	0.5478	1.085	5.642	2.185	1.20	0.1408
9	6	16.0	0.0000	1.044	5.620	2.101	1.20	0.1516
9	7	16.0	0.1141	0.960	5.168	1.932	1.20	0.1695
9	8	16.0	0.1936	1.095	5.893	2.203	1.20	0.1464
9	9	16.0	0.2739	1.561	8.401	3.141	1.20	0.4527
9	10	16.0	0.3426	0.896	4.021	1.805	1.20	0.1420
9	11	16.0	0.4565	1.035	5.561	2.079	1.20	0.1527
9	12	15.0	0.1141	0.987	5.314	1.987	1.20	0.1454
9	13	15.0	0.2739	1.106	5.956	2.227	1.20	0.1515
9	14	15.0	0.4565	1.087	5.652	2.188	1.20	0.1085
9	15	16.0	0.1141	1.252	6.736	2.519	1.20	0.2685
9	16	16.0	0.2739	1.264	6.004	2.544	1.20	0.2676
9	17	16.0	0.4565	1.242	6.685	2.500	1.20	0.2584
10	9	2.0	0.2812	1.174	8.425	3.150	0.90	0.1595
10	10	2.0	0.4602	1.295	9.292	3.475	0.90	0.2047
10	11	2.0	0.1169	1.168	8.586	3.156	0.90	0.2062
10	12	3.0	0.2739	1.195	8.576	3.207	0.90	0.1250
10	13	3.0	0.4565	1.350	9.693	3.624	0.90	0.1660
10	14	7.0	0.1169	1.093	7.645	2.935	0.90	0.1255
10	16	7.0	0.1917	1.105	7.934	2.967	0.90	0.1529
10	17	7.0	0.2739	1.305	9.551	3.496	0.90	0.1892
10	18	7.0	0.3698	1.122	8.056	3.012	0.90	0.1572
12	5	3.5	0.3698	0.777	8.368	3.129	0.60	0.0562
12	6	3.5	0.4565	0.852	9.177	3.431	0.60	0.0907
12	7	3.5	0.5296	0.724	7.795	2.915	0.60	0.0875
12	8	6.0	0.1169	0.728	7.837	2.930	0.60	0.0450
12	9	6.0	0.2739	0.688	7.408	2.770	0.60	0.0755
12	10	6.0	0.3698	0.716	7.704	2.881	0.60	0.0720
12	11	8.0	0.1169	0.711	7.652	2.861	0.60	0.0427
12	12	8.0	0.2739	0.724	7.797	2.916	0.60	0.0450
12	13	8.0	0.4565	0.740	7.962	2.977	0.60	0.0752
12	14	10.0	0.1169	0.710	7.644	2.856	0.60	0.0644
12	15	10.0	0.2739	0.785	8.453	3.161	0.60	0.0765
12	16	10.0	0.4565	0.784	8.444	3.157	0.60	0.1027
12	17	12.0	0.1169	0.721	7.764	2.905	0.60	0.0661



contd. APPENDIX A.4.1

Run	No.	h	$u_d$	$d_{xt}$	DVT	DVC	$d_b$	C.L.
12	18	12.0	0.2739	0.711	7.057	2.865	0.60	0.0619
12	19	12.0	0.4565	0.718	7.725	2.889	0.60	0.0595
12	20	12.0	0.5478	0.685	7.374	2.757	0.60	0.0747
13	6	2.0	0.0822	0.914	6.558	2.452	0.90	0.1215
13	7	2.0	0.1096	0.895	6.421	2.401	0.90	0.0960
13	8	2.0	0.1917	0.827	5.936	2.220	0.90	0.0770
13	9	2.0	0.2739	0.800	5.743	2.147	0.90	0.0899
13	10	2.0	0.3652	0.929	6.069	2.494	0.90	0.1161
13	11	2.0	0.4565	0.864	6.205	2.320	0.90	0.0655
13	12	6.0	0.0822	0.970	6.006	2.470	0.90	0.1125
13	13	6.0	0.1096	0.910	6.532	2.443	0.90	0.1490
13	14	6.0	0.1917	0.842	6.046	2.261	0.90	0.0992
13	15	6.0	0.2739	0.878	5.946	2.223	0.90	0.0572
13	16	6.0	0.3652	0.861	6.176	2.310	0.90	0.0800
13	17	6.0	0.4565	0.920	6.001	2.460	0.90	0.1150
14	7	4.0	0.0730	0.856	4.009	1.725	1.20	0.0755
14	8	4.0	0.0822	0.864	4.049	1.750	1.20	0.1019
14	9	4.0	0.1004	0.765	4.121	1.541	1.20	0.0602
14	10	4.0	0.1461	0.714	3.845	1.457	1.20	0.1200
14	11	4.0	0.2739	0.814	4.582	1.659	1.20	0.1500
14	12	4.0	0.3652	0.801	4.512	1.612	1.20	0.0741
14	13	4.0	0.4565	0.907	4.081	1.825	1.20	0.1166
14	14	6.0	0.0730	0.831	4.474	1.675	1.20	0.2041
14	15	6.0	0.0822	0.982	5.288	1.977	1.20	0.1504
14	16	6.0	0.1004	0.891	4.790	1.795	1.20	0.1509
14	17	6.0	0.1461	0.991	5.533	1.994	1.20	0.1850
14	18	6.0	0.2739	0.890	4.794	1.792	1.20	0.0705
14	19	6.0	0.3652	1.044	5.514	2.062	1.20	0.1630
14	20	8.5	0.0730	0.909	4.694	1.830	1.20	0.1760
14	21	8.5	0.0822	0.910	4.697	1.831	1.20	0.1500
14	22	8.5	0.1004	1.044	5.018	2.101	1.20	0.2255
14	23	8.5	0.1461	1.017	5.475	2.040	1.20	0.1180
14	27	11.0	0.0822	0.977	5.259	1.966	1.20	0.1161
14	28	11.0	0.1461	0.960	5.167	1.952	1.20	0.1144
14	29	11.0	0.3652	0.884	4.758	1.779	1.20	0.1165
14	30	11.0	0.4565	0.818	4.405	1.647	1.20	0.1050
15	2	3.0	0.0730	0.706	7.598	2.841	0.60	0.0755
15	3	3.0	0.0822	0.700	7.537	2.818	0.60	0.0675
15	4	3.0	0.1004	0.704	7.584	2.830	0.60	0.0024
15	5	3.0	0.1461	0.683	7.549	2.740	0.60	0.0010
15	6	3.0	0.2739	0.655	7.654	2.630	0.60	0.0775
15	7	3.0	0.3652	0.650	6.995	2.615	0.60	0.1059
15	8	3.0	0.5022	0.640	6.086	2.575	0.60	0.0757
15	9	6.0	0.0274	0.717	7.716	2.885	0.60	0.0645
15	10	6.0	0.0520	0.677	7.286	2.724	0.60	0.0027
15	11	6.0	0.0475	0.743	7.997	2.990	0.60	0.1150
15	12	6.0	0.0730	0.705	7.595	2.840	0.60	0.0797
15	13	6.0	0.1096	0.778	8.374	3.151	0.60	0.0795
15	14	6.0	0.1461	0.741	7.982	2.984	0.60	0.0024
15	15	6.0	0.1826	0.719	7.738	2.895	0.60	0.0746
15	16	6.0	0.2739	0.698	7.514	2.810	0.60	0.0704
15	17	8.0	0.0274	0.711	7.059	2.864	0.60	0.1169
15	18	8.0	0.0365	0.659	7.095	2.655	0.60	0.0772
15	19	8.0	0.0457	0.735	7.911	2.950	0.60	0.0780
15	20	8.0	0.0730	0.763	8.217	3.072	0.60	0.0504
15	21	8.0	0.1096	0.710	7.641	2.857	0.60	0.0720
15	22	8.0	0.1461	0.750	8.070	3.017	0.60	0.0767
15	23	8.0	0.2009	0.742	7.987	2.980	0.60	0.0825
15	26	8.0	0.2739	0.734	7.898	2.955	0.60	0.0065
15	25	11.0	0.0274	0.729	7.647	2.934	0.60	0.0245



contd. APPENDIX A.4.1

Run	No.	h	$u_d$	$d_{xt}$	DST	DSC	$d_b$	C.L.
15	26	11.0	0.0365	0.760	8.185	3.061	0.50	0.0340
15	27	11.0	0.0457	0.739	7.955	2.975	0.50	0.0721
15	28	11.0	0.0730	0.743	7.998	2.991	0.50	0.0774
15	29	11.0	0.1096	0.709	7.632	2.854	0.50	0.0620
15	32	11.0	0.2739	0.786	8.464	3.165	0.50	0.0936
16	2	2.0	0.0274	0.951	6.673	2.551	0.50	0.0376
16	3	2.0	0.0274	0.951	6.627	2.533	0.50	0.0479
16	4	2.0	0.0411	1.040	7.324	2.738	0.50	0.0607
16	5	2.0	0.0657	0.949	6.612	2.547	0.50	0.1266
16	5	2.0	0.1096	0.902	6.471	2.420	0.50	0.0633
16	6	2.0	0.1808	0.826	5.927	2.216	0.50	0.0697
16	7	2.0	0.2757	0.969	6.958	2.602	0.50	0.1293
16	8	2.0	0.2757	0.938	6.733	2.516	0.50	0.1376
16	9	4.0	0.0274	0.842	6.040	2.259	0.50	0.1420
16	10	4.0	0.0301	0.816	5.856	2.190	0.50	0.1457
16	11	4.0	0.0411	0.851	5.965	2.230	0.50	0.1016
16	12	4.0	0.0657	0.875	6.279	2.346	0.50	0.1333
16	13	4.0	0.1096	0.906	6.501	2.431	0.50	0.1401
16	14	4.0	0.1808	0.834	5.985	2.236	0.50	0.1002
16	15	4.0	0.2757	0.914	6.558	2.432	0.50	0.2010
16	16	6.0	0.0274	0.877	6.293	2.333	0.50	0.1361
16	17	6.0	0.0301	1.052	7.547	2.822	0.50	0.1216
16	18	6.0	0.0411	0.930	6.677	2.497	0.50	0.1006
16	17	6.0	0.0657	0.951	6.626	2.532	0.50	0.1433
16	20	6.0	0.1096	0.918	6.391	2.463	0.50	0.1053
16	21	6.0	0.1808	0.926	7.149	2.673	0.50	0.1467
16	22	6.0	0.2757	0.927	6.651	2.487	0.50	0.1064
16	23	8.0	0.0274	0.850	6.103	2.282	0.50	0.1467
16	24	8.0	0.0301	0.789	5.089	1.903	0.50	0.0717
16	25	8.0	0.0411	0.745	5.346	1.999	0.50	0.0337
16	25	8.0	0.0657	0.802	5.757	2.153	0.50	0.1092
16	26	8.0	0.1096	0.813	5.636	2.182	0.50	0.1030
16	27	8.0	0.1808	0.916	6.374	2.436	0.50	0.1764
16	28	8.0	0.2757	0.929	6.666	2.493	0.50	0.1262
16	29	8.0	0.4492	0.933	6.700	2.503	0.50	0.1377
16	30	8.0	0.0000	0.861	6.179	2.311	0.50	0.1053
16	31	8.0	0.0000	0.772	5.339	2.071	0.50	0.1386
16	32	8.0	0.0000	0.926	7.148	2.673	0.50	0.2066
16	33	8.0	0.0000	0.824	6.419	2.406	0.50	0.1333
16	34	8.0	0.0000	0.826	6.433	2.406	0.50	0.1263
17	3	1.5	0.0301	0.332	1.893	0.706	1.20	0.0694
17	4	1.5	0.0411	0.567	3.138	1.181	1.20	0.2374
17	5	1.5	0.0657	0.663	3.367	1.334	1.20	0.2214
17	6	1.5	0.1077	0.706	3.603	1.422	1.20	0.2627
17	7	1.5	0.1808	0.679	3.656	1.366	1.20	0.1963
17	8	1.5	0.2757	0.655	3.689	1.379	1.20	0.1836
17	9	1.5	0.4657	0.911	4.904	1.834	1.20	0.1883
17	10	1.5	0.0000	0.979	5.271	1.971	1.20	0.2033
17	11	3.0	0.0256	0.936	5.147	1.924	1.20	0.2066
17	12	3.0	0.0301	0.903	4.860	1.817	1.20	0.1610
17	13	3.0	0.0411	0.900	4.848	1.813	1.20	0.1734
17	14	3.0	0.0657	0.964	5.190	1.941	1.20	0.1613
17	15	3.0	0.1077	0.865	4.657	1.741	1.20	0.1040
17	16	3.0	0.1808	1.014	5.460	2.042	1.20	0.2119
17	17	3.0	0.2757	0.971	5.226	1.934	1.20	0.1436
17	18	3.0	0.4657	0.931	5.009	1.873	1.20	0.1117
17	19	3.0	0.0000	1.001	5.389	2.013	1.20	0.1284
17	20	3.0	0.0256	0.972	5.231	1.956	1.20	0.1761
17	21	3.0	0.0301	0.939	5.056	1.890	1.20	0.1142



contd. APPENDIX A.4.1

Run	No.	h	$u_d$	$d_{xt}$	DST	DSC	$d_b$	C.L.
17	23	5.0	0.0657	1.009	5.429	2.030	1.20	0.1432
17	24	5.0	0.1077	0.955	5.141	1.922	1.20	0.1432
17	25	5.0	0.1308	0.977	5.261	1.967	1.20	0.2013
17	26	5.0	0.2757	1.039	5.594	2.072	1.20	0.2082
17	27	5.0	0.4657	0.934	5.026	1.879	1.20	0.1770
17	28	5.0	0.0000	1.109	5.900	2.232	1.20	0.1717
17	29	10.0	0.0256	0.931	5.012	1.874	1.20	0.0060
17	30	10.0	0.0301	0.878	4.728	1.750	1.20	0.1074
17	31	10.0	0.0411	0.920	4.955	1.855	1.20	0.1111
17	32	10.0	0.0657	0.880	4.757	1.771	1.20	0.0887
17	33	10.0	0.1077	0.986	5.300	1.984	1.20	0.1370
17	34	10.0	0.1308	0.916	4.930	1.845	1.20	0.1332
17	35	10.0	0.2757	0.928	4.997	1.860	1.20	0.1241
18	1	2.0	0.0301	0.616	3.315	1.240	1.20	0.1212
18	2	2.0	0.0411	0.656	3.334	1.321	1.20	0.2384
18	3	2.0	0.0657	0.575	3.095	1.157	1.20	0.1330
18	4	2.0	0.2757	0.950	5.114	1.912	1.20	0.2280
18	5	4.0	0.0256	0.748	8.056	3.012	0.60	0.1267
18	6	4.0	0.0301	0.809	8.712	3.258	0.60	0.1380
18	7	4.0	0.0411	0.729	7.849	2.935	0.60	0.1120
18	8	4.0	0.0657	0.665	7.379	2.759	0.60	0.0895
18	9	4.0	0.1077	0.658	7.085	2.649	0.60	0.0837
18	10	4.0	0.1780	0.701	7.548	2.822	0.60	0.0593
18	11	4.0	0.2757	0.694	7.475	2.795	0.60	0.0613
18	12	4.0	0.0000	0.772	8.514	3.109	0.60	0.0751
18	13	6.0	0.0301	0.651	6.799	2.542	0.60	0.0794
18	14	6.0	0.0411	0.650	6.780	2.557	0.60	0.1125
18	15	6.0	0.1370	0.620	6.076	2.490	0.60	0.1090
18	16	6.0	0.1077	0.642	6.910	2.587	0.60	0.0703
18	25	8.0	0.2757	0.693	7.460	2.789	0.60	0.0774
18	26	8.0	0.0000	0.657	7.078	2.647	0.60	0.1010
18	27	12.0	0.0301	0.619	6.662	2.491	0.60	0.0544
18	28	12.0	0.0411	0.696	7.498	2.805	0.60	0.1302
18	29	12.0	0.0657	0.669	7.201	2.693	0.60	0.0570
18	30	12.0	0.1077	0.595	6.407	2.395	0.60	0.0735
18	31	12.0	0.1308	0.668	7.194	2.690	0.60	0.0750
18	32	12.0	0.2757	0.731	7.867	2.942	0.60	0.0932
18	33	12.0	-0.0000	0.609	7.421	2.775	0.60	0.0524
19	1	4.0	0.0256	0.880	6.518	2.362	0.90	0.0815
19	2	4.0	0.0329	0.954	6.846	2.560	0.90	0.0882
19	3	4.0	0.0411	0.897	6.435	2.406	0.90	0.1340
19	4	4.0	0.0657	0.861	6.177	2.310	0.90	0.0662
19	5	4.0	0.1096	0.887	6.365	2.380	0.90	0.0740
19	6	4.0	0.1826	0.454	3.257	1.218	0.90	0.1121
19	7	4.0	0.2785	0.934	6.705	2.507	0.90	0.1405
19	8	4.0	0.4565	0.916	6.578	2.460	0.90	0.1459
19	9	4.0	0.0000	0.848	6.089	2.277	0.90	0.0999
19	10	4.0	0.0000	0.838	6.012	2.246	0.90	0.0909
19	11	6.0	0.0256	1.025	7.360	2.752	0.90	0.2014
19	12	6.0	0.0329	0.922	6.619	2.475	0.90	0.1235
19	13	6.0	0.0411	0.970	6.962	2.605	0.90	0.1955
19	14	6.0	0.0657	0.932	6.691	2.502	0.90	0.1754
19	15	6.0	0.1096	0.933	6.695	2.505	0.90	0.1415
19	16	6.0	0.1826	0.942	6.764	2.529	0.90	0.2449
19	17	6.0	0.2785	1.006	7.219	2.699	0.90	0.1315
20	1	10.0	0.0256	0.830	5.958	2.228	0.90	0.0750
20	2	10.0	0.0329	0.949	6.610	2.540	0.90	0.1250
20	3	10.0	0.0411	0.876	6.289	2.352	0.90	0.0822
20	4	10.0	0.0657	0.859	6.163	2.304	0.90	0.1284



contd. APPENDIX A.4.1

Run	No.	h	$u_d$	$d_{xt}$	DST	DSC	$d_b$	C.L.
20	5	10.0	0.1096	0.905	6.497	2.429	0.90	0.1510
20	6	10.0	0.1826	0.947	6.798	2.542	0.90	0.1136
20	7	10.0	0.2739	0.902	6.474	2.421	0.90	0.1725
20	8	10.0	0.4565	0.904	6.491	2.427	0.90	0.1521
20	9	3.0	0.0247	0.969	5.215	1.950	1.20	0.1194
20	10	3.0	0.0329	0.912	4.911	1.850	1.20	0.2285
20	11	3.0	0.0411	0.918	4.939	1.847	1.20	0.1589
20	12	3.0	0.0657	0.954	5.135	1.920	1.20	0.2501
20	13	3.0	0.1096	1.003	5.400	2.019	1.20	0.2029
20	14	3.0	0.1826	1.073	5.776	2.160	1.20	0.1075
20	15	3.0	0.2739	0.871	4.689	1.755	1.20	0.1545
20	16	3.0	0.0000	0.889	4.787	1.790	1.20	0.1260
20	17	5.0	0.0256	0.855	4.602	1.721	1.20	0.1544
20	18	5.0	0.0329	0.965	5.197	1.945	1.20	0.1507
20	19	5.0	0.0411	0.943	5.074	1.897	1.20	0.1509
20	20	5.0	0.0657	0.876	4.715	1.765	1.20	0.1207
20	21	5.0	0.1096	0.954	5.137	1.921	1.20	0.1505
20	22	5.0	0.1826	0.901	4.850	1.814	1.20	0.1750
20	23	5.0	0.2739	0.945	5.087	1.902	1.20	0.1140
20	24	5.0	0.0000	0.888	4.781	1.780	1.20	0.1662
20	25	9.0	0.0256	0.776	4.180	1.565	1.20	0.0767
20	26	9.0	0.0329	0.921	4.958	1.854	1.20	0.0951
20	27	9.0	0.0411	0.962	5.178	1.956	1.20	0.1492
20	29	9.0	0.0657	0.925	4.981	1.862	1.20	0.1712
21	1	3.0	0.0256	1.173	12.025	4.721	0.50	0.2080
21	2	3.0	0.0329	1.051	11.096	4.149	0.50	0.2525
21	3	3.0	0.0329	1.024	11.028	4.124	0.50	0.2225
21	4	3.0	0.0411	0.974	10.484	3.920	0.50	0.2401
21	5	3.0	0.0657	0.977	10.521	3.934	0.50	0.1555
21	6	3.0	0.1096	1.047	11.271	4.214	0.50	0.1950
21	7	3.0	0.1826	0.973	10.477	3.916	0.50	0.1220
21	8	3.0	0.2739	0.904	9.735	3.640	0.50	0.1411
21	9	3.0	0.0000	1.054	11.549	4.244	0.50	0.2035
21	10	5.0	0.0256	0.595	6.411	2.397	0.50	0.0618
21	11	5.0	0.0274	0.519	5.592	2.091	0.50	0.0539
21	12	5.0	0.0411	0.567	6.109	2.284	0.50	0.0944
21	13	5.0	0.0657	0.680	7.320	2.737	0.50	0.1107
21	14	5.0	0.1096	0.751	8.082	3.022	0.50	0.0979
21	15	5.0	0.1826	0.743	7.996	2.990	0.50	0.1022
21	16	5.0	0.2739	0.824	8.868	3.316	0.50	0.1522
21	17	5.0	0.0000	0.638	6.071	2.569	0.50	0.1507
21	18	8.0	0.0256	0.753	8.109	3.052	0.50	0.1427
21	19	8.0	0.0329	0.760	8.184	3.060	0.50	0.1197
21	20	8.0	0.0411	0.668	7.189	2.680	0.50	0.0659
21	21	8.0	0.0657	0.677	7.292	2.720	0.50	0.1050
21	22	8.0	0.1096	0.763	8.215	3.072	0.50	0.1257
21	23	8.0	0.1826	0.670	7.216	2.690	0.50	0.0679
21	24	8.0	0.0000	0.824	8.868	3.310	0.50	0.1400
21	25	11.0	0.0256	0.774	8.539	3.110	0.50	0.0912
21	26	11.0	0.0329	0.668	7.197	2.691	0.50	0.1142
21	27	11.0	0.0411	0.688	7.408	2.770	0.50	0.0629
21	28	11.0	0.0657	0.752	7.881	2.947	0.50	0.0695
21	29	11.0	0.1096	0.735	7.910	2.950	0.50	0.0755
21	30	11.0	0.1826	0.698	7.512	2.809	0.50	0.0869
21	31	11.0	0.2739	0.689	7.419	2.774	0.50	0.0878
21	32	11.0	0.0000	0.751	7.869	2.942	0.50	0.0700
22	1	2.0	0.0256	0.903	6.478	2.422	0.90	0.1170
22	2	2.0	0.0329	0.915	6.564	2.454	0.90	0.1274
22	3	2.0	0.0411	0.939	6.739	2.520	0.90	0.1290
22	4	2.0	0.0657	1.073	7.705	2.881	0.90	0.1000



contd. APPENDIX A.4.1

Run	No.	h	$u_d$	$d_{xt}$	DST	DSC	$d_b$	C.L.
22	5	2.0	0.1096	0.990	7.108	2.658	0.90	0.1073
22	0	4.0	0.0329	0.993	7.127	2.665	0.90	0.1174
22	11	4.0	0.0411	0.981	7.043	2.634	0.90	0.1477
22	12	4.0	0.0639	0.807	5.791	2.165	0.90	0.1798
22	13	4.0	0.1096	1.011	7.256	2.715	0.90	0.1427
22	14	4.0	0.1826	0.997	7.154	2.675	0.90	0.1145
22	15	4.0	0.2739	0.923	6.023	2.470	0.90	0.1404
22	16	4.0	0.0000	0.934	6.701	2.505	0.90	0.1555
22	17	6.0	0.0256	0.836	5.999	2.245	0.90	0.1115
22	18	6.0	0.0329	0.844	6.055	2.264	0.90	0.1267
22	19	6.0	0.0411	0.968	6.947	2.596	0.90	0.1571
22	20	6.0	0.0657	0.975	6.996	2.610	0.90	0.1501
22	21	6.0	0.1096	0.998	7.163	2.670	0.90	0.1590
22	22	6.0	0.1826	0.968	6.946	2.597	0.90	0.1592
22	23	6.0	0.2739	0.813	5.833	2.181	0.90	0.1285
22	25	10.0	0.0256	0.841	6.037	2.257	0.90	0.1442
22	26	10.0	0.0292	0.867	6.223	2.327	0.90	0.0917
22	27	10.0	0.0411	1.000	7.179	2.684	0.90	0.2540
22	28	10.0	0.0657	0.870	6.241	2.334	0.90	0.1955
22	29	10.0	0.1096	0.890	6.391	2.390	0.90	0.2040
22	30	10.0	0.1826	0.973	6.987	2.613	0.90	0.2180
22	31	10.0	0.2739	1.049	7.532	2.816	0.90	0.2660
22	32	10.0	0.0000	0.958	6.077	2.571	0.90	0.2167
23	1	3.0	0.0256	0.938	10.094	3.774	0.60	0.2598
23	2	3.0	0.0329	1.074	11.560	4.322	0.60	0.2194
23	3	3.0	0.0411	1.007	10.846	4.055	0.60	0.2489
23	4	3.0	0.0657	0.990	10.656	3.964	0.60	0.2536
23	5	3.0	0.1096	1.138	12.254	4.582	0.60	0.1607
23	6	3.0	0.1826	0.984	10.599	3.963	0.60	0.1594
23	7	3.0	0.2739	1.004	10.815	4.044	0.60	0.1534
23	8	3.0	0.0000	0.941	10.135	3.790	0.60	0.0767
23	9	5.0	0.0256	0.747	8.045	3.008	0.60	0.1045
23	10	5.0	0.0329	0.783	8.429	3.152	0.60	0.0666
23	11	5.0	0.0411	0.711	7.652	2.861	0.60	0.0452
23	12	5.0	0.0657	0.705	7.588	2.837	0.60	0.0767
23	13	5.0	0.1096	0.807	8.689	3.249	0.60	0.1281
23	14	5.0	0.1826	0.761	8.197	3.065	0.60	0.1501
23	15	5.0	0.2739	0.772	8.315	3.109	0.60	0.1252
23	16	5.0	0.0000	0.614	6.608	2.471	0.60	0.0709
23	17	5.0	0.0000	0.682	7.345	2.746	0.60	0.0961
23	18	9.0	0.0256	0.757	8.148	3.047	0.60	0.1277
23	19	9.0	0.0329	0.796	8.566	3.205	0.60	0.1284
23	20	9.0	0.0411	0.765	8.236	3.079	0.60	0.1175
23	21	9.0	0.0657	0.708	7.623	2.850	0.60	0.1025
23	22	9.0	0.1096	0.644	6.939	2.595	0.60	0.1161
23	23	9.0	0.1826	0.740	7.970	2.980	0.60	0.1025
23	24	9.0	0.2739	0.701	7.544	2.821	0.60	0.1251
23	25	9.0	0.0000	0.750	7.861	2.939	0.60	0.0911
23	26	9.0	0.0000	0.765	8.236	3.079	0.60	0.0896
23	26	9.0	0.0000	0.744	8.008	2.994	0.60	0.0991
23	27	11.0	0.0256	0.693	7.457	2.786	0.60	0.1070
23	28	11.0	0.0329	0.660	7.109	2.650	0.60	0.0677
23	29	11.0	0.0411	0.824	8.874	3.316	0.60	0.1016
23	30	11.0	0.0657	0.762	8.208	3.069	0.60	0.0604
23	31	11.0	0.1096	0.727	7.830	2.928	0.60	0.1136
23	32	11.0	0.1826	0.730	7.864	2.940	0.60	0.0880
23	33	11.0	0.2739	0.670	7.213	2.697	0.60	0.0867
23	34	11.0	0.0000	0.679	7.516	2.755	0.60	0.0421
23	35	11.0	0.0000	0.704	8.221	3.074	0.60	0.0769
24	1	4.0	0.0256	0.964	5.192	1.941	1.20	0.1794



contd. APPENDIX A.4.1

Run	No.	h	$u_d$	$d_{xt}$	DST	DSC	$d_b$	C.L.
24	2	4.0	0.0329	0.899	4.637	1.809	1.20	0.1465
24	3	4.0	0.0411	0.868	4.673	1.747	1.20	0.1657
24	4	4.0	0.0657	1.014	5.459	2.041	1.20	0.2744
24	5	4.0	0.1096	0.889	4.787	1.790	1.20	0.1402
24	6	4.0	0.1826	0.947	5.097	1.906	1.20	0.1544
24	7	4.0	0.2739	0.946	5.095	1.905	1.20	0.2044
24	8	4.0	0.0000	1.044	5.621	2.102	1.20	0.1879
24	9	7.0	0.0256	0.840	4.523	1.691	1.20	0.1135
24	10	7.0	0.0329	0.870	4.685	1.752	1.20	0.0717
24	11	7.0	0.0411	0.815	4.389	1.641	1.20	0.1259
24	12	7.0	0.0657	1.022	5.501	2.057	1.20	0.2679
24	13	7.0	0.1096	1.063	5.723	2.140	1.20	0.1969
24	14	7.0	0.1826	0.950	5.112	1.912	1.20	0.1075
24	15	7.0	0.2739	1.000	5.583	2.015	1.20	0.1601
24	16	7.0	0.0000	0.847	4.559	1.705	1.20	0.1615
24	17	10.0	0.0256	1.076	5.791	2.165	1.20	0.2744
24	18	10.0	0.0329	1.062	5.717	2.156	1.20	0.2041
24	19	10.0	0.0411	1.045	5.623	2.102	1.20	0.1866
24	20	10.0	0.0657	0.996	5.560	2.004	1.20	0.1815
24	21	10.0	0.1096	1.044	5.619	2.101	1.20	0.1081
24	22	10.0	0.1826	0.968	5.211	1.948	1.20	0.1535
24	23	10.0	0.2739	1.058	5.697	2.150	1.20	0.1850
24	24	10.0	0.0000	1.088	5.660	2.191	1.20	0.1258
24	25	10.0	0.0000	0.985	5.503	1.985	1.20	0.2465
24	26	10.0	0.0000	1.178	6.541	2.371	1.20	0.2057



APPENDIX A.4.2

Data Obtained from 9" Diameter Column  
with dispersed phase flow only

Ref	h	$u_d$	$d_{xt}$	DVC	DVT	$d_b$
2FR1	2.0	0.0100	0.110	0.221	0.592	1.20
3FR1	5.0	0.0100	0.110	0.221	0.592	1.20
3F11	5.0	0.0530	0.110	0.221	0.592	1.20
4FR1	7.5	0.0100	0.110	0.221	0.592	1.20
4F10	7.5	0.0260	0.110	0.221	0.592	1.20
4F11	7.5	0.0530	0.110	0.221	0.592	1.20
6F10	4.0	0.0530	0.150	0.403	1.077	0.90
7FR3	8.0	0.0100	0.320	0.859	2.297	0.90
7F17	8.0	0.0260	0.338	0.907	2.426	0.90
7F20	8.0	0.0530	0.358	0.961	2.570	0.90
8FR3	11.0	0.0100	0.340	0.913	2.440	0.90
8F15	11.0	0.0260	0.390	1.047	2.799	0.90
8F27	11.0	0.0530	0.550	1.476	3.948	0.90
9FR1	13.0	0.0100	0.562	1.508	4.034	0.90
9F14	13.0	0.0260	0.538	1.444	3.862	0.90
9F22	13.0	0.0530	0.580	1.557	4.163	0.90
10F3	7.0	0.0100	0.622	2.504	6.697	0.60
0F25	7.0	0.0530	0.603	2.428	6.492	0.60
0F15	7.0	0.0260	0.615	2.476	6.621	0.60
1FR4	11.0	0.0100	0.550	2.214	5.922	0.60
1F20	11.0	0.0260	0.590	2.375	6.352	0.60
1F28	11.0	0.0530	0.630	2.536	6.783	0.60
2FR3	12.5	0.0100	0.540	2.174	5.814	0.60
2F15	12.5	0.0260	0.550	2.214	5.922	0.60
2F19	2.0	0.0530	0.110	0.221	0.592	1.20
3FR1	4.0	0.0100	0.100	0.201	0.538	1.20
3FR6	4.0	0.0260	0.100	0.201	0.538	1.20
3F10	4.0	0.0530	0.100	0.201	0.538	1.20
4FR1	8.0	0.0100	0.110	0.221	0.592	1.20
4FR6	8.0	0.0260	0.110	0.221	0.592	1.20
4F10	8.0	0.0530	0.110	0.221	0.592	1.20
5FR1	12.0	0.0100	0.120	0.242	0.646	1.20
5FR6	12.0	0.0260	0.120	0.242	0.646	1.20
5F11	12.0	0.0530	0.120	0.242	0.646	1.20
5FR1	12.0	0.0100	0.110	0.221	0.592	1.20
5F10	12.0	0.0260	0.130	0.262	0.700	1.20
5F11	12.0	0.0530	0.150	0.302	0.807	1.20
6FR1	4.0	0.0100	0.140	0.376	1.005	0.90
7FR1	5.0	0.0100	0.012	0.032	0.086	0.90
7FR6	5.0	0.0260	0.012	0.032	0.086	0.90
7F11	5.0	0.0530	0.012	0.032	0.086	0.90
8FR1	8.0	0.0100	0.012	0.032	0.086	0.90
8FR6	8.0	0.0260	0.013	0.035	0.093	0.90
8F11	8.0	0.0530	0.015	0.040	0.108	0.90
9FR1	11.0	0.0100	0.141	0.378	1.012	0.90

Toluene

M.I.B.K.



contd. APPENDIX A.4.2

Ref	h	$u_d$	$d_{xt}$	DVC	DVT	$d_b$
9FR6	11.0	0.0260	0.161	0.432	1.156	0.90
9F11	11.0	0.0530	0.171	0.459	1.227	0.90
0FR1	13.0	0.0100	0.161	0.432	1.156	0.90
0FR7	13.0	0.0260	0.161	0.432	1.156	0.90
0F14	13.0	0.0530	0.181	0.486	1.299	0.90
1FR2	7.0	0.0100	0.201	0.809	2.164	0.60
1FR8	7.0	0.0260	0.251	1.010	2.702	0.60
1F14	7.0	0.0530	0.310	1.248	3.338	0.60
2FR1	10.0	0.0100	0.251	1.010	2.702	0.60
2FR7	10.0	0.0260	0.351	1.413	3.779	0.60
2F13	10.0	0.0530	0.401	1.614	4.317	0.60
3FR1	14.0	0.0100	0.301	1.212	3.241	0.60
3FR7	14.0	0.0260	0.401	1.614	4.317	0.60
3F13	14.0	0.0530	0.351	1.413	3.779	0.60
4FR1	3.5	0.0100	0.100	0.201	0.538	1.20
4FR6	3.5	0.0260	0.120	0.242	0.646	1.20
4F12	3.5	0.0360	0.110	0.221	0.592	1.20
4F17	3.5	0.0450	0.110	0.221	0.592	1.20
4F22	3.5	0.0530	0.130	0.262	0.700	1.20
5FR1	7.5	0.0100	0.110	0.221	0.592	1.20
5FR7	7.5	0.0260	0.120	0.242	0.646	1.20
5F13	7.5	0.0530	0.120	0.242	0.646	1.20
6FR1	12.0	0.0100	0.100	0.201	0.538	1.20
6FR6	12.0	0.0260	0.110	0.221	0.592	1.20
6F11	12.0	0.0530	0.120	0.242	0.646	1.20
7FR1	7.0	0.0100	0.200	0.537	1.436	0.90
7FR7	7.0	0.0260	0.170	0.456	1.220	0.90
7F13	7.0	0.0530	0.170	0.456	1.220	0.90
8FR1	11.5	0.0100	0.200	0.537	1.436	0.90
8FR7	11.5	0.0260	0.170	0.456	1.220	0.90
8F13	11.5	0.0530	0.170	0.456	1.220	0.90
9FR1	12.5	0.0100	0.220	0.590	1.579	0.90
9FR7	12.5	0.0260	0.190	0.510	1.364	0.90
0FR3	6.0	0.0100	0.390	1.570	4.199	0.60
0FR8	6.0	0.0160	0.460	1.852	4.953	0.60
0F15	6.0	0.0260	0.480	1.932	5.168	0.60
0F22	6.0	0.0360	0.481	1.936	5.179	0.60
1FR2	10.0	0.0100	0.398	1.602	4.285	0.60
1FR7	10.0	0.0160	0.430	1.731	4.630	0.60
1F12	10.0	0.0260	0.463	1.864	4.985	0.60
1F18	10.0	0.0360	0.493	1.985	5.308	0.60
2FR1	14.0	0.0100	0.457	1.840	4.920	0.60
2FR6	14.0	0.0160	0.598	2.407	6.438	0.60
2F11	14.0	0.0260	0.477	1.920	5.136	0.60
2F16	14.0	0.0360	0.481	1.936	5.179	0.60
2F21	14.0	0.0440	0.437	1.759	4.705	0.60
2F26	14.0	0.0530	0.469	1.888	5.050	0.60

M.I.B.K.

Iso - Octane



APPENDIX A.4.3 Data Obtained From 9" Diam. Column  
 Operating Under Counter - Current Flow  
 Toluene - Water

Ref	h	$u_d$	$d_{xt}$	DVC	DVT	$d_b$	$u_c$
7R19	8.0	0.0260	0.206	0.553	1.479	0.90	0.0220
7R20	8.0	0.0260	0.202	0.542	1.450	0.90	0.0220
7R29	8.0	0.0530	0.242	0.649	1.737	0.90	0.0050
7R30	8.0	0.0530	0.298	0.800	2.139	0.90	0.0050
7R31	8.0	0.0530	0.352	0.945	2.527	0.90	0.0115
7R32	8.0	0.0530	0.326	0.875	2.340	0.90	0.0115
7R33	8.0	0.0530	0.276	0.741	1.981	0.90	0.0220
7R34	8.0	0.0530	0.358	0.961	2.570	0.90	0.0220
7R35	8.0	0.0530	0.541	1.452	3.883	0.90	0.1200
7R36	8.0	0.0530	0.371	0.996	2.663	0.90	0.1200
7R37	8.0	0.0750	0.509	1.366	3.653	0.90	0.0000
8RR5	11.0	0.0100	0.352	0.945	2.527	0.90	0.0050
8RR7	11.0	0.0100	0.662	1.777	4.752	0.90	0.0115
8RR8	11.0	0.0100	0.645	1.731	4.630	0.90	0.0115
8RR9	11.0	0.0100	0.626	1.680	4.493	0.90	0.0220
8R10	11.0	0.0100	0.166	0.446	1.192	0.90	0.0220
8R11	11.0	0.0100	0.645	1.731	4.630	0.90	0.0000
8R12	11.0	0.0100	0.371	0.996	2.663	0.90	0.0000
8R20	11.0	0.0260	0.393	1.055	2.821	0.90	0.0220
8R22	11.0	0.0260	0.706	1.895	5.067	0.90	0.0000
8R23	11.0	0.0530	0.301	0.808	2.160	0.90	0.0000
8R24	11.0	0.0530	0.377	1.012	2.706	0.90	0.0000
8R25	11.0	0.0530	0.550	1.476	3.948	0.90	0.0050
8R26	11.0	0.0530	0.495	1.329	3.553	0.90	0.0050
8R27	11.0	0.0530	0.616	1.653	4.421	0.90	0.0115
8R28	11.0	0.0530	0.562	1.508	4.034	0.90	0.0115
8R29	11.0	0.0530	0.640	1.718	4.594	0.90	0.0220
8R30	11.0	0.0530	0.593	1.592	4.256	0.90	0.0220
8R31	11.0	0.0530	0.504	1.353	3.618	0.90	0.0000
8R32	11.0	0.0530	0.586	1.573	4.206	0.90	0.0000
8R33	11.0	0.0530	0.581	1.559	4.170	0.90	0.0000
8R34	11.0	0.0530	0.520	1.396	3.732	0.90	0.0000
9RR2	14.0	0.0100	0.477	1.280	3.424	0.90	0.0000
9RR4	14.0	0.0100	0.465	1.248	3.338	0.90	0.0050
9RR5	14.0	0.0100	0.627	1.683	4.500	0.90	0.0115
9RR6	14.0	0.0100	0.713	1.914	5.118	0.90	0.0115
9RR7	14.0	0.0100	0.641	1.720	4.601	0.90	0.0220
9RR8	14.0	0.0100	0.509	1.366	3.653	0.90	0.0220
9RR9	14.0	0.0100	0.578	1.551	4.149	0.90	0.0000
9R10	14.0	0.0100	0.681	1.828	4.888	0.90	0.0000
9R11	14.0	0.0260	0.709	1.903	5.089	0.90	0.0000
9R12	14.0	0.0260	0.651	1.747	4.673	0.90	0.0000
9R13	14.0	0.0260	0.692	1.857	4.967	0.90	0.0050
9R14	14.0	0.0260	0.538	1.444	3.862	0.90	0.0050
9R15	14.0	0.0260	0.707	1.897	5.075	0.90	0.0115
9R17	14.0	0.0260	0.618	1.659	4.436	0.90	0.0220
9R18	14.0	0.0260	0.576	1.546	4.134	0.90	0.0220
9R19	14.0	0.0260	0.633	1.699	4.543	0.90	0.0000
9R20	14.0	0.0260	0.687	1.844	4.931	0.90	0.0000
9R21	14.0	0.0530	0.710	1.906	5.096	0.90	0.0000
9R22	14.0	0.0530	0.532	1.428	3.819	0.90	0.0000
9R23	14.0	0.0530	0.657	1.763	4.716	0.90	0.0050
9R24	14.0	0.0530	0.583	1.565	4.185	0.90	0.0050
9R27	14.0	0.0530	0.581	1.559	4.170	0.90	0.0220
9R28	14.0	0.0530	0.672	1.804	4.823	0.90	0.0220
9R31	14.0	0.0530	0.640	1.718	4.594	0.90	0.0000
0RR3	7.0	0.0100	0.647	2.605	6.966	0.60	0.0000
0RR4	7.0	0.0100	0.630	2.536	6.783	0.60	0.0000
0RR5	7.0	0.0100	0.633	2.548	6.815	0.60	0.0050
0RR6	7.0	0.0100	0.593	2.387	6.385	0.60	0.0050



Ref	h	$u_d$	$d_{xt}$	DVC	DVT	$d_b$	$u_c$
0RR8	7.0	0.0100	0.476	1.916	5.125	0.60	0.0115
0RR9	7.0	0.0100	0.619	2.492	6.665	0.60	0.0220
0R10	7.0	0.0100	0.682	2.746	7.343	0.60	0.0220
0R11	7.0	0.0100	0.606	2.440	6.525	0.60	0.0000
0R12	7.0	0.0100	0.637	2.564	6.858	0.60	0.0000
0R13	7.0	0.0260	0.648	2.609	6.977	0.60	0.0000
0R14	7.0	0.0260	0.613	2.468	6.600	0.60	0.0000
0R15	7.0	0.0260	0.663	2.669	7.138	0.60	0.0050
0R17	7.0	0.0260	0.709	2.854	7.634	0.60	0.0115
0R18	7.0	0.0260	0.679	2.733	7.311	0.60	0.0115
0R19	7.0	0.0260	0.631	2.540	6.794	0.60	0.0220
0R20	7.0	0.0260	0.674	2.713	7.257	0.60	0.0220
0R21	7.0	0.0260	0.695	2.798	7.483	0.60	0.0000
0R22	7.0	0.0260	0.747	3.007	8.043	0.60	0.0000
0R23	7.0	0.0530	0.630	2.536	6.783	0.60	0.0000
0R24	7.0	0.0530	0.664	2.673	7.149	0.60	0.0000
0R25	7.0	0.0530	0.602	2.424	6.481	0.60	0.0050
0R26	7.0	0.0530	0.621	2.500	6.686	0.60	0.0050
0R27	7.0	0.0530	0.671	2.701	7.224	0.60	0.0115
0R28	7.0	0.0530	0.631	2.540	6.794	0.60	0.0115
0R29	7.0	0.0530	0.660	2.657	7.106	0.60	0.0220
0R30	7.0	0.0530	0.626	2.520	6.740	0.60	0.0220
0R31	7.0	0.0530	0.661	2.661	7.117	0.60	0.0000
0R32	7.0	0.0530	0.664	2.673	7.149	0.60	0.0000
1RR4	11.0	0.0100	0.680	2.738	7.321	0.60	0.0000
1RR5	11.0	0.0100	0.672	2.705	7.235	0.60	0.0000
1RR6	11.0	0.0100	0.613	2.468	6.600	0.60	0.0050
1RR7	11.0	0.0100	0.639	2.572	6.880	0.60	0.0050
1RR8	11.0	0.0100	0.611	2.460	6.578	0.60	0.0115
1RR9	11.0	0.0100	0.691	2.782	7.440	0.60	0.0115
1R10	11.0	0.0100	0.619	2.492	6.665	0.60	0.0220
1R11	11.0	0.0100	0.682	2.746	7.343	0.60	0.0220
1R12	11.0	0.0100	0.601	2.419	6.471	0.60	0.0500
1R14	11.0	0.0100	0.719	2.895	7.741	0.60	0.0100
1R15	11.0	0.0100	0.642	2.585	6.912	0.60	0.0120
1R17	11.0	0.0180	0.568	2.287	6.115	0.60	0.0000
1R18	11.0	0.0260	0.608	2.448	6.546	0.60	0.0000
1R19	11.0	0.0260	0.571	2.299	6.148	0.60	0.0000
1R20	11.0	0.0260	0.586	2.359	6.309	0.60	0.0050
1R21	11.0	0.0260	0.613	2.468	6.600	0.60	0.0050
1R22	11.0	0.0260	0.439	1.767	4.727	0.60	0.0075
1R24	11.0	0.0260	0.666	2.681	7.171	0.60	0.0115
1R25	11.0	0.0260	0.669	2.693	7.203	0.60	0.0220
1R28	11.0	0.0530	0.600	2.415	6.460	0.60	0.0000
1R29	11.0	0.0530	0.635	2.556	6.837	0.60	0.0000
1R30	11.0	0.0530	0.617	2.484	6.643	0.60	0.0050
1R31	11.0	0.0530	0.638	2.568	6.869	0.60	0.0050
1R32	11.0	0.0530	0.661	2.661	7.117	0.60	0.0115
1R34	11.0	0.0530	0.661	2.661	7.117	0.60	0.0220
2RR4	12.5	0.0100	0.540	2.174	5.814	0.60	0.0000
2RR5	12.5	0.0100	0.580	2.335	6.245	0.60	0.0000
2RR6	12.5	0.0100	0.670	2.697	7.214	0.60	0.0050
2RR7	12.5	0.0100	0.665	2.677	7.160	0.60	0.0050
2RR8	12.5	0.0100	0.620	2.496	6.675	0.60	0.0115
2RR9	12.5	0.0100	0.584	2.351	6.288	0.60	0.0115
2R10	12.5	0.0100	0.616	2.480	6.632	0.60	0.0220
2R12	12.5	0.0100	0.739	2.975	7.957	0.60	0.0000
2R13	12.5	0.0100	0.770	3.100	8.290	0.60	0.0000
2R14	12.5	0.0260	0.563	2.267	6.062	0.60	0.0000
2R15	12.5	0.0260	0.547	2.202	5.889	0.60	0.0000
2R17	12.5	0.0260	0.568	2.287	6.115	0.60	0.0050



contd. APPENDIX A.4.3

Ref	Iso-Octane - Water						
	h	$u_d$	$d_{xt}$	DVC	DVT	$d_b$	$u_c$
0FR3	6.0	0.0100	0.387	1.558	4.167	0.60	0.0050
0FR4	6.0	0.0100	0.392	1.578	4.220	0.60	0.0115
0FR7	6.0	0.0100	0.491	1.977	5.286	0.60	0.0000
0FR9	6.0	0.0160	0.504	2.029	5.426	0.60	0.0050
0R10	6.0	0.0160	0.424	1.707	4.565	0.60	0.0115
0R12	6.0	0.0160	0.428	1.723	4.608	0.60	0.0220
0R13	6.0	0.0260	0.594	2.391	6.395	0.60	0.0000
0R14	6.0	0.0260	0.465	1.872	5.006	0.60	0.0050
0R15	6.0	0.0260	0.471	1.896	5.071	0.60	0.0115
0R16	6.0	0.0260	0.448	1.804	4.823	0.60	0.0220
0R17	6.0	0.0260	0.449	1.808	4.834	0.60	0.0000
0R18	6.0	0.0360	0.405	1.630	4.360	0.60	0.0000
0R19	6.0	0.0360	0.468	1.884	5.039	0.60	0.0050
0R20	6.0	0.0360	0.438	1.763	4.716	0.60	0.0150
0R21	6.0	0.0360	0.448	1.804	4.823	0.60	0.0220
0R22	6.0	0.0360	0.621	2.500	6.686	0.60	0.0000
0R23	6.0	0.0450	0.484	1.948	5.211	0.60	0.0000
0R24	6.0	0.0450	0.362	1.457	3.898	0.60	0.0050
0R25	6.0	0.0450	0.455	1.832	4.899	0.60	0.0115
0R26	6.0	0.0450	0.470	1.892	5.060	0.60	0.0220
0R27	6.0	0.0450	0.500	2.013	5.383	0.60	0.0000
0R28	6.0	0.0530	0.538	2.166	5.792	0.60	0.0000
0R29	6.0	0.0530	0.496	1.997	5.340	0.60	0.0050
0R30	6.0	0.0530	0.424	1.707	4.565	0.60	0.1150
0R31	6.0	0.0530	0.500	2.013	5.383	0.60	0.0220
1FR3	10.0	0.0100	0.418	1.683	4.500	0.60	0.0050
1FR4	10.0	0.0100	0.391	1.574	4.210	0.60	0.0115
1FR5	10.0	0.0100	0.426	1.715	4.587	0.60	0.0220
1FR6	10.0	0.0100	0.453	1.824	4.877	0.60	0.0000
1FR8	10.0	0.0160	0.429	1.727	4.619	0.60	0.0050
1R14	10.0	0.0260	0.481	1.936	5.179	0.60	0.0115
1R15	10.0	0.0260	0.489	1.969	5.265	0.60	0.2200
1R16	10.0	0.0260	0.454	1.828	4.888	0.60	0.0000
1R19	10.0	0.0360	0.480	1.932	5.168	0.60	0.0050
1R20	10.0	0.0360	0.494	1.989	5.319	0.60	0.0115
1R21	10.0	0.0360	0.452	1.820	4.866	0.60	0.0220
1R26	10.0	0.0450	0.447	1.800	4.813	0.60	0.0220
1R27	10.0	0.0450	0.427	1.719	4.597	0.60	0.0000
1R29	10.0	0.0530	0.466	1.876	5.017	0.60	0.0050
1R30	10.0	0.0530	0.478	1.924	5.146	0.60	0.0050
1R32	10.0	0.0530	0.476	1.916	5.125	0.60	0.0220
2FR3	14.0	0.0010	0.569	2.291	6.126	0.60	0.0115
2FR5	14.0	0.0010	0.499	2.009	5.373	0.60	0.0220
2FR7	14.0	0.0160	0.454	1.828	4.888	0.60	0.0050
2FR8	14.0	0.0160	0.454	1.828	4.888	0.60	0.0115
2FR9	14.0	0.0160	0.437	1.759	4.705	0.60	0.0220
2F10	14.0	0.0160	0.480	1.932	5.168	0.60	0.0000
2F12	14.0	0.0260	0.495	1.993	5.329	0.60	0.0050
2F14	14.0	0.0260	0.451	1.816	4.856	0.60	0.0220
2F18	14.0	0.0360	0.450	1.812	4.845	0.60	0.0115
2F22	14.0	0.0440	0.481	1.936	5.179	0.60	0.0050
2F23	14.0	0.0440	0.437	1.759	4.705	0.60	0.0115
2F24	14.0	0.0440	0.469	1.888	5.050	0.60	0.0220
2F27	14.0	0.0530	0.482	1.940	5.189	0.60	0.0050
2R28	14.0	0.0530	0.489	1.969	5.265	0.60	0.0115
2R31	14.0	0.0530	0.330	1.329	3.553	0.60	0.1000
2R36	10.0	0.0010	0.449	1.808	4.834	0.60	0.1000



Data Obtained Using GreaCo-Latin Factorial Experimental Analysis  
With 6" Diameter Column; Exit Drop Diameter Evaluated from  
Shadowgraphs Using Image Analysing Computer (Quantimet 720)

Ref.	$\rho_d$	$\Delta\rho$	g	$d_{in}$	$d_{xt}$	$d_b$	h	$\gamma$	$\mu_d$	$u_d$	
1RR1	0.8640	0.136	981.1	0.10	0.328	0.90	1.50	55.20	0.0058	0.0175	1
1RR2	0.8640	0.136	981.1	0.10	0.383	0.90	1.50	55.20	0.0058	0.0176	
1RR3	0.8640	0.136	981.1	0.10	0.435	0.90	1.50	55.20	0.0058	0.0276	
1RR4	0.8640	0.136	981.1	0.10	0.320	0.90	1.50	55.20	0.0058	0.0258	
1RR5	0.8640	0.136	981.1	0.10	0.376	0.90	1.50	55.20	0.0058	0.0296	
1RR6	0.8640	0.136	981.1	0.10	0.295	0.90	1.50	55.20	0.0058	0.0370	
1R11	0.8640	0.136	981.1	0.10	0.439	0.90	3.75	55.20	0.0058	0.0175	
1R18	0.8640	0.136	981.1	0.10	0.366	0.90	3.75	55.20	0.0058	0.0500	
1R26	0.8640	0.136	981.1	0.10	0.481	0.90	20.00	55.20	0.0058	0.0850	
2RR2	0.8640	0.136	981.1	0.10	0.600	0.60	1.00	55.20	0.0058	0.0166	
2RR3	0.8640	0.136	981.1	0.10	0.600	0.60	1.00	55.20	0.0058	0.0175	
3RR1	0.8640	0.136	981.1	0.20	0.563	1.20	2.00	55.20	0.0058	0.0195	
3RR3	0.8640	0.136	981.1	0.20	0.427	1.20	2.00	55.20	0.0058	0.0197	
3RR8	0.8640	0.136	981.1	0.20	0.460	1.20	2.00	55.20	0.0058	0.0450	
3R18	0.8640	0.136	981.1	0.20	0.454	1.20	8.00	55.20	0.0058	0.0250	
4RR1	0.8640	0.136	981.1	0.50	0.501	1.20	2.00	55.20	0.0058	0.0232	
4RR3	0.8640	0.136	981.1	0.50	0.510	1.20	2.00	55.20	0.0058	0.0380	
4R26	0.8640	0.136	981.1	0.50	0.493	1.20	20.00	55.20	0.0058	0.0580	
4R29	0.8640	0.136	981.1	0.50	0.467	1.20	20.00	55.20	0.0058	0.2222	
5RR1	0.8640	0.136	981.1	0.50	0.487	0.60	2.00	55.20	0.0058	0.0186	
5RR3	0.8640	0.136	981.1	0.50	0.465	0.60	2.00	55.20	0.0058	0.0308	
5RR5	0.8640	0.136	981.1	0.50	0.562	0.60	2.00	55.20	0.0058	0.0500	
5R10	0.8640	0.136	981.1	0.50	0.534	0.60	2.00	55.20	0.0058	0.0308	
5R14	0.8640	0.136	981.1	0.50	0.446	0.60	6.50	55.20	0.0058	0.0168	
5R28	0.8640	0.136	981.1	0.50	0.510	0.60	20.00	55.20	0.0058	0.0168	
3RR1	0.6930	0.307	981.1	0.50	0.411	1.20	2.50	51.10	0.0051	0.0214	
3R19	0.6930	0.307	981.1	0.50	0.408	1.20	2.00	51.10	0.0051	0.0590	
4RR1	0.6930	0.307	981.1	0.50	0.464	0.60	3.50	51.10	0.0051	0.0213	
4RR2	0.6930	0.307	981.1	0.50	0.550	0.60	3.50	51.10	0.0051	0.0279	
4RR6	0.6930	0.307	981.1	0.50	0.480	0.60	7.00	51.10	0.0051	0.0860	
4RR8	0.6930	0.307	981.1	0.50	0.470	0.60	7.00	51.10	0.0051	0.0214	
4R12	0.6930	0.307	981.1	0.50	0.464	0.60	7.00	51.10	0.0051	0.0558	
4R21	0.6930	0.307	981.1	0.50	0.550	0.60	10.00	51.10	0.0051	0.2222	
4R29	0.6930	0.307	981.1	0.50	0.502	0.60	20.00	51.10	0.0051	0.0800	
5RR1	0.6930	0.307	981.1	0.10	0.100	0.90	2.00	51.10	0.0051	0.0200	
6RR2	0.6930	0.307	981.1	0.10	0.355	0.60	3.00	51.10	0.0051	0.0288	
6RR4	0.6930	0.307	981.1	0.10	0.470	0.60	8.00	51.10	0.0051	0.0445	
6R11	0.6930	0.307	981.1	0.10	0.454	0.60	8.00	51.10	0.0051	0.0445	
6R13	0.6930	0.307	981.1	0.50	0.467	1.20	23.00	51.10	0.0051	0.0550	
7RR1	0.6930	0.307	981.1	0.20	0.200	1.20	8.00	51.10	0.0051	0.0185	
7RR2	0.6930	0.307	981.1	0.20	0.201	1.20	20.00	51.10	0.0051	0.0350	
9RR3	0.8000	0.200	981.1	0.10	0.100	0.60	1.50	2.80	0.0062	0.0288	
9RR4	0.8000	0.200	981.1	0.10	0.100	1.20	15.00	2.80	0.0062	0.0352	
9RR5	0.8000	0.200	981.1	0.50	0.203	0.60	3.50	2.80	0.0062	0.0635	
9RR6	0.8000	0.200	981.1	0.20	0.193	1.20	3.50	2.80	0.0062	0.0550	
9RR7	0.8000	0.200	981.1	0.20	0.203	1.20	3.50	2.80	0.0062	0.0890	
9RR8	0.8000	0.200	981.1	0.10	0.100	0.90	10.00	2.80	0.0062	0.2500	
9RR8	0.9760	0.024	981.1	0.10	0.795	1.20	3.00	13.10	0.0082	0.2220	
9R33	0.9760	0.024	981.1	0.10	0.554	0.90	20.00	13.10	0.0082	0.0167	
9R34	0.9760	0.024	981.1	0.10	0.662	0.90	20.00	13.10	0.0082	0.0232	
9R35	0.9760	0.024	981.1	0.10	0.681	0.90	20.00	13.10	0.0082	0.0500	
0RR8	0.9760	0.024	981.1	0.10	0.584	0.60	3.00	13.10	0.0082	0.0232	
0R10	0.9760	0.024	981.1	0.10	0.615	0.60	6.50	13.10	0.0082	0.0232	
0R12	0.9760	0.024	981.1	0.10	0.780	0.60	6.50	13.10	0.0082	0.0380	
0R12	0.9760	0.024	981.1	0.10	0.655	0.60	3.00	13.10	0.0082	0.0232	
0R24	0.9760	0.024	981.1	0.10	0.540	0.60	15.00	13.10	0.0082	0.0232	
0R26	0.9760	0.024	981.1	0.10	0.550	0.60	15.00	13.10	0.0082	0.0580	
0R27	0.9760	0.024	981.1	0.10	0.674	0.60	15.00	13.10	0.0082	0.0500	
1R20	0.9760	0.024	981.1	0.40	1.096	1.20	7.00	13.10	0.0082	0.0232	
2RR1	0.9760	0.024	981.1	0.40	0.750	0.60	7.00	13.10	0.0082	0.0195	
2R18	0.9760	0.024	981.1	0.20	0.890	1.20	15.00	13.10	0.0082	0.0500	
1R22	0.9760	0.024	981.1	0.20	1.100	1.20	15.00	13.10	0.0082	0.0550	

1. Toluene-Water
2. Iso Octane - Water
3. M.I.B.K. - Water
4. Diethyl Carbonate - Water



## APPENDIX A.4.4

Ref	Property No.	Void No.	Archimedes No.	Drop Exp.	Number Calc.	% Dif..	calc c
1RR1	178.52	0.4682	0.0450	3.2800	3.6259	-0.1055	3.7582
1RR2	178.52	0.4682	0.0450	3.8300	3.6259	0.0533	3.7582
1RR3	178.52	0.4682	0.0450	4.3500	3.6259	0.1665	3.7582
1RR4	178.52	0.4682	0.0450	3.2000	3.6259	-0.1331	3.7582
1RR5	178.52	0.4682	0.0450	3.7600	3.6259	0.0357	3.7582
1RR6	178.52	0.4682	0.0450	2.9500	3.6259	-0.2291	3.7582
1R11	178.52	0.4682	0.0450	4.3900	3.6259	0.1741	3.7582
1R18	178.52	0.4682	0.0450	3.6600	3.6259	0.0093	3.7582
1R26	178.52	0.4682	0.0450	4.8100	3.6259	0.2462	3.7582
2RR2	178.52	0.5386	0.0450	6.0000	4.1709	0.3049	4.3230
2RR3	178.52	0.5386	0.0450	6.0000	4.1709	0.3049	4.3230
3RR1	178.52	0.5386	0.0204	2.8150	1.8882	0.3292	1.9571
3RR3	178.52	0.5386	0.0204	2.1350	1.8882	0.1156	1.9571
3RR8	178.52	0.5386	0.0204	2.3000	1.8882	0.1790	1.9571
3R18	178.52	0.5386	0.0204	2.2700	1.8882	0.1682	1.9571
4RR1	178.52	0.7391	0.0071	1.0020	0.9089	0.0929	0.9420
4RR3	178.52	0.7391	0.0071	1.0200	0.9089	0.1090	0.9420
4R26	178.52	0.7391	0.0071	0.9860	0.9089	0.0782	0.9420
4R29	178.52	0.7391	0.0071	1.2820	0.9089	0.2911	0.9420
5RR1	178.52	0.9390	0.0071	0.9740	1.1547	-0.1855	1.1968
5RR3	178.52	0.9390	0.0071	0.9300	1.1547	-0.2416	1.1968
5RR5	178.52	0.9390	0.0071	1.1240	1.1547	-0.0273	1.1968
5R10	178.52	0.9390	0.0071	1.0680	1.1547	-0.0811	1.1968
5R14	178.52	0.9390	0.0071	0.8920	1.1547	-0.2945	1.1968
5R28	178.52	0.9390	0.0071	1.0200	1.1547	-0.1320	1.1968
3RR1	190.14	0.7391	0.0052	0.8220	0.7000	0.1485	0.7255
3R19	190.14	0.7391	0.0052	0.8160	0.7000	0.1422	0.7255
4RR1	190.14	0.9390	0.0052	0.9280	0.8893	0.0418	0.9217
4RR2	190.14	0.9390	0.0052	1.1000	0.8893	0.1916	0.9217
4RR6	190.14	0.9390	0.0052	0.9600	0.8893	0.0737	0.9217
4RR8	190.14	0.9390	0.0052	0.9400	0.8893	0.0540	0.9217
4R12	190.14	0.9390	0.0052	0.9280	0.8893	0.0418	0.9217
4R21	190.14	0.9390	0.0052	1.1000	0.8893	0.1916	0.9217
4R29	190.14	0.9390	0.0052	1.0040	0.8893	0.1143	0.9217
5RR1	190.14	0.4682	0.0325	1.0000	2.7925	-1.7925	2.8943
6RR2	190.14	0.5386	0.0325	3.3500	3.2122	0.0411	3.3293
6RR4	190.14	0.5386	0.0325	4.7000	3.2122	0.3166	3.3293
6R11	190.14	0.5386	0.0325	4.5400	3.2122	0.2925	3.3293
6R13	190.14	0.7391	0.0052	0.9340	0.7000	0.2506	0.7255
7RR1	190.14	0.5386	0.0147	1.0000	1.4542	-0.4542	1.5073
7RR2	190.14	0.5386	0.0147	1.0050	1.4542	-0.4470	1.5073
9RR3	70.30	0.5386	0.0421	1.0000	1.5363	-0.5363	1.5923
9RR4	70.30	0.4240	0.0421	1.0000	1.2093	-0.2093	1.2534
9RR5	70.30	0.9390	0.0067	0.4060	0.4253	-0.0476	0.4408
9RR6	70.30	0.5386	0.0190	0.9650	0.6955	0.2793	0.7209
9RR7	70.30	0.5386	0.0190	1.0150	0.6955	0.3148	0.7209
9RR8	70.30	0.4682	0.0421	1.0000	1.3356	-0.3356	1.3843
9RR8	110.25	0.4240	0.1082	7.9500	4.8813	0.3860	5.0594
9R33	110.25	0.4682	0.1082	5.5400	5.3911	0.0269	5.5878
9R34	110.25	0.4682	0.1082	6.6200	5.3911	0.1856	5.5878
9R35	110.25	0.4682	0.1082	6.8100	5.3911	0.2083	5.5878
0RR8	110.25	0.5386	0.1082	5.8400	6.2014	-0.0619	6.4276
0R10	110.25	0.5386	0.1082	6.1500	6.2014	-0.0084	6.4276
0R12	110.25	0.5386	0.1082	7.8000	6.2014	0.2049	6.4276
0R13	110.25	0.5386	0.1082	6.5500	6.2014	0.0532	6.4276
0R24	110.25	0.5386	0.1082	5.4000	6.2014	-0.1484	6.4276
0R26	110.25	0.5386	0.1082	5.5000	6.2014	-0.1275	6.4276
0R27	110.25	0.5386	0.1082	6.7400	6.2014	0.0799	6.4276
1R20	110.25	0.6843	0.0222	2.7400	1.6147	0.4107	1.6736
2RR1	110.25	0.8693	0.0222	1.8750	2.0514	-0.0941	2.1262
2R18	110.25	0.5386	0.0490	4.4500	2.8075	0.3691	2.9099
1R22	110.25	0.5386	0.0490	5.5000	2.8075	0.4895	2.9099



APPENDIX A.4.5 Typical Evaluation of Inlet Drop Model  
 Showing Relationship between Drop Diameter, Physical Properties  
 & Packing Geometry

DIAMETER OF SPHERE 1.2  
 MINIMUM VOID DIAMETER .33  $d_v = 0.27 d_b$

DROP DIA.	BOUYANCY NO.	CHI	F VALUE	PREDICTION
.5	1	20.3125	.392292	PASSAGE
.55	1	24.3125	.194542E-01	PASSAGE
.56	1	25.5625	-.495439E-01	HOLD-UP
.57	1	26.3125	-.117922	HOLD-UP

DIAMETER OF SPHERE .9  
 MINIMUM VOID DIAMETER .2475  $d_v = 0.27 d_b$

DROP DIA.	BOUYANCY NO.	CHI	F VALUE	PREDICTION
.33	1	14.9375	.193132	PASSAGE
.34	1	16.3125	.233573E-01	PASSAGE
.35	1	17.6375	-.152354	HOLD-UP
.41	2	24.6375	.367772	PASSAGE
.42	2	25.5625	.263761	PASSAGE
.43	2	26.5625	.146331	PASSAGE
.44	2	27.4375	.45259E-01	PASSAGE
.45	2	28.3125	-.541232E-01	HOLD-UP

DIAMETER OF SPHERE .6  
 MINIMUM VOID DIAMETER .165  $d_v = 0.27 d_b$

DROP DIA.	BOUYANCY NO.	CHI	F VALUE	PREDICTION
.2	1	10.0625	.201395E-01	PASSAGE
.21	1	12.5625	-.373065	HOLD-UP
.21	2	12.5625	.431553	PASSAGE
.22	2	14.9375	.695953E-01	PASSAGE
.23	2	17.0625	-.332252	HOLD-UP
.24	3	19.0625	.133695	PASSAGE
.25	3	20.3125	-.15251	HOLD-UP

DIAMETER OF SPHERE 1.2  
 MINIMUM VOID DIAMETER .24  $d_v = 0.2 d_b$

DROP DIA.	BOUYANCY NO.	CHI	F VALUE	PREDICTION
.35	1	16.0625	.433757E-01	PASSAGE
.36	1	17.1375	-.123932	HOLD-UP
.5	2	23.9375	.332433E-01	PASSAGE
.51	2	29.5625	-.304265E-01	HOLD-UP

DIAMETER OF SPHERE .9  
 MINIMUM VOID DIAMETER .13  $d_v = 0.2 d_b$

DROP DIA.	BOUYANCY NO.	CHI	F VALUE	PREDICTION
.22	1	3.5625	.463555	PASSAGE
.23	1	10.4375	.16972	PASSAGE
.24	1	12.3125	-.164663	HOLD-UP
.27	2	17.1375	.110315	PASSAGE
.23	2	13.5625	-.170351	HOLD-UP
.32	3	23.5625	.170391	PASSAGE
.33	3	24.6375	-.344791E-01	HOLD-UP



Contd. APPENDIX A.4.5

DIAMETER OF SPHERE .6  $d_v = 0.185 d_b$   
 MINIMUM VOID DIAMETER .927E-01

DROP DIA.	BOUYANCY NO.	CHI	F VALUE	PREDICTION
.1	1	2.4375	.562756	PASSAGE
.11	1	5.9375	-.105274	HOLD-UP
.12	1	9.3125	-1.20366	HOLD-UP
.11	2	5.9375	.625315	PASSAGE
.12	2	9.3125	-.449539	HOLD-UP
.13	2	12.3125	-1.67477	HOLD-UP
.11	3	5.9375	1.3559	PASSAGE
.12	3	9.3125	.304581	PASSAGE
.13	3	12.3125	-.898324	HOLD-UP
.17	10	21.6875	.741896	PASSAGE
.18	10	23.4375	.689468E-01	PASSAGE
.19	10	25.1875	-.569284	HOLD-UP

DIAMETER OF SPHERE .9  $d_v = 0.185 d_b$   
 MINIMUM VOID DIAMETER .13905

DROP DIA.	BOUYANCY NO.	CHI	F VALUE	PREDICTION
.17	1	7.0625	.330081	PASSAGE
.18	1	9.3125	-.174007	HOLD-UP
.18	2	9.3125	.957173	PASSAGE
.19	2	11.3125	.451684	PASSAGE
.2	2	13.1875	-.713968E-01	HOLD-UP
.22	3	16.6875	.960064E-01	PASSAGE
.23	3	18.1875	-.34639	HOLD-UP

DIAMETER OF SPHERE 1.2  $d_v = 0.185 d_b$   
 MINIMUM VOID DIAMETER .1854

DROP DIA.	BOUYANCY NO.	CHI	F VALUE	PREDICTION
.25	1	10.8125	.246601	PASSAGE
.26	1	12.3125	-.609369E-01	HOLD-UP
.27	1	13.6875	-.359438	HOLD-UP
.31	2	18.5625	.174863	PASSAGE
.32	2	19.6875	-.661149E-01	HOLD-UP
.33	2	20.6875	-.277713	HOLD-UP
.41	3	27.4375	.251337	PASSAGE
.42	3	28.1875	.141165	PASSAGE
.43	3	28.8125	.527391E-01	PASSAGE
.44	3	29.4375	-.32526E-01	HOLD-UP

DIAMETER OF SPHERE .6  $d_v = 0.2 d_b$   
 MINIMUM VOID DIAMETER .12.

DROP DIA.	BOUYANCY NO.	CHI	F VALUE	PREDICTION
.14	1	6.4375	.151652	PASSAGE
.15	1	9.4375	-.432921	HOLD-UP
.16	2	12.3125	-.443755	HOLD-UP
.16	3	12.3125	.353295	PASSAGE
.17	3	14.3125	-.366992	HOLD-UP



APPENDIX 5.

MEISTER & SCHEELE'S CORRELATIONS FOR  
PREDICTING DROP DIAMETER FORMED AT SHARP EDGED NOZZLES

Fig. A.5

PREDICTION OF EXIT DROP DIAMETER  
USING MEISTER & SCHEELE CORRELATIONS

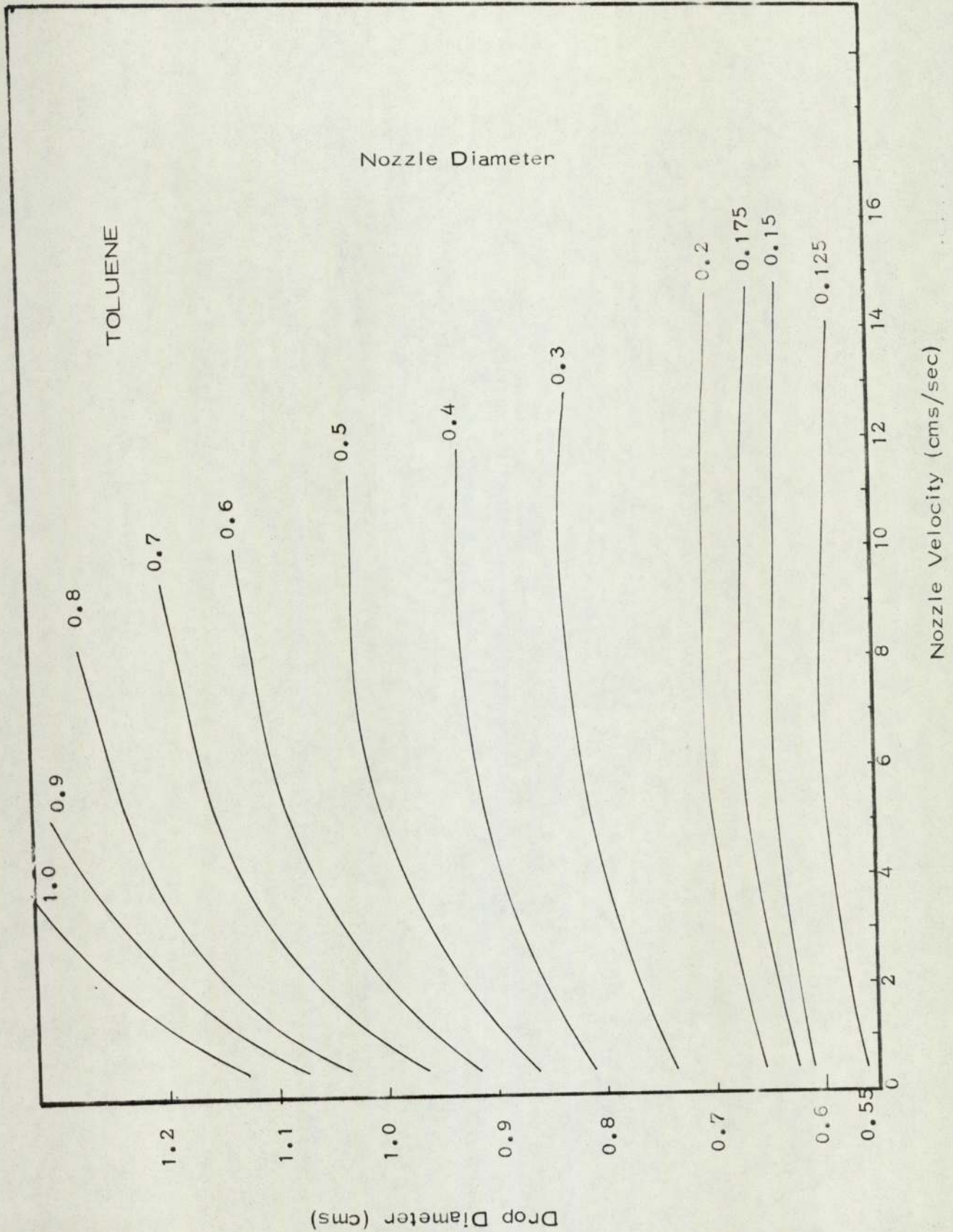




Fig. A.5

PREDICTION OF EXIT DROP DIAMETER  
USING MEISTER & SCHEELE CORRELATIONS

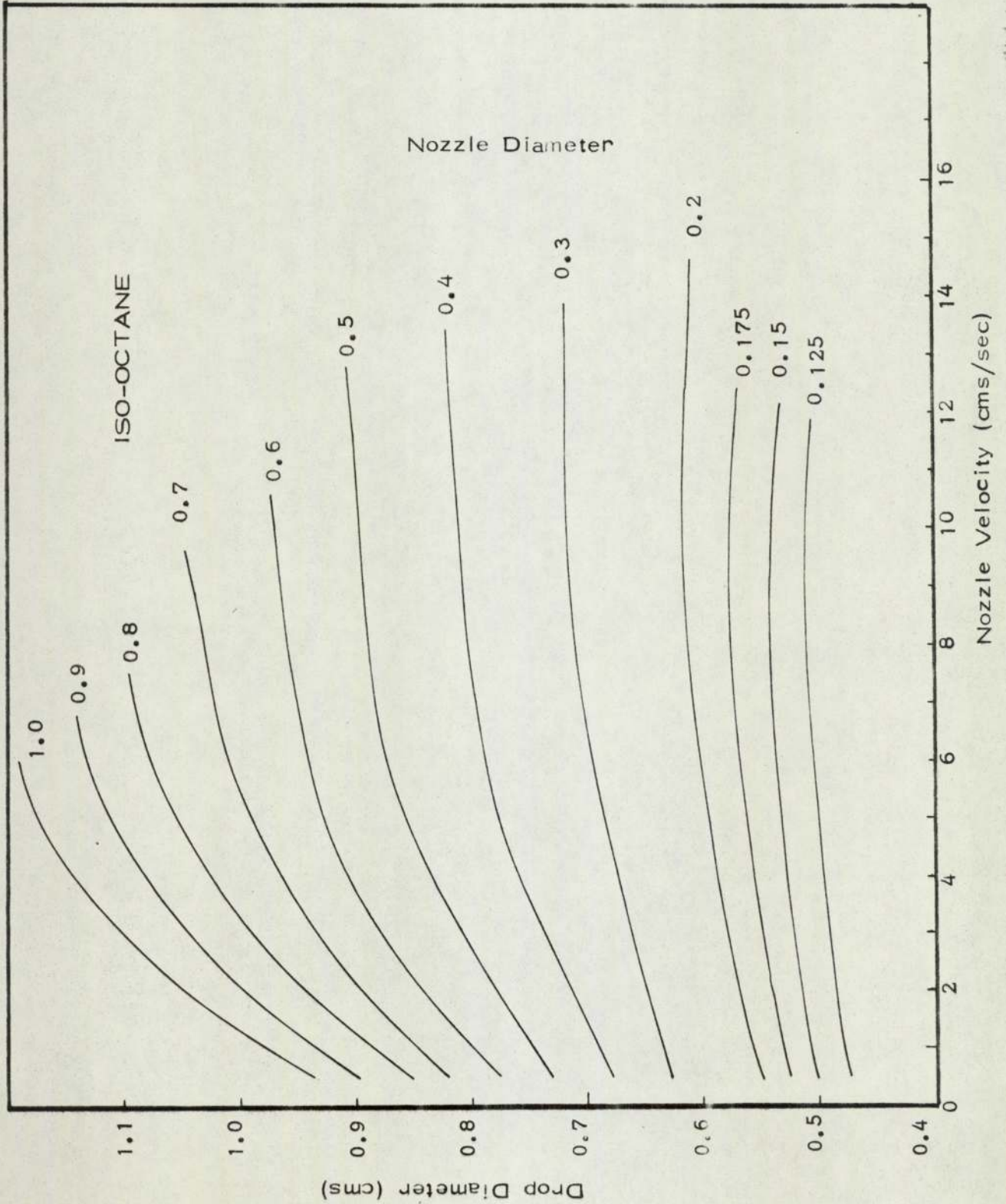
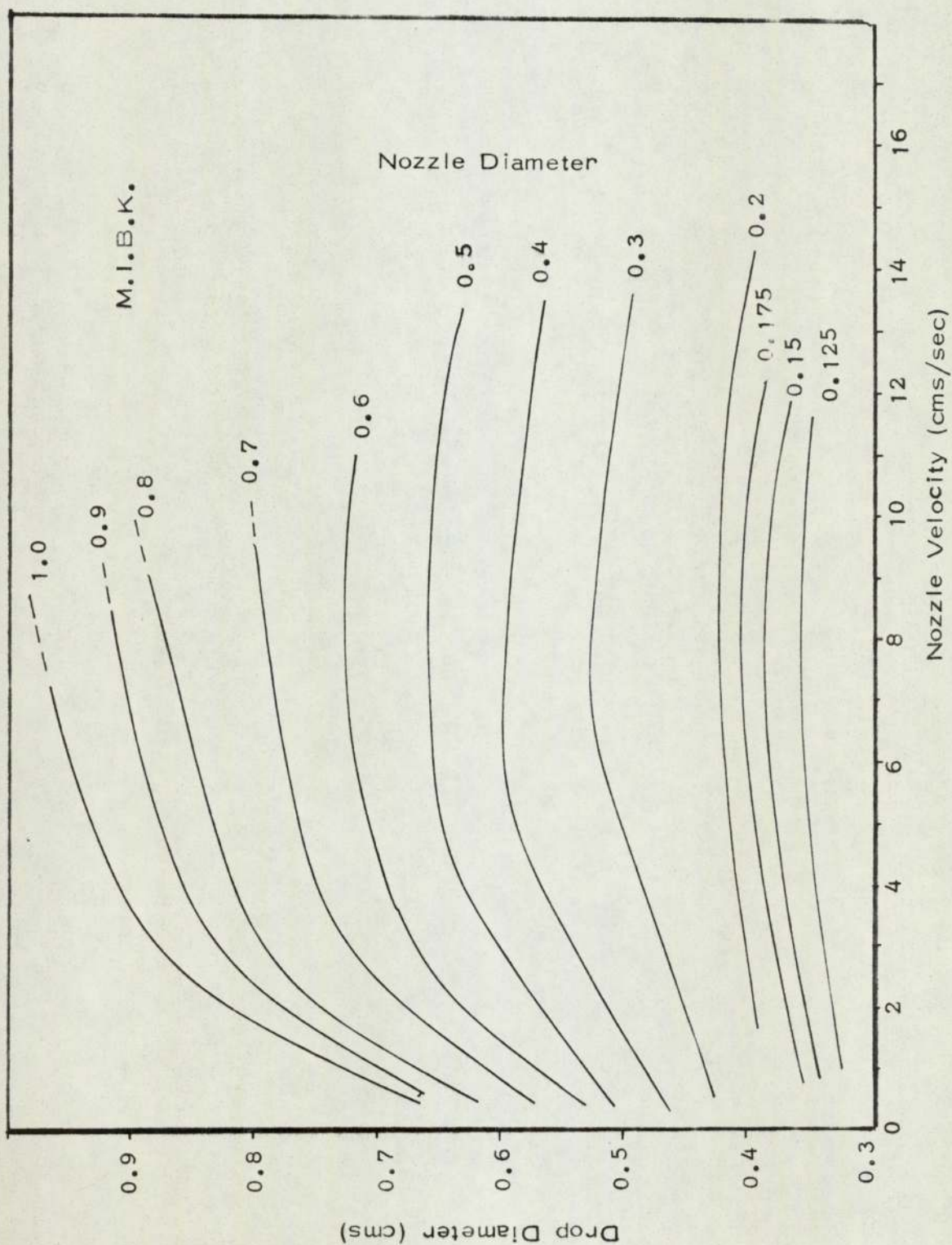


Fig. A.5

PREDICTION OF EXIT DROP DIAMETER  
USING MEISTER & SCHEELE CORRELATIONS





## NOMENCLATURE

Symbols have the following meanings except where specifically indicated in the text.

A	=	Area ( $\text{cms}^2$ )
a	=	Jet radius $\bar{a} = \frac{2a}{d_n}$ (cms)
b	=	Radius of curvature of a sessile drop (cms)
c	=	$(\rho g/\gamma)^{\frac{1}{2}}$ ( $\text{cms}^{-1}$ )
$d_b$	=	Diameter of ballotini (cms)
$d_c$	=	Diameter of critical packing size (cms)
$d_d$	=	Diameter of exit drop (cms)
$d_{dj}$	=	Diameter of exit drop evaluated by Jenkinson (cms)
$d_{dm}$	=	Diameter of exit drop predicted by Meister and Scheele (cms)
$d_{ec}$	=	Diameter of critical drop size predicted by Thornton and Ramshaw (cms)
$d_{exp}$	=	Diameter of drop obtained during this study (cms)
$d_f$	=	Diameter of fibre (cms)
$d_h$	=	Hydraulic mean diameter defined by Jenkinson (cms)
$d_{in}$	=	Diameter of inlet drop (cms)
$d_n$	=	Diameter of nozzle (cms)
$d_p$	=	Equivalent diameter of packing (cms)
$d_{xt}$	=	Mean exit drop diameter evaluated at one operating condition for ballotini packings (cms)
$d_{xt \text{ average}}$	=	Exit drop diameter evaluated from a series of operating conditions with ballotini packings (cms)
$d_{xt \text{ theory}}$	=	Theoretical maximum exit drop size for ballotini packing (cms)
$d_v$	=	Diameter of void (cms)
$d_{vc}$	=	Diameter of void - cubic geometry (cms)
$d_{vt}$	=	Diameter of void - triangular geometry (cms)

$d_{vs}$	=	Mean diameter of exit dispersion for all packings except ballotini (cms)
$d_{vs}^o$	=	Characteristic mean drop diameter (cms)
$D_{vo}$	=	Original drop diameter before deformation (cms)
$D_e$	=	Diameter of restriction (cms)
$D_g$	=	Diameter of packing element (cms)
DV	=	Drop Void Number
DVC	=	Drop Void Number based on cubic geometry
DVT	=	Drop Void Number based on triangular geometry
$(DE_1)_{crit}$	=	Maximum stable drop diameter (cms)
e	=	Eccentricity
E	=	E  Factor (residual of eqn. 7.9)
F	=	Harkins-Brown factor (residual after drop detachment)
g	=	Gravitational acceleration (cms sec <sup>-2</sup> )
$h_b$	=	Packing height (ballotini) (cms)
$h_1$	=	Film thickness before drainage commences (cms)
$h_2$	=	Film thickness at rupture (cms)
K	=	Constant relating to active sites
k	=	Constant relating to geometry of exit packing
L	=	Length of drop fall (cms)
N	=	Total number of drops
n	=	Number of packing restrictions
P	=	Pressure (gm cms <sup>-2</sup> )
$\Delta P$	=	Pressure drop (gm cms <sup>-2</sup> )
Q	=	Volumetric flow rate into a nozzle (cms sec <sup>-1</sup> )
$R_1$	=	$r_1$ ; radius of upper segment (cms)
$R_2$	=	$r_b$ ; radius of lower segment (cms)
$r_v$	=	Radius of drop formed at a nozzle (cms)
S	=	Spreading coefficient eqn(4.3) or saturation coefficient eqn.(2.20-22)



T	=	Temperature ( $^{\circ}\text{C}$ )
t	=	Coalescence time (secs)
$t_{\frac{1}{2}}$	=	Coalescence time - half life
$t_m$	=	Coalescence time - mean
u	=	U; superficial velocity ( $\text{cms sec}^{-1}$ )
$U_o$	=	Orifice velocity ( $\text{cms sec}^{-1}$ )
$U_n$	=	Nozzle velocity ( $\text{cms sec}^{-1}$ )
$U_j$	=	Jetting velocity ( $\text{cms sec}^{-1}$ )
$U_x$	=	Nozzle velocity (experimental)( $\text{cms sec}^{-1}$ )
$\bar{V}$	=	Mean velocity of drops in packing ( $\text{cms sec}^{-1}$ )
$V_t$	=	Terminal velocity ( $\text{cms sec}^{-1}$ )
$V_o$	=	Characteristic droplet velocity ( $\text{cms sec}^{-1}$ )
$V_{cf}; V_{df}$	=	Volumetric flow rate at flooding for continuous and dispersed phase respectively ( $\text{cms}^3 \text{sec}^{-1}$ )
$V_f$	=	Volume of drop formed at nozzle ( $\text{cms}^3$ )
v	=	Volume of a sessile drop ( $\text{cms}^3$ )
$x_c; x_{90}$	=	Sessile drop dimensions in horizontal plane
$z_c; z_{90}$	=	Sessile drop dimensions in vertical plane
XZV	=	Dimensionless drop values
x	=	Dispersed phase hold-up

#### SUBSCRIPTS

c	=	Denotes continuous phase when used with velocity, volumetric, density or viscosity terms
d	=	Denotes dispersed phase when used with velocity, volumetric, density or viscosity terms

#### POSTSCRIPTS

t	=	Denotes total area of $d_v$ min
s	=	Denotes exit drop evaluated from surface area
v	=	Denotes exit drop evaluated from volume

## GREEK LETTERS

$\beta$	=	bc
$\gamma$	=	Interfacial tension (dynes cms <sup>-1</sup> )
$\epsilon$	=	Voidage
$\zeta$	=	Probability of retention
$\eta$	=	Packing efficiency
$\lambda$	=	Deposition coefficient or ratio R/d used in models for coalescence times
$\mu$	=	Viscosity (poise)
$\rho$	=	Density (gm cms <sup>-1</sup> )
$\Delta\rho$	=	Density difference (gm cms <sup>-1</sup> )
$\sigma$	=	Surface tension (dynes cms <sup>-1</sup> )
$\sigma'$	=	Standard deviation
$\phi$	=	Angle of packing geometry
$\theta_c$	=	Contact angle
$\overline{\theta}_{ca}$	=	Contact angle advancing
$\theta_{cr}$	=	Contact angle receding
$\theta, \psi$	=	Angles used in inlet model to evaluate volumes of drop segment, $V_1; V_{II}; V_{III}; V_o$



## REFERENCES

- 1) Jeffreys, G.V., and Hawkesley, J.L., *A.I.Ch.E.J.* 11 413 (1965)
- 2) Hitit, A., Ph.D. Thesis. Univ. of Aston (1972)
- 3) Frankel, S.P., and Mysels, K.S., *J. Phys. Chem.*, 66 190 (1962)
- 4) Lawson, G.B., *Chem. and Proc. Eng.*, V.48 No.5 45 (1967)
- 5) Jeffreys, G.V., Davies, G.A., and Pitt, K., *A.I.Ch.E.J.*, 18 833 (1970)
- 6) Smith, D.V., Ph.D. Thesis. Univ. of Manchester (1969)
- 7) Gillespie, T., and Rideal, E.K., *Trans. Faraday Soc.* 52 173 (1956)
- 8) Jeffreys, G.V., and Hawkesley, J.L., *J. Appl. Chem.* 12 329 (1962)
- 9) Cockbain, E.G., and McRoberts, T.S., *J. Colloid Sci.* 8 440 (1953)
- 10) Elton, G.A., and Picknett, R.G., *Proceedings of the 2nd International Congress on Surface Activity, Vol. 1.* 288 307, Butterworths, Lon. (1957)
- 11) Misek, T., *Coll. Czech., Chem. Commun.* 29 2086 (1964)
- 12) Jeffreys, G.V., and Davies, G.A., *Recent Advances in Liquid-Liquid Extraction.* Pergamon Press (1971)
- 13) Bashforth, F., and Adams, J.C., *Attempt to Test the Theories of Capillary Action.* Cambridge Univ. Press (1883)
- 14) Lang, S.B., and Wilke, C.R., *Ind. Eng. Chem. Fund.* 10 No.3 329 (1971)
- 15) Princen, H.M., *J. Colloid Sci.*, 18, 178 (1963)
- 16) Jeffreys, G.V., and Hawkesley, J.L., *A.I.Ch.E.J.* 11 413 (1965)
- 17) Lawson, G.B., Ph.D. Thesis Univ. of Manchester (1967)
- 18) Davies, G.A., Jeffreys, G.V., and Smith, D.V., *I.S.E.C. Hague* (1971)
- 19) Hawkesley, J.L., Ph.D. Thesis Univ. of Birmingham (1963)
- 20) Sawistowski, H., "Recent Adv. in L-L Extraction" Perg. Press Ltd (1971)
- 21) Lang, S.B., Ph.D. Thesis Univ. of California (1962)
- 22) Brown, A.H. and Hanson, C., *Trans. Faraday Soc.* 61 1754 (1965)
- 23) Hartland, S.J., *Colloid Sci.*, 26 383 (1968)

- 24) Davies, J.T., and Rideal, E.K., *Interfacial Phenomena*, Academy Press, New York (1963)
- 25) Jeffreys, G.V., and Lawson, G.B., *Trans. Inst. Chem. Eng.* V.43, T.294 (1965)
- 26) Hodgson, T.D., and Lee, J.C., *J. Colloid Interface Sci.*, 30 94 (1969)
- 27) Hartland, S.J., *Can. J. Chem. Eng.* 47 221 (1969)
- 28) MacCay, G.D.M., and Mason, S.G., *J. Colloid Sci.*, 18 674 (1963)
- 29) Hartland, S.J., *Trans. Instn. Chem. Engrs.* 45, T 102 (1957)
- 30) Van den Tempel., *Rec. Trav. Chim.*, 72 419 (1953)
- 31) Levich, G., *Physicochemical Hydrodynamics* Prentice Hall ( )
- 32) Howarth, W.J., *Chem. Eng. Sci* 19 33 (1964)
- 33) Scheele, G.F., and Leng, D.E., *Chem. Eng. Sci* 26 1867 (1971)
- 34) Murdoch, P.G., and Leng, D.E., *Chem. Eng. Sci* 26 1881 (1971)
- 35) Allan, R.S., Charles, G.E., and Mason, S.G. *J. Colloid Sci* 16 150 (1961)
- 36) Allak, A.M.A., Ph.D. Thesis Univ. of Aston (1973)
- 37) Perut, M., *Petr. Ann. Comb. Liquides* 27(5) 763 (1972)
- 38) Lewis, S.B., Jones, I., and Pratt, H.R.C., *Trans. Instn. Chem. Engrs.* 29, 136 (1951)
- 39) Gayler, R., and Pratt, H.R.C. *Trans. Instn. Chem. Engrs.* 31 69 (1953)
- 40) *Ibid.* *Trans. Instn. Chem. Engrs.* 29 110 (1951)
- 41) Gayler, R., Roberts, N.W., and Pratt, H.R.C., *Trans. Instn. Chem. Engrs.* 31 57 (1953)
- 42) Dell, F.R., and Pratt, H.R.C., *Trans. Instn. Chem. Engrs.* 29 270 (1951)
- 43) *Ibid.* *Trans. Instn. Chem. Engrs.* 29 89 (1951)
- 44) Wicks, C., and Beckman, R.B., *Ind. Engng. Chem.* 42 1078 (1950)
- 45) Puranik, S.A., and Sharma, M.M., *Chem. Engng Sci.* 25 257 (1970)
- 46) Morrello, V.S., and Beckman, R.B., *Ind. Engng. Chem. Ind. Int. Edition* 42 1078 (1950)



- 47) Ballard, J.H., and Piret, E.L., *Ind. Engng. Chem. Eng.* 29 39 (1951)
- 48) Ramshaw, C., and Thornton, R.D., *Instn Chem. Engrs Symp. Series* 26 73 (1967)
- 49) *Ibid.* *Instn Chem. Engrs Symp. Series* 26 86 (1967)
- 50) Thomas, R.J., and Mumford, C.J., *I.S.E.C. Hague Vol 1* 400 (1971)
- 51) Chin, H.L., *M. Ch.E. Thesis Univ. of New York* (1956)
- 52) Crawford, J.W. and Wilke, C.R. *Chem. Eng. Prog.* 47 423 (1951)
- 53) Hoffing, E.H., and Lockart, F.J., *Chem. Eng. Prog.* 50 94 (1962)
- 54) Breckenfield, R.R., and Wilke, C.R., *Chem. Engng. Prog.* 40 187 (1950)
- 55) Blanding, F.H., and Elgin, J.C., *A.I.Ch.E. JI* 33 305 (1942)
- 56) Mumford, C.J., and AlHemeri, A.A.A., *I.S.E.C. Hague Vol 2* 1591 (1974)
- 57) Lewis, B., and von Elbe, G., "*Combustion Flames & Explosions of Gases*" Acad. Press Inc. New York (1951)
- 58) Honeykamp, J.R., and Burkart, L.E., *Ind. Engng. Chem. Process Des. Dev.* 1 177 (1962)
- 59) Slatter, M.A., *M.Sc. Thesis Univ. of Aston* (1968)
- 60) Piper, H., *Ph.D. Thesis Univ. of Manchester Inst. Sci & Tech* (1969)
- 61) Scheibel, E.G., *Chem. Eng. Prog.* 44 681 (1948)
- 62) Jeffreys, G.V., and Davies, G.A., *Filtration Separation* 349 (1969)
- 63) Selka, A.H., and Skicher, C.A., *Can. J. Chem. Eng.* 43 298 (1965)
- 64) Farkir-Din, S.M., *M.Sc. Thesis Univ. of Manchester* (1969)
- 65) Luhnig, R.W., and Sawistowski, H., *I.S.E.C. Hague* 873 (1971)
- 66) Ali, F.A., *Ph.D. Thesis University of Manchester* (1971)
- 67) Davies, G.A., and Jeffreys, G.V., *Machevo Congress Utrecht* (1971)
- 68) Azfal, M., Jeffreys, G.V. and Davies, G.A., *Brit. Chem. Eng. Proc. Tech.* 17 9 (1972)
- 69) Morrow, N.R., *Ind. Engng. Chem.* 62 32 (1970)
- 70) Spielman, L.A., *Ph. D. Thesis Univ. of California Berkeley* (1968)
- \* 71) Sareen, S.S., Rose, P.M., Gudson, R.C., and Kintner, R.C., *A.I.Ch.E. J.* 12 1045 (1966)



- 72) Davies, G.A., Jeffreys, G.V., and Price-Bailey, D., A new packing for gas-liquid & liquid-liquid sep. process Knitmesh Ltd. (1971)
- 73) Schniedegger, A.E., The Physics of Flow through Porous Media Macmillan New York (1957)
- 74) Schwartz, A.M., Ind. Engng. Chem. 61 No. 1 10 (1967)
- 75) Liepman, H.W., and Puckett, A.E., "Intro. to Aerodynamics" J. Wiley & sons incor. N.Y. (1947)
- 76) Padday, J.F., Proc. 2nd Int. Cong. Surface Activity Vol 3 London Butterworth (1957)
- 77) Hazlett, R.N., Ind. Eng. Chem. Fundam. 9 520 (1970)
- 78) Hazlett, R.N., and Corhort, H.W., Filt. and Sep. 9 456 (1972)
- 79) Spielman, L.A., and Goren, S.L., Ind. Eng. Chem. Fund 11 63 (1972)
- 80) Sherony, D.F., and Kintner, R.C., Can. J. Chem Eng. 43 314 (1971)
- 81) Sherony, D.F., Ph.D. Thesis I.I.T. (1969)
- 82) Rosenfeld, J.I., and Wasan, D.T., Can. J. Chem. Eng. 52 Feb. (1974)
- 83) Bartle, J.W., Filt. and Sep. (Sept/Oct) (1966)
- X 84) Shackleton, L.R.B., Douglas, E., and Walsh, T, Trans. Inst. Mar. Eng. 72 409 (1960)
- X 85) Douglas, E., and Elliot, I. G., Trans. Inst. Mar. Eng. 74 164 (1962)
- X 86) Farley, R., and Valentine, F.H.H., Joint Meeting A.I. Ch. E and I. Chem. Eng. Symp. London (1965)
- X 87) Smith, G.J., Ph.D. Thesis Univ. of Southampton (1969)
- 88) Hubburst, H.M., and Katz, S., Chem. Eng. Sci 19 555 (1964)
- 89) Newall, H.J., Group Research Report J. Lucas Ltd GR 90 502
- 90) Rushton, E., and Davies, G.A., I.S.E.C. Lyons (1974)
- 91) Tate, T.T., Phil. Mag. 27 176 (1864)
- 92) Perry, J.H., Chemical Engineers' Handbook 4th Edition New York McGraw-Hill
- 93) Hanson, C., Recent Advances in Liquid-Liquid Extraction Pergamon Press (1971)



- 94) Harkins, W.D., and Brown, F.E., *J. Am. Chem. Soc.* 41 499 (1919)
- 95) Hayworth, C.B., and Treybal, R.E., *Ind. Eng. Chem.* 42 1174 (1950)
- 96) Scheele, G.F., and Meister, B.J., *A. I. Ch. E. J.* 14 9 (1968)
- 97) Null, H.R., and Johnson, H.F., *A. I. Ch. E. J.* 4 273 (1958)
- 98) Rao, E.V.L.N., Kumar, R., and Kuloor, N.R., *Chem. Eng. Sci* 21 867 (1966)
- 99) Davidson, J.F., and Schuler, B.O.G., *Trans. Inst. Chem. Eng.* 38 335 (1960)
- 100) Kalyanasundaram, C.V., Kumar, R., and Kuloor, N.R.,  
Tech. Report No. CE-67-3 *Ind. Inst Sci* (1967)
- 101) Heertjes, P.M., de Nie, L.H., and de Vries, H.J., *Chem. Eng. Sci.* 26 441 (1971)
- 102) de Chazal, L.E.M., and Ryan, J.T., *A. I. Ch. E. J.* 17 1226 (1971)
- 103) Griegar, K., Prochazka, J., and Landau, J., *Coll. Czech. Chem. Comm.* 37 1943 (1972)
- 104) Izard, J.A., *A. I. Chem. E. J.* 18 634 (1972)
- 105) Narayanan, S., Anjali, Basu, and Roy, N.K., *Chem. Eng. Sci.* 25 1950 (1970)
- 106) Halligan, J.E., and Burkhardt, L.E., *A. I. Chem. E. J.* 14 411 (1968 a)
- 107) Ryan, J.T., Ph.D. Thesis Univ. of Missouri (1966)
- 108) Perrut, M., and Loutati, R., *Chem. Eng. J.* 3 286 (1972)
- 109) Scheele, J.F., and Meister, B.J., *A. I. Chem. E. J.* 14 15 (1968)
- 110) *Ibid.* *A. I. Chem. E. J.* 15 689 (1969)
- 111) Becher, P., "Emulsions Theory and Practice" New York :Reinhold (1965)
- 112) Shiffler, D.A., Ph.D. Thesis Cornell Uni. Ithaca (1966)
- 113) Tyler, E., and Richardson, E.C., *Prod. Phys. Soc.* 37 297 (1925)
- 114) Rayleigh, Lord, *Prod. Royal Soc.* 29 71 (1819)
- 115) Christiansen, R.M., and Hixson, A.N., *Ind. Engng. Chem.* 49 1017 (1957)

- 116) Meister, B. J., and Scheele, G. F., *A. I. Chem. E. J.* 13 682 (1967)
- 117) *Ibid.* *A. I. Chem. E. J.* 15 700 (1969)
- 118) Haynes, L. G., Himenbleu, D. M., and Schechter, G., *I. E. and C. Proc. Des. Dev.* 7 4 508 (1968)
- 119) Laplace, P. S., "Supplément a la Théorie de L'action Capillaire" page 64 Book \*10 of series "Trete de Mechanique Celeste" Dupret Paris (1798 - 1823)
- 120) Sudgen, S., *J. Chem. Soc.* 1483 (1921)
- 121) Staicopolous, D. N., *J. Coll. Int. Sci.* 23 453 (1967)
- 122) *Ibid.* *J. Coll. Int. Sci.* 17 439 (1962)
- 123) *Ibid.* *J. Coll. Int. Sci.* 18 793 (1963)
- 124) Parvatikar, K. G., *J. Coll. Int. Sci.* 23 274 (1967)
- 125) Mack, G. L., and Lee, D., *J. Phys. Chem.* 40 169 (1936)
- 126) Hartland, S. J., and Hartley, R., to be published
- 127) Davies, R., *Ind. Engng. Chem.* 62 1287 (1970)
- 128) Appino, J. B., *Annals of N. Y. Acad. of Sci.* 158 3 680 (1969)
- 129) Young, T. H., *Phil. Trans.* 65 84 (1805)
- 130) Johnson, R. E., *J. Phys. Chem* 63 1655 (1959)
- 131) Smolders, S., *Rev. Trans. Chem.* 80 650 (1961)
- 132) Buff, F. P., "Handbuch der Physik" Vol 10 Springer-verlog Berlin (1958)
- 133) Rayleigh, Lord., *Phil. Mag.* 30 397 (1890)
- 134) Gibbs, J. W., "Collected Works" Vol 1 Yale Uni Press Newhaven (1928)
- 135) Elliot, G. E. P., and Riddiford, A. C., "Recent Progress in Surface Science" Vol 2 (1964)
- 136) Pettica, B. A., and Pettica, T. J. P., *Proc. 2nd Int. Cong. Surface Activity Vol 3 London Butterworth (1957)*
- 137) Lester, G. R., *J. Coll. Sci.* 16 315 (1961)



- 138) Goodrich, F.C., "Surface and Colloidal Science"  
Vol 1 Wiley Interscience (1969)
- 139) Zisman, W.A., Adv. in Chem. Services 43 1 (1964)
- 140) Binkerman, J.J., Proc. 2nd Int. Cong. Surface Activity  
Vol 3 London Butterworth (1957)
- 141) Harkins, W.D., Phys. Chem. of Surface Films Rheinhold  
Pub. Co. (1952)
- 142) Temperley, H.N.D., Proc. Cambridge Phil. Soc. 48 683 (1952)
- 143) Mizrahi, J., and Barnea, E., Brit. Chem. Eng. 15 4 497 (1970)
- 144) Binkerman, J.J., Surface Chemistry Academy Press  
N.Y. 2nd Edition
- 145) Shuttleworth, R., and Bailey, G.L.J., Dis. Faraday Soc.  
3 16 (1948)
- 146) Johnson, R.E., and Dettre, R.H., Adv. in Chem. Series  
43 Am. Chem. Soc. Washington DC (1964)
- 147) Wenzel, R.N., J. Phys. Chem. 53 1466 (1949)
- 148) Ibid. Ind. Engng. Chem. 28 988 (1936)
- 149) Bartell, F.E., and Shepard, J.W., J. Phys. Chem. 57 211 (1953)
- 150) Ibid. J. Phys. Chem. 57 455 (1953)
- 151) Reay, D., and Ratcliff, G.A., J. Can. Chem. Eng. 51 178 (1973)
- 152) Phillips, M.C., and Riddiford, A.C., Wetting Sci. Monograph  
No. 25 Soc. of Chem. Ind. London (1967)
- 153) Zisman, W.A., Record of Chem. Prog. 26 1 13 (1964)
- 154) Adam, N.K., Dis. of Faraday Soc. 3 5 (1948)
- 155) Gregg, S.J., Journal of Chem. Phys 16 549 (1948)
- 156) Kowoski, K., J. Coll. Sci. 17 167 (1962)
- 157) Hansen, R.S., and Miotto, M., J. Am. Chem. Soc. 79 1765 (1957)
- 158) Johnson, R.E., and Dettre, R.H., J. Phys. Chem. 68 1744 (1964)
- 159) Yarnold, G.D., and Mason, B.J., Proc. Phys. Soc. B62 125 (1949)
- 160) Elliot, G.E.P., and Riddiford, A.C., J. Coll. Sci. 23 389 (1967)



- 161) Davies, J.T. and Rideal, E.K., "Interfacial Phenomena"  
Academy Press N.Y. (1961)
- 162) Fowkes, F.M., and Harkins, W.D., J. Am. Chem. Soc. 62 3372 (1940)
- 163) Adams, N.K., and Elliot, G.E.P., J. Chem. Soc. 2206 (1962)
- 164) Mason, G., J. Coll. Int. Sci. 35 286 (1971)
- 165) Houghley, D.P., and Beveridge, G.S.G., Chem. Eng. Sci.  
22 715 (1967)
- 166) Ridgeway, K., and Tarbuck, K.J., Brit. Chem. Eng. 12 384 (1967)
- 167) Verman, L.C., and Banerjee, S., Nature 157 584 (1946)
- 168) Jacobs, M.B., and Schefan, L., "Chemical Analysis of Solvents"  
McGraw Hill N.Y. Interscience (1955)
- 169) Bowden, F.P., Semaine d'etude sur la theme forces  
Moleculaires 285 Pontificae Academiae Scientiarum Scripto 31
- 170) Andreevskaya, G., High Strength Orientated Plastics  
p 192 Nueka Publ. Moscow (1966)
- 171) Hair, M.L., "Clean Surfaces" M. Dekka Incor. N.Y. (1970)
- 172) Davies, G.A., and Jeffreys, G.V.,
- 173) Jenkinson, L., M. Sc. Thesis Univ. of Aston (1973)
- 174) Edge, R.M., and Kalofatoglu, I.E., ISEC Vol 1 (1974)
- 175) Edge, R.M., and Grant, C.D., Chem Engng. Sci 27 1709 (1972)
- 176) O'Brien, V., J. Met. 18 549 (1961)
- 177) Hertzberg, W.J., Ph.D. Thesis Univ. of California Berkeley (1968)
- 178) Blaisdell, B.E., J. Math. Phys. 19 186 217 (1940)
- 179) Abrimonity, R., and Sergun, B., Handbook of Mathematical  
Functions p 416
- 180) Hussein, K.T., M.Sc. Thesis, Univ. of Aston (1972)
- 181) Cited by Lashkari, M., Proc. Phys. Soc. 59 1 (1947)
- 182) Kintner, R.C., "Advances in Chemical Engineering" Vol 4  
Academy Press (1963)
- 183) Tavlarides, L.L., Coufaloglou, C.A., Zeiten, M.A., Klinzing, G.E.,  
and Gobor, B., Ind. Engng. Chem. 62 11 15 (1970)



- 184) Dupre, Théorie mecanizue de la chaleur 359 (1869)
- 185) Treybal, R.E., "Liquid Extraction" McGraw Hill 2nd Edition
- 186) Schlieren Photography Kodak Scientific & Tech. Data
- 187) Photography applied to flow visualization Kodak Data Sheet 1N-1 Issue A
- 188) Mayer, P.R., and Stowe, R.A., J. Coll. Sci. 20 893 (1965)
- 189) Purchas, D.B., "Industrial Filtration of Liquids" Leonard Hill London (1967)
- 190) Davies, O.L., "Design & Analysis of Industrial Experiments" Oliver & Boyd London (1967)
- 191) Brown, A.H., and Hanson, C., Brit. Chem. Eng. 11, 7, 695 (1966)
- 192) Wilkinson, P., Chem. Reviews Vol 72 No. 6 577 (1972)
- 193) I.C.L. Statistical Package (XDS3) Users Handbook Section 0301 Univ. of Aston August (1972)
- 194) Topliss, J.A., 1st Chem. Eng. Dept. Research Symp. Univ. of Aston May (1970)